VICTORIA UNIVERSITY OF TECHNOLOGY

DAMAGE DETECTION IN STRUCTURES USING MEASURED FREQUENCY RESPONSE FUNCTION DATA

by

Abhijit Roy Choudhury

A thesis submitted to the Victoria University of Technology for the degree of Doctor of Philosophy.

Department of Mechanical Engineering

ACKNOWLEDGMENTS

I would like to express my sincere gratitude to Dr. Jimin He for his untiring supervision, advice and guidance which have greatly contributed to the success of this project.

My thanks are also due to Professor Geoffrey Lleonart for his helpful guidance in writing this thesis. Other members of the staff in the department of mechanical engineering are also acknowledged for their help at different stages of this work.

Sincere thanks are also due to all colleagues for their friendly cooperation and fruitful discussions during the course of the present work.

The author is also thankful to Victoria University of Technology for the financial support provided over the period in which this work was carried out. More personally, the author owe most to his parents, wife Amba and sister Mousumi for their constant support and encouragement, without which this work might never have culminated in this thesis.

ABSTRACT

Modern engineering structures such as offshore oil platforms, transmission towers, bridges and aircraft frames are regularly monitored and maintained in order to avert catastrophic failure. Despite our best efforts, sporadic failures, which may have disastrous consequences in terms of human life and resources, still occur. It is therefore important to develop techniques which lead to significant improvements in the reliability of the structures.

A challenging area of structural dynamics research is concerned with the development and practical implementation of monitoring systems which can identify and quantify damage as it occurs in a structure. The development of a number of techniques that contribute to providing means to detect structural damage is the goal of the work presented in this thesis.

A structural damage detection technique based on constrained minimization theory, which can both locate and quantify damage in a structure has been successfully developed. For locating damage only in a structure, a method which works well in the presence of appreciable measurement noise and coordinate incompleteness was demonstrated. In addition, a submatrix procedure was successfully applied to directly identify damaged elements in a structure instead of the degrees of freedom.

Each of the methods required a finite element model of the undamaged structure. For applications where such a model was not available, a new method was developed which used only the frequency response function from

addition to presenting the damage detection methods, consideration of problems associated with measurement noise and coordinate incompleteness pertaining to the proposed methods have been investigated, and appropriate steps suggested to overcome the problems.

NOMENCLATURE

The following list gives the principal use of the symbols in this thesis. However, a given symbol might be used to denote different quantities under special situations. The interpretation to be given to a symbol will be clear from the context in which it is employed.

$[A_1]$	- as given in equation (3.3.8)
$[A_2]$	- as given in equation (3.3.9)
$[A_D]$	- as explained in equation (2.2.25)
$[A_{MIX}]$	- as defined in equation (3.3.14)
$[B]$	- as defined in equation (5.4.1)
$\{b\}$	- as defined in equation (5.4.1)
$[C]$	- viscous damping matrix
$[D]$	- as explained in equation (2.2.31)
$\{\underline{D}\}$	- vector derived from matrix [D]
$\{d_f(\Omega)\}$	- as defined in equation (2.4.3)
$\{d(\Omega)\}$	- as defined in equation (3.2.7) in Chapter 3
d	- number of frequency pairs
E	- Young's Modulus
e	- error function as defined in equation (2.2.9)
e1 to e5	- random errors
F	- number of unknown non-zero coefficients in the stiffness matrix
$\{F(\Omega)\}$	- excitation at frequency Ω
$[G^i]$	- $-[A^D]^T[KSQ^i][A^D]$
g_1, g_2	- constraints in the Lagrange equation
$[H]$	- structural damping matrix in Chapter 1
$[H]_{ij}$	- $\{\underline{A}_D\}_j\{R^j\}_i^T$ in Chapter 2
$\{h\}$	- vector comprising of scaling factors
h_n	- n^{th} scaling factor

[I]	- identity matrix
I_{YY}	- moment of inertia of cross sectional area about axis Y-Y
I_{ZZ}	- moment of inertia of cross sectional area about axis Z-Z
[K]	- stiffness matrix of the structure
$[K]_j$	- j^{th} submatrix of stiffness matrix transformed to global coordinate system
[KSQ]	- $[K]_{UD} \otimes [K]_{UD}$
$[\Delta K]$	- differential stiffness matrix of the structure due to damage
K_{nn}	- coefficient of stiffness matrix at nn coefficient location in the matrix.
$[k_r]$	- diagonal modal stiffness matrix
k_r	- r^{th} modal stiffness
L	- Lagrange function
[M]	- mass matrix of the structure
$[\Delta M]$	- differential mass matrix of the structure due to damage
$[M]_j$	- j^{th} submatrix of mass matrix transformed to global coordinate system
$[m_r]$	- diagonal modal mass matrix
m_r	- r^{th} modal mass
mm	- number of measured modes
m	- number of measured coordinates
N	- number of degrees of freedom of the system
n_d	- number of averages
[P]	- contains orthonormalized eigenvectors of ([T] + [S])
$[Q_M]$	- damage quantification matrix due to change in mass only
$[Q_K]$	- damage quantification matrix due to change in stiffness matrix
$[Q_Z]$	- damage quantification matrix due to change in dynamic stiffness matrix
$Q_{Z,ij}$	- ij^{th} element of matrix $[Q_Z]$
{R}	- as defined in equation (4.2.12)
$\{R^j\}_i$	- ith column of $[A_D]^T[KSQ_j]$ in Chapter 2
[S]	- as explained in equation (2.2.32)
s	- number of frequency points
[T]	- as explained in equation (2.2.32)

[TR]	- transformation matrix
[U]	- as defined in equation (2.2.10)
u	- number of unmeasured coordinates
[V]	- diagonal matrix whose diagonal elements are the eigenvalues of ([T] + [S])
{X}	- as defined equation (2.2.20) in Chapter 2
{x}	- as defined equation (5.4.1) in Chapter 3
{Y}	- as defined in equation (4.2.13)
[Y]	- as defined in equation (4.2.14)
$[Z(\Omega)]$	- dynamic stiffness matrix of the structure
$Z(\Omega)_{D,ij}$	- ij^{th} element of dynamic stiffness matrix of damaged structure at frequency Ω
$\{Z_{UD}(\Omega)\}j$	- j^{th} row of $[Z(\Omega)]_{UD}$
[ZSQ]	- $0.25\ [Z]_{UD} \otimes [Z]_{UD}$
$[\Delta Z(\Omega)]$	- differential dynamic stiffness matrix of the structure due to damage at frequency Ω
$[\alpha(\Omega)]$	- receptance matrix at frequency Ω
$\{\alpha_D(\Omega)\}_k$	- k^{th} column of the RFRF matrix of the damaged structure at frequency Ω
$\{\alpha_{D(f)}(\Omega)\}_k$	- k^{th} column of the filtered RFRF matrix of the damaged structure at frequency Ω
$\{\alpha_{UD}(\Omega)\}_k$	- k^{th} column of the RFRF matrix of the undamaged structure at frequency Ω
$\{\Delta\alpha(\Omega)\}_k$	- k^{th} column of the differential RFRF matrix between damaged and undamaged structure at frequency Ω
$\alpha_{kk}(\Omega)$	- kk^{th} element of receptance matrix at frequency Ω
$\{\beta(\Omega)\}$	- damage location vector
$\{\delta\}_K$	- delta vector whose k^{th} element is unity
$\gamma_{xy}^2(\Omega)$	- coherence at frequency Ω
$[\phi]$	- mass normalised mode shapes
η_K	- k^{th} modal damping factor

λ, μ	- Lagrange multipliers
$[\psi]$	- eigenvector matrix
$[\lambda_r]$	- diagonal matrix whose diagonal elements are the eigenvalues
λ_k	- k^{th} eigenvalue
θ_Ω^j	- defined in equation (3.2.20) in Chapter 3
Ω	- frequency of the system
ω_K	- k^{th} natural frequency

Operators and symbols

Σ	- summation
$\{\ \}^T, [\ ]^T$	- transpose
$\otimes$	- matrix element by element operation
[ ]-1	- standard inverse
[ ]+	- pseudo inverse
$\lVert\ \rVert$	- matrix norm
$[\ ]_D$	- represents damaged structure
$[\ ]_{UD}$	- represents undamaged structure
$\{^m\}$	- superscript m refers to measured coordinate
$\{^u\}$	- superscript u refers to unmeasured coordinate

Abbreviations

CDLV	- cumulative damage location vector
CMDQ	- constrained minimization damage quantification
COMAC	- coordinate modal assurance criterion
D. E	- dynamic expansion
DLP	- damage location plot
DLV	- damage location vector
DOF	- degree of freedom
FE	- finite element

FEM	- finite element model
FRF	- frequency response function
IRS	- improved reduced system
MAC	- modal assurance criterion
MDOF	- multiple degree of freedom
MRPT	- minimum rank perturbation technique
PMAC	- partial modal assurance criterion
RFRF	- receptance frequency response function
SDOF	- single degree of freedom
SEREP	- system equivalent reduction expansion process
SSC	- signal subspace correlation

LIST OF FIGURES

Figure	Title	Page
2.1	Graph showing variation of normalized random error as a function of coherence and number of averages	58
2.2	Graph of normalized random error and number of averages	58
2.3	Flowchart of program for computer implementation of CMDQ method	59
2.4	A 12 DOF mass-spring system (Model 2.1)	60
2.5	An 8 DOF mass-spring system (Model 2.2)	60
2.6	A 20 member plane truss structure (Model 2.3)	61
2.7	Actual [ΔK] for model 2.1	62
2.8	Calculated [ΔK] using CMDQ method for pure data in model 2.1 (29 valid eigenvalues; 3, 12, 14 rad/s)	62
2.9	Calculated [ΔK] using CMDQ method for pure data in model 2.1 (26 valid eigenvalues; 3, 12, 14 rad/s)	62
2.10	Calculated [ΔK] using CMDQ method for pure data in model 2.1 (23 valid eigenvalues; 3, 12, 14 rad/s)	62
2.11	Calculated [ΔK] using CMDQ method for pure data in model 2.1 (23 valid eigenvalues; 8, 10, 11 rad/s)	63
2.12	Calculated [ΔK] using CMDQ method for pure data in model 2.1 (25 valid eigenvalues; 8, 10, 11, 13 rad/s)	63
2.13	Calculated [ΔK] using CMDQ method for pure data in	63

	model 2.1 (29 valid eigenvalues; 8, 10, 11, 13, 15.4rad/s)	
2.14	Calculated [ΔK] using CMDQ method for 2% noisy data in model 2.1 (29 valid eigenvalues; 3, 12, 14 rad/s)	63
2.15	Calculated [ΔK] using CMDQ method for 2% noisy data in model 2.1 (29 valid eigenvalues; 3, 12, 14, 13 rad/s)	64
2.16	Calculated [ΔK] using CMDQ method for 2% noisy data in model 2.1 (29 valid eigenvalues; 3, 12, 14, 13, 16 rad/s)	64
2.17	Calculated [ΔK] using CMDQ method, 2% noisy data in model 2.1 (29 valid eigenvalues; 3, 12, 14, 13, 16, 9 rad/s)	64
2.18	Calculated [ΔK] using CMDQ, noise filtering for 2% noisy data in model 2.1 (3, 12, 14, 13, 16 rad/s)	64
2.19	Actual [ΔK] for model 2.2	65
2.20	Calculated [ΔK] using CMDQ method for pure data in model 2.2 (16 valid eigenvalues; 8, 14 rad/s)	65
2.21	Calculated [ΔK] using CMDQ method for pure data in model 2.2 (16 valid eigenvalues; 8, 14, 19 rad/s)	65
2.22	RFRF for model 2.3 before and after damage	66
2.23	Actual [ΔK] for model 2.3	66
2.24	Calculated [ΔK] using CMDQ method for pure data in model 2.3 (12, 19, 25, 43 rad/s)	66
2.25	Calculated [ΔK] using CMDQ method for 2% noisy data in model 2.3 (12, 19, 25, 43 rad/s)	67
2.26	Calculated [ΔK] using CMDQ method for 2% noisy data in model 2.3 (12, 19, 25, 37, 43 rad/s)	67
2.27	Calculated [ΔK] using CMDQ method for filtered data in model 2.3 (12, 19, 25, 37, 43 rad/s)	67

3.1	A 5 DOF mass-spring system	110
3.2	A 12 DOF mass-spring system (Model 3.2)	110
3.3	A truss structure (Model 3.3)	111
3.4A	3-D DLP using D.E A (Case I/ Subcase 1 in section 3.4)	112
3.4B	3-D DLP using D.E B (Case I/ Subcase 1 in section 3.4)	112
3.4C	3-D DLP using D.E C (Case I/ Subcase 1 in section 3.4)	112
3.4D	3-D DLP using FRF mix (Case I/ Subcase 1 in section 3.4)	112
3.4E	3-D DLP using SEREP1 (Case I/ Subcase 1 in section 3.4)	113
3.4F	3-D DLP using SEREP2 (Case I/ Subcase 1 in section 3.4)	113
3.4G	3-D DLP using SEREP3 (Case I/ Subcase 1 in section 3.4)	113
3.4H	3-D DLP using SEREP4 (Case I/ Subcase 1 in section 3.4)	113
3.5A	3-D DLP using D.E A (Case I/ Subcase 2 in section 3.4)	114
3.5B	3-D DLP using D.E B (Case I/ Subcase 2 in section 3.4)	114
3.5C	3-D DLP using D.E C (Case I/ Subcase 2 in section 3.4)	114
3.5D	3-D DLP using FRF mix (Case I/ Subcase 2 in section 3.4)	114
3.5E	3-D DLP using SEREP1 (Case I/ Subcase 2 in section 3.4)	115
3.5F	3-D DLP using SEREP2 (Case I/ Subcase 2 in section 3.4)	115
3.5G	3-D DLP using SEREP3 (Case I/ Subcase 2 in section 3.4)	115
3.5H	3-D DLP using SEREP4 (Case I/ Subcase 2 in section 3.4)	115
3.6A	3-D DLP using D.E A (Case II/ Subcase 1 in section 3.4)	116
3.6A/1	CDLV using D.E A (Case II/ Subcase 1 in section 3.4)	116

3.6B	3-D DLP using D.E B (Case II/ Subcase 1 in section 3.4)	116
3.6B/1	CDLV using D.E B (Case II/ Subcase 1 in section 3.4)	116
3.6C	3-D DLP using D.E C (Case II/ Subcase 1 in section 3.4)	117
3.6C/1	CDLV using D.E B (Case II/ Subcase 1 in section 3.4)	117
3.6D	3-D DLP using FRF mix (Case II/Subcase 1 in section 3.4)	117
3.6D/1	CDLV using FRF mix (Case II/ Subcase 1 in section 3.4)	117
3.7A	3-D DLP using D.E A (Case II/ Subcase 2 in section 3.4)	118
3.7A/1	CDLV using D.E A (Case II/ Subcase 2 in section 3.4)	118
3.7B	3-D DLP using D.E B (Case II/ Subcase 2 in section 3.4)	118
3.7B/1	CDLV using D.E B (Case II/ Subcase 2 in section 3.4)	118
3.7C	3-D DLP using D.E C (Case II/ Subcase 2 in section 3.4)	119
3.7C/1	CDLV using D.E C (Case II/ Subcase 2 in section 3.4)	119
3.7D	3-D DLP using FRF mix (Case II/Subcase 2 in section 3.4)	119
3.7D/1	CDLV using FRF mix (Case II/ Subcase 2 in section 3.4)	119
3.8A	3-D DLP using D.E A (case 1/ subcase I; fig.3.3 model)	120
3.8B	3-D DLP using D.E A (case 1/ subcase II; fig.3.3 model)	120
3.8C	3-D DLP using D.E A (case 1/ subcase III; fig.3.3 model)	120
3.9A	3-D DLP using D.E A (case 2/ subcase I; fig.3.3 model)	121
3.9B	3-D DLP using D.E A (case 2/ subcase II; fig.3.3 model)	121
3.9C	3-D DLP using D.E A (case 2/ subcase III; fig.3.3 model)	121
4.1	A 3 DOF mass-spring system	143

4.2	A 10 DOF mass-spring system	143
4.3	A cantilever truss structure	144
4.4	Scaling factor due to damage in model 3.2	145
4.5	Identified scaling factor (Approach 1; 2 frequency points, no noise)	145
4.6	Identified scaling factor (Approach 1; 4 frequency points, no noise)	146
4.7	Identified scaling factor (Approach 2; no noise)	146
4.8	Identified scaling factor (Approach 1; 4% noise)	147
4.9	Identified scaling factor (Approach 2; 4% noise)	147
4.10	Identified scaling factor (Approach 2 and DLP; 4% noise)	148
4.11	Identified scaling factor (Approach 2, incomplete measurement; 4% noise)	148
4.12	Identified scaling factor (Approach 2 and DLP; measurement available; 4% noise)	149
4.13	Identified scaling factor (Approach 2 and DLP; interpolated data; 4% noise)	149
4.14	Scaling factor of the truss structure in fig. 4.3 (Case 1)	150
4.15	Scaling factor of the truss structure in fig. 4.3 (Case 2)	150
4.16	3-D DLP for case 1 damage in fig. 4.3 model	151
4.17	Identified scaling factor for the truss structure in fig.4.3 (Case1)	151
4.18	3-D DLP for case 2 damage in fig. 4.3 model	152

4.19	Identified scaling factor for the truss structure in fig.4.3 (Case2)	152
5.1	A 3 DOF mass-spring system	179
5.2	A continous beam and its lumped mass model	179
5.3	[ΔK] for the 12 DOF mass-spring system in fig. 3.2	180
5.4	Calculated [ΔK] for the 12 DOF mass-spring system in fig. 3.2 (using Method I in section 5.5.1)	180
5.5	Calculated [ΔK] for the 12 DOF mass-spring system in fig. 3.2 (using Method II in section 5.5.2)	181
5.6	Identified scaling factor for fig. 3.2 system (Method III in section 5.5.3; 4% noise)	181
5.7	Calculated [ΔK] for fig. 3.2 system (using Method II, frequency points different from case represented in fig.5.5)	182
5.8	Identified scaling factor for fig. 3.2 system (Method III in section 5.5.3; 4% noise, frequency different from case represented in fig. 5.6)	182
5.9	Calculated [ΔK] for fig. 3.2 system (using Method II, 4% noise, incomplete coordinates measured)	183
5.10	Identified scaling factor for fig. 3.2 system (Method III in section 5.5.3; 4% noise, incomplete coordinates measured)	183
5.11	Calculated [ΔK] for fig. 3.2 system (using Method II, 4% noise, incomplete coordinates interpolated)	184
5.12	Identified scaling factor for fig. 3.2 system (Method III in section 5.5.3; 4% noise, incomplete coordinates interpolated)	184
6.1	A beam structure	223
6.2	A cross stiffened grid structure	224

6.3a	Location on the beam where measurements were taken	225
6.3b	Location on the grid where measurements were taken	225
6.4	Schematic diagram of the measurement set-up	226
6.5	Photograph of the experimental rig	226
6.6	$\alpha_{11,11}(\Omega)$ for the beam from measurement and FE model	227
6.7	Coherence of RFRF ($\alpha_{11,11}(\Omega)$) for the undamaged beam	228
6.8	$\alpha_{7,7}(\Omega)$ for the grid from measurement and FE model	229
6.9	Frequency response of different forms of attachment	229
6.10	$\alpha_{11,11}(\Omega)$ for the beam before and after damage	230
6.11a	3-D DLP for the beam	231
6.11b	CDLV for the beam	231
6.12	$\alpha_{7,7}(\Omega)$ for the grid before and after damage	232
6.13a	3-D DLP for the grid structure	233
6.13b	CDLV for the grid structure	233
6.14A	$\alpha_{11,11}(\Omega)$ for the beam (regenerated, before and after damage) for case A	234
6.14B	$\alpha_{11,11}(\Omega)$ for the beam (regenerated, before and after damage) for case B	234
6.14C	$\alpha_{11,11}(\Omega)$ for the beam (regenerated, before and after damage) for case C	235
6.15A	$\alpha_{11,11}(\Omega)$ for the beam (regenerated, before and after damage) using scaling factor .15	235
6.15B	$\alpha_{11,11}(\Omega)$ for the beam (regenerated, before and after	236

	damage) using scaling factor .17	
6.15C	$\alpha_{11,11}(\Omega)$ for the beam (regenerated, before and after damage) using scaling factor .26	236
6.16A	$\alpha_{7,7}(\Omega)$ for the grid (regenerated, before and after damage) for case A	237
6.16B	$\alpha_{7,7}(\Omega)$ for the grid (regenerated, before and after damage) for case B	237
6.16C	$\alpha_{7,7}(\Omega)$ for the grid (regenerated, before and after damage) for case C	238
6.16D	$\alpha_{7,7}(\Omega)$ for the grid (regenerated, before and after damage) for case D	238
6.17A	$\alpha_{7,7}(\Omega)$ for the grid (regenerated, before and after damage) using scaling factor .38	239
6.17B	$\alpha_{7,7}(\Omega)$ for the grid (regenerated, before and after damage) using scaling factor ..24	239
6.17C	$\alpha_{7,7}(\Omega)$ for the grid (regenerated, before and after damage) using scaling factor .37	240
6.17D	$\alpha_{7,7}(\Omega)$ for the grid (regenerated, before and after damage) using scaling factor .34	240
6.18	$\alpha_{7,7}(\Omega)$ for the grid (undamaged and after both damages)	241
6.19a	3-D DLP for the grid for both damages	242
6.19b	CDLV for the grid for both damages	242

TABLE OF CONTENTS

TITLE i

ABSTRACT ii

ACKNOWLEDGEMENTS iv

NOMENCLATURE v

LIST OF FIGURES x

TABLE OF CONTENTS xviii

1. INTRODUCTION 1

1.1 Damage location using measured receptance FRF data 1

1.2 System models 4

1.3 Review of previous work 10

1.4 Assumptions of this study 16

1.4 Scope of present work 17

2. DETERMINATION OF STRUCTURAL DAMAGE EXTENT USING CONSTRAINED MINIMIZATION THEORY 20

2.1 Introduction 20

2.2 Constrained minimization damage quantification (CMDQ) method 23

2.3 Discussion 34

2.3.1 Determining the number of valid eigenvalues 35

2.3.2 Determining the number of frequency points 37

2.3.3 Simultaneous mass and stiffness changes due to damage 38

2.4 Noise filtering algorithm for proposed method 40

2.5 Results of numerical analysis 43

2.6 Summarising remarks 51

3. DAMAGE LOCATION IN A STRUCTURE USING MEASURED FRF DATA 68

3.1 Introduction 68

3.2 Theory of damage location using FRF data 71

3.3 Compatibility of measured and analytical data 77

3.3.1 Reduction Techniques 78

3.3.2 Expansion Techniques 81

3.4 Results of numerical simulations 89

3.5 Analysis of numerical results 99

3.6 Summarising remarks 106

4. SUBMATRIX APPROACH FOR DETERMINING DAMAGE EXTENT IN A STRUCTURE 122

4.1 Introduction 122

4.2 Theory of determining damage extent using submatrix approach 124

4.3 Discussions 131

4.4 Results of numerical analysis 134

4.5 Summarising remarks 140

5. USING SPATIAL MODEL TO DETERMINE DAMAGE EXTENT 153

5.1 Introduction 153

5.2 Review of previous works for spatial model derivation 154

5.3 Theory to generate spatial model 157

5.4 Discussion 163

5.5 Application of the method for determining damage extent 166

5.5.1 Method I (Direct Method) 166

5.5.2 Method II (Indirect Method) 167

5.5.3 Method III (Using Submatrix Approach) 168

5.6 Results of numerical case studies 169

5.7 Summarising remarks 174

6. EXPERIMENTAL CASE STUDY 185

6.1 Introduction 185

6.2 The test structures 186

6.3 Measurement equipment 186

6.4 Calibration of the measurement equipment 188

6.5 FE modelling of undamaged structure 189

6.5.1 Beam structure 189

6.5.2 Cross stiffened grid structure 190

6.6 Test structure preparation for measurement 190

6.6.1 Support Condition 190

6.6.2 Type of Excitation 191

6.6.3 Attachment and location of transducer 192

6.7 Introduction of damage in the structure 193

6.8 Execution of the measurement 193

6.9 Damage location 194

6.10 Discussion of location results 197

6.11 Determination of damage severity 198

6.12 Discussion of damage severity results 207

6.13 Location of multiple damage 211

6.14 Summarising remarks 211

7. CONCLUSION AND SUGGESTIONS FOR FUTURE RESEARCH 243

7.1 General conclusion 243

7.2 New contributions of present research 245

7.3 Suggestions for further work 246

REFERENCES 248

APPENDIX A 263

APPENDIX B 265

APPENDIX C 269

APPENDIX D 272

APPENDIX E 277

CHAPTER 1

INTRODUCTION

With the progress of materials science, new materials have been introduced which have made it possible to build large and complicated structures with reduced weight. However, due to the large size and complexity of such structures and the possible catastrophic effect associated with their failure, it is imperative to develop a technique which is able to locate, and determine the extent, of structural damage as it develops in a structure. Advancement in recent years in the capability of modern electronic instrumentation for signal processing have resulted in the development of superior instruments for monitoring the condition of machines. From experience gained in the machinery health monitoring field, it is expected that the vibration signature of a structure should provide adequate and useful information to detect possible structural damage.

1.1 DAMAGE LOCATION/QUANTIFICATION USING MEASURED RECEPTANCE FRF (RFRF) DATA

As a result of the consequences associated with the failure of some present day structures, in terms of both human life and resources, a lot of effort has been directed towards developing a suitable technique for detecting damage in structures. Most of the work in structural damage detection uses the general framework of model refinement or model updatings where the analytical spatial model of the undamaged structure (mass and stiffness properties) and the experimental modal model of the damaged structure (natural frequencies and mode shapes) have been used together to determine damage location and its extent. In these approaches it is assumed that the analytical model of the undamaged structure truly represents the structure within certain frequency ranges of interest.

Although the system identification technique is a promising method in structural damage detection, use of modal parameters introduces some disadvantages and limitations into these methods. The experimental modal parameters of a system by themselves usually present a limited amount of data. This is because these modal parameters are restricted only to natural frequencies and mode shapes of the system within the measured frequency range. For most practical applications the measured frequency range contains only a limited number of natural frequencies. In addition, if the modal parameters available are not severely affected by damage, then it would be difficult to detect damage by applying existing methods using modal parameters.

To generate a true analytical model of a structure, it is required to discretize it into a large number of degrees of freedom (DOFs). If the number of DOFs is N, then the complete modal model of the structure should have information about all N natural frequencies and their corresponding mode shapes. However, the experimental modal model obtained for a structure is incomplete, as it becomes difficult to measure over a wide frequency band if the value of N is large. In addition, it is impractical to measure as many coordinates as an analytical model has. A few of the earlier methods which required a complete experimental modal model to detect damage consequently performed unsatisfactorily when working in practical situation. In addition, use of modal parameters for detecting damage involves the extraction of them from measured frequency response function (FRF) data by an analysis method called experimental modal analysis, which may introduce additional computational burden and errors.

However, if a suitable technique can be developed which makes use of the analytical spatial model and the experimental response model (FRF data) instead of the modal model, then it is possible to eliminate most of the limitations and disadvantages associated with using the modal model. Therefore, in contrast to the existing structural damage detection methods based on system identification using the,

> Spatial Model Of The Undamaged Structure + Modal Model Of The Damaged Structure,

the method proposed in this work will use the,

> Spatial Model Of The Undamaged Structure + Response Model Of The Damaged Structure

to locate and quantify damage in the structure. These models are described in the next section.

However, two problems which confront any structural damage detection algorithm have to be addressed. These are :

- effect of noise - in spite of all the technological advances in electronic instrumentation, it is hard to envisage a condition where no noise of any type has contaminated the measured vibration data. When using FRF data directly, it is possible to judiciously select frequency points with a high signal to noise ratio but it is unlikely that the noise effect will be zero.

- effect of DOF incompleteness - when developing a finite element model of a structure, it is possible to use a large number of DOFs to discretize it in order to better resemble the structure. However, while taking measurements of the structure, it is not possible to measure at all the DOFs corresponding to the finite element model (FEM) of the structure. One way to tackle this problem of DOF incompatibility is either to expand the measured DOFs to equal to FE model DOFs or to reduce the FE model in accordance with the measured DOFs. However, both the expansion and reduction methods introduce inaccuracy into the data.

These two problems will be addressed in the context of using FRF data to locate and determine the extent of structural damage.

1.2 SYSTEM MODELS

The dynamic properties of a system, analytically or experimentally derived, can be represented in the following model formats: spatial model, modal model and response model. For the application of damage detection, either the experimental modal model or the experimental response model of the damaged structure can be used along with the analytical spatial model of the undamaged structure to detect the possible location and extent of damage. These three models used to describe the dynamic properties of the system are defined below.

(1) Spatial Model

When a given structure is discretized analytically, spatially distributed properties, such as the mass, stiffness and damping, are assigned to each of the N DOFs. These properties are presented in matrix form as given below:

$[M]_{NxN}$ - mass matrix whose diagonal terms define the inertia force assigned to each DOF when they experience an acceleration and whose off-diagonal terms contain inertia coupling information.

$[K]_{NxN}$ - stiffness matrix whose diagonal terms define the inherent restoring forces due to relative displacement at each DOF and the off-diagonal terms express the static coupling between DOFs.

$[C]_{NxN}$ or $[H]_{NxN}$ - viscous and structural damping matrices respectively. In cases where the dissipative forces are negligible, they are often neglected.

If a spatial model has N co-ordinates, then it is expected to have N modes. However, if it is reduced by one of the reduction methods to be discussed in Chapter 3, to 'm' co-ordinates ($m < N$), it will contain information on 'm' modes only.

Spatial models are also referred to as "Time Models", since equations of motion formulated by using spatial properties contain the response motions of system as functions of time.

(2) <u>Modal Model</u>

Dynamic properties of a system are also often described in terms of natural frequencies, modal damping factors and associated mode shapes. A mathematical model comprising these data is called a modal model.

Mathematically, the mode shapes are represented as vectors in which each element represents a deflection of one DOF relative to the other (N-1) DOFs in the model. The mode shapes (or eigenvectors) can be grouped together in the, so called Modal Matrix which is represented by $[\Psi]_{Nxm}$. This is a square or rectangular matrix containing information about N co-ordinates and m modes. The eigenvalues related to system natural frequencies can be grouped together forming a diagonal matrix represented by $[\lambda_r]_{mxm}$. Generally, both matrices are complex. The k^{th} eigenvalue is given here as λ_k and the corresponding mode shape as $\{\Psi\}_k$. The diagonal matrix corresponding to system natural frequencies and the modal matrix is presented next:

$$[\lambda_r]_{mxm} = \begin{bmatrix} \cdot & & \\ & \cdot & \\ & \omega_k^2(1+i\eta_k) & \\ & & \cdot \end{bmatrix} \tag{1.1}$$

$$[\psi]_{N\times m} = \begin{bmatrix} . & . & a_1^k + ib_1^k & . \\ . & . & a_2^k + ib_2^k & . \\ . & . & . & . \\ . & . & . & . \\ . & . & a_N^k + ib_N^k & . \end{bmatrix} \tag{1.2}$$

The kth eigenvalue contains information related to the kth natural frequency (ω_k) and modal damping (η_k). The kth mode shape $\{\psi\}_k$ is represented by a real part and an imaginary part.

Since the mode shapes represent relative amplitudes at the DOFs, rather than absolute deflections of the structure, the elements of each mode shape can be scaled arbitrarily. For instance, they can be scaled in such a way that the largest element becomes unity for graphical visualisation purposes. On other occasions, mode shapes may be required to be uniquely defined. This can be achieved by making use of the concept of modal mass and modal stiffness. Due to the orthogonality theory of a multi-degree-of-freedom system, the following relationships hold (if $m < N$):

$$[m_r]_{mxm} = [\psi]^T_{m\times N}[M]_{N\times N}[\psi]_{N\times m} \tag{1.3}$$

$$[k_r]_{mxm} = [\psi]^T_{m\times N}[K]_{N\times N}[\psi]_{N\times m} \tag{1.4}$$

With [K] assumed as a complex stiffness matrix, equations (1.3) and (1.4) gives the diagonal modal mass and modal stiffness matrices whose elements are interrelated as $\lambda_r = {}^{k_r}\!/_{m_r} = \omega_r^2(1+i\eta_r)$. The mode shapes of the system can be normalized using the modal mass such that :

$$[\phi] = [\psi][m_r]^{-0.5} \tag{1.5}$$

where $[\phi]$ is called the mass normalized mode shape. This will result in a new set of orthogonality equations given below as:

$$[\phi]^T_{m\times N}[M]_{N\times N}[\phi]_{N\times m} = [I]_{mxm} \tag{1.6}$$

$$[\phi]^T_{m\times N}[K]_{N\times N}[\phi]_{N\times m} = [\lambda_r]_{m\times m} \tag{1.7}$$

These mass normalized mode shapes can be experimentally obtained from a modal analysis process, as illustrated by Ewins [1].

(3) <u>Response Model</u>

A linear, time invariant dynamic system, when subjected to a certain input, will generate a definite output. The basic system equation is:

$$\text{OUTPUT} = \text{SYSTEM CHARACTERISTICS x INPUT} \tag{1.8}$$

It can be seen that the output response is related to the input via its dynamic characteristics. Using the same system equation for any linear system excited by harmonic excitation, the input/output relationship in the frequency domain at frequency Ω can be written as:

$$\{X(\Omega)\} = [\alpha(\Omega)]\{F(\Omega)\} \tag{1.9}$$

$$\{F(\Omega)\} = [Z(\Omega)]\{X(\Omega)\} \tag{1.10}$$

where $[\alpha(\Omega)]$ and $[Z(\Omega)]$ are related by the following relationship,

$$[Z(\Omega)] = [\alpha(\Omega)]^{-1} \tag{1.11}$$

$[\alpha(\Omega)]$ is called the receptance frequency response function matrix of the system. The receptance FRF matrix $[\alpha(\Omega)]$ will become the Mobility matrix or Inertance matrix if the response measured is velocity or acceleration. In these matrices each element is a complex ratio (response/force) called the FRF which covers a certain frequency range. In addition, there exists three other formats for FRF data, these being the inverse of receptance, mobility and inertance. They are generally known as 'dynamic stiffness', 'mechanical impedance' and 'apparent mass' respectively. The response model is then expressed as an FRF matrix which may be derived either analytically or experimentally.

It is important to comprehend different practical implications if measuring $[\alpha(\Omega)]$ or $[Z(\Omega)]$. Consider an element $\alpha_{ij}(\Omega)$in matrix $[\alpha(\Omega)]$. It represents the amplitude and relative phase of a harmonic displacement at DOF 'i' due to a harmonic force applied at DOF 'j' (no other external forces are applied to the system). However, $Z_{ij}(\Omega)$ represents the amplitude and relative phase of a harmonic force applied to DOF 'i' due to a unit displacement at DOF 'j' (when no other displacement exists in the system).

For a SDOF system it is easy to measure or calculate either $\alpha(\Omega)$ or $Z(\Omega)$. For a MDOF system, it is physically impossible to measure $[Z(\Omega)]$ since it is impossible to ensure displacement response only at one DOF while displacements at all other DOFs are equal to zero.

Elements in a particular column of matrix $[\alpha(\Omega)]$ can be measured by changing the point of response while force location is the same. According to the reciprocity principle, matrix $[\alpha(\Omega)]$ is symmetric. Therefore, measuring one column is equivalent to measuring one row, although the mechanism of measurement is different.

To summarize, the Response model of a dynamic system can be described by the FRF matrix whose elements can be either measured or analytically calculated or sometimes, a mixture of both.

1.3 REVIEW OF PREVIOUS WORKS

Using vibration test data to locate structural damage has been attempted by many researchers in recent years. A brief review is given here. More details are given in later chapters where some specific techniques are studied.

Most of the prior work in structural damage detection is based on the general framework of FEM refinement (System Identification) techniques. The need for FEM refinement of a structure arose because of the deviation that occurred between the modal properties predicted by the Finite Element Model and that measured. To reduce this deviation, the technique of FEM refinement was used where measurement data of a structure was used to tune or correct the FEM of the structure. The tuned or correlated FEM is expected to represent the actual structure more accurately. Unlike model refinement, where the deviation is credited to modelling errors, in the case of damage location, the deviation is attributed to the damage in the structure. This explains the reason behind the application of the FEM refinement algorithm to damage location problems.

The FEM refinement algorithms which may be used for structural damage detection may be broadly divided into three categories: optimal matrix updating, eigenstructure assignment and sensitivity analysis. Among these categories, perhaps the most widely used is optimal matrix updating. Early work in this area included that of Rodden [3] who used vibration test data to determine the structural influence coefficients of a structure. The problem of finding a matrix that satisfies a set of measurements as well as symmetry and positive definiteness was addressed by Brock [4]. Berman and Flannely [5] discussed the calculation of system matrices when the number of DOFs and the number of measured modes do not coincide.

Several optimal matrix update algorithms are based on the problem formulation set forth by Baruch and Bar Itzhack [6]. In their work, a closed form solution was developed for the minimal Frobenius norm matrix adjustment to the structural stiffness matrix incorporating measured natural frequencies and mode shapes. Berman and Nagy [7] adopted a similar formulation but included approaches to improve both the mass and stiffness matrices. In their work, the refined stiffness (mass) takes a form in which the original physical connectivity of the system is destroyed. In separate publications Kabe [8] and Smith and Beattie [9] suggested algorithms which preserved the original connectivity of the stiffness matrix.

The Kabe [8] algorithm utilised a percentage change in the stiffness value cost function and preserved the connectivity of the original structure. Assuming that the accurately measured mode shapes of the damaged structure were available at every finite element DOFs of the structure, Smith and Hendricks [9] investigated the extent of structural damage. However, in this case the stiffness matrix coefficients corresponding to undamaged members were significantly affected, making the detection uncertain. Although the minimization of the matrix norm of the stiffness difference before and after damage might be a promising mathematical method, the success of such a method depends heavily on the introduction of adequate and necessary physical constraints.

The control-based eigenstructure assignment technique determines the pseudo-control that would be required to produce the measured modal properties with the initial Finite Element model. The pseudo-control is then translated into matrix adjustments applied to the initial FEM. Among the approaches described by Inman and Minas [10], the first approach corrected the stiffness matrix using information about the eigenparameters. The symmetry in the resultant model was enforced by using an unconstrained numerical non-linear optimization approach. The second approach based upon eigenvalue information used a state space formulation to find the errors due to damage. Zimmerman [11] used a symmetry preserving eigenstructure assignment theorem where the information regarding eigenparameters of the damaged structure was incorporated in the spatial model of the undamaged structure. This algorithm used the solution of a generalized algebraic Riccati equation whose dimension was defined solely by the number of measured modes.

Sensitivity analysis for damage detection makes use of the derivatives of modal parameters with respect to physical design variables. The derivatives are then used to update the physical parameters. These algorithms result in updated models consistent within the original finite element programme framework. Hajela and Soeiro [12] and Soeiro [13] made direct application of non-linear optimization to the damage detection problem. Among other works reported that uses sensitivity analysis, Jung and Ewins [14] described the application of an inverse eigensensitivity method for model updating using arbitrarily chosen macro elements to a simple frame. Although the method has been shown to be reasonably insensitive to noise, the number of eigensensitivity vectors (derived from eigenvectors) required for the method to succeed might become prohibitively large for complicated structures.

In addition to the methods discussed above, Liu and Yao [15] considered the development of the probabilistic methodology for the prediction of multiple crack distribution in a structure of beam elements. The probabilistic measure of crack distribution could then be used for probabilistic diagnosis of crack location and extent. Several other authors have also shown that crack locations could be identified by using the concept of fracture mechanics along with information about change in natural frequencies due to damage. Among them was Gudmundson [16] who used saw cuts to simulate open cracks and the experimental results obtained by him from vibration measurements agreed remarkably well with the predictions from the open crack mathematical model he developed.

Chondros and Dimarogonas [17] also created actual fatigue cracks in welded joints and established a simple relationship between the crack depth and its flexibility using concepts of fracture mechanics. However, although it is relatively easy to create an open crack mathematical model of a simple beam, it may be difficult to apply it to real life structures. Among other researchers in this area who tried to analyse the change in natural frequencies due to damage by using fracture mechanics, a notable contribution has been made by Ju [18] who used the concept of structural modal frequency and concluded that it would change with the presence of fracture damages in the structure. In his approach, Ju used fracture mechanics to define a damage characteristic and assumed that the changes in modal frequencies were functions of damage characteristics.

A different approach to identifying system matrices was suggested by Lim [19] which was described as a 'submatrix' approach. Instead of working with individual coefficients in the stiffness matrix affected by damage, the submatrix approach focused on individual blocks or submatrices which often coincided with individual physical components in the structure. Hearn and Testa [20] studied the dependence of natural frequencies and modal damping coefficients on structural deterioration and tried to establish the magnitude of change in natural frequencies as a function of location and severity of deterioration.

Adams et al. [21] used the decrease in natural frequencies and increase in damping to detect cracks in fibre reinforced plastics. They developed a theoretical model to detect the damage location but the model seems to be valid only for simple beam structures. Adams and Cawley [22] employed sensitivity analysis to deduce the location of damage in two-dimensional structures, based on the finite element analysis method. but this method appears to be computationally intensive. Yuen [23] showed in his paper that for a cantilever beam there is a systematic change in the first mode shape with respect to damage location. However this method seems to work only when the first mode is sensitive to change and for simple structures like beams.

Instead of comparing the shifts of modal parameters such as natural frequencies and mode shapes to detect structural damage, Cherng and Abdelhamid [24] tried to introduce a new variable called the Signal Subspace Correlation (SSC) index derived from the impulse response function. However, this parameter contained no information about damage location. Numerical examples given assumed that all modes are present and there was noise free measurement, which is impossible to obtain in a practical situation. Therefore, it is not clear how the method will behave with incomplete modes and noise present in measurement, and in which way it is advantageous to use the SSC index instead of commonly used parameters like natural frequency and mode shapes to detect structural change. Chen and Garba [25] developed a three step damage location procedure that initially used residual force vectors to locate potential damage areas; then a least squares approach was used to determine scalars for the appropriate element stiffness matrice and finally, damage was located in structural members where the calculated element scalars were less than unity.

Measured modal test data along with an analytical model was used by Ricles and Kosmatka [26] to locate damaged regions using residual force vectors and to conduct a weighted sensitivity analysis to assess the extent of variations, where damage was characterized by stiffness reduction. Penny, et al. [27] used a statistical method of identification based on generalised least square theory to detect structural damage. In addition to the works referred to above, Wang and Liou [28] tried structural damage detection by observing the change in the FRFs of the damaged substructure. A comparison of some of the structural damage detection methods has been given by Salawu and Williams [29].

Some of the model updating and damage detection methods discussed above have already been applied to detect structural damage with encouraging results. However, almost all of them have to rely on modal parameters. In addition, adequate emphasis has not been given to address the problems of measurement noise and DOF incompatibility. Both these factors can be determinants in the ultimate success of these methods. This thesis aims at using measured FRF data to detect structural damage. In this context, it addresses the question of measurement noise and the DOF incompatibility between the analytical and experimental data.

1.4 ASSUMPTIONS OF THIS STUDY

In the present study certain assumptions have been made regarding the behaviour of structures on which the methods to be proposed in this work can be applied successfully. These assumptions are made after an extensive literature review on the existing methods for structural damage detection and conditions based on which the methods operate:

The first assumption made is that, following structural damage, the major change in characteristics manifests itself as a change in the stiffness only, with changes in mass and damping small enough to be neglected. This is in line with assumptions made by other researchers in the field of damage detection. Although the theory developed is valid for changes in mass also, the numerical and experimental case studies presented are based on stiffness change only.

It is also assumed that the damping in the structures is small and the structure can be safely regarded as undamped without introducing appreciable error. For many practical applications, this might be regarded as a reasonable assumtion as it is often found that the dissipative forces in the structure are negligible compared to its inertial and restoring forces. For structures, where damping is big enough to be neglected, the methods to be proposed in this study can be readily extended as shown in the appendix.

Finally, it was assumed that the structures were linear. This means that the response of a structure to a combination of forces applied simultaneously is the summation of the responses corresponding to each individual force. This is a reasonable assumption as most of the real life structures exhibit linear behaviour within a certain frequency and dynamic range. Therefore, the FRF data used in this study should reflect the linear behaviour of a structure.

1.5 SCOPE OF PRESENT WORK

The research program presented in this thesis is concerned with developing a technique for structural damage detection using measured FRF data and it is comprised of the following parts :

Chapter 2 introduces a method called Constrained Minimization Damage Quantification (CMDQ) method to identify structural damage. This method uses receptance FRF data at different frequencies and information about structural connectivity to determine damage extent in a structure. The constraint minimization theory behind the CMDQ method is presented along with numerical examples to demonstrate the effectiveness of the method. When determining damage extent, the CMDQ method works with the whole structural model. This increases the computational burden and results in difficulties in dealing with noise and incomplete coordinates. To overcome these difficulties the next part of the thesis presents a method that concentrates on locating the damage in a structure, and then determining the damage extent by focussing only on that part of the structure where damage has been located.

Location of damage in a structure is the subject of Chapter 3. In this chapter, a brief review of existing damage location techniques is given. The central part of this chapter is devoted to the introduction of a new method of locating damage in a structure by using measured RFRF data. The performance of the method with noise contaminated data is explored. In addition, the sensitivity of the method to coordinate incompleteness is investigated. In this connection, different expansion and reduction methods currently available are discussed and the suitability of the method proposed in conjunction with different expansion methods to locate structural damage has been examined.

In Chapter 4, the use of the submatrix approach in the field of damage detection has been illustrated. Instead of identifying the DOFs affected due to damage, the algorithm presented in this chapter makes use of the measured receptance

FRF data along with the submatrix technique to identify the damaged element and the severity of the damage.

For determining structural damage extent, a new technique has been proposed in Chapter 5. For situations where the finite element model of the structure is not available, this method can be used to derive the spatial parameters of the structure prior to damage. Subsequent to damage, the same procedure can be repeated to obtain the spatial parameters of the damaged structure. A simple comparison of the spatial parameters thus derived before and after damage provide valuable information about the location and extent of damage. In addition, this method, when used in conjunction with the damage location method proposed in Chapter 3, utilises the information regarding damage location and can work only in that part of the structure where damage is located. Numerical examples have been provided to demonstrate these two applications of the method.

Experimental case studies are presented in Chapter 6. Central to this chapter are the results obtained from two different structures by applying the damage location and quantification methods proposed in earlier chapters. The results reflect the application of the methods proposed, to real structures, in determining the location and extent of damage in a structure using measured FRF data.

Finally, Chapter 7 presents the general conclusions, contributions of the current research work and suggestions for further research.

CHAPTER 2

DETERMINATION OF STRUCTURAL DAMAGE EXTENT USING CONSTRAINED MINIMIZATION THEORY

2.1 INTRODUCTION

Any real life structure under impact, operating and fatigue load is susceptible to structural damage over its operating life. Undetected and unattended structural damage can lead to structural deterioration ultimately resulting in failure. To detect such damage numerous inspection and monitoring procedures have been developed. Examples of such endeavours include x-ray, ultrasonic testing, magnetic response, dye penetration and visual inspection. These methods are time consuming and are local assessments. An alternative approach to damage location and quantification is the system identification technique which utilizes changes in the vibration signature of a structure before and after damage occurs to determine both the location and extent of the structural damage.

Determining damage location and extent is an area which has seen considerable research effort in recent years. He and Ewins [30] in their work proposed the use of an error matrix method both to locate and to quantify system changes in the field of model updating. Adelman and Haftka [31] made use of a sensitivity method to detect damage in a structural system. Wolff and Richardson [32] published a paper in 1989 in which they investigated the correlation between a physical change and changes in a structure's modal parameters. Using changes in modal parameters the authors attempted to detect variations in the tightness of a bolt between a plate and a rib. Martinez, et al. [33] used system identification techniques to detect changes in electronic packages by analysing the changes in their modal parameters. This work may be regarded more as an effort to make practical applications of the concept that the change in modal parameters can be used as an effective tool to study changes in the system.

In addition to the publications mentioned above, a modal model based method for the tasks of model updating and identification of joint models in structural assemblies has been proposed by Nobari, et al. [34]. Lallement, et al. [35] introduced a parametric optimization technique based on sensitivity analysis of static deformation with regard to stiffness parameters of a FEM. This numerical process is based on static deformations which naturally introduces the difficulty of constructing a sufficiently rigid support during measurement. Law and Li [36] presented a perturbation study of a dynamic system involving an investigation of the effect of change in the system matrices on the eigenvalues. Assuming damage in a structural system affects stiffness only, the changes in eigenvalues can be expanded in Taylor's series where only the first term is considered. The method used by Law and Li claimed to improve the accuracy of the calculated changes in eigenvalues due to large damage by including the second term for consideration. This method seems to be more appropriate for structural modification than for damage detection.

Dong, et al. [37] in a more recent publication attempted to examine the sensitivity of modal parameters to both crack location and extent. They made use of fracture theory to generate finite element model of a cracked beam. Using the finite element model, they analytically studied the variations of the modal parameters by altering crack size and location. This work is similar to that of Yuen [23]. Even for simple structures like beams the technique has been found to work only if the first mode is affected by damage.

An algorithm proposed by Zimmerman and Kaouk [38] made use of an original finite element model and a subset of measured eigenvalues and eigenvectors to locate damage. After locating the damage they endeavoured to determine the extent of stiffness change due to damage by using a method based on minimum rank stiffness perturbation constraint which they named as the minimum rank perturbation technique (MRPT) method. Assuming that there are N_e damaged portions and each damaged portion has rank r stiffness model, this technique would require $N_e$xr modes of vibration to determine damage extent if the data were noise free.

This places a severe constraint on this method since it may not be always possible to obtain the required number of eigenvalues and eigenvectors if the number of rank change due to damage is large or unknown. Kaouk and Zimmerman [39] extended the concept of MRPT presented in [38] by applying the MRPT to each portion of the structure seperately. Although the improvement resulted in a significant decrease in the number of modes required, the authors did not discuss the performance of the method for situations where the data contained noise and/or expansion errors.

Most of the methods mentioned above have their origin in system identification techniques, where the analytical model of the undamaged structure and the modal parameters of the damaged structure are used together to determine damage location and extent in one step. However, use of modal parameters introduced certain limitations into these methods as described in Chapter 1.

The outcomes however, can be improved by use of measured FRF data instead of modal data. The successful use of FRF data instead of modal data was demonstrated by Lin and Ewins [40] in the area of model updating; further, Zimmerman et al. [41] in a more recent publication have also made a preliminary attempt to use FRF data for structural damage detection. The fact that the abundance of data available when using FRF data instead of modal data can be advantageous was appreciated by all the authors mentioned above. In addition, FRF data not only eliminates the computational burden associated with extracting modal parameters from measured FRF data, but also circumvents the errors introduced when extracting modal parameters from measured FRF data with curve fitting techniques.

In this chapter a new technique named Constrained Minimization Damage Quantification (CMDQ) method based on system identification techniques has been presented. The method makes use of the measured receptance Frequency Response Function (RFRF) data of the damaged structure and the spatial model of the undamaged structure to detect damage in a structure. It employs measured RFRF data at different frequencies and applies the concept of constrained minimization theory to both locate and quantify damage in a structure at the same time.

2.2 CONSTRAINED MINIMIZATION DAMAGE QUANTIFICATION (CMDQ) METHOD

Consider an N-DOF undamped system whose mass and stiffness properties are given by NxN matrices $[M]_{UD}$ and $[K]_{UD}$ respectively. According to vibration theory [2], the dynamic stiffness matrix of the system at frequency Ω is given by:

$$[Z(\Omega)]_{UD} = ([K]_{UD} - \Omega^2[M]_{UD}) \tag{2.2.1}$$

It is assumed the mass and stiffness matrices of the undamaged system have changed to $[M]_D$ and $[K]_D$ respectively due to damage and they are related by the following equations:

$$[M]_D = [M]_{UD} - [\Delta M] \tag{2.2.2}$$

$$[K]_D = [K]_{UD} - [\Delta K] \tag{2.2.3}$$

Since the dynamic stiffness matrix of the undamaged structure at a frequency Ω is given by $[Z(\Omega)]_{UD}$, on introduction of damage, the dynamic stiffness matrix of the undamaged structure at the same frequency Ω will be altered to $[Z(\Omega)]_D$ where

$$[Z(\Omega)]_D = ([K]_D - \Omega^2[M]_D) \tag{2.2.4}$$

Most of the damage detection methods based on system identification reasonably assumes that the analytical model of the undamaged structure represents the structure correctly from the connectivity point of view. This essentially means that the model of the undamaged structure truly reflects how a particular member is connected to the remaining members of the structure.

However, if the algorithm used for generating the model of the damaged structure develops a model which shows different connectivity between structural members of the damaged structure, then it would become difficult to compare the models before and after damage and isolate the area of damage. In fact, structural damage should not usually alter the connectivity of the undamaged structure. For this reason, one important feature of the algorithm to be developed for determining damage extent in a structure should be to ensure that the structural connectivity of the model before and after damage is identical.

In order to ensure that the constraint of connectivity is preserved in the following development, it is assumed that the dynamic stiffness matrices at a particular frequency Ω before and after damage are related by the following equation:

$$[Z(\Omega)]_D = [Z(\Omega)]_{UD} \otimes [Q_Z] \tag{2.2.5}$$

where the operator $\otimes$ defines the element operation $Z(\Omega)_{D,ij} = Z(\Omega)_{UD,ij}\ Q_{Z,ij}$; Here the matrix $[Q_Z]$ is denoted as damage quantification coefficient matrix due to changes in both mass and stiffness. The use of the operator $\otimes$ in equation (2.2.5) ensures that all elements of dynamic stiffness matrix with values of zero prior to damage occurrence remains zero afterwards. This means that if

$Z(\Omega)_{UD,ij}$ has a value of zero, $Z(\Omega)_{D,ij}$ will also have a value of zero. As a result, the connectivity of the undamaged and damaged structure remains the same.

If the difference in dynamic stiffness of the structure at a frequency Ω due to damage is denoted by $[\Delta Z(\Omega)]$, then

$$[\Delta Z(\Omega)] = [Z(\Omega)]_{UD} - [Z(\Omega)]_{D} \tag{2.2.6}$$

Combining equations (2.2.5) and (2.2.6) together yields

$$[\Delta Z(\Omega)] = [Z(\Omega)]_{UD} - [Z(\Omega)]_{UD} \otimes [Q_Z] \tag{2.2.7}$$

or

$$[\Delta Z(\Omega)] = [Z(\Omega)]_{UD} \otimes ([U] - [U] \otimes [Q_Z]) \tag{2.2.8}$$

Following the method suggested by Kabe [8], any unrealistic changes in dynamic stiffness elements can be minimized by defining an error function such that it is independent of the magnitude of dynamic stiffness elements. This is done by defining the error function as the norm of matrix ($[U]- [U]\otimes[Q_Z]$) which can be denoted as:

$$e = \left\| [U] - [U] \otimes [Q_Z] \right\| \tag{2.2.9}$$

$$e = \sum_{i=1}^{n}\sum_{j=1}^{n} (U_{ij} - U_{ij} Q_{Z,ij})^2 \tag{2.2.10}$$

where $U_{ij} = 1$ if $Z_{UD,ij} \neq 0$ and $U_{ij} = 0$ if $Z_{UD,ij} = 0$

From a mathematical viewpoint, the objective is to determine a matrix $[Q_Z]$ which will result in minimum deviation between the dynamic stiffness matrix before the development of damage and that after such damage. As can be seen from equation (2.2.5), a known $[Q_Z]$ will lead to the dynamic stiffness matrix $[Z(\Omega)]_D$. This mathematical operation needs to be performed under certain physical constraints. These constraints ensure that the resultant dynamic stiffness matrix (dynamic stiffness matrix corresponding to damaged structure) satisfies the physical reality of the structure. If an adequate number of such constraints can be imposed when determining $[Q_Z]$, it is both mathematically and physically feasible to expect that the dynamic stiffness matrix obtained will represent the damaged structure. The mathematical formulation of the problem is as follows:

Given a vector $\{\alpha_D(\Omega)\}_k$ which is the measured k^{th} column of receptance matrix of the damaged structure, find a matrix $[Q_Z]$ which minimizes the norm given by equation (2.2.9) and also satisfies the constraints given by equations (2.2.11) and (2.2.12) below:

$$([Z(\Omega)]_{UD} \otimes [Q_Z])\{\alpha_D(\Omega)\}_k - \{\delta\}_k = \{0\} \tag{2.2.11}$$

where $\{\delta\}_k$ is a vector whose elements are zero except that the k^{th} element is unity and

$$[Q_Z] - [Q_Z]^T = [0] \tag{2.2.12}$$

From a physical viewpoint, the first constraint ensures that the calculated $[Q_Z]$ should be such that the dynamic stiffness derived is orthogonal to any column of the receptance matrix of the damaged structure. The second constraint is imposed to guarantee that the derived dynamic stiffness matrix of the damaged structure is symmetric. Using the method of Lagrange Multipliers, as discussed in appendix C, to incorporate these constraints, a Lagrange function can be defined as:

$$L = e + \lambda g_1 + \mu g_2 \tag{2.2.13}$$

where λ and μ are the Lagrange multipliers, g_1 and g_2 are the given constraints and L is the Lagrange function. It can be written as

$$L = e + \sum_{i=1}^{n} \lambda_i (\sum_{l=1}^{n} Z(\Omega)_{UD,il} Q_{Z,il} \alpha_{D,l}) - Y + \sum_{i=1}^{n}\sum_{j=1}^{n} \mu_{ij} (Q_{Z,ij} - Q_{Z,ji}) \tag{2.2.14}$$

where Y represents the second term on left hand side of equation (2.2.11). Taking the partial derivative of L with respect to $Q_{Z,ij}$ and setting them equal to zero yields an equation that $Q_{Z,ij}$ has to satisfy for L to be minimal:

$$\partial L / \partial Q_{Z,ij} = -2(U_{ij} - Q_{Z,ij}) + \lambda_i Z(\Omega)_{UD,ij} \alpha_{D,j} + \mu_{ij} - \mu_{ji} = 0 \tag{2.2.15}$$

Equation (2.2.15) can be written in a matrix form yielding:

$$-2([U] - [Q_Z]) + [Z(\Omega)]_{UD} \otimes (\{\lambda\}\{\alpha_D(\Omega)\}_K^T) + [\mu] - [\mu]^T = [0] \tag{2.2.16}$$

Since the physical constraints are applied at a single frequency Ω, the Lagrange multiplier has a single column corresponding to the frequency point used. Taking the transpose of equation (2.2.16) and adding it to equation (2.2.16) itself gives:

$$- 4([U] - [Q_Z]) + [Z(\Omega)]_{UD} \otimes (\{\lambda\}\{\alpha_D(\Omega)\}_k^T + \{\alpha_D(\Omega)\}_k\{\lambda\}^T) = [0] \qquad (2.2.17)$$

Multiplying equation (2.2.17) by $0.25[Z(\Omega)]_{UD}$ and rearranging terms it yields,

$$[Z(\Omega)]_{UD} \otimes [Q_Z] = [Z(\Omega)]_{UD} - [ZSQ] \otimes (\{\lambda\}\{\alpha_D(\Omega)\}_k^T + \{\alpha_D(\Omega)_k \{\lambda\}^T)\} \qquad (2.2.18)$$

where $[ZSQ] = 0.25[Z(\Omega)]_{UD} \otimes [Z(\Omega)]_{UD}$

Replacing equations (2.2.18) into (2.2.11), the following equation is derived:

$$[Z(\Omega)]_{UD}\{\alpha_D(\Omega)\}_k - [ZSQ] \otimes (\{\lambda\}\{\alpha_D(\Omega)\}_k^T + \{\alpha_D(\Omega)\}_k\{\lambda\}^T)\{\alpha_D(\Omega)\}_k = \{\delta\}_k \qquad (2.2.19)$$

$$[ZSQ] \otimes (\{\lambda\}\{\alpha_D(\Omega)\}^T_k + \{\alpha_D(\Omega)\}_k \{\lambda\}^T)\{\alpha_D(\Omega)\}_k = \{X\} \qquad (2.2.20)$$

where $\{X\} = ([Z(\Omega)]_{UD}\{\alpha_D(\Omega)\}_k - \{\delta\}_k)$

Now the left hand side of equation (2.2.20) can be written as:

$$\begin{bmatrix} \sum_{i=1}^{n} ZSQ_{1i}\alpha_{ik,D}^2 & .. & 0 \\ .. & ... & .. \\ 0 & .. & \sum_{i=1}^{n} ZSQ_{n1}\alpha_{ik,D}^2 \end{bmatrix} \begin{Bmatrix} \lambda_1 \\ .. \\ \lambda_n \end{Bmatrix} + \begin{bmatrix} ZSQ_{11}\alpha_{1k,D}^2 & .. & ZSQ_{1n}\alpha_{1k,D}\alpha_{nk,D} \\ .. & .. & .. \\ ZSQ_{n1}\alpha_{nk,D}\alpha_{1k,D} & & ZSQ_{nn}\alpha_{nk,D}^2 \end{bmatrix} \begin{Bmatrix} \lambda_1 \\ .. \\ \lambda_n \end{Bmatrix}$$

Hence equation (2.2.20) can be written as:

$$([a] + [b])\{\lambda\} = \{X\}$$

or, $$\{\lambda\} = ([a]+[b])^{-1}\{X\} \qquad (2.2.21)$$

Once $\{\lambda\}$ is derived, it can be put back into equation (2.2.18) to derive the dynamic stiffness matrix of the damaged structure at a particular frequency Ω.

The dynamic stiffness matrix $[Z(\Omega)]$ is a function of frequency. Therefore, at a different frequency the matrix $[Q_Z]$ will also be different, resulting in a different error function defined in equation (2.2.9). The constraint equations will also be frequency dependant.

However, if it is assumed that due to structural damage, only stiffness characteristics have been affected, while variations in mass are small enough to be neglected, then the error function may be simplified. In such case, it can be written as

$$[\Delta K] = [K]_{UD} - [K]_D \tag{2.2.22}$$

or,

$$[\Delta K] = [K]_{UD}([U] - [U] \otimes [Q_K]) \tag{2.2.23}$$

where matrix $[Q_K]$ is denoted as the damage quantification matrix due to change in stiffness only. Since the stiffness matrix does not vary with frequency, the constraint equations may be used repeatedly for multiple frequency points. Therefore the constraint equation becomes :

$$([K]_{UD} \otimes [Q_K])[\{\alpha_D(\Omega_1)\}_k,...\{\alpha_D(\Omega_n)\}_k] - [M]_{UD}[\{\alpha_D(\Omega_1)\}_k,...,\{\alpha_D(\Omega_n)\}_k][\Omega_n^2]$$
$$- [\{\delta\}_k...\{\delta\}_k] = [0] \tag{2.2.24}$$

or,

$$([K]_{UD} \otimes [Q_K])[A_D] - [M]_{UD}[A_D][\Omega_n^2] - [\{\delta\}_k,.....,\{\delta\}_k] = [0] \tag{2.2.25}$$

where $[\Omega_n^2]$ is a diagonal matrix. Ω_i ($i = 1, 2, ..., n$) is the frequency at which RFRF data have been measured , and

$$[A_D] = [\{\alpha_D(\Omega_1)\}_k,...\{\alpha_D(\Omega_n)\}_k]$$

The second physical constraint is again the symmetry of matrix $[Q_K]$,

$$[Q_K] - [Q_K]^T = [0] \tag{2.2.26}$$

The Lagrange function in equation (2.2.14) can then be defined as:

$$L = e + \sum_{i=1}^{n}\sum_{j=1}^{s}\lambda_{ij}\left(\sum_{l=1}^{n}K_{UD,il}Q_{K,il}A_{D,lj}\right) - Y + \sum_{i=1}^{n}\sum_{j=1}^{n}\mu_{ij}(Q_{K,ij} - Q_{K,ji}) \tag{2.2.27}$$

Here 's' represents the number of frequency points used. The term Y represents the second and third terms of the left hand side of equation (2.2.25) which are not a function of $Q_{K,ij}$ and need not be defined. They do not contribute to the derivative of L with respect to $Q_{K,ij}$.

Taking the partial derivative of L with respect to $Q_{K,ij}$ and setting them equal to zero yields equations that $Q_{K,ij}$ have to satisfy for L to be minimal. Repeating the same procedure for the case of the dynamic stiffness matrix gives:

$$-2([U] - [Q_K]) + [K]_{UD} \otimes ([\lambda][A_D]^T) + [\mu] - [\mu]^T = [0] \tag{2.2.28}$$

In contrast to equation (2.2.16), the constraint has been applied here at multiple frequency points and hence the Lagrange multiplier is given by a matrix $[\lambda]$ where each column corresponds to a particular frequency point. Adding the transpose of equation (2.2.28) to itself yields :

$$-4([U] - [Q_K]) + [K]_{UD} \otimes ([\lambda][A_D]^T + [A_D][\lambda]^T) = [0] \tag{2.2.29}$$

Multiplying equation (2.2.29) by $0.25[K]_{UD}$ and rearranging terms yields,

$$[K]_{UD} \otimes [Q_K] = [K]_{UD} - 0.25\,[KSQ] \otimes ([\lambda][A_D]^T + [A_D][\lambda]^T) \qquad (2.2.30)$$

where $[KSQ] = [K]_{UD} \otimes [K]_{UD}$

Substituting equation (2.2.30) into equation (2.2.25) leads to :

$$[D] + \{[KSQ] \otimes ([\lambda][A_D]^T)\}[A_D] + \{[KSQ] \otimes ([A_D][\lambda]^T)\}[A_D] = [0] \qquad (2.2.31)$$

where $[D] = 4.0([K]_{UD}[A]_D - [M]_{UD}[A]_D[\,\Omega_n^2] - [\{\delta\}_k \ldots \{\delta\}_k])$

Equation (2.2.31) can be used to establish $[\lambda]$ which when put back into equation (2.2.30), will yield $[K]_D$. From equation (2.2.31) the following relationship can be derived

$$\{\underline{D}\} = ([T]+[S])\{\underline{\lambda}\} \qquad (2.2.32)$$

where the column vector $\{\underline{D}\}$ is formed by putting columns of [D] into a single column consecutively. The same happens to column vector $\{\underline{\lambda}\}$. Matrix [T] can be represented by the following matrix

$$\begin{bmatrix} [G^{1}] & .. & 0 \\ .. & .. & .. \\ 0 & .. & [G^{n}] \end{bmatrix}$$

Here $[G^i] = -[A_D]^T[KSQ^i][A_D]$ and $[KSQ^i]$ is a diagonal matrix whose diagonal terms are the i^{th} row of [KSQ]. Matrix [S] can be represented as:

$$\begin{bmatrix} [H]^{11} & .. & [H]^{1n} \\ .. & .. & .. \\ [H]^{n1} & .. & [H]^{nn} \end{bmatrix}$$

where $[H]^{ij} = -\{\underline{A_D}\}_j \{R^j\}_i^T$

$\{\underline{A_D}\}_j = j^{th}$ column of $[A_D]^T$

$\{R^j\}_i = i^{th}$ column of $[A_D]^T[KSQ^j]$

Equation (2.2.32) can be used to determine $\{\underline{\lambda}\}$. However, in most cases ([T] + [S]) will be ill-conditioned and simple inversion is not possible for obtaining $\{\underline{\lambda}\}$. To overcome this, ([T] + [S]) can be written as:

$$[T] + [S] = [P][V][P]^T \tag{2.2.33}$$

where [P] contains orthonormalised eigenvectors of ([T] + [S]) and [V] is a diagonal matrix whose diagonal elements are the eigenvalues of ([T] + [S]). Hence, equation (2.2.32) can be written as

$$\{\underline{D}\} = ([P][V][P]^T)\{\underline{\lambda}\} \tag{2.2.34}$$

Considering only the non-zero elements in [V] and the corresponding columns of eigenvectors in [P] and inverting them results in

$$\{\underline{\lambda}\} = [P]\,[V]^{-1}[P]^{T}\{\underline{D}\} \qquad (2.2.35)$$

Once $\{\underline{\lambda}\}$ has been obtained it can be used to rebuild $[\lambda]$ and which, in turn, can be used in equation (2.2.30) to derive $[K]_D$, the stiffness matrix of the damaged structure. With $[K]_D$ determined, the location and extent of damage can be easily determined.

The above derivation to determine $[K]_D$ was based on the assumption that the system was undamped. However, the CMDQ method can be extended even for damped systems and appendix A1 suggest a possible method of doing so.

2.3 DISCUSSION

From the theory in the preceding section, it is apparent that the success of the proposed CMDQ method to locate and quantify damage in a structure rests largely on accurate computation of the vector $\{\underline{\lambda}\}$ given in equation (2.2.35). However, due to the possible ill-conditioning of matrix ([T] + [S]), the CMDQ method needs to be applied with prudence in order to accurately estimate $\{\underline{\lambda}\}$.

If matrix ([T] + [S]) is not ill-conditioned, then matrix [P] obtained in equation (2.2.33) through the spectral decomposition of ([T] + [S]) will be orthogonal. In such a case, the product of $[P]^T$ and [P] is expected to yield a unity matrix. However, in practice it is found that due to ill-conditioning of matrix ([T] + [S]), the product $[P]^T[P]$ is not an identity matrix. To remove the effect of ill-conditioning, it is essential to construct $([P][V][P]^T)$ by discarding those diagonal elements (eigenvalues of ([T] + [S])) in matrix [V] which are due to ill-conditioning.

It was found that the product of $[P]^T$ and [P] provided a very useful indicator regarding eigenvalues to be included or discarded. The product $[P]^T[P]$ will yield a matrix which has a few diagonal elements equal to one, but there are others which yield values different from unity. The diagonal elements in [V] corresponding to the non-unity diagonal elements in $[P]^T[P]$ should then be ignored along with those corresponding columns in [P]. The best results are obtained if ([T]+[S]) is rebuilt by using only those diagonal elements in [V] which correspond to unity diagonal elements in the product $[P]^T[P]$ and the corresponding columns in the matrix [P].

To elaborate further, if matrix ([T] + [S]) is a 24 by 24 matrix, then it will have 24 eigenvalues which are the diagonal elements in the diagonal matrix [V]. Matrix $[P]^T[P]$ will have twenty four diagonal elements. If the first eighteen of these diagonal elements are unity and the remainder are not, then the best decomposition of ([T] + [S]) using $[P][V][P]^T$ is by using the first eighteen diagonal elements of [V] and the first eighteen columns of [P]. In such a case, matrices [P], [V] and $[P]^T$ are of size 24x18, 18x18 and 18x24 respectively and their product $[P][V][P]^T$ is a new 24x24 matrix which is used to compute $\{\underline{\lambda}\}$.

2.3.1 Determining the number of valid eigenvalues

An important question to be addressed, is how many valid eigenvalues are needed for the CMDQ method to exactly locate and quantify damage of a structure in cases where the damage has affected the stiffness of the structure. The sum of the number of diagonal elements in the stiffness matrix and the number of non-zero non-diagonal coefficients on one side of the diagonal line gives an indication of the minimum number of valid eigenvalues required for the CMDQ method to work. If the sum is 'F', then it has been found that the method is able to quantify damage, provided the number of valid eigenvalues is greater than or equal to 'F'. The reason behind this is explained in the following paragraph.

The relationship between the number of eigenvalues considered and accuracy of the result obtained can be explained mathematically by considering equation (2.2.15). The equation is obtained by partially differentiating the Lagrange function L with respect to a particular element in matrix $[Q_K]$ and equating it to zero. The approach taken in this algorithm, is to correct individually the elements (diagonal elements and non-zero non-diagonal elements on one side) of the undamaged stiffness matrix. If the number of such stiffness elements is 'F', then the algorithm would need to solve for 'F' unknowns of $Q_{K,ij}$ which naturally require at least 'F' independent equations.

Referring to equation (2.2.33) if the matrix [V] has 'F' valid eigenvalues (validity can be checked by examining the product $[P]^T[P]$, as already discussed), then it automatically ensures the existence of 'F' linearly independent equations. Therefore, 'F' unknowns can be computed. If the number of eigenvalues obtained is greater than 'F', then mathematically it is a case of an overdetermined set of equations. Although for the noise free case, it was found that the result obtained is most accurate by considering only 'F' valid eigenvalues, for noisy data, better results can be expected by considering all valid eigenvalues.

If the number of valid eigenvalues becomes smaller than 'F', then the number of linearly independent equations reduces and the results therefore becomes more and more inaccurate. It was also found that the number of valid eigenvalues that can be obtained do not increase indefinitely with increase in the number of frequency points. Once the number of valid eigenvalues obtained reaches 'F' or for certain systems slightly higher than 'F', it does not increase any further even with more frequency points. Although the number of valid eigenvalues does not increase any further, the individual values of the eigenvalues changes by considering additional frequency points. For noisy FRF data, inclusion of additional frequency points proved specially beneficial in reducing the effect of noise.

2.3.2 Determining the number of frequency points

The number of frequency points to be chosen for CMDQ method plays a significant role in the success of this method, since generation of an adequate number of valid eigenvalues can be ensured only if the number of frequency points chosen is sufficient. The number of valid eigenvalues required for CMDQ method can be calculated from the stiffness matrix of the structure. For an N DOF structure which requires 'F' valid eigenvalues, it is not possible to have more than N eigenvalues if the number of frequency point selected is one. Similarly, if "s" frequency points are selected, then the maximum possible number of valid eigenvalues that can be obtained is "s×N". Hence, in order to obtain the required number of eigenvalues, the number of frequency points selected should be such that:

$$s \geq F/N \tag{2.3.1}$$

Once the number of valid eigenvalues required for a particular system is decided, the minimum number of frequency points required can be easily computed. A simple illustration is given to explain it in more detail. If for a 10 DOF system, it is found that the number of valid eigenvalues required for the method to work is 23, then using equation (2.3.1), it is possible to obtain the minimum number frequency points required as:

$$s \geq 23/10$$

or, $s \geq 2.3$

Hence, the minimum number of frequency point required to generate 23 valid eigenvalues is 3. However, if by selecting 3 frequency points it is found that, the number of valid eigenvalues obtained is less than 23, then it will require reselecting frequency points or increasing the number of frequency points. It has been found that depending on the load path indeterminancy of certain structures and quality of measured FRF data, one may require using additional frequency points to obtain more accurate results.

In Section 2.5, numerical examples are given to illustrate situations where additional frequency points are required. In brief, once the value of 'F' is known from the stiffness matrix, the first step is to ensure that at least 'F' number of valid eigenvalues is obtained. The next step is to consider whether additional frequency points are required.

2.3.3 Simultaneous mass and stiffness changes due to damage

When only the stiffness of a structure is affected by damage, the damage coefficient matrix $[Q_K]$ due to change in stiffness is independent of frequency. In other words, equation (2.2.23) is valid at all frequency points. Since $[Q_K]$ is frequency independent, the constraint equation may be used repeatedly for different frequency points, as suggested by equation (2.2.24).

However, in some applications it may be possible that both mass and stiffness are affected by damage. In these case, the dynamic stiffness changes due to damage can be expressed as given in equation (2.2.8). Unlike the case where damage affected stiffness only, the correction coefficient matrix $[Q_Z]$ is dependant on frequency. The constraint equations in this case are related only to a particular frequency, as given by equations (2.2.11) and (2.2.12). No constraint equation with multi frequency points is available. As a result, the number of valid eigenvalues obtained is no more than the number of DOFs of the system as the number of frequency points usable each time is one. This is often not sufficient to determine the dynamic stiffness matrix after damage. However, even in this case, the method can still indicate the location of damage.

From $[Q_Z]$ alone a rough idea about $[Z(\Omega)]_D$ can be formed but from $[Q_Z]$ only it is not possible to decide in what proportion the damage has affected the mass and stiffness of the structure. However, this information can be extracted from

$[Q_Z]$ by a simple mathematical manipulation as shown below. Assuming that the damage coefficient matrix due to change in mass is given by $[Q_M]$, it is possible to write:

$$[Z(\Omega)]_D = [K]_D - \Omega^2[M]_D = [K]_{UD} \otimes [Q_K] - \Omega^2[M]_{UD} \otimes [Q_M] \tag{2.3.2}$$

Using equation (2.2.5), gives

$$[K]_{UD} \otimes [Q_K] - \Omega^2[M]_{UD} \otimes [Q_M] = [K]_{UD} \otimes [Q_Z] - \Omega^2[M]_{UD} \otimes [Q_Z] \tag{2.3.3}$$

or, $$[K]_{UD} \otimes ([Q_Z] - [Q_K]) = \Omega^2[M]_{UD} \otimes ([Q_Z] - [Q_M]) \tag{2.3.4}$$

or, $$([M]^{-1}{}_{UD}[K]_{UD}) \otimes ([Q_Z] - [Q_K]) = \Omega^2 ([Q_Z] - [Q_M]) \tag{2.3.5}$$

Hence, once $[Q_Z]$ is computed at multiple frequency points, $[Q_K]$ and $[Q_M]$ can be computed from which a rough idea can be formed regarding contribution of stiffness change and mass change towards total damage. Nevertheless, since only one frequency point can be used each time to estimate $[Q_Z]$, the resultant $[Q_Z]$ will be inaccurate. This in turn will make the estimated $[Q_M]$ and $[Q_K]$ in this case deviate from the correct estimate.

2.4 NOISE FILTERING ALGORITHM FOR CMDQ METHOD

To be of practical use, the CMDQ method should be capable to produce good results when imperfect FRF data are used. Measured FRF data are inevitably contaminated by noise, instrument inaccuracy, etc. The random error in a typical FRF measurement as per J.S Bendat's *Non linear System Analysis and Identification from Random Data* can be quantified by:

$$\varepsilon\left[\left|\hat{H}_{XY}(\Omega)\right|\right] = \frac{\left[1-\gamma_{xy}^{2}(\Omega)\right]^{1/2}}{\left|\hat{\gamma}_{xy}(\Omega)\right|\sqrt{2n_d}} \tag{2.4.1}$$

where γ_{xy}^{2} = coherence and n_d = number of averages.

If the coherence of the measurement is 1.0, then the normalised random error is zero. However in reality coherence is always less than 1.0. This may be attributed to the following :

- the presence of uncorrelated noise in the input and output signal in time domain;
- a non-linear relationship between input and output signal;
- to insufficient resolution or wrong choice of windows, power from discrete frequency components may leak into adjacent bands. This phenomenon is commonly referred to as leakage;
- a time delay between the input and output signal when this is of the same order as the length of the record. This implies that if a possible signal is the direct output of another signal, the apparent relationship will not be very strong if the delay between the input and output signal is large with respect to record length. This bias error can be minimized by applying what is known as pre computational delay to the output signal so that the sections analyzed correspond to each other.

However unsatisfactory coherence due to random noise can be improved by increasing the number of averages. Figure 2.1 gives an indication of the variation of Normalised Random Error as a function of coherence and number of averages. Figure 2.2 shows the exponential relation existing between normalized random error and number of averages.

The proposed CMDQ method using constrained minimization theory was assessed for FRF data with noise levels of around 2% on the amplitude of vibration. It was found that with that noisy data the CMDQ method does not quantify the damage exactly, although the location of damage can still be easily identified. Therefore, it is proposed that once the location of damage has been ascertained using the CMDQ method, a noise filtering algorithm may be used to reduce the effect of noise in the CMDQ method in order to obtain a better estimate of the damage. The procedure is explained below in more detail.

The noise filtering algorithm consists simply of replacing the $\{\alpha_D(\Omega)\}_k$ vectors by $\{\alpha_{D(f)}(\Omega)\}_k$. Here $\{\alpha_D(\Omega)\}_k$ is the noisy receptance FRF data at a particular frequency Ω obtained from measurement for the damaged structure and $\{\alpha_{D(f)}(\Omega)\}_k$ is the corresponding 'noise filtered' receptance FRF data. The filtering is done by using the relationship :

$$[Z_{UD}(\Omega)]\{\alpha_D(\Omega)\}_k = \{d\} \tag{2.4.2}$$

In equation (2.4.2) all elements in the vector $\{d\}$ are expected to be zero except those which correspond to the damaged DOFs. Such a result can be obtained if the measured data is free of error of any type. In practical situations, due to the effect of noise, it is found that almost all the elements in the vector $\{d\}$ will have non-zero values. The values in the elements of the vector $\{d\}$ which correspond to undamaged DOFs is entirely due to the effect of noise while the values in elements which correspond to damaged DOFs is due largely to damage and, to much less extent, to noise. As mentioned above, using noisy data the CMDQ method successfully indicates the location of damage.

Once damage has been located, the non-zero elements in the vector $\{d\}$ (obtained by direct multiplication of matrix $[Z_{UD}(\Omega)]$ and vector $\{\alpha_D(\Omega)\}_k$) which are due to measurement errors can be easily identified. These elements can then be set to zero leaving the elements in the vector $\{d\}$ due to damage to its original value. Consequently the revised $\{d\}$ may be written as $\{d_f\}$ and the vector $\{d\}$ in the equation (2.4.2) is replaced by $\{d_f\}$. Therefore equation (2.4.2) can rewritten as:

$$[Z_{UD}(\Omega)]\{\alpha_{D(f)}(\Omega)\}_k = \{d_f\} \qquad (2.4.3)$$

where $\{\alpha_{D(f)}(\Omega))\}_k$ is the filtered receptance FRF data at a frequency Ω and this can be obtained from equation (2.4.3) by using Gaussian elimination. Once $\{\alpha_{D(f)}(\Omega)\}_k$ is computed, it can be used in the CMDQ method to obtain a better estimate of the extent of damage. Hence, the steps involved in using the CMDQ method in conjunction with the noise filtering algorithm are as follows:

- Use the CMDQ method with measured FRF data to determine the location of damage and a preliminary estimate of the magnitude of damage.
- Use the information regarding damage location in the noise filtering algorithm to derive 'noise-filtered' FRF data.
- Use the filtered FRF data in the CMDQ method to obtain a more accurate estimate of damage.

2.5 RESULTS OF NUMERICAL ANALYSIS

A computer programme written in Fortran for the CMDQ method has been developed and implemented on an HP Unix workstation. Frequency points are specified at random and using the information regarding a particular column of RFRF of a damaged structure, the damage location and quantification was carried out using the CMDQ method. In figure 2.3 the flowchart for the program is presented.

Numerical case studies were carried out on three different systems to examine the effectiveness of the CMDQ method. These systems have been given in figures 2.4, 2.5 and 2.6.

Example 1

The first system studied was a 12 DOF undamped mass-spring system as shown in figure 2.4. The stiffness matrix for the undamaged system is given in Table 2.1 and that for the damaged system is given in Table 2.2. In both cases, the mass matrix is as given by Table 2.3 (assume that the mass matrix is unaffected by the introduction of damage). It was assumed that the location of damage lies between co-ordinates 5 and 6. The actual stiffness change due to damage is given in figure 2.7. Table 2.4 tabulates the natural frequency of the 12 DOF system both before and after damage. In the following, the results of CMDQ method are presented in the form of $[\Delta K]$ instead of $[K]_D$.

Firstly, the proposed method was applied using three frequency points at random and assuming that the RFRF data available for the damaged structure were noise free. The frequency points chosen were 3 rad/s, 12 rad/s and 14 rad/s. All three frequency points chosen lie within the first two modes for this system. Only the first column of the receptance matrix (without loosing generality) at these three frequency points were used to build up matrix ([T] + [S]). As already given in equation (2.2.33), matrix ([T] + [S]) can be decomposed to the product of [P], [V] and $[P]^T$. It was found that the matrix product $[P]^T[P]$ as shown in Table 2.5 has unity in the first thirty one diagonal elements. However, the 32nd diagonal element has a value of 1.59 and from here onwards the values of diagonal elements deviate significantly from unity.

Although by considering the first thirty or thirty one eigenvalues a fairly good estimate of the extent of damage can be obtained, the most accurate results were obtained when considering the first twenty nine eigenvalues - the number of non-zero elements in [K]. The diagonal elements of the diagonal matrix [V] have been tabulated in Table 2.6. For noise free data, as already mentioned in Section 2.3.1, the best results are obtained when the number of valid eigenvalues used are exactly equal to the number of unknowns in the stiffness matrix. Therefore, only the first twenty nine eigenvalues of [V] and the corresponding columns of eigenvectors in [P] were used to compute $\{\underline{\lambda}\}$ using equation (2.2.35) which was then used to compute $[K]_D$. The method successfully indicates the location and extent of damage as shown in figure 2.8.

Instead of using the first twenty nine eigenvalues, the same example was also tried using the first twenty six eigenvalues and first twenty three eigenvalues, the results of which have been shown in figures 2.9 and 2.10 respectively. The method locates damage successfully, but the accuracy of the damage extent starts to deteriorate. The decrease in accuracy of results was expected. Referring to Section 2.3.1, it was mentioned that the sum 'F', which is 29 in this example, represents the number of unknowns and the number of valid eigenvalues indicate the number of independent equations available to solve for those unknowns. Therefore, using only twenty six or twenty three eigenvalues in this example essentially means an effort to solve for twenty nine unknowns using twenty six or twenty three equations. Naturally for such cases, the exact solution cannot be obtained , as reflected in the results plotted in figures 2.9 and 2.10.

Secondly, the same numerical example was tried with a different set of frequency points. This time the frequency points were close to each other and chosen at random. They were 8 rad/s, 10 rad/s and 11 rad/s. In this case it was found that the number of valid eigenvalues were less than 29. As shown in figure 2.11, the location of damage is clear but the extent of damage is inaccurate. An important observation was that in spite of using three frequency points, the method fails to give an accurate estimate of the damage extent, since the number of valid eigenvalues was less than the required number for the method to succeed. In this particular case the required number was 29 but the number of valid eigenvalues obtained was 23.

The situation however can be improved by either selecting a new set of frequency points or by adding more frequency points. In this example an attempt was made to increase the number of valid eigenvalues by using an additional frequency point at 13 rad/s. As a result, the number of valid eigenvalues increased from 23 to 25 and the results are as shown in figure 2.12. Since, from theory it is known that best results in this example can be obtained when the number of valid eigenvalues is 29, the same case was repeated by adding 15.4 rad/s to the existing set of four frequency points. With five frequency points, the number of valid eigenvalues obtained became just equal to 29 and the results as plotted in figure 2.13 are almost identical to the correct results.

The two numerical examples use the same system to locate and quantify damage. In both the cases, the correct results were obtained although the frequency points selected were different. However, both cases had one thing in common. The number of valid eigenvalues in both cases equals the sum 'F' of the number of unknown elements in the stiffness matrix which for this particular example was 29. Therefore, it may be concluded that for any set of frequency points the method will correctly quantify the change in stiffness provided the number of valid eigenvalues is equal to the sum 'F' mentioned above. If for certain cases the number of valid eigenvalues obtained is greater than the sum 'F', then for noise free data most accurate results can be obtained by considering the first 'F' eigenvalues.

To resemble a practical situation, a random noise of 2% was incorporated in the amplitudes of the RFRF data and a repetition of the same numerical case as described above was carried out. With 2% noise and using three frequency points (points used were 3 rad/s, 12 rad/s and 14 rad/s) which generated 29 valid eigenvalues, the performance of the method in identifying damage deteriorated sharply as evident from the results plotted in figure 2.14. However, it was found that by using additional frequency points, the effect of noise can be reduced and a reasonably good estimate of the damage location can be determined.

To illustrate, the example was repeated by considering four frequency points (3 rad/s, 12 rad/s, 14 rad/s and 13 rad/s), five frequency points (3 rad/s, 12 rad/s, 14 rad/s, 13 rad/s and 16 rad/s) and six frequency points (3 rad/s, 12 rad/s, 14 rad/s, 13 rad/s, 16 rad/s and 9 rad/s) and the results have been plotted in figures 2.15, 2.16 and 2.17. It is found that from figures 2.16 or 2.17, the location of damage and an estimate of the damage extent can be easily ascertained. The results were expected since by considering additional frequency points, mathematically more constraints were imposed which helped in diminishing the effect of noise and approach the accurate results (as already discussed in Section 2.0). The additional frequency points selected were in the frequency region where the most severely affected natural frequencies were situated.

The improvement in results would not be as significant if the frequency points were selected in the region where there was not much change in FRF due to damage. However, it has been found that beyond a certain number of frequency points the effect of noise does not change significantly as demonstrated by the similarity of figures 2.16 and 2.17. Therefore, it is suggested that with noisy data once the damage has been located, the method should be used in conjunction with the noise filtering algorithm to obtain a better estimate of the damage extent. Figure 2.18 shows the [ΔK] results after applying the noise filtering algorithm. Comparing figures 2.17 and 2.18, it is apparent that after applying the noise filtering algorithm, the effects of noise vanished leaving only the peak due to genuine damage.

An important point to be noted is that while using noise free RFRF data the frequency points selected were all within the first two modes. This is significant and can be readily attributed to the use of RFRF data rather than modal data. If the same example was repeated using modal data then more modes will be needed to get the desired results. The use of RFRF data leads to the same results but with data measured over a narrower frequency band.

Example 2

The minimum number of frequency points needed to run CMDQ is given by equation (2.3.1). In example 1 it has been shown that the effect of noise can be reduced by using more frequency points. This example will show that depending on the load path indeterminancy of a system, more frequency points in addition to the minimum number may be needed. To demonstrate this, the system shown in figure 2.5 was used. This was the same system used by Kabe in [9]. The difference in stiffness matrix due to damage is given in figure 2.19 and the stiffness and mass matrix prior to damage is given by Tables 2.7 and 2.8. The stiffness matrix after damage has also been tabulated in Table 2.9. In this case, the sum of diagonal elements and non zero off-diagonal elements on one side of the stiffness matrix was 16. Therefore the number of valid eigenvalues required for this system was 16.

Frequency points selected here were again at random and they were equal to 8, 14, 19 rad/s. Accurate results as shown in figure 2.21 were obtained as the number of valid eigenvalues were 16. However, with two frequency points (8 and 14 rad/s), even when the number of valid eigenvalues were sixteen, the method did not successfully quantify damage if it was in the region of DOFs 6, 7 and 8 although the extent of damage located between DOFs 3 and 5 could be estimated accurately as shown in figure 2.20. This was because DOFs 6, 7 and 8 involved a load path indeterminancy of three as shown in figure 2.5. This essentially means that since m_1 is connected to only m_2, one frequency point is good enough for this region. Once this was identified, m_2 to m_5 has a maximum of two unknowns and so two frequency points were good enough. However, for m_6, even if the stiffness between m_4 and m_6 was known from m_4, it still has three unknowns. Therefore, at least three frequency points were required. However, if the system given in figure 2.5 was such that, the mass m_6 was not connected to ground, then two frequency points would have been good enough for the entire system. This can be readily determined from the connectivity of the system.

Once the minimum number of frequency points required for this constrained minimization method is determined, examination of the connectivity of a structure is needed to determine whether more frequency points are required. In practice, because of abundant FRF data and due to use of more FRF data points to combat noise effect, this load path indeterminancy should not become a problem.

Example3 : A truss structure

A truss structure as shown in figure 2.6 was considered in this example. The mass and stiffness matrices of this 20 member plane truss structure was generated using PAFEC FE software. The data file used in PAFEC FE is shown in Table 2.10. The structure was modelled using bar elements (element number 34400), each element having two nodes and each node having only translational degrees of freedom in the -x and -y directions. Young's Modulus was taken to be $E = 2.09 \times 10^5$ N/m^2 and the density 7860 kg/m^3. Nodes 1 and 14 had been totally restrained. It was assumed that each member of the truss has a cross sectional area of .0002 m^2, IYY is equal to 1.666E-9 m^4 and IZZ equal to 6.666E-9 m^4.

Damage was simulated between nodes 4 and 5 and this was done by changing the Young's Modulus of that particular element to half of its original value. Figure 2.22 shows the point RFRF curve ($\alpha_{2,2}$) of the truss structure before and after damage. The stiffness matrix change due to damage has been given in figure 2.23. RFRF data used were at frequency 12 rad/s, 19 rad/s, 25 rad/s and 43 rad/s to build up the matrix ([T] + [S]) and the results using the CMDQ method are shown in figure 2.24. From the figure it is clear that besides locating the damage, the extent of damage has also been correctly identified.

The above results were obtained using RFRF data at 4 frequency points. When random noise of 2% was introduced into the amplitude of the RFRF data of the damaged structure, the results are as plotted in figure 2.25. The location of damage is clear although its quantification is not accurate. Besides, there are a few additional peaks. To identify peaks due to genuine damage, the number of frequency points used were increased by adding a point at 37 rad/s. As already demonstrated in Example 1, by increasing the number of frequency points the effects of noise can be reduced.

There was a degree of improvement as the peaks due to noise seemed to diminish as shown in figure 2.26. From figure 2.26 the location of damage can be identified distinctly. Once the damage location was obtained clearly, the noise filtering algorithm was applied to the RFRF data. By using the filtered RFRF data, the CMDQ method was re-applied to get a more accurate estimate of the changes in stiffness due to damage which have been shown in figure 2.27. By comparing figures 2.26 and 2.27, it appears that the noise filtering algorithm achieved marginal improvement. However, in reality, the usefulness of the noise filtering algorithm will not be known unless it is applied. To assure better results for CMDQ method, it is suggested to use noise filtering algorithm.

2.6 SUMMARISING REMARKS

A new method called the CMDQ method has been developed in this chapter for determining the damage extent using measured RFRF data. The use of measured RFRF data instead of modal data provides a number of advantages in the endeavour of structural damage detection.

The method has been tested with simulated data to examine its feasibility and check the variation in results that occurs due to the use of FRF data at different frequency points. It has been found that with noise free data, the method accurately locate and estimate structural damage. The number of valid eigenvalues that are required by the CMDQ method to obtain accurate results is given by the number of unknown non-zero coefficients 'F' in the stiffness matrix of the undamaged structure. To identify the validity of eigenvalues calculated, a numerical technique has been developed. To obtain reliable results, the number of valid eigenvalues obtained should be at least equal to 'F'. If it is less than 'F', then the CMDQ method cannot successfully determine the damage extent although it can still indicate damage location.

To improve the results with noisy FRF data, the use of FRF data with more frequency points and the noise filtering algorithm presented in this chapter are suggested. In doing so, a preliminary damage estimate can be made by using measured FRF data and then the noise filtering algorithm can be employed to obtain a more accurate estimate of the damage.

For some applications measurements cannot be taken on all coordinates in the damaged structure (which corresponds to coordinates used to define the analytical model of the undamaged structure). It is possible to interpolate the FRF data corresponding to those unmeasured coordinates by using expansion techniques to be discussed in Chapter 3.

In conclusion, it can be stated that the CMDQ method is a promising technique for quantifying structural damage affecting the stiffness of a dynamic system. The method has been found to work well with measured RFRF data. Numerical examples using mass spring models and truss structures have successfully shown the effectiveness of the method as a damage detection algorithm.

6000	-2000	0	0	0	0	-2000	0	0	0	0	0
-2000	6000	-2000	0	0	0	0	-2000	0	0	0	0
0	-2000	6000	-2000	0	0	0	0	-2000	0	0	0
0	0	-2000	6000	-2000	0	0	0	0	-2000	0	0
0	0	0	-2000	6000	-2000	0	0	0	0	-2000	0
0	0	0	0	-2000	6000	-2000	0	0	0	0	-2000
-2000	0	0	0	0	-2000	6000	-2000	0	0	0	0
0	-2000	0	0	0	0	-2000	6000	-2000	0	0	0
0	0	-2000	0	0	0	0	-2000	6000	-2000	0	0
0	0	0	-2000	0	0	0	0	-2000	6000	-2000	0
0	0	0	0	-2000	0	0	0	0	-2000	6000	-2000
0	0	0	0	0	-2000	0	0	0	0	6000	-2000

Table 2.1: Stiffness matrix of the undamaged system in Fig.2.4

6000	-2000	0	0	0	0	-2000	0	0	0	0	0
-2000	6000	-2000	0	0	0	0	-2000	0	0	0	0
0	-2000	6000	-2000	0	0	0	0	-2000	0	0	0
0	0	-2000	6000	-2000	0	0	0	0	-2000	0	0
0	0	0	-2000	**5200**	**-1200**	0	0	0	0	-2000	0
0	0	0	0	**-1200**	**5200**	-2000	0	0	0	0	-2000
-2000	0	0	0	0	-2000	6000	-2000	0	0	0	0
0	-2000	0	0	0	0	-2000	6000	-2000	0	0	0
0	0	-2000	0	0	0	0	-2000	6000	-2000	0	0
0	0	0	-2000	0	0	0	0	-2000	6000	-2000	0
0	0	0	0	-2000	0	0	0	0	-2000	6000	-2000
0	0	0	0	0	-2000	0	0	0	0	6000	-2000

Table 2.2: Stiffness matrix of the damaged system in Fig.2.4

1	0	0	0	0	0	0	0	0	0	0	0
0	2	0	0	0	0	0	0	0	0	0	0
0	0	3	0	0	0	0	0	0	0	0	0
0	0	0	4	0	0	0	0	0	0	0	0
0	0	0	0	5	0	0	0	0	0	0	0
0	0	0	0	0	6	0	0	0	0	0	0
0	0	0	0	0	0	7	0	0	0	0	0
0	0	0	0	0	0	0	8	0	0	0	0
0	0	0	0	0	0	0	0	9	0	0	0
0	0	0	0	0	0	0	0	0	10	0	0
0	0	0	0	0	0	0	0	0	0	11	0
0	0	0	0	0	0	0	0	0	0	0	12

Table 2.3: Mass matrix of the undamaged/damaged system in Fig.2.4

NATURAL FREQUENCY OF THE FIG.2.4 SYSTEM (RAD/S)					
	BEFORE DAMAGE	AFTER DAMAGE		BEFORE DAMAGE	AFTER DAMAGE
1	5.8	5.8	7	31.8	31.3
2	15.7	15.7	8	34.9	34.8
3	18.5	17.8	9	40.1	38.0
4	24.9	24.8	10	46.0	45.7
5	26.9	26.7	11	56.4	56.4
6	28.9	28.5	12	81.7	81.7

Table 2.4: Natural frequency for the system in Fig.2.4 before and after damage

1	2	3	4	5	6
1.00	1.00	1.00	1.00	1.00	1.00
7	8	9	10	11	12
1.00	1.00	1.00	1.00	1.00	1.00
13	14	15	16	17	18
1.00	1.00	1.00	1.00	1.00	1.00
19	20	21	22	23	24
1.00	1.00	1.00	1.00	1.00	1.00
25	26	27	28	29	30
1.00	1.00	1.00	1.00	1.00	1.00
31	32	33	34	35	36
1.00	1.59	5.18	1.58	1.03	1.18

Table 2.5: Diagonal elements in product $[P]^T[P]$ for the system in Fig.2.4

1	2	3	4	5	6
25.86	17.47	16.46	15.19	14.98	13.18
7	8	9	10	11	12
12.52	11.72	11.24	10.49	7.20	6.25
13	14	15	16	17	18
0.73	0.56	0.44	0.19	0.17	0.15
19	20	21	22	23	24
0.12	0.07	0.05	0.04	.013	.0075
25	26	27	28	29	30
.0057	.0024	.001	.0005	.18E-03	.45E-05
31	32	33	34	35	36
.23E-05	.52E-06	.52E-06	.35E-06	-.19E-05	-.36E-05

Table 2.6: Diagonal elements in the matrix [V] for the system in Fig.2.4

1000	-1000	0	0	0	0	0	0
-1000	3000	-1000	0	0	0	0	0
0	-1000	3000	0	-1000	0	0	0
0	0	0	3000	-1000	-1000	0	0
0	0	-1000	-1000	3000	0	0	0
0	0	0	-1000	0	4000	-1000	-1000
0	0	0	0	0	-1000	3000	-1000
0	0	0	0	0	-1000	-1000	3000

Table 2.7: Stiffness matrix of the undamaged system in Fig.2.5

1	0	0	0	0	0	0	0
0	2	0	0	0	0	0	0
0	0	3	0	0	0	0	0
0	0	0	4	0	0	0	0
0	0	0	0	5	0	0	0
0	0	0	0	0	6	0	0
0	0	0	0	0	0	7	0
0	0	0	0	0	0	0	8

Table 2.8: Mass matrix of the undamaged system in Fig.2.5

1000	-1000	0	0	0	0	0	0
-1000	**2400**	**-400**	0	0	0	0	0
0	**-400**	**2400**	0	-1000	0	0	0
0	0	0	3000	-1000	-1000	0	0
0	0	-1000	-1000	3000	0	0	0
0	0	0	-1000	0	4000	-1000	-1000
0	0	0	0	0	-1000	**2500**	**-500**
0	0	0	0	0	-1000	**-500**	**2500**

Table 2.9: Stiffness matrix of the damaged system in Fig.2.5

```
CONTROL
CONTROL.END
NODES
NODE     X      Y        NODE     X       Y
1        0      0        2        .85     1.50
3        .85    2.35     4        2.25    2.75
5        2.25   3.75     6        4.05    3.40
7        4.05   4.50     8        5.95    3.40
9        5.95   4.50     10       7.75    2.75
11       7.75   3.75     12       9.15    1.50
13       9.15   2.35     14       10.00   0
ELEMENTS
ELEMENT.TYPE = 34400
NUMBER  PROP  TOPOLOGY   NUMBER  PROP  TOPOLOGY
1       1     1 2        2       1     1 3
3       1     2 3        4       1     3 5
5       1     2 4        6       1     4 5
7       1     5 7        8       1     4 6
9       1     6 7        10      1     7 9
11      1     6 8        12      1     8 9
13      1     9 11       14      1     8 10
15      1     10 11      16      1     11 13
17      1     10 12      18      1     12 13
19      1     13 14      20      1     12 14
BEAMS
SECTION   MATERIAL   IYY        IZZ        TORS.CONST   AREA
1         11         1.666E-9   6.666E-9   4.6E-9       2.0E-4
MATERIAL
MATERIAL.NUMBER   E       NU   RO
11                209E5   .3   7860
LOADS
CASE     NODE     DIRECTIONS.OF.LOAD     VALUE.OF.LOAD
1        4        2                      10
ACTIVE.FREEDOMS
NODE     DIRECTION     PRINT.CONTROL
2        12            2
R20      00            0
RESTRAINTS
NODE     DIRECTION
1        0
2        3
R11  1   0
14       0
MODES.AND.FREQUENCIES
AUTOMATIC.MASTERS     MODES
0                     10
MASTERS
NODE.NUMBER     DIRECTION
2               12
R11    1        00
END.OF.DAT
```

Table 2.10: Data file in PAFEC FE for deriving mass and stiffness for truss in fig.2.6

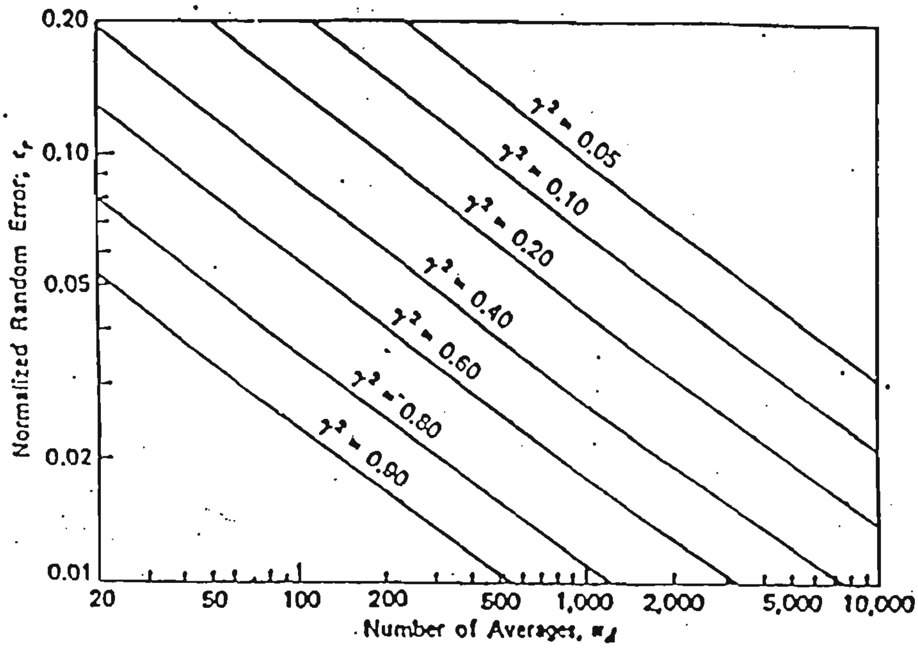

FIG.2.1: Normalized random error as a function of coherence and number of averages (Reference B & K 2032 Manual; Volume 1)

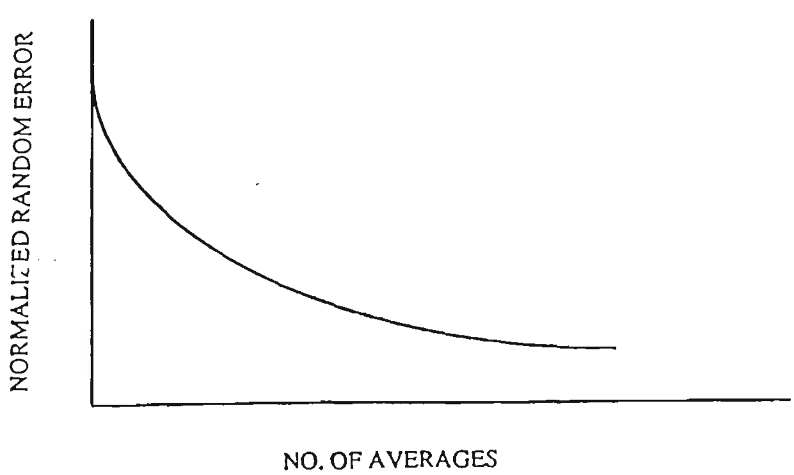

FIG.2.2: Normalized random error vs number of averages

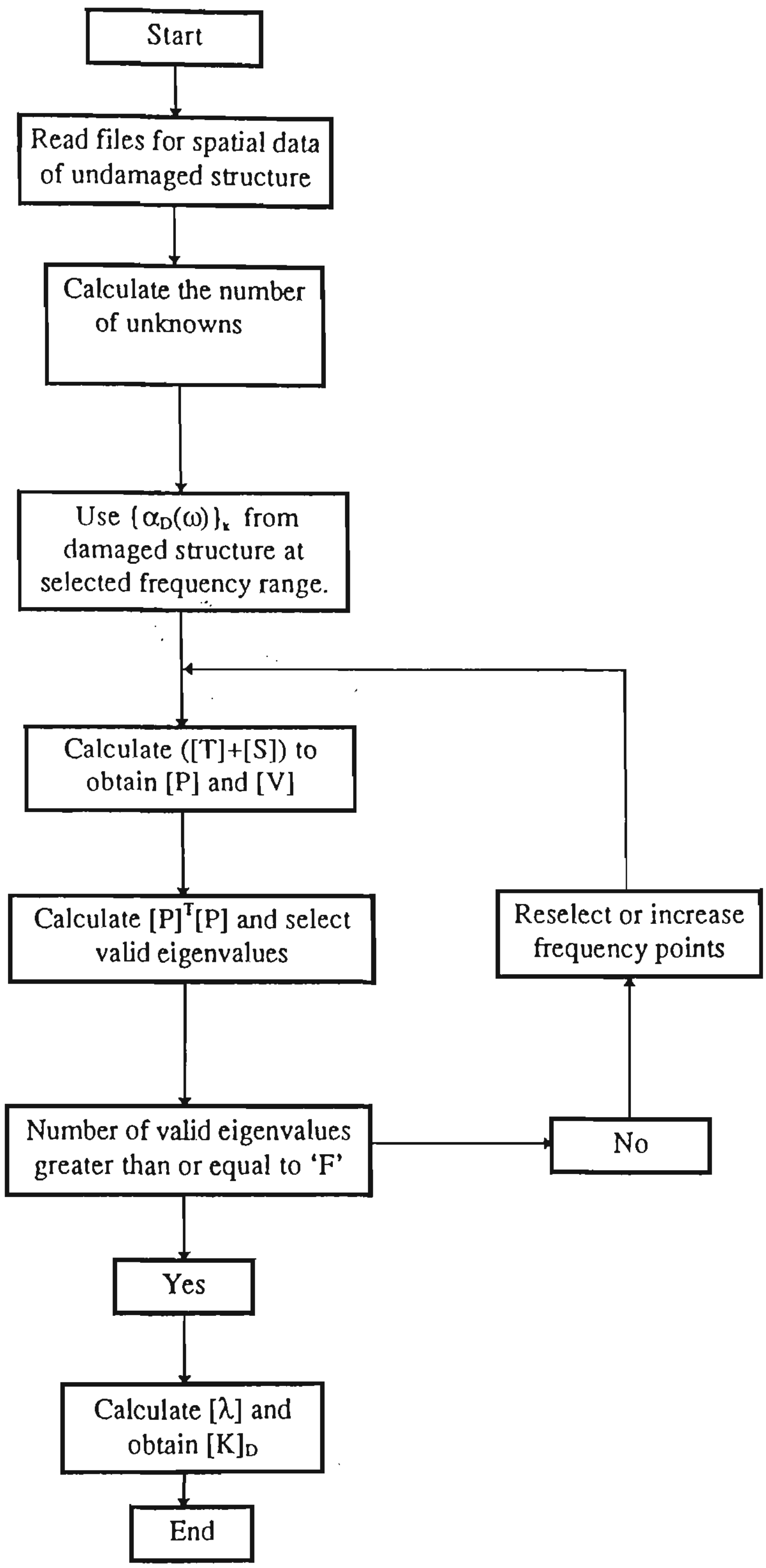

FIG.2.3: A flowchart of program for computer implementation of CMDQ method

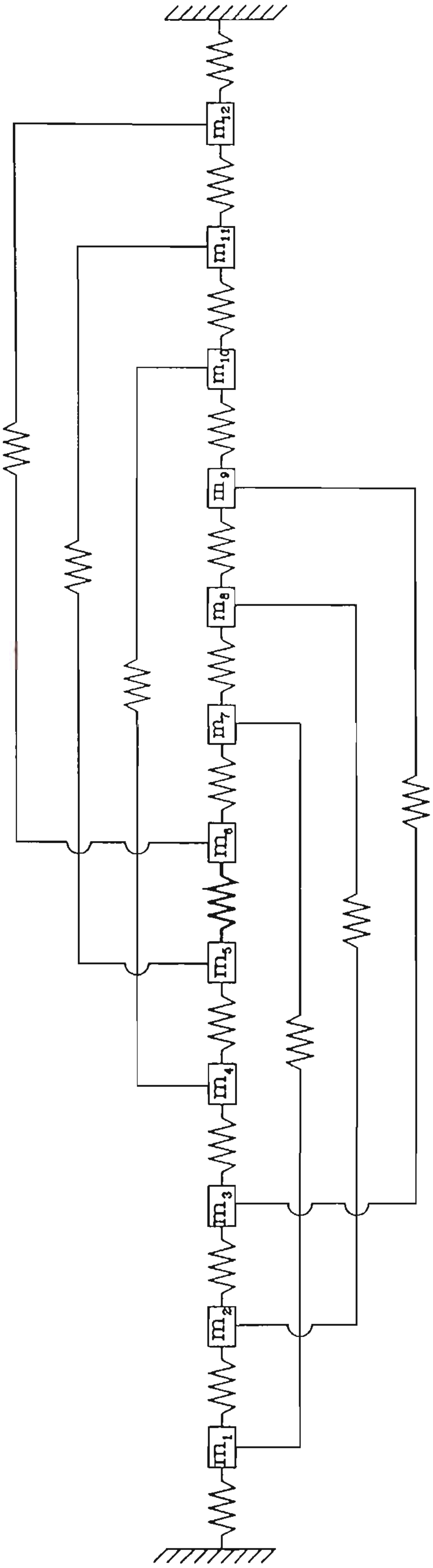

FIG.2.4: A12 DOF mass spring system (Model 2.1)

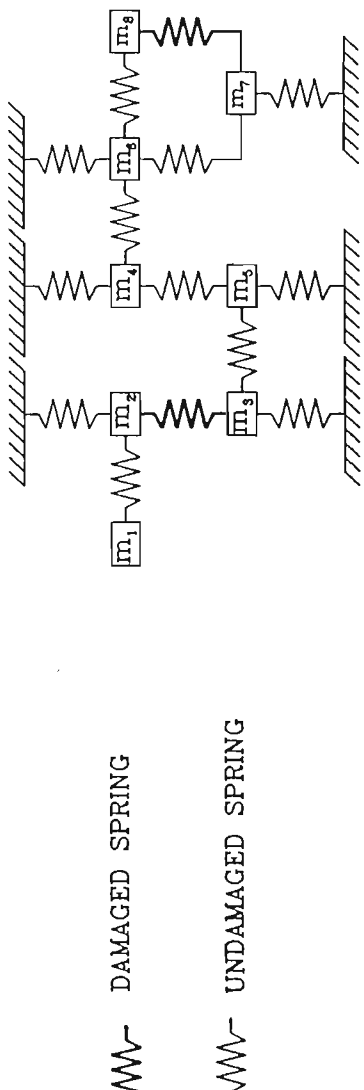

FIG.2.5: An 8 DOF undamped mass spring system (Model 2.2)

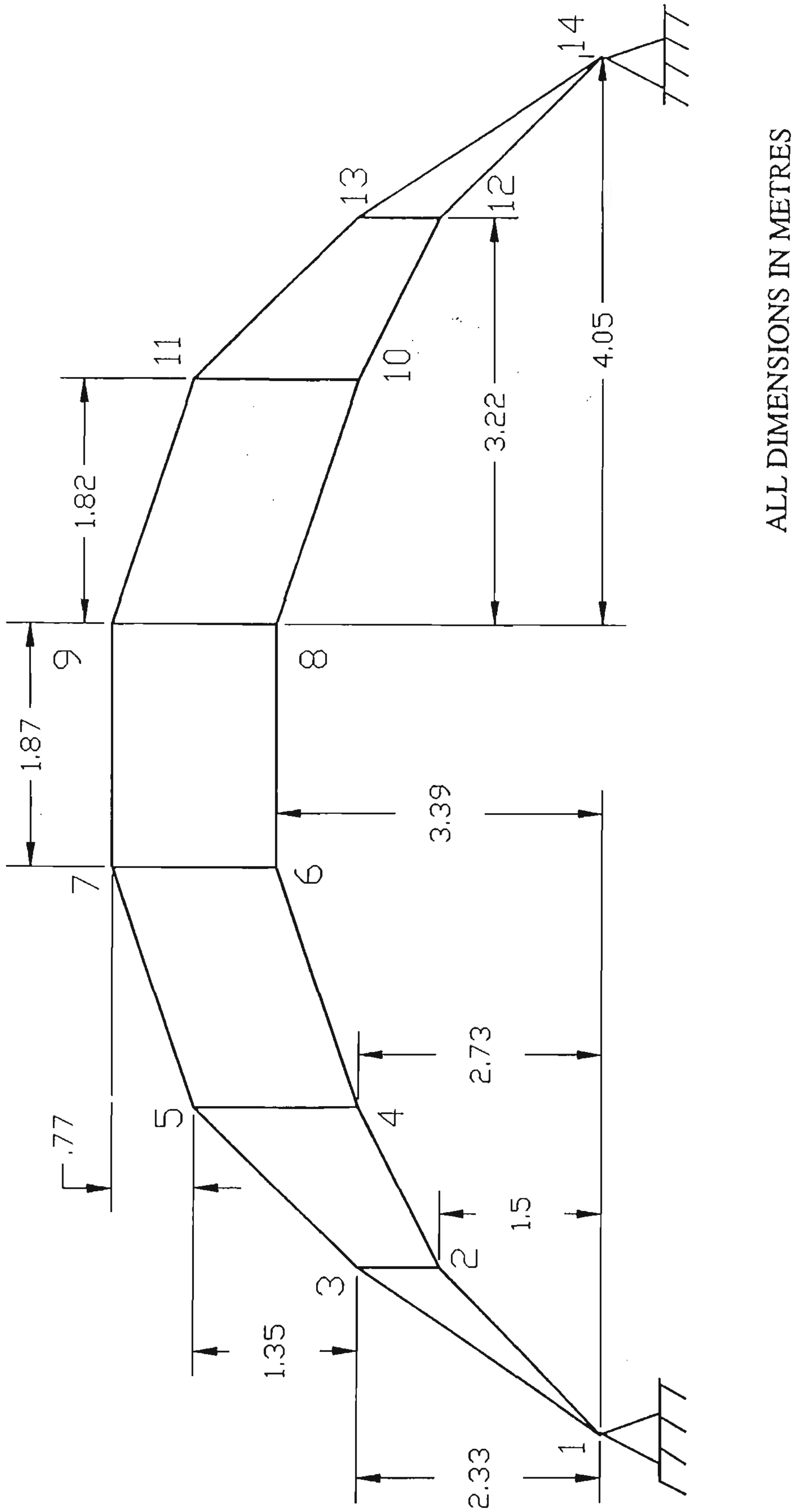

FIG.2.6: A 20 member plane truss structure (Model 2.3)

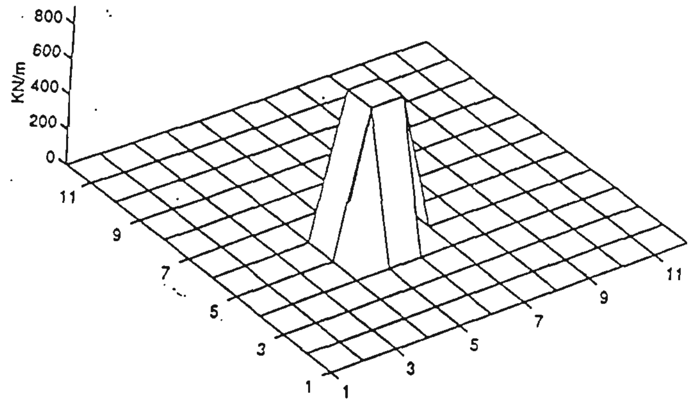

FIG.2.7: Actual [ΔK] for model 2.1

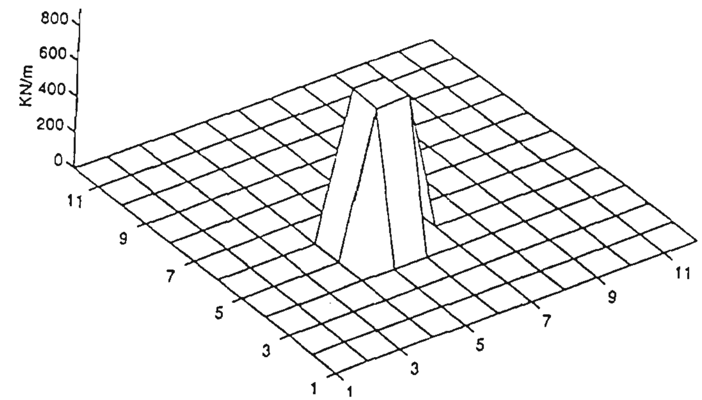

FIG.2.8: Calculated [ΔK] using CMDQ method for pure data in model 2.1 (29 valid eigenvalues; frequency points 3, 12, 14 rad/s)

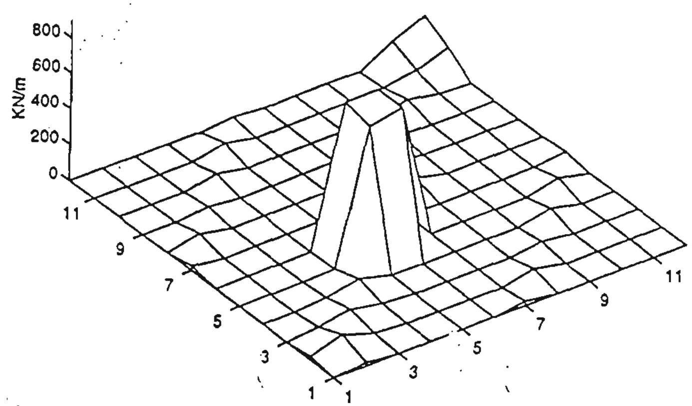

FIG.2.9: Calculated [ΔK] using CMDQ method for pure data in model 2.1 (26 valid eigenvalues; frequency points 3, 12, 14 rad/s)

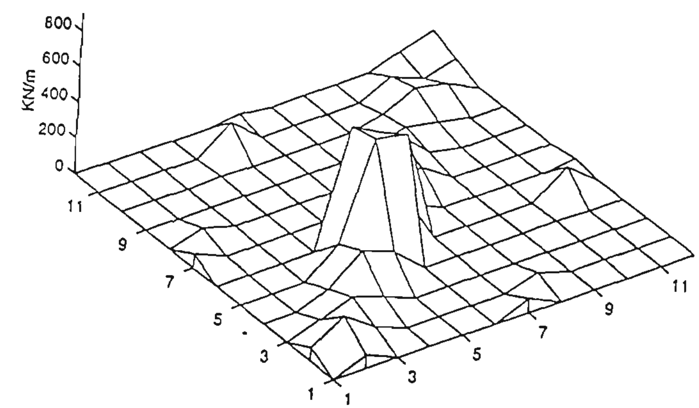

FIG.2.10: Calculated [ΔK] using CMDQ method for pure data in model 2.1 (23 valid eigenvalues; frequency points 3, 12, 14 rad/s)

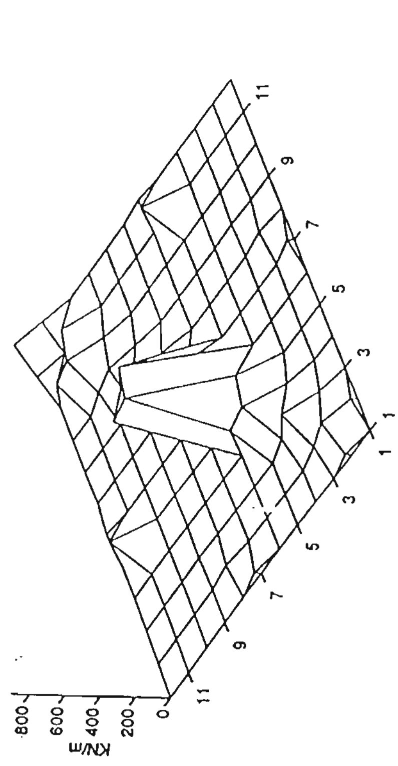

FIG.2.11: Calculated [ΔK] using CMDQ method for pure data in model 2.1 (23 valid eigenvalues; frequency points 8, 10, 11 rad/s)

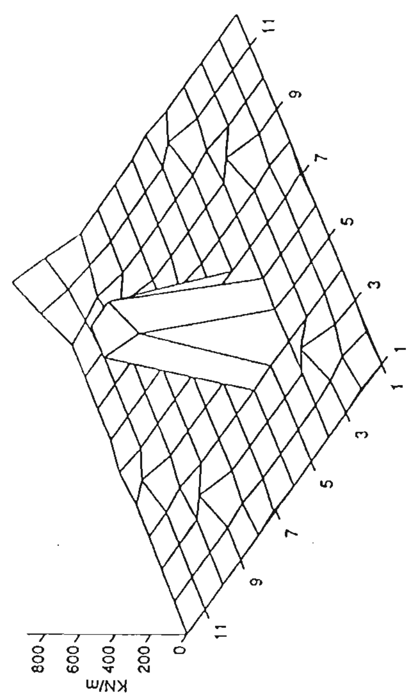

FIG.2.12: Calculated [ΔK] using CMDQ method for pure data in model 2.1 (25 valid eigenvalues; frequency points 8, 10, 11, 13 rad/s)

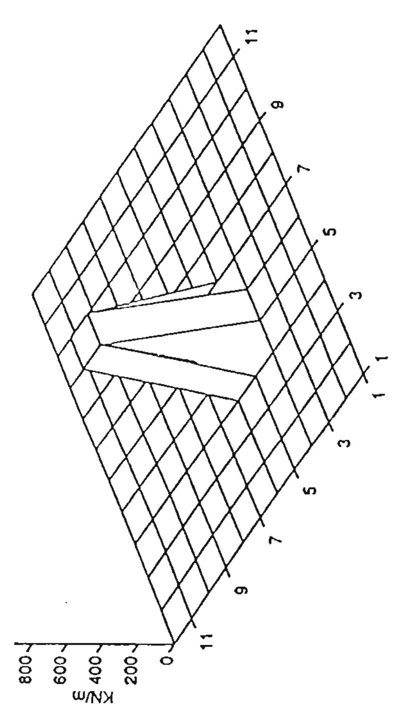

FIG.2.13: Calculated [ΔK] using CMDQ method for pure data in model 2.1 (29 valid eigenvalues; frequency points 8, 10, 11, 13, 15.4 rad/s)

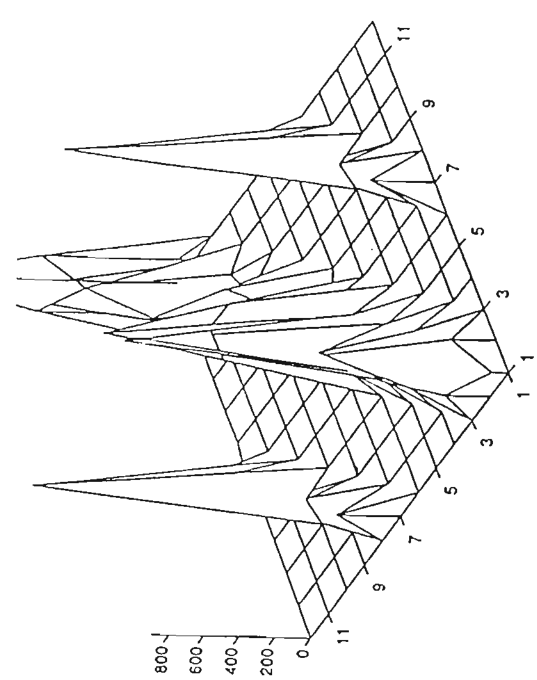

FIG.2.14: Calculated [ΔK] using CMDQ method for 2% noise in data in model 2.1(29 valid eigenvalues; frequency points 3, 12, 14 rad/s)

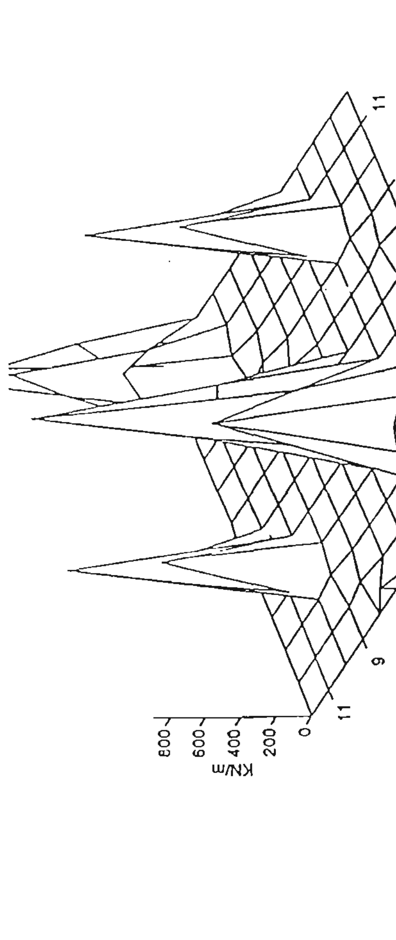

FIG.2.15: Calculated [ΔK] using CMDQ method for 2% noise in data in model 2.1 (29 valid eigenvalues; frequency points 3, 12, 14, 13 rad/s)

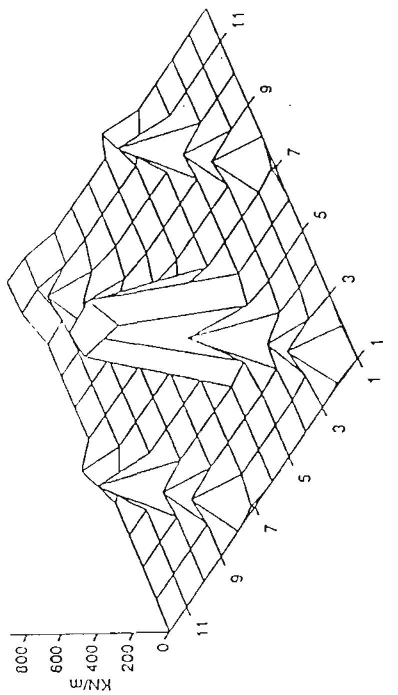

FIG.2.16: Calculated [ΔK] using CMDQ method for 2% noise in data in model 2.1 (29 valid eigenvalues; frequency points 3, 12, 14, 13, 16 rad/s)

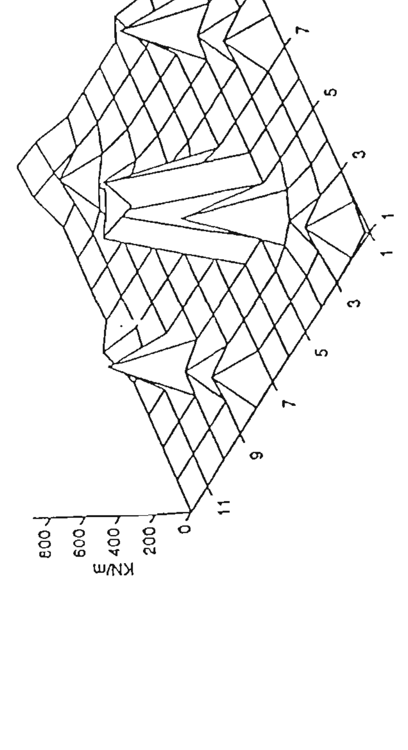

FIG.2.17: Calculated [ΔK] using CMDQ method for 2% noise in data in model 2.1 (29 valid eigenvalues; frequency points 3, 12, 14, 13, 16, 9 rad/s)

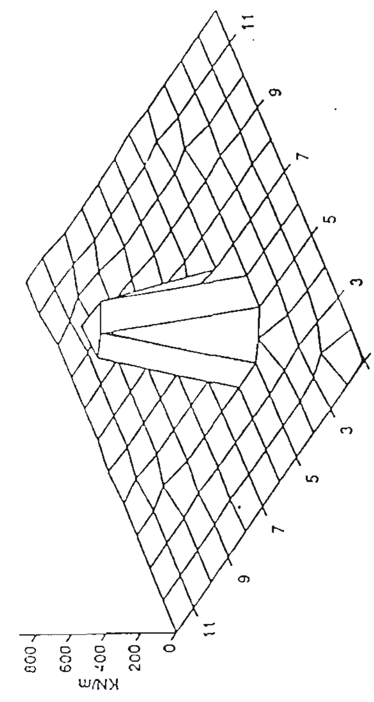

FIG.2.18: Calculated [ΔK] using CMDQ and noise filtering technique for 2% noise in data in model 2.1(frequency points 3, 12, 14, 13, 16 rad/s)

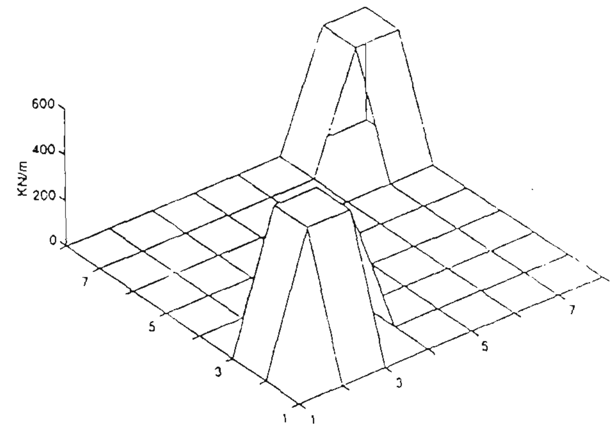

FIG.2.19: Actual [ΔK] for model 2.2

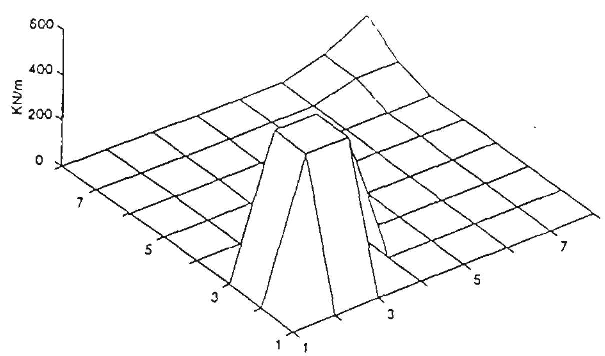

FIG.2.20: Calculated [ΔK] using CMDQ method for pure data in model 2.2
(16 valid eigenvalues; frequency points 8, 14 rad/s)

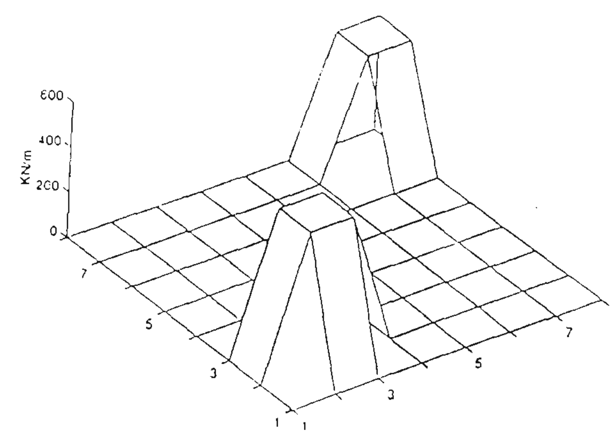

FIG.2.21: Calculated [ΔK] using CMDQ method for pure data in model 2.2
(16 valid eigenvalues and frequency points 8, 14, 19 rad/s)

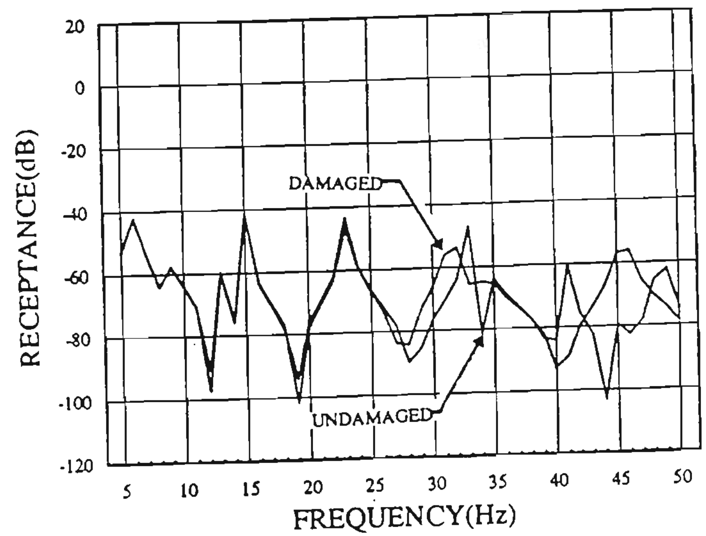

FIG.2.22: RFRF ($\alpha_{22}(\Omega)$) for model 2.3 before and after damage

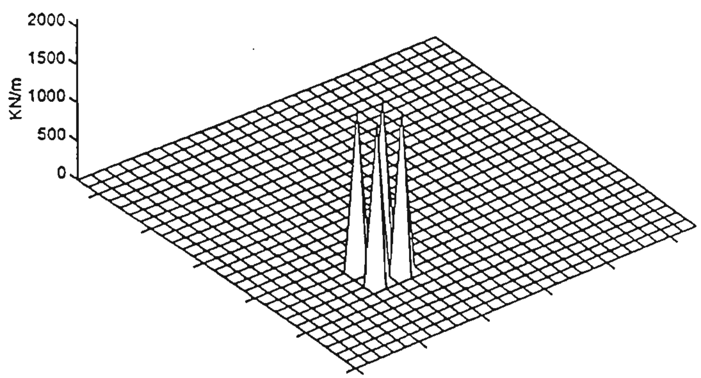

Fig.2.23: Actual [ΔK] for model 2.3

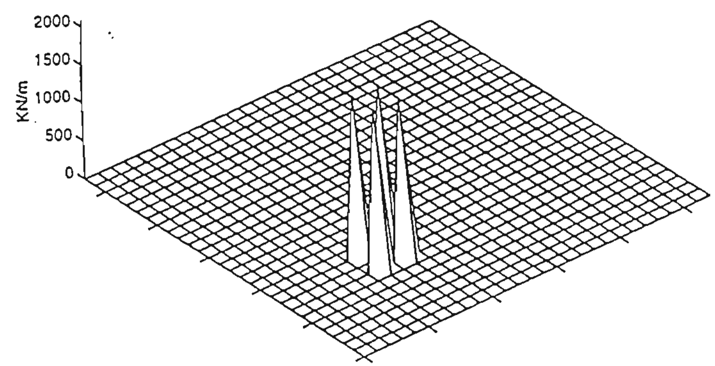

FIG.2.24: Calculated [ΔK] using CMDQ method for pure data in model 2.3 (frequency points 12, 19, 25, 43 rad/s)

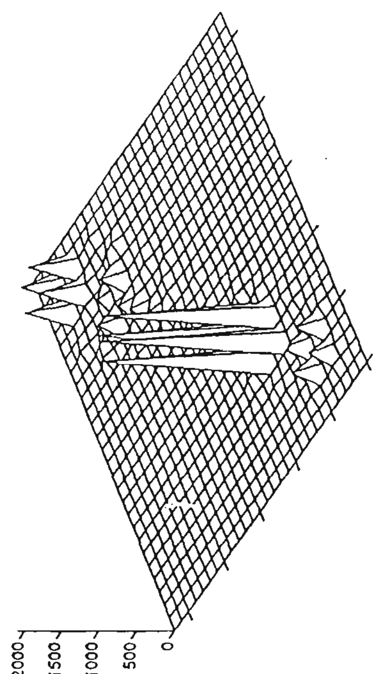

FIG.2.25: Calculated [ΔK] using CMDQ for data containing 2% noise in model 2.3
(frequency points 12, 19, 25, 43 rad/s)

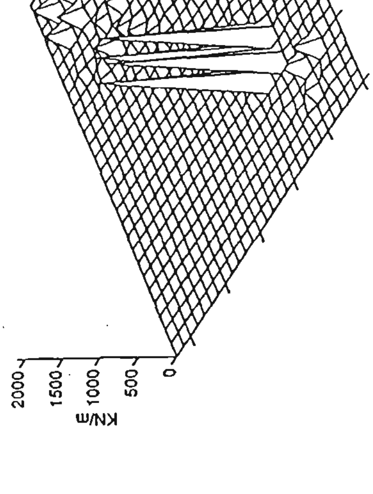

FIG.2.26: Calculated [ΔK] using CMDQ for data containing 2% noise in model 2.3
(frequency points 12, 19, 25, 43, 37 rad/s)

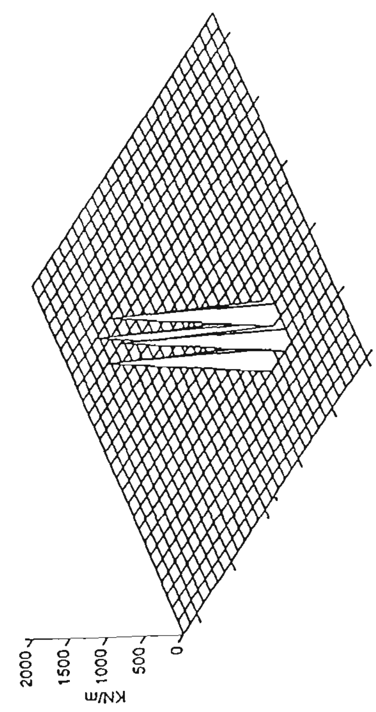

FIG.2.27: Calculated [ΔK] using CMDQ for filtered data in model 2.3
(frequency points 12, 19, 25, 43, 37 rad/s)

CHAPTER 3

DAMAGE LOCATION IN A STRUCTURE USING MEASURED FREQUENCY RESPONSE FUNCTION DATA

3.1 INTRODUCTION

The CMDQ method suggested in Chapter 2 was aimed at determining directly the extent of damage in a structure. An alternative procedure is to treat the problem in a decoupled fashion: first determine the location of damage and then concentrate only on the damaged area of the structure to find the extent of damage. If the damage can be located beforehand, an algorithm which works only with the part of the structure where the damage is located, need to handle matrices of much smaller size. This reduces the computational effort and increases the capacity to accommodate inaccuracies in the FRF data.

With this concept in mind, a technique suitable for locating structural damage is next developed. The outcome is used in later chapters where techniques which work only with the damaged part of a structure are presented.

Researchers in the past have explored the possibility of locating structural faults. However, almost all the methods developed for this purpose depend on modal parameters. The application of the Cross Random Decrement method for locating damage in a scale model of an offshore platform structure had been demonstrated by Tsai, et al. [42]. Their paper demonstrates that the correlation between changes of relative phases at various positions can be succesfully used to locate damage in a structure.

In another publication by Akgun and Ju [43] the authors used transmissibility changes in a structure caused by damage as a feasible means to diagnose structural damage. Rizos, et al. [44] made an attempt to locate a crack in a cantilever beam by using vibration modes. In addition to the methods discussed above, Lin [45] in his work suggested determining the flexibility matrix using experimental data and then multiplying it by the original stiffness matrix to identify the row and/ or column that differs significantly from a row and/ or columns of the identity matrix, thereby indicating the DOFs affected. However, with the flexibility matrix built up using noisy data it is hard to obtain the pattern suggested by Lin and often damage location becomes uncertain. Pandey, et al. [46] suggested a method of damage detection using the change in the curvature of mode shapes as the indicating factor associated with damage location. The authors have also shown that even for situations where the MAC and COMAC are not sensitive enough to detect damage, the application of the curvature mode shapes succeeded in detecting damage.

A comparison between some techniques which used natural frequency and mode shape data to locate damage has been given by Fox [47]. Based on his findings, Fox concluded that the change in natural frequencies and MAC values were reasonable indicators of the presence of damage but by themselves they were not sufficient enough to indicate the correct location of damage accurately enough. According to Fox, plots of the difference and relative difference in the mode shapes of a particular mode whose frequency has been affected provides a better tool for damage location. Law, et al. [48] applied the sensitivity equations which relate the changes in FRF and phase differences to elemental change for detecting damage in a scale model of a bridge deck. However, the experimental results obtained by the author using this technique failed to give good results.

Joon-Ho Kim, et al. [49] showed the feasibility of locating faults by combining the concepts of the Partial MAC (PMAC) and the Co-ordinate MAC (COMAC). The important issues associated with the use of experimentally derived modal parameters as a means of structural fault detection have been discussed by Richardson and Mannan [50]. This paper may be regarded as a report aimed at highlighting the most common problems likely to be faced while trying to detect structural damage from changes in modal parameters. The authors suggested the application of neural networks in the field of damage detection to utilise it as an effective on-line monitoring system.

Doebling, et al. [51] presented the experimental results obtained when a model updating algorithm which relied on an unconstrained minimization of the Frobenius norm of modal dynamic residuals was employed to detect damage in a suspended truss. Although the method worked well for a cantilevered truss structure it failed to locate damage for the suspended truss. Lim and Kashangaki [52] presented a method which used measured modes and frequencies to compute the Euclidean distances between the measured mode shapes and the best achievable eigenvectors to identify the damaged element directly without identifying the DOFs affected by damage. Although the method was found to be successful in locating a single area of damage, multiple areas of damage could not be located by the algorithm in a single attempt. Sheinman [53] located damage directly by identifying the DOFs where force residue was not zero. This can be done with a single measured mode provided the concerned mode is affected by damage in question.

All the research work reviewed in the previous paragraph had their origins in system identification techniques, where the analytical model of the undamaged structure along with modal parameters of the damaged structure have been used to locate damage. To eliminate the disadvantages associated with the use of modal data, the damage location method to be presented in this chapter uses the measured FRF data of the damaged structure instead of modal data. This location method will be computationally attractive as it involves only matrix multiplication. As a result, the method has been found to be robust to measurement noise and expansion errors. As the discrepancy increases between the RFRFs of the structure before and after damage, the level of robustness of the method to accomodate measurement noise also increases.

3.2 THEORY OF DAMAGE LOCATION USING FRF DATA

It is assumed that an N DOF finite element model of the undamaged structure exists and is given by,

$$[M]\{\ddot{x}\} + [K]\{x\} = \{0\} \tag{3.2.1}$$

where [M] and [K] are the NxN analytical mass and stiffness matrices, $\{x\}$ is an Nx1 vector of displacements.

If a single column of RFRF at a particular frequency Ω is given by $\{\alpha(\Omega)\}$, then it follows that:

$$([K]_{UD} - \Omega^2[M]_{UD})\{\alpha_{UD}(\Omega)\}_k = ([K]_D - \Omega^2[M]_D)\{\alpha_D(\Omega)\}_k \tag{3.2.2}$$

or, $$([Z(\Omega)]_{UD})\{\alpha_{UD}(\Omega)\}_k = ([Z(\Omega)]_D)\{\alpha_D(\Omega)\}_k \tag{3.2.3}$$

The dynamic stiffness matrix before and after damage is related by:

$$([Z(\Omega)]_D = [Z(\Omega)]_{UD} - [\Delta Z(\Omega)] \tag{3.2.4}$$

Hence, equation (3.2.3) can be written as

$$[Z(\Omega)]_{UD}\{\alpha_{UD}(\Omega)\}_k = ([Z(\Omega)]_{UD} - [\Delta Z(\Omega)])\{\alpha_D(\Omega)\}_k \tag{3.2.5}$$

or, $$[Z(\Omega)]_{UD}(\{\alpha_D(\Omega)\}_k - \{\alpha_{UD}(\Omega)\}_k) = [\Delta Z(\Omega)]\{\alpha_D(\Omega)\}_k \tag{3.2.6}$$

or, $$[Z(\Omega)]_{UD}\{\Delta\alpha(\Omega)\}_k = \{d(\Omega)\} \tag{3.2.7}$$

where the vector $\{\Delta\alpha(\Omega)\}_k$ represents the difference in RFRFs between the damaged and undamaged structure at a frequency Ω. The right hand side of equation (3.2.7) represents a vector which indicates damage. The j^{th} element of that vector will be zero if the j^{th} row of matrix $[\Delta Z(\Omega)]$ is zero. In contrast, a degree of freedom which has been affected by damage will result in a non-zero entry in the vector $\{d(\Omega)\}$. Hence, a straight multiplication of the undamaged dynamic stiffness matrix and the vector $\{\Delta\alpha(\Omega)\}_k$ will generate a vector $\{d(\Omega)\}$ which will have non-zero values corresponding to damaged DOFs and zero for undamaged DOFs.

For measurements which are free of error, it is relatively simple to obtain the zero non-zero pattern as described above. However, in practical applications where the measurements are contaminated by various errors, it is impossible to obtain the pattern described above. In addition, if the norm of a few rows of dynamic stiffness matrix are much larger or smaller than others, then the vector $\{d(\Omega)\}$ generated by this method may not be successful in locating damage.

This can be further explained by reference to the simple 5 DOF chain system shown in figure 3.1 for which the stiffness element between DOFs 2 and 3 is much stiffer than the other elements. This results in rows 2 and 3 of the undamaged dynamic stiffness matrix of this system having a much bigger norm compared to other rows.

For this 5 DOF system, equation (3.2.7) becomes:

$$\begin{bmatrix} Z_{11}(\Omega) & Z_{12} & - & - & - \\ Z_{21} & Z_{22}(\Omega) & Z_{23} & - & - \\ - & Z_{32} & Z_{33}(\Omega) & Z_{34} & - \\ - & - & Z_{43} & Z_{44}(\Omega) & Z_{45} \\ - & - & - & Z_{54} & Z_{55}(\Omega) \end{bmatrix} \begin{Bmatrix} \Delta\alpha_{1k}(\Omega) \\ \Delta\alpha_{2k}(\Omega) \\ \Delta\alpha_{3k}(\Omega) \\ \Delta\alpha_{4k}(\Omega) \\ \Delta\alpha_{5k}(\Omega) \end{Bmatrix} = \{d(\Omega)\}$$

Assuming the damage is located between DOFs 4 and 5, error free FRF data will lead to:

$$Z_{11}(\Omega)\Delta\alpha_{1k}(\Omega) + Z_{12}\Delta\alpha_{2k}(\Omega) = 0.0 \tag{3.2.8}$$

$$Z_{21}\Delta\alpha_{1k}(\Omega) + Z_{22}(\Omega)\Delta\alpha_{2k}(\Omega) + Z_{23}\Delta\alpha_{3k}(\Omega) = 0.0 \tag{3.2.9}$$

$$Z_{32}\Delta\alpha_{2k}(\Omega) + Z_{33}(\Omega)\Delta\alpha_{3k}(\Omega) + Z_{34}\Delta\alpha_{4k}(\Omega) = 0.0 \tag{3.2.10}$$

$$Z_{43}\Delta\alpha_{3k}(\omega) + Z_{44}(\Omega)\Delta\alpha_{4k}(\omega) + Z_{45}\Delta\alpha_{5k}(\Omega) \neq 0.0 \tag{3.2.11}$$

$$Z_{54}\Delta\alpha_{4k}(\Omega) + Z_{55}(\Omega)\Delta\alpha_{5k}(\Omega) \neq 0.0 \tag{3.2.12}$$

In the following section between equations (3.2.13) and (3.2.19), the frequency sign Ω is omitted from dynamic stiffness and RFRF terms in order to accomodate the equations in a single line. Since the measured FRF data will be inevitably contaminated by noise, what actually results are the following:

$$Z_{11}(\Delta\alpha_{1k} + e1) + Z_{12}(\Delta\alpha_{2k} + e2) = Z_{11}e1 + Z_{12}e2 \tag{3.2.13}$$

$$Z_{21}(\Delta\alpha_{1k} + e1) + Z_{22}(\Delta\alpha_{2k} + e2) + Z_{23}(\Delta\alpha_{3k} + e3) = Z_{21}e1 + Z_{22}e2 + Z_{23}e3 \tag{3.2.14}$$

$$Z_{32}(\Delta\alpha_{2k} + e2) + Z_{33}(\Delta\alpha_{3k} + e3) + Z_{34}(\Delta\alpha_{4k} + e4) = Z_{32}e2 + Z_{33}e3 + Z_{34}e4 \tag{3.2.15}$$

$$Z_{43}(\Delta\alpha_{3k} + e3) + Z_{44}(\Delta\alpha_{4k} + e4) + Z_{45}(\Delta\alpha_{5k} + e5) = Z_{43}e3 + Z_{44}e4 + Z_{45}e5 + \text{Non zero value} \tag{3.2.16}$$

$$Z_{54}(\Delta\alpha_{4k} + e4) + Z_{55}(\Delta\alpha_{5k} + e5) = Z_{54}e4 + Z_{55}e5 + \text{Non zero value} \tag{3.2.17}$$

where e1, e2, e3, e4 and e5 are the random errors associated with FRFs $\alpha_{D,1k}$, $\alpha_{D,2k}$, $\alpha_{D,3k}$, $\alpha_{D,4k}$, $\alpha_{D,5k}$ respectively. As assumed $Z_{22}(\Omega)$, Z_{23} and $Z_{33}(\Omega)$ are much greater than $Z_{11}(\Omega)$, Z_{12}, Z_{34}, $Z_{44}(\Omega)$, Z_{45}, $Z_{55}(\Omega)$. Therefore, unless the error due to damage is appreciably large, the following equations will be accurate,

$$(Z_{21}e1 + Z_{22}e2 + Z_{23}e3) >> (Z_{43}e3 + Z_{44}e4 + Z_{45}e5 + \text{Non zero value}) \text{ or, } (Z_{54}e4 + Z_{55}e5 + \text{Non zero value}) \tag{3.2.18}$$

and

$$(Z_{32}e2 + Z_{33}e3 + Z_{34}e4) >> (Z_{43}e3 + Z_{44}e4 + Z_{45}e5 + \text{Non zero value}) \text{ or, } (Z_{54}e4 + Z_{55}e5 + \text{Non zero value}) \tag{3.2.19}$$

In such cases, the method will wrongly identify DOFs 2 and 3 as damage affected DOFs rather than the DOFs 4 and 5.

One solution to address this problem is to write equation (3.2.7) as,

$$d_j(\Omega) = \{Z_{UD}(\Omega)\}_j\{\Delta\alpha(\Omega)\}_k = \|Z_{UD}(\Omega)_j\|\ \|\Delta\alpha(\Omega)\|\cos(\theta_\Omega^{\ j}) \tag{3.2.20}$$

where $d_j(\Omega)$ is the j^{th} component (or the j^{th} DOF) of the vector at a frequency Ω, $\{Z_{UD}(\Omega)\}_j$ is the j^{th} row of the matrix $[Z_{UD}(\Omega)]$ and $\theta_\Omega^{\ j}$ is the angle between the vectors $\{Z_{UD}(\Omega)\}_j$ and $\{\Delta\alpha(\Omega)\}_k$ at a frequency Ω. Since in this case, the product of $\{Z_{UD}(\Omega)\}_j$ and $\{\Delta\alpha(\Omega)\}_k$ is divided by the norm of a particular row, it effectively normalises each row and eliminates the imbalance if a particular row has a bigger norm compared to other rows.

It is apparent in this case that a zero $d_j(\Omega)$ corresponds to a $\theta_\Omega^{\ j}$ of ninety degrees whereas a non-zero $d_j(\Omega)$ corresponds to an angle different than ninety degrees. It is also possible to calculate a vector $\{\beta(\Omega)\}$ whose elements are:

$$\beta_\Omega^{\ j} = 90 - \theta_\Omega^{\ j} \tag{3.2.21}$$

Therefore a zero $\beta_\Omega^{\ j}$ corresponds to an undamaged DOFs and a non-zero $\beta_\Omega^{\ j}$ corresponds to damaged DOFs. In this case, the vector $\{\beta(\Omega)\}$ is called the 'Damage Location Vector' or DLV.

Although using the vector angle assisted in eliminating the problem caused by the difference in matrix/vector norms as described in the preceding paragraphs, the effects of measurement noise on the damage location algorithm still remain to be properly addressed. Due to the presence of measurement noise, the zero/non-zero pattern will not exist. Even for DOFs unaffected by damage, the effect of noise may result in a value for the corresponding element in the 'Damage Location Vector' which is too large to be ignored.

The use of FRF data over a frequency range helps significantly in reducing uncertainties caused by the effect of noise while trying to locate damage in a structure. In general, the effect of noise on measurement varies randomly depending on the frequency of measurement. If the elements (corresponding DOFs) in the 'Damage Location Vector' are plotted over a certain frequency range, then the values of elements due to noise in the measurement only will follow a random pattern, becoming negligible at certain frequency points and becoming notable at others. In contrast, the elements in the 'Damage Location Vector' due to genuine damage, will occur more consistently with a greater amplitude and with a definite pattern.

A 3-D graph can be drawn to locate damage. The first axis of the graph corresponds to the DOFs in the 'Damage Location Vector', the second axis indicates the frequency range over which the damage location algorithm is applied and the third axis represents the values obtained for the elements in the 'Damage Location Vector'. Using such a 3-D graph, a regular pattern can be identified corresponding to the damaged DOFs. In contrast, the elements in the 'Damage Location Vector' whose values are due only to the effect of noise, will follow a random pattern with insignificant amplitudes when plotted over a certain frequency range. This 3-D graph is referred to as 3-D 'Damage Location

Plot' or DLP and it enables a more reliable identification of damage. This 3-D graph is attributable to the use of FRF data since FRF data at different frequencies provide abundant information which can be used to locate damage with greater reliability. Such a feature would not have been possible if modal data were used.

Instead of drawing a 3-D DLP, it is possible to obtain similar results by projecting the 3 dimensional DLP onto a 2 dimensional plane. This means that the absolute values of the DLV obtained over a frequency range be added to each other to obtain a resultant vector called here a 'Cumulative Damage Location Vector' or CDLV. This CDLV can be plotted in a 2 dimensional graph where the first axis corresponds to the DOFs and the second axis represents the elements of the CDLV. Since the elements in the DLV due to damage will be mostly bigger than that due to noise, the CDLV will magnify it greatly making it easier to isolate the location of damage.

3.3 COMPATIBILITY OF MEASURED AND ANALYTICAL DATA

In creating an analytical model, it is possible to discretize a structure into a large number of DOFs to represent the structure accurately. This model is often used in conjunction with the measured FRF data of the same structure after it has suffered damage in order to locate structural damages. However, an important issue to be addressed is the incompatibility between the analytical model and the measured FRF data in respect to the coordinates employed. Usually, an analytical model will use a far greater number of coordinates to describe the vibration characteristics of a structure than is practicable with measured data.

The approach to resolving the incompatibility problem can be broadly classified in either of the following two ways:

(i) by reducing the analytical model of the undamaged structure to the corresponding measured DOFs
(ii) by implementing a procedure that will expand the measured data so that they are compatible coordinate wise with the analytical model.

3.3.1 Reduction techniques

The computational cost of eigenparameters of large systems can be large. At the same time only the information in a limited low frequency range is needed. As a result, different condensation techniques have been developed for reducing the full eigenproblem to a much smaller one. The earliest and probably the most commonly used reduction technique is usually referred to as static condensation or Guyan Reduction and can be found in publications by Guyan [54] and Irons [55]. In contrast to Guyan's method for reducing the size of stiffness and mass matrices based on the displacement method, Kaufman and Hall [56] derived a reduced mass matrix identical to Guyan by using a force method.

The error introduced while using static condensation is heavily dependent on the selection of DOFs to be retained. Hu and Zheng [57] attempted to minimize the loss of accuracy induced by the poor or improper selection of masters by the use of a perturbation technique. Similar attempts to improve the accuracy of the Guyan Reduction method were attempted by Conti [58]. A better technique than static condensation was found to be dynamic condensation and Kidder's approach [59] was one of the earliest. Subsequently, publications by Leung [60], Downs [61], Paz [62] and Petersman [63] all used techniques which can be broadly categorised as dynamic condensation.

Suarez and Singh [64] also used a dynamic condensation method in proposing an iterative method which starts with a trial condensation matrix to form a condensed eigenvalue problem. Some work in this area has been reported which can be classified under system balancing. Moore [65] used balanced controllability and observability to obtain a reduced model. Yae and Inman [66] proposed a method in which the Guyan reduced model was converted to state space and further reduced by system balancing.

In addition to the methods discussed above, the Improved Reduced System (IRS) by O'Callahan [67] extended the Guyan method by adjusting the modal matrix estimate by taking into account inertial effects associated with the deleted DOFs in the transformation matrix. The System Equivalent Reduction Expansion process (SEREP) by O'Callahan, et al. [68] had been suggested in recent years and was found to be more accurate than previous methods.

All the methods mentioned above use modal parameters to carry out the reduction of the original model. The measure of success of the reduction techniques is gauged by the degree of similarity of the eigenparameters generated by the reduced model and those of the original model. In other words, reduction techniques employed to reduce the original model can be regarded as successful only if the eigenproperties of the original model and reduced model are similar.

Instead of using modal parameters, an attempt was made in this study to use RFRF data to reduce the original model. However, while using RFRF data it was found that the modal parameters generated by the reduced model were similar to that of the original model when the RFRF data chosen for reduction were at frequencies very close to the natural frequencies of the system. This can result in problems in practical applications while trying to measure RFRF data at the natural frequency of the system.

Irrespective of whether modal data or FRF data is used, the reduced model is never found to be physically identical to the original model. This feature was quite expected since the idea behind obtaining a reduced model was not to ensure that the reduced model and the original structure had the same physical properties, but only to ensure that their modal properties were as similar as possible. It was found that the connectivity of the reduced model was not similar to the original model. This meant that if in the original model DOF 1 was not connected to DOF 4, the model obtained after reduction might indicate that they were connected. It essentially means that the reduced model fails to reflect the physical characteristics of the original system. This particular feature makes it difficult to use the reduced model for structural damage location.

Most of the damage location algorithms based on system identification techniques need a spatial model of the undamaged structure which is used along with the measured data from the damaged structure to determine the location and extent of damage. Therefore, for the damage location method to succeed it is important for the spatial model to physically represent the structure correctly. If the model used for damage location represents connectivities which do not exist in the actual structure, the algorithms for damage location may falsely find locations of damage in areas which are practically impossible. Hence, the use of a reduced model, which does not correctly represent the connectivity of the original structure, fail to produce satisfactory results from the damage location point of view. As a result, for damage location, the only way to solve the problem of compatibility is to expand the measured RFRF data so that they are compatible with the analytical model.

3.3.2 Expansion techniques

The process of interpolating data corresponding to coordinates or DOFs which have not been measured may be termed coordinate expansion. The task of expanding measured mode shapes using analytically derived properties has been the subject of considerable investigation and three different approaches have been identified. The first approach for mode shape expansion was proposed by Kidder [59] who used the mass and stiffness matrices of the analytical model to compute the missing DOFs in the measured mode shape. The approach is equivalent to an inverse Guyan Reduction where the slave co-ordinates are recovered in terms of masters.

The second approach as discussed seperately by O'Callahan, et al [68] and Roy, et al [76] relied on the assumption that the mode shape values corresponding to the full system model can be expressed as a linear combination of the mode shape values corresponding to the DOFs to be retained in the reduced model. The SEREP method discussed by O'Callahan, et al [68] was originally formulated as a global mapping technique to develop rotational DOFs for modal test data by the same author [69]. In addition to that SEREP has been successfully employed in a variety of applications such as checking correlation and orthogonality between analytical and experimental modal vectors by Avitable, et al [70], linear and nonlinear forced response studies by Avitable, et al [71], and analytical model improvement by O'Callahan, et al [72].

Although, O'Callahan, et al [68] applied SEREP on a simple structure to demonstrate the accuracy of the reduced model, the method has been found to be reversible in the sense that expanding the reduced system's mode shapes back to the full system's space, develops mode shapes that are exactly identical to the original mode shapes of the full system model. The third approach which involved the interpolation/extrapolation of the measured DOFs to those of the full model by adopting a spatial interpolation approach was employed by Williams and Green [73] and Waters and Lieven [74]. Due to the problems associated with complex spatial descriptions and sudden changes of geometry, there have been relatively few examples of this technique being applied to structural dynamics. The main application area of this technique is the wing aeroelasticity where the mesh sizes for fluid and structure are incompatible as shown by Harder, et al [75].

In what follows, the expansion techniques mentioned in the first and second approaches for expanding mode shapes are used here to interpolate RFRF data. Subsequently these interpolated FRF data will be used together with measured FRF data in order to locate damage in a structure. The coordinates in the damaged structure for which RFRF data has been measured are given the superscript "m" and those which have not been measured and need to be interpolated are given the superscript "u".

(i) **Dynamic expansion techniques:**

Using equation (3.2.6):

$$[Z(\Omega)]_{UD}\{\Delta\alpha(\Omega)\}_k = [\Delta Z(\Omega)]\{\alpha_D(\Omega)\}_k \tag{3.2.6}$$

The vectors $\{\Delta\alpha(\Omega)\}_k$ and $\{\alpha_D(\Omega)\}_k$ are partitioned into measured and unmeasured parts so that it can be written as:

$$\{\Delta\alpha(\Omega)\}_k = \begin{Bmatrix} \Delta\alpha^m(\Omega) \\ \Delta\alpha^u(\Omega) \end{Bmatrix}_k \quad \text{and} \quad \{\alpha_D(\Omega)\}_k = \begin{Bmatrix} \alpha_D^m(\Omega) \\ \alpha_D^u(\Omega) \end{Bmatrix}_k \tag{3.3.1}$$

As per the ordering of $\{\Delta\alpha(\Omega)\}_k$ and $\{\alpha_D(\Omega)\}_k$, the dynamic stiffness matrix for the undamaged structure, for which it is assumed that a complete FE model is available, is reordered to become $[\underline{Z(\Omega)}]_{UD}$, thus

$$\begin{bmatrix} [\underline{Z_{11}(\Omega)}] & [\underline{Z_{12}(\Omega)}] \\ [\underline{Z_{21}(\Omega)}] & [\underline{Z_{22}(\Omega)}] \end{bmatrix}_{UD} \begin{Bmatrix} \Delta\alpha^m(\Omega) \\ \Delta\alpha^u(\Omega) \end{Bmatrix}_k = [\Delta Z(\Omega)] \begin{Bmatrix} \alpha_D^m(\Omega) \\ \alpha_D^u(\Omega) \end{Bmatrix}_k \tag{3.3.2}$$

This expansion method basically ignores the right hand side of equation (3.3.2) and tries to interpolate $\{\Delta\alpha^u(\Omega)\}_k$ by equating the left hand side of equation (3.3.2) to zero. By doing so, the interpolated DOFs will not contain information about structural damage although a full RFRF vector becomes available for using in equation (3.2.7) for damage location. In this work $\{\Delta\alpha(\Omega)\}$ has been interpolated instead of $\{\alpha_D(\Omega)\}$. This have been done for two main reasons. Firstly, the use of $\{\Delta\alpha(\Omega)\}$ ensures that the only non zero elements in the right hand side of equation (3.2.7) are due to damage in the structure. Otherwise use of $\{\alpha_D(\Omega)\}$ would mean that the vector to be used for locating damage will contain a unity element other than the elements due to damage. The position of the unity element in the vector will vary depending on the coloumn of FRF matrix being used. This will introduce unnecessary complexities which can be avoided by interpolating $\{\Delta\alpha(\Omega)\}$.

Secondly, the damage location vector proposed in this work uses $\{\Delta\alpha(\Omega)\}$ and once $\{\Delta\alpha(\Omega)\}$ is known, it can be used directly to locate damage. However, regarding $\{\Delta\alpha(\Omega)\}$ and $\{\alpha_D(\Omega)\}$, if either is known, the other can be readily computed. Equation (3.3.2) can be written as two matrix equations as follows:

$$\left[\underline{Z_{11}(\Omega)}\right]_{UD}\left\{\Delta\alpha^{m}(\Omega)\right\}_k+\left[\underline{Z_{12}(\Omega)}\right]_{UD}\left\{\Delta\alpha^{u}(\Omega)\right\}_k=\{0\} \tag{3.3.3}$$

$$\left[\underline{Z_{21}(\Omega)}\right]_{UD}\left\{\Delta\alpha^{m}(\Omega)\right\}_k+\left[\underline{Z_{22}(\Omega)}\right]_{UD}\left\{\Delta\alpha^{u}(\Omega)\right\}_k=\{0\} \tag{3.3.4}$$

Three methods are available to calculate the RFRF data for unmeasured co-ordinates from equations (3.3.3) and (3.3.4), all being in the form of:

$$\left\{\Delta\alpha^{u}(\Omega)\right\}_k=[TR]\left\{\Delta\alpha^{m}(\Omega)\right\}_k \tag{3.3.5}$$

Each method has a different transformation matrix [TR] which are discussed next:

Dynamic expansion A (D.E A)

From equation (3.3.4), it can be shown that by calculating the inverse of the partitioned dynamic stiffness matrix corresponding to unmeasured DOFs, the transformation matrix becomes:

$$[TR] = -\left[\left[\underline{K_{22}}\right]_{UD} - \Omega^2\left[\underline{M_{22}}\right]_{UD}\right]^{-1}\left[\left[\underline{K_{21}}\right]_{UD} - \Omega^2\left[\underline{M_{21}}\right]_{UD}\right] \tag{3.3.6}$$

Here, the partitioned dynamic stiffness matrix corresponding to unmeasured DOFs is a square matrix and has a dimension of (N-m)x(N-m) where "N" is the number of DOFs for the structure and "m" is the number of measured DOFs.

Dynamic expansion B (D.E B)

From equation (3.3.3), the transformation matrix given below in equation (3.3.7) can be derived:

$$[TR] = -\left[\left[\underline{K_{12}}\right]_{UD} - \Omega^2\left[\underline{M_{12}}\right]_{UD}\right]^{+}\left[\left[\underline{K_{11}}\right]_{UD} - \Omega^2\left[\underline{M_{11}}\right]_{UD}\right] \tag{3.3.7}$$

In this method, the transformation matrix is obtained by calculating the generalised inverse of the partitioned dynamic stiffness matrix $[[K_{12}]_{UD} - \Omega^2[M_{12}]_{UD}]$ which has a dimension of N x (N-m), and then carrying out a matrix multiplication with the dynamic stiffness matrix corresponding to measured DOFs.

Dynamic expansion C (D.E C)

From equations (3.3.3) and (3.3.4), one can define matrices $[A_1]$ and $[A_2]$ as:

$$[A_1] := \begin{bmatrix} \left[\underline{K_{11}}\right]_{UD} - \Omega^2\left[\underline{M_{11}}\right]_{UD} \\ \left[\underline{K_{21}}\right]_{UD} - \Omega^2\left[\underline{M_{21}}\right]_{UD} \end{bmatrix} \tag{3.3.8}$$

$$[A_2] := \begin{bmatrix} \left[\underline{K_{12}}\right]_{UD} - \Omega^2\left[\underline{M_{12}}\right]_{UD} \\ \left[\underline{K_{22}}\right]_{UD} - \Omega^2\left[\underline{M_{22}}\right]_{UD} \end{bmatrix} \tag{3.3.9}$$

which leads to the following transformation matrix :

$$[TR] = [A_2]^+ [A_1] \tag{3.3.10}$$

This method, in contrast to methods D.E A and D.E B, uses the entire matrix of the undamaged structure to build the transformation matrix. Once the transformation matrix is built up using any of the three equations given above as (3.3.6), (3.3.7) and (3.3.10), the FRF data corresponding to unmeasured coordinates can be interpolated using equation (3.3.5).

(ii)RFRF mixing

The second expansion method is one that just fills the FRFs at unmeasured coordinates with the corresponding FRFs from the FE model of the undamaged structure. As a result, a hybrid FRF vector is formed which will be used as the FRF vector for the location of structural damage.

(iii) System equivalent reduction expansion process (SEREP)

This method was originally derived for mode shape expansion which solely used modal data for expansion. Therefore, in contrast to the dynamic expansion techniques which relied on use of spatial model, the SEREP approach promised a significant departure. While using the SEREP approach for interpolating modal data corresponding to unmeasured coordinates, the basic assumption was that the total modal matrix of a system can be expressed as a linear combination of the eigenvectors corresponding to measured coordinates of the same system. In the present study, the same concept as suggested by SEREP has been used for FRF data. It assumes that the FRF data of the damaged structure at a set of frequency points is a linear combination of the FRF data of the same system for measured coordinates at the same set of frequency points. In this case the transformation matrix may be written as:

$$\left[\left\{\{\alpha_D(\Omega_1)\}_k\right\}_{N\times 1},\ldots\ldots\left\{\{\alpha_D(\Omega_s)\}_k\right\}_{N\times 1}\right]=[TR]\left[\left\{\{\alpha_D(\Omega_1)\}_k\right\}_{m\times 1},\ldots\ldots\left\{\{\alpha_D(\Omega_s)\}_k\right\}_{m\times 1}\right]$$

$$\text{or,}\quad [A_D]_{Nxs} = [TR]_{Nxm}\,[A_D]_{mxs} \tag{3.3.11}$$

where s = number of frequency points at which FRF has been measured.

Here, [TR] may be taken as a global curve fitting function which projects the receptance FRF elements from the group comprising only measured co-ordinates to the complete group. This is exactly what is expected from an expansion process. Besides, it is assumed that the transformation matrix built up using a set of frequency values is valid for all frequency values within that range.

Since the matrix on the left hand side of equation (3.3.11) is not fully known, it is possible to adopt the following approaches for calculating the transformation matrix [TR] in equation (3.3.11).

1.Undamaged structure based (SEREP1)

$$[TR] = [A_{UD}]_{Nxs} [A_{UD}]^{+}_{sxm} \tag{3.3.12}$$

Here, the transformation matrix is built up using the data only from the undamaged structure.

2.Damaged structure based (SEREP2)

$$[TR] = [A_{UD}]_{Nxs} [A_{D}]^{+}_{sxm} \tag{3.3.13}$$

Here, the transformation matrix is built up by multiplying two matrices. The first matrix is built up from data from the undamaged structure and the second one from the damaged structure.

3.Mixing data of damaged and undamaged structure (SEREP3)

In this approach the matrix on the left hand side of equation (3.3.11) is written as a mixture of data from the damaged and undamaged structure. This essentially means that each column of the above mentioned matrix comprises two parts: the first part corresponds to coordinates which have been measured and the second part corresponds to unmeasured coordinates whose value have been approximated by the corresponding values for the undamaged structure.

$$[A_{MIX}]_{Nxs} = \begin{bmatrix} [A_D]_{mxs} \\ [A_{UD}]_{(N-m)xs} \end{bmatrix}$$

Hence the transformation matrix in this case may be written as:

$$[TR] = \left[A_{MIX}\right]_{N\times s}\left[A_{UD}\right]^{+}_{s\times m} \tag{3.3.14}$$

4.Mixing damaged and undamaged structure (SEREP4)

For this case the transformation matrix may be defined as:

$$[TR] = \left[A_{MIX}\right]_{N\times s}\left[A_{D}\right]^{+}_{s\times m} \tag{3.3.15}$$

Once these transformation matrix [TR] has been formed using one of the approaches described above, it can be used to compute the RFRF corresponding to the unmeasured coordinates for the damaged structure using equation (3.3.11).

3.4. RESULTS OF NUMERICAL SIMULATIONS

In this section numerical studies have been carried out based on a 12 DOF mass-spring system (figure 3.2) and a truss structure (figure 3.3) to examine the effectiveness of the damage location theory presented in this chapter.

The 12 DOF mass-spring system shown in figure 3.2 is used to demonstrate the damage location algorithm in conjunction with the various expansion methods discussed in this chapter. The mass and stiffness matrices corresponding to the undamaged case of this system are given in Tables 3.1 and 3.2. It is assumed that the mass matrix remains unchanged as a result of damage while the stiffness matrix is changed as given in Table 3.3. The expansion methods were evaluated for two cases: (I) no noise is present in the simulated 'measured' FRF data and (II) random noise of 4% is incorporated in the FRF data to resemble a practical application.

For each of these two cases, subcases have been studied by including and not including the adjacent coordinates, between where the damage was located, in the list of measured coordinates. A three dimensional graph entitled 3-D Damage Location Plot has been plotted for each of the case and subcase to indicate the location of damage in the system. In the graph, the x-axis indicates DOFs, the y-axis represents the frequency range and the z-axis shows values describing the damage location. The frequency range used in this numerical simulation spans from 20 rad/s to 200 rad/s which essentially covers the first four modes of the system.

Case I

In the first case, it was assumed that no noise was present in the measured FRF data. Damage has caused the stiffness between DOFs 7 and 8 to be reduced by 30% of the original value leaving the mass of the system unchanged.

Sub case 1: (co-ordinates included adjacent coordinates between which damage was located.)

This numerical simulation case assumed that measurements were taken at coordinates 1, 2, 3, 5, 7, 8 and 11. Since not all coordinates have been measured, the RFRFs corresponding to unmeasured coordinates were interpolated using the different expansion methods presented in this chapter. The interpolated RFRF data corresponding to each expansion technique was combined with the measured RFRF data and used to locate damage existing in the structure represented. Figures 3.4A to 3.4H represent the 3-D damage location plots obtained by using the damage location algorithm in conjunction with different expansion methods discussed. Figure 3.4A represents the case in which D.E A was the expansion technique used. It clearly shows that the location of damage was between DOFs 7 and 8, since there was a consistent peak between DOFs 7 and 8 running over the entire frequency range. At certain frequency points there is a crest. However, by using a frequency range, damage location appears consistently. This highlights the advantage of using FRF data over other data for damage location.

Figures 3.4B to 3.4D represent cases where the method of expansion used were D.E B, D.E C and RFRF mixing. However none of these figures show the correct location of damage. Of the three cases, D.E C is more preferable, since in this case a peak can be located in the region of damage although it is still not comparable to D.E A. Figures 3.4E to 3.4H represents the cases using SEREP1 to SEREP4 as expansion methods, but the 3D graph obtained completely fails to indicate the location of damage.

Therefore, in this particular case, D.E A and to certain extent D.E C can be identified as methods working reasonably well when RFRF values interpolated for unmeasured coordinate are used in conjunction with measured RFRF data to locate damage.

Sub case 2: (measured coordinates exclude coordinates between which damage is located.)

In this case, the situation was identical to subcase 1 except that the measured coordinates here were 1, 2, 3, 6 8, 11 and 12. This meant one of the co-ordinates between which damage was located (coordinate 7 in this case) was not measured. Using D.E A, the damage location results obtained have been plotted in figure 3.5A. Again the peaks consistently occured at DOFs 6 and 8. Although the DOFs affected due to damage were 7 and 8, the results shown in figure 3.5A pinpoints the location of damage between DOFs 6 and 8. This is a reasonable result, since DOFs 6 and 8 were the measured coordinates closest to the location of the damage. FRF data at DOF 7 have been interpolated by using data corresponding to undamaged structure and therefore it cannot reflect damage. Thus the peaks occured at the nearest measured coordinate with respect to damage. It was also found that if the measured coordinates had been 1, 3, 11 and 12 (neither DOF 7 nor 8 measured), then this method indicates the location of damage between DOFs 3 and 11, which are the nearest measured coordinates with respect to the damage. However, in the high frequency region the situation deteriorates and the reasons will be explained in Section 3.5.

Figure 3.5B represents the results plotted for D.E B. The results indicate that the location of damage was between DOFs 7 and 9. This result may appear to be encouraging, but it was obtained when the number of measured coordinates was greater than the number of unmeasured coordinates. For situations where the number of measured coordinates was less than the number of unmeasured coordinates, which is most often the case, the results dramatically worsen. Therefore, D.E B may not be regarded as a very reliable method to interpolate FRF data to be used subsequently for damage location. Figure 3.5C plots the result when using D.E C, and from the figure the location of damage can be roughly estimated to be lying between DOFs 6 and 8 which were the nearest measured coordinates. Figure 3.5D is the 3D graph obtained using the FRF mixing method from which no indication can be obtained regarding the location of damage. The results obtained using SEREP1 to SEREP4 have been plotted in figures 3.5E to 3.5H. However, using these figures, no estimate can be made regarding location of damage.

As in subcase 1, D.E A seems to be the best choice for interpolating RFRF for unmeasured coordinates to locate damage. Although not as good, the results generated using D.E C seems to be the only other alternative as all the remaining methods failed completely to give any indicitation of damage location.

Case II

In this case, measurement noise was simulated by introducing a 4% random error to the amplitude of the real part of the generated FRFs. Since in these examples, the system was undamped, the FRFs had zero imaginary part. For the same system as defined in Tables 3.1, 3.2 and 3.3, subcases 1 and 2 in case I were repeated with the difference that FRF data now contains random noise.

Subcase 1

Assume that measurements at coordinates 1, 2, 3, 5, 7, 8 and 11 has been taken. Figures 3.6A to 3.6C represent the cases where location was attempted after interpolating the unmeasured coordinates using expansion methods D.E A, D.E B and D.E C respectively. Similar to the noise free case, D.E A succeeded in locating the damage clearly, while a reasonable result was achieved using D.E C. In comparison to noise free cases, spurious peaks due to noise can be observed throughout the range. Unlike the peaks due to damage which are consistent over the entire frequency range, the peaks due to noise occured off and on becoming more prominent in regions where the peak due to damage reaches a crest. In general, the peaks due to noise were found to be not as prominent as the peak due to damage. By running the algorithm over a wide frequency range, instead of at a few frequency points, damage could be located easily and with reliability.

Results obtained using D.E B and FRF mixing are plotted in figures 3.6B and 3.6D. Both of them failed to locate the damage. Since the examples with pure data have already shown the uselessness of SEREP in the context of damage location, the results have not been shown here.

For noisy FRF data, the Cumulative Damage Location Vector (CDLV) is an alternative to the 3-D damage location plot for locating damage. For this particular subcase, an attempt was made to locate damage by using the CDLV (using FRF data from frequency points spanning between 20 to 200 rad/s in steps of 1). Using D.E A, D.E B, D.E C and FRF mixing to interpolate the unmeasured coordinates, the CDLV was plotted as given in figures 3.6A/1 to 3.6D/1. From the results obtained, it appears that the CDLV follows the same trend as seen in the 3-D damage location plot. The damage could be readily located when using D.E A as shown in figure 3.6A/1. For

D.E C, a rough estimate can be made as shown in figure 3.6C/1. However, no indication about damage location is available from figures 3.6B/1 and 3.6D/1 which used D.E B and FRF mixing to interpolate unmeasured coordinates.

Subcase 2

As in subcase 2 of case I, measurement at coordinates 1, 2, 3, 6, 8, 11 and 12 were assumed to be available. With noise, the results obtained followed the same trend as for the noisefree case, except that the presence of noise in the measurement caused spurious peaks, thereby making the damage location less distinct. Using D.E A as the expansion method, figure 3.7A indicates the location of damage between DOFs 6 and 8 which were the nearest measured coordinates. In addition to peaks in the region of damage, spurious peaks due to noise were also present but were much less consistent and prominent. In figure 3.7C, D.E C was used for expansion and the results obtained, though clear enough, were less prominent than for D.E A.

For both D.E A and D.E C, the results for damage location progressively deteriorates into the higher frequency region and are consistent with the results obtained for case I subcase 2. Figures 3.7B and 3.7D show the results obtained using D.E B and FRF mixing. RFRF data interpolated using these methods failed altogether to locate damage, as is evident from figures 3.7B and 3.7D. For this subcase too, the CDLV was plotted for D.E A, D.E B, D.E C and FRF mixing as given in figures 3.7A/1, 3.7B/1, 3.7C/1 and 3.7D/1 respectively. Like using 3-D damage location plot, the CDLV also indicated the location of damage between DOFs 6 and 8 when using D.E A (figure 3.7A/1) and an approximate damage location when using D.E C (figure

3.7C/1). The CDLV generated using D.E B and FRF mixing provides no indication of damage location.

To summarize, D.E A is the most promising method among all methods studied for interpolating FRF data corresponding to unmeasured coordinates. An alternative is D.E C, although it is not comparable to D.E A in accuracy. All other methods studied for interpolating FRF data have proved to be of no use in the context of damage location. Moreover, in the context of damage location, both the 3-D damage location plot and the CDLV produce similar types of results and hence either of them can be used for successful damage location with noisy data.

For a more thorough evaluation, a truss structure as shown in figure 3.3 was modelled and damage location method in conjunction with D.E A for interpolating unmeasured coordinates was attempted on this model. The PAFEC FE data file used to generate the mass and stiffness matrix for this structure is given in Table 3.4. A random error of 4% was incorporated into the amplitude of RFRF data to simulate noise. The error was introduced into the amplitude of the RFRF data which did not have an imaginary part since it was assumed that the system was undamped.

The structure was modelled using PAFEC FE software. The element type selected during this modelling was element number 34400 in the PAFEC routine. This particular element has three DOFs at each node which are all translational. For this particular truss structure, it is assumed that nodes 1 and 2 were totally encastered. For the remaining nodes movement was allowed in the

X- and Y- direction only. Each element was assumed to have a cross sectional area of .0002 m^2 with IYY equal to 1.666E-9 m^4 and IZZ equal to 6.666E-9 m^4.

The material selected for the structure had a Young's Modulus of 209E+4 N/m^2, Poisson's ratio of 0.3 and density of 7860 kg/m^3. The horizontal and vertical members of the truss structure each has a length of 0.1 m and the diagonal elements have a length of 0.14 m each. Mass and stiffness matrices of the structure were generated using PAFEC FE software. In this particular study, two damage cases were simulated seperately.

(1) The horizontal member between Nodes 7 and 8 have been damaged.
(2) The diagonal member between Nodes 8 and 9 have been damaged.

In both the cases, damage was simulated by changing the Young's Modulus of that particular member by 40% to ensure that only the stiffness is affected. The mass of the structure was not altered as structural damage was supposed to affect the stiffness of the structure much more significantly than mass.

For each of these two cases, subcases were studied by varying the coordinates measured. For case 1, three subcases have been studied each having the measured coordinates:

(I) 3-x, 4-x, 6-x, 7-x, 8-x, 9-x, 10-x, 14-y.
(II) 3-x, 4-x, 6-x, 7-x, 8-y, 9-x, 10-x, 14-y.
(III) 3-x, 4-x, 6-x, 7-x, 10-x, 14-y.

For case2, the subcases studied had the following measured coordinates:

(I) 3-x, 4-x, 5-x, 6-x, 7-x, 8-x, 8-y, 9-x, 9-y, 12-x, 13-x, 14-x

(II) 3-x, 4-x, 5-x, 6-x, 7-x, 8-x, 9-x, 10-x, 11-x, 12-x, 13-x, 14-x

(III) 3-x, 3-y, 4-y, 5-y, 6-y, 7-y, 8-y, 9-y, 10-y, 11-y, 12-y, 14-y.

Since the dynamic stiffness matrix of this particular structure was not tri-diagonal, the data interpolated using D.E A cannot be used successfully to locate damage unless the measured coordinates include 7-x, 7-y, 8-x and 8-y (i.e coordinates between which the damage was located). The reason behind that has been explained later in in Section 3.5. Figures 3.8B and 3.8C plots the 3-D damage location plot when the measured coordinates were as given in subcase II and III for case 1 and were in agreement with the above conclusions. Neither of these two results indicates the location of damage successfully.

However, figure 3.8A which shows the results corresponding to measured coordinates as for subcase I case 1, demonstrates successful location of damage, (using D.E A to interpolate data corresponding to unmeasured coordinate) even when the measured coordinates excluded 7-y and 8-y. In contrast, when the damaged member is the diagonal member between nodes 8 and 9, the damage location plot given in figure 3.9A succeeded in locating the damage only for subcase I case 2 when the measured coordinates included 8-x, 8-y, 9-x and 9-y. For both subcases II and III in case 2, the damage location plots given in figures 3.9B and 3.9C respectively do not provide any idea about damage location.

On comparing cases 1 and 2 for the truss structure, it is clear that when the damaged member between nodes 7 and 8 is a horizontal one, damage could be located even when measurement had not been taken at 7-y and 8-y which are at right angles to the orientation of the member. However, when the damage affected the diagonal member situated between nodes 8 and 9, measurements were required at 8-x, 8-y, 9-x and 9-y to indicate damage location. From this it appears, that the orientation of a particular member plays a significant role in deciding the direction of measurement for a particular node. This fact can be explained by considering that for the horizontal truss member in this example, the component of displacement in the vertical direction was negligible. Therefore, by not using actual measurement in the direction 7-y and 8-y, the error introduced in the the damage location vector at a particular frequency was too small to affect the ultimate result.

On the contrary, the diagonal member considered in case 2 for the truss structure, has a significant component of displacement in both the x- and y-direction. This results in a significant error in the damage location vector if any of these are not measured. Since the member 7-8 is oriented in x-direction it is more important to measure translational displacement in the x- direction than in any other direction for this particular member and for the diagonal member 8-9, measurement in both the -x and -y direction for both coordinates 8 and 9 has to be taken to ascertain the damage location

3.5 ANALYSIS OF NUMERICAL RESULTS

It is apparent from the numerical studies that except for D.E A, none of the expansion methods investigated in this work can be accepted as working satisfactorily in locating damage. Using a suitable expansion method, it was possible to interpolate the RFRF data corresponding to the unmeasured coordinates in the damaged structure. However, due to limitations of the existing expansion methods, in most cases the interpolated FRF data are different from the FRF data otherwise measured resulting in a difference which can be referred to as 'Expansion Errors'. The effect of inaccuracy in FRF data introduced due to expansion error has been found to be much more substantial than that due to measurement noise.

Of the different expansion methods studied, the only method which worked consistently well in locating damage was the D.E A. It was found that for cases where the measured coordinate included the coordinates between which damage was located, this damage location method in conjunction with D.E A for interpolating values for unmeasured coordinate worked successfully in locating damage. However for cases, where the measured coordinates excluded the coordinates where damage was located, the method worked successfully only if the dynamic stiffness matrix of the model was effectively a tri-diagonal matrix with other elements outside the tri-diagonal band appreciably smaller than those inside the band. The model (in figure 3.2) used in this study satisfied the above constraint at lower frequencies.

The reason these methods successfully located damage in such cases was because the number of unknowns in a particular equation derived from equation (3.3.5) was either two or at the most three due to tridiagonality of the dynamic stiffness matrix. As a result, the two measured coordinates which were nearest to the location of damage acted as a barrier and ensured only the receptance interpolated for coordinates within this barrier were erroneous. Consequently, the receptance for coordinates outside this barrier were interpolated correctly.

However, if the dynamic stiffness matrix was not tri-diagonal, then one coordinate may have been connected to more than two coordinates.

In such cases, the error due to interpolation could not be restricted within the limit mentioned above but spread to almost all the interpolated co-ordinates. As a result, the damage location method would fail to indicate the damage when using such receptance. To elaborate the above explanation further, an eight DOF structure was used for which the dynamic stiffness matrix of the undamaged structure was given by $[Z(\Omega)]_{UD}$ and it was assumed that the only damage was located between coordinates two and three, represented by $[\Delta Z(\Omega)]$. Let the measured coordinates on the damaged structure be 1, 3, 5, 7. Without losing generality, it is assumed that the first column of receptance had been measured. Hence, $\alpha_{D,11}(\Omega)$ $\alpha_{D,31}(\Omega)$, $\alpha_{D,51}(\Omega)$ and $\alpha_{D,71}(\Omega)$ were measured and were known.

As $\Delta\alpha(\Omega) = \alpha_D(\Omega) - \alpha_{UD}(\Omega)$,

it was possible to compute $\Delta\alpha_{11}(\Omega)$, $\Delta\alpha_{31}(\Omega)$, $\Delta\alpha_{51}(\Omega)$ and $\Delta\alpha_{71}(\Omega)$. However, $\Delta\alpha_{21}(\Omega)$, $\Delta\alpha_{41}(\Omega)$, $\Delta\alpha_{61}(\Omega)$ and $\Delta\alpha_{81}(\Omega)$ were obtained by expansion using equation (3.3.5). If $[Z(\Omega)]_{UD}$ is represented by equation (3.5.1) as given next:

$$Z(\Omega)]_{UD} = \begin{bmatrix} a_1 & b_1 & c_1 & d_1 & e_1 & f_1 & g_1 & h_1 \\ b_1 & b_2 & c_2 & d_2 & e_2 & f_2 & g_2 & h_2 \\ c_1 & c_2 & c_3 & d_3 & e_3 & f_3 & g_3 & h_3 \\ d_1 & d_2 & d_3 & d_4 & e_4 & f_4 & g_4 & h_4 \\ e_1 & e_2 & e_3 & e_4 & e_5 & f_5 & g_5 & h_5 \\ f_1 & f_2 & f_3 & f_4 & f_5 & f_6 & g_6 & h_6 \\ g_1 & g_2 & g_3 & g_4 & g_5 & g_6 & g_7 & h_7 \\ h_1 & h_2 & h_3 & h_4 & h_5 & h_6 & h_7 & h_8 \end{bmatrix} \qquad (3.5.1)$$

then equation (3.3.2) yielded the following eight equations, where the symbol Ω has been omitted from $\Delta\alpha$ to accomodate each of the following equations in a single line:

$$a_1\Delta\alpha_{11} + b_1\Delta\alpha_{21} + c_1\Delta\alpha_{31} + d_1\Delta\alpha_{41} + e_1\Delta\alpha_{51} + f_1\Delta\alpha_{61} + g_1\Delta\alpha_{71} + h_1\Delta\alpha_{81} = 0 \quad (3.5.2)$$

$$b_1\Delta\alpha_{11} + b_2\Delta\alpha_{21} + c_2\Delta\alpha_{31} + d_2\Delta\alpha_{41} + e_2\Delta\alpha_{51} + f_2\Delta\alpha_{61} + g_2\Delta\alpha_{71} + h_2\Delta\alpha_{81} = X \quad (3.5.3)$$

$$c_1\Delta\alpha_{11} + c_2\Delta\alpha_{21} + c_3\Delta\alpha_{31} + d_3\Delta\alpha_{41} + e_3\Delta\alpha_{51} + f_3\Delta\alpha_{61} + g_3\Delta\alpha_{71} + h_3\Delta\alpha_{81} = Y \quad (3.5.4)$$

$$d_1\Delta\alpha_{11} + d_2\Delta\alpha_{21} + d_3\Delta\alpha_{31} + d_4\Delta\alpha_{41} + e_4\Delta\alpha_{51} + f_4\Delta\alpha_{61} + g_4\Delta\alpha_{71} + h_4\Delta\alpha_{81} = 0 \quad (3.5.5)$$

$$e_1\Delta\alpha_{11} + e_2\Delta\alpha_{21} + e_3\Delta\alpha_{31} + e_4\Delta\alpha_{41} + e_5\Delta\alpha_{51} + f_5\Delta\alpha_{61} + g_5\Delta\alpha_{71} + h_5\Delta\alpha_{81} = 0 \quad (3.5.6)$$

$$f_1\Delta\alpha_{11} + f_2\Delta\alpha_{21} + f_3\Delta\alpha_{31} + f_4\Delta\alpha_{41} + f_5\Delta\alpha_{51} + f_6\Delta\alpha_{61} + g_6\Delta\alpha_{71} + h_6\Delta\alpha_{81} = 0 \quad (3.5.7)$$

$$g_1\Delta\alpha_{11} + g_2\Delta\alpha_{21} + g_3\Delta\alpha_{31} + g_4\Delta\alpha_{41} + g_5\Delta\alpha_{51} + g_6\Delta\alpha_{61} + g_7\Delta\alpha_{71} + h_7\Delta\alpha_{81} = 0 \quad (3.5.8)$$

$$h_1\Delta\alpha_{11} + h_2\Delta\alpha_{21} + h_3\Delta\alpha_{31} + h_4\Delta\alpha_{41} + h_5\Delta\alpha_{51} + h_6\Delta\alpha_{61} + h_7\Delta\alpha_{71} + h_8\Delta\alpha_{81} = 0 \quad (3.5.9)$$

Because the unmeasured coordinates were 2, 4, 6, 8, equations (3.5.3), (3.5.5), (3.5.7) and (3.5.9) were used for solving the receptance of unmeasured coordinates. However, since the values on the right hand side of the above equations (equations 3.5.2 to 3.5.9) were not known, it was assumed that they were all zero. Therefore in this case it is apparent that this assumption resulted in incorrect value for the right hand side of equation (3.5.3) although it was correct for equations (3.5.5), (3.5.7) and (3.5.9). Due to the wrong assumption regarding the right hand side of equation (3.5.3), the data interpolated for $\Delta\alpha_{21}(\Omega)$, $\Delta\alpha_{41}(\Omega)$, $\Delta\alpha_{61}(\Omega)$ and $\Delta\alpha_{81}(\Omega)$ were also erroneous.

However, it may be noted at this point that if the measured coordinates included the adjacent coordinate between which damage was located, then all the interpolated values would be correct. To illustrate such a situation, if it was assumed that $\alpha_{11}(\Omega)$, $\alpha_{21}(\Omega)$ and $\alpha_{31}(\Omega)$ were measured, then the equations selected for interpolating the unknown receptance would be equations (3.5.5) to (3.5.9) and since the assumption regarding the right hand side of these equations were correct, the interpolated values using these equations would be accurate.

Once the values were interpolated, they were put back into equations (3.2.7) or (3.2.20) to locate damages. It is apparent in this case that when the measured coordinates were 1, 3, 5, 7 the second, fourth, sixth and eighth rows would be zero, since they had been equated to zero to interpolate the receptance for unmeasured coordinates. However, when the wrongly interpolated values were put back into first, third, fifth and seventh rows which corresponded to measured coordinates, it changed the actual values for these rows. Consequently, the damage location vector took a form which had non-zero values in all the elements that corresponded to measured coordinates and zero values for rows corresponding to unmeasured coordinates. In this particular case, the first, third, fifth and seventh elements would return non-zero values with the remaining elements being zero.

However, if the model was for a chain system with tri-diagonal dynamic stiffness matrix, then equations (3.5.2) to (3.5.9) becomes:

$$a_1\Delta\alpha_{11}(\Omega) + b_1\Delta\alpha_{21}(\Omega) = 0 \tag{3.5.10}$$

$$b_1\Delta\alpha_{11}(\Omega) + c_1\Delta\alpha_{21}(\Omega) + d_1\Delta\alpha_{31}(\Omega) = X_1 \tag{3.5.11}$$

$$d_1\Delta\alpha_{21}(\Omega) + e_1\Delta\alpha_{31}(\Omega) + f_1\Delta\alpha_{41}(\Omega) = Y_1 \tag{3.5.12}$$

$$f_1\Delta\alpha_{31}(\Omega) + g_1\Delta\alpha_{41}(\Omega) + h_1\Delta\alpha_{51}(\Omega) = 0 \tag{3.5.13}$$

$$h_1\Delta\alpha_{41}(\Omega) + i_1\Delta\alpha_{51}(\Omega) + j_1\Delta\alpha_{61}(\Omega) = 0 \tag{3.5.14}$$

$$j_1\Delta\alpha_{51}(\Omega) + k_1\Delta\alpha_{61}(\Omega) + l_1\Delta\alpha_{71}(\Omega) = 0 \tag{3.5.15}$$

$$l_1\Delta\alpha_{61}(\Omega) + m_1\Delta\alpha_{71}(\Omega) + n_1\Delta\alpha_{81}(\Omega) = 0 \tag{3.5.16}$$

$$n_1\Delta\alpha_{71}(\Omega) + p_1\Delta\alpha_{81}(\Omega) = 0 \tag{3.5.17}$$

Here, if the measured coordinates were 1, 4, 6 then the equations selected for interpolating the $\Delta\alpha(\Omega)$ for the remaining coordinates would be equations (3.5.11), (3.5.12), (3.5.14), (3.5.16) and (3.5.17). Hence due to the wrong assumption regarding right hand side of equations (3.5.11) and (3.5.12), $\Delta\alpha_{21}(\Omega)$ and $\Delta\alpha_{31}(\Omega)$ had wrongly interpolated values. However the effect of wrong values did not fall on equations (3.5.14), (3.5.16) and (3.5.17) and the values obtained for unknowns in these equations were correct.

Therefore, while calculating the 'Damage Location Vector' $\{\beta(\Omega)\}$ only the first and fourth rows which contained wrongly interpolated $\Delta\alpha_{21}(\Omega)$ and $\Delta\alpha_{31}(\Omega)$ returned non-zero values indicating damage location between DOFs 1 and 4 which were the nearest measured coordinates with respect to damage. Since the right hand side of equations (3.5.11), (3.5.12), (3.5.14), (3.5.16) and (3.5.17) were to be zero while interpolating unknown values, all these rows in the 'Damage Location Vector' would also be zero. Regarding the sixth row, since the values interpolated for $\Delta\alpha_{51}(\Omega)$ and $\Delta\alpha_{71}(\Omega)$ were correct, it also returned correct values.

From the above discussions, it may be said that if any model had a tri-diagonal dynamic stiffness matrix (i.e similar to a chain model) then the interpolated receptance data obtained by the D.E A can be used successfully to locate errors. For any model to have a tridiagonal dynamic stiffness matrix, the following conditions need to be satisfied:

(i) stiffness matrix must be tridiagonal
(ii) mass matrix must be lumped.

However for models which have a tridiagonal stiffness matrix and a consistent mass matrix, the dynamic stiffness matrix is not tridiagonal. The elements outside the tridiagonal band in the dynamic stiffness matrix are due to the effect of elements of the mass matrix which lie outside the tridiagonal band in the mass matrix, and the frequency at which dynamic stiffness matrix is calculated. Even in such cases, if in the dynamic stiffness matrix the elements outside the tridiagonal band are very small compared to those inside the band, then they can be effectively ignored without introducing any appreciable error. Consequently, in such cases the dynamic stiffness matrix can be looked upon as a tri-diagonal one. However, in order to ensure that the elements outside the tri-diagonal band in the dynamic stiffness are small enough to be neglected the following conditions need to be satisfied:

i) the stiffness connecting the DOFs has a magnitude which is quite large compared to the magnitude of the mass of the DOFs;

ii) dynamic stiffness matrix must be measured at very low values of frequency.

In the dynamic stiffness matrix if the value of Ω is large, it will push up the value of $\Omega^2[M]$ even if the elements in matrix [M] are small. In such a case, the terms outside the tridiagonal band may not be small enough to be neglected. Although in such cases the best results are obtained if Ω is zero, but even for small values of Ω the method works, because the elements outside the tridiagonal band in the dynamic stiffness matrix still remain small enough compared to elements inside the band that they can be neglected.

3.6 SUMMARISING REMARKS

A method has been presented to locate damage in a structure using measured Frequency Response Function (FRF) data. In addition, an attempt has been made to study the effectiveness of the method in handling FRF data containing measurement noise and expansion error.

A major problem associated with using measured vibration data for locating structural damage is the effect of noise on such data. Because of this, it was often found that it becomes very difficult to identify the actual location of damage. The 3 dimensional Damage Location Plot and the Cumulative Damage Location Vector suggested in this chapter provides a useful technique for identifying the actual location of damage when using noisy data. The use of the FRF data instead of modal data in these techniques provide the user with an abundance of data. By using these data over a wide frequency band, the more prominent peaks due to damage can be easily identified from the spurious peaks occurring due to noise in the 3 dimensional Damage Location Plot. The summation effect in the CDLV helps to magnify the peaks caused by damage, making their identification easier.

In addition to noise in the data, the problem of coordinate incompleteness as discussed in Chapter 1 is another problem faced while attempting to locate structural damage using vibration data. The expansion methods commonly used to tackle the problem of coordinate incompleteness while using modal data were used here for expanding FRF data. The suitability of the expanded FRF data in the context of damage location was examined. A comparitive study of the different expansion methods from the point of damage location has also been carried out. Based on the study carried out in this work, it appears that D.E A is the most suitable expansion method in the context of damage location. However, when the measured coordinates do not include the coordinates between which damage is located, it was found that the data obtained using D.E A produces reliable results in the low frequency region and for certain types of structures.

1	0	0	0	0	0	.9	0	0	0	0	0
0	1	0	0	0	0	0	.9	0	0	0	0
0	0	1	0	0	0	0	0	.9	0	0	0
0	0	0	1	0	0	0	0	0	.9	0	0
0	0	0	0	1	0	0	0	0	0	.9	0
0	0	0	0	0	1	0	0	0	0	0	.9
.9	0	0	0	0	0	1	0	0	0	0	0
0	.9	0	0	0	0	0	1	0	0	0	0
0	0	.9	0	0	0	0	0	1	0	0	0
0	0	0	.9	0	0	0	0	0	1	0	0
0	0	0	0	.9	0	0	0	0	0	1	0
0	0	0	0	0	.9	0	0	0	0	0	1

Table 3.1: Mass matrix of the undamaged/damaged system in Fig.3.2

60000	-30000	0	0	0	0	0	0	0	0	0	0
-30000	60000	-30000	0	0	0	0	0	0	0	0	0
0	-30000	50000	-20000	0	0	0	0	0	0	0	0
0	0	-20000	50000	-30000	0	0	0	0	0	0	0
0	0	0	-30000	50000	-20000	0	0	0	0	0	0
0	0	0	0	-20000	50000	-30000	0	0	0	0	0
0	0	0	0	0	-30000	50000	-20000	0	0	0	0
0	0	0	0	0	0	-20000	50000	-30000	0	0	0
0	0	0	0	0	0	0	-30000	60000	-30000	0	0
0	0	0	0	0	0	0	0	-30000	60000	-30000	0
0	0	0	0	0	0	0	0	0	-30000	60000	-30000
0	0	0	0	0	0	0	0	0	0	-30000	60000

Table 3.2: Stiffness matrix of the undamaged system in Fig.3.2

60000	-30000	0	0	0	0	0	0	0	0	0	0
-30000	60000	-30000	0	0	0	0	0	0	0	0	0
0	-30000	50000	-20000	0	0	0	0	0	0	0	0
0	0	-20000	50000	-30000	0	0	0	0	0	0	0
0	0	0	-30000	50000	-20000	0	0	0	0	0	0
0	0	0	0	-20000	50000	-30000	0	0	0	0	0
0	0	0	0	0	-30000	44000	-14000	0	0	0	0
0	0	0	0	0	0	-14000	44000	-30000	0	0	0
0	0	0	0	0	0	0	-30000	60000	-30000	0	0
0	0	0	0	0	0	0	0	-30000	60000	-30000	0
0	0	0	0	0	0	0	0	0	-30000	60000	-30000
0	0	0	0	0	0	0	0	0	0	-30000	60000

Table 3.3: Stiffness matrix of the damaged system in Fig.3.2

```
CONTROL
CONTROL.END
NODES
NODE      X       Y        NODE     X      Y
1         0       0        2        .1     0
3         0       .1       4        .1     .1
5         0       .2       6        .1     .2
7         0       .3       8        .1     .3
9         0       .4       10       .1     .4
11        .2      .3       12       .2     .4
13        .3      .4       14       .3     .4
ELEMENTS
ELEMENT.TYPE = 34400
NUMBER   PROP   TOPOLOGY    NUMBER   PROP   TOPOLOGY
1         1       1 3          2       1      1 4
3         1       2 3          4       1      2 4
5         1       3 5          6       1      3 6
7         1       3 4          8       1      4 5
9         1       4 6          10      1      5 6
11        1       5 7          12      1      5 8
13        1       6 7          14      1      6 8
15        1       7 8          16      1      7 9
17        1       8 9          18      1      7 10
19        1       8 10         20      1      9 10
21        1       10 11        22      1      8 12
23        1       8 11         24      1      10 12
25        1       11 12        26      1      11 13
27        1       12 13        28      1      11 14
29        1       12 14        30      1      13 14
BEAMS
SECTION     MATERIAL    IYY        IZZ        TORS.CONST    AREA
1              11       1.666E-9   6.666E-9   4.6E-9        2.0E-4
MATERIAL
MATERIAL.NUMBER        E        NU      RO
11                  209E4       .3     7860
LOADS
CASE          NODE          DIRECTIONS.OF.LOAD           VALUE.OF.LOAD
1              4                  2                          10
ACTIVE.FREEDOMS
NODE          DIRECTION              PRINT.CONTROL
3                12                       2
R11   1          00                       0
RESTRAINTS
NODE          DIRECTION
1                0
2                0
3                3
R11      1       0
MODES.AND.FREQUENCIES
AUTOMATIC.MASTERS             MODES
0                               10
MASTERS
NODE.NUMBER            DIRECTION
3                          12
R11            1           00
END.OF.DAT
```

Table 3.4: Data file in PAFEC FE for deriving mass and stiffness for truss in fig.3.3

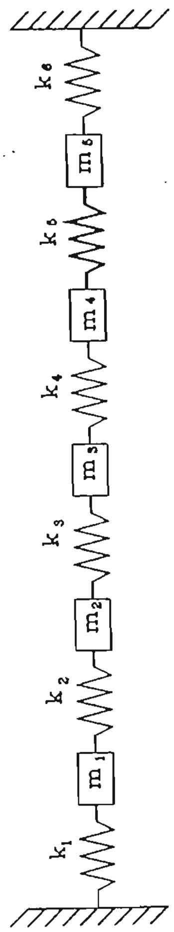

FIG.3.1: A 5 DOF mass-spring system

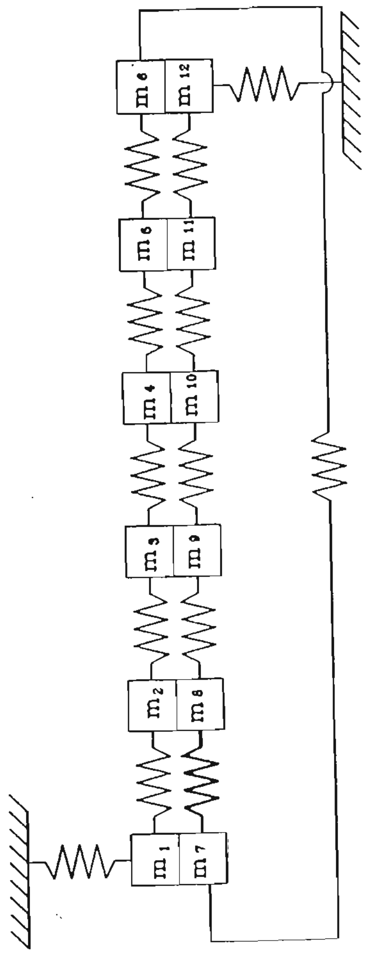

FIG.3.2: A 12 DOF mass-spring system (Model 3.2)

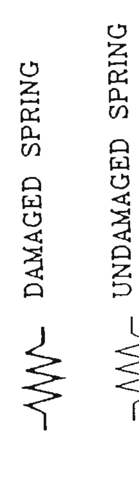

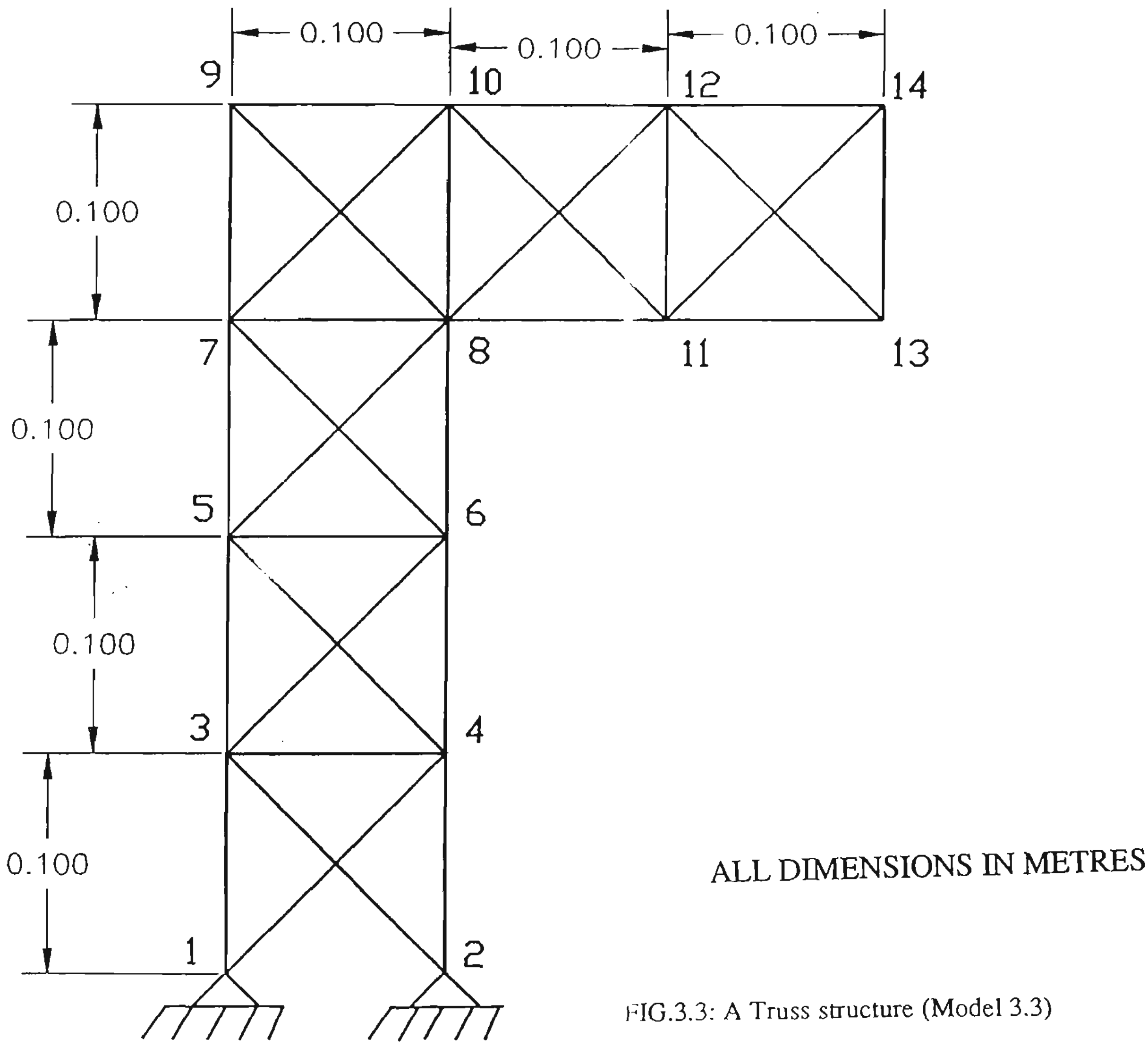

FIG.3.3: A Truss structure (Model 3.3)

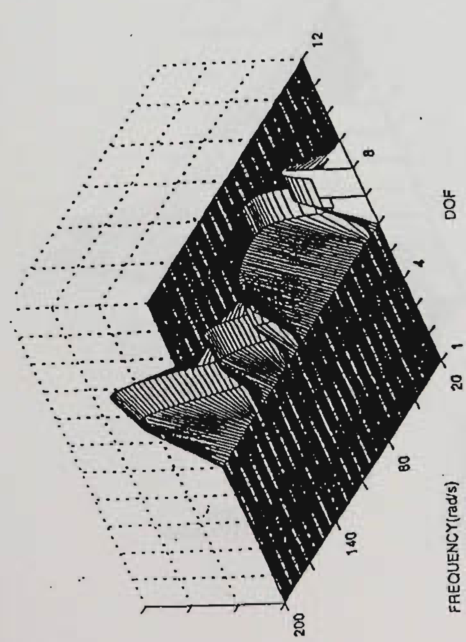

FIG.3.4A: 3-D DLP using D.E A (Case I/ Subcase 1 in section 3.4)

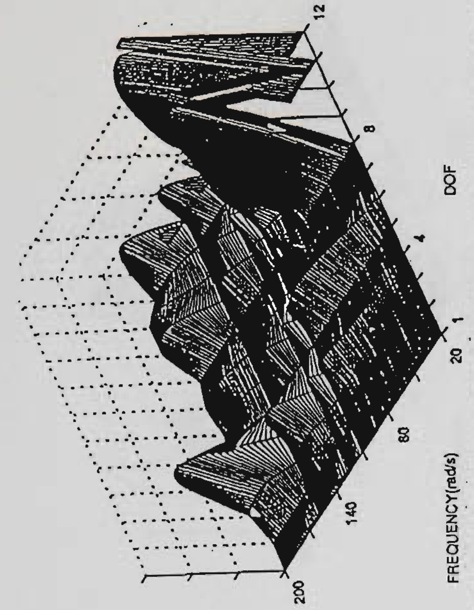

FIG.3.4B: 3-D DLP using D.E B (Case I/ Subcase 1 in section 3.4)

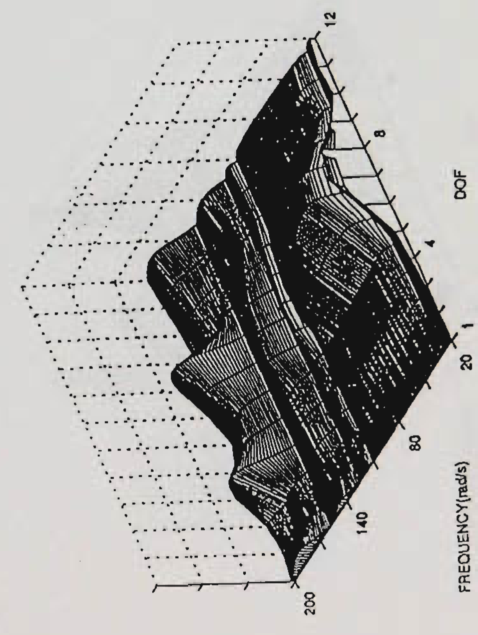

FIG.3.4C: 3-D DLP using D.E C (Case I/ Subcase 1 in section 3.4)

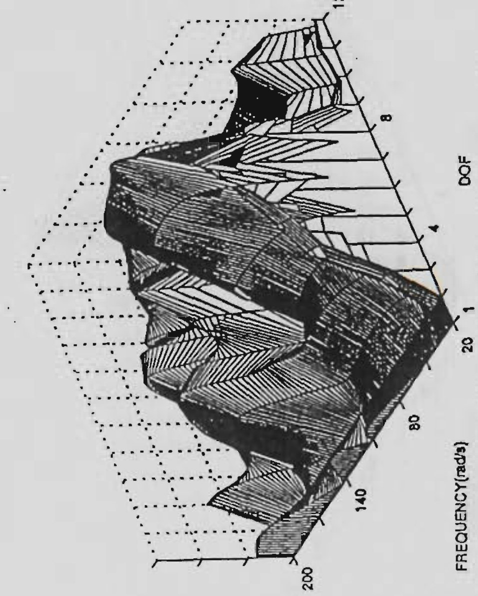

FIG.3.4D: 3-D DLP using RFRF mixing (Case I/ Subcase 1 in section 3.4)

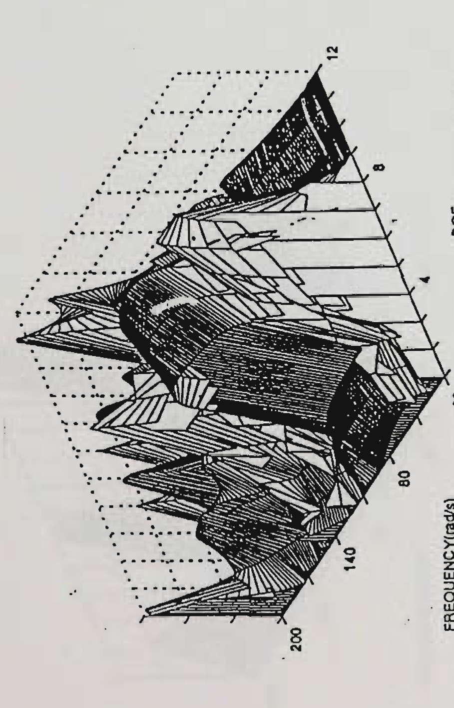

FIG.3.4E: 3-D DLP using SEREP 1 (Case I/ Subcase 1 in section 3.4)

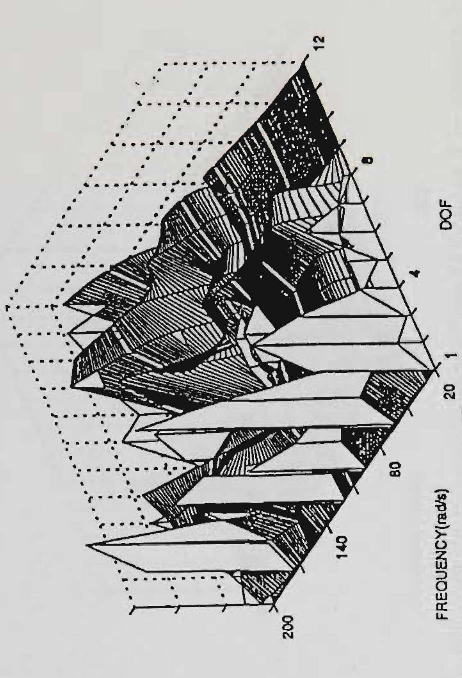

FIG.3.4F: 3-D DLP using SEREP 2 (Case I/ Subcase 1 in section 3.4)

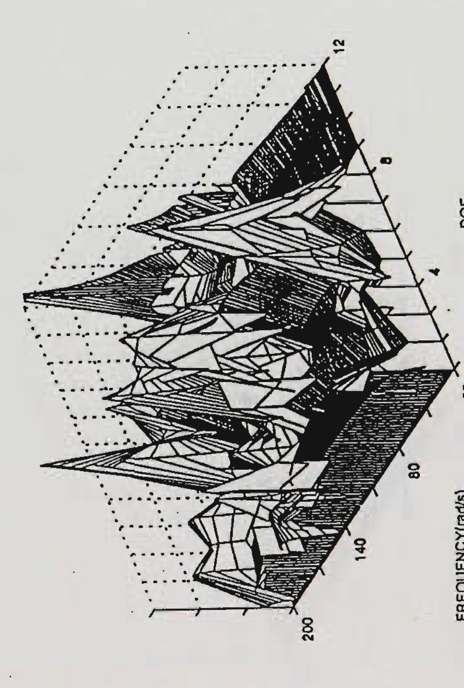

FIG.3.4G: 3-D DLP using SEREP 3 (Case I/ Subcase 1 in section 3.4)

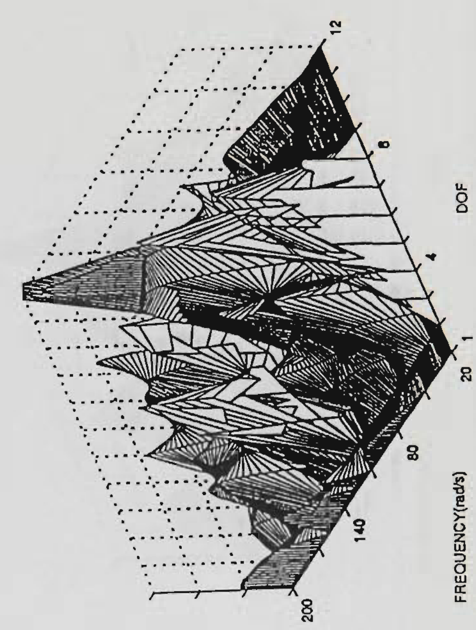

FIG.3.4H: 3-D DLP using SEREP 4 (Case I/ Subcase 1 in section 3.4)

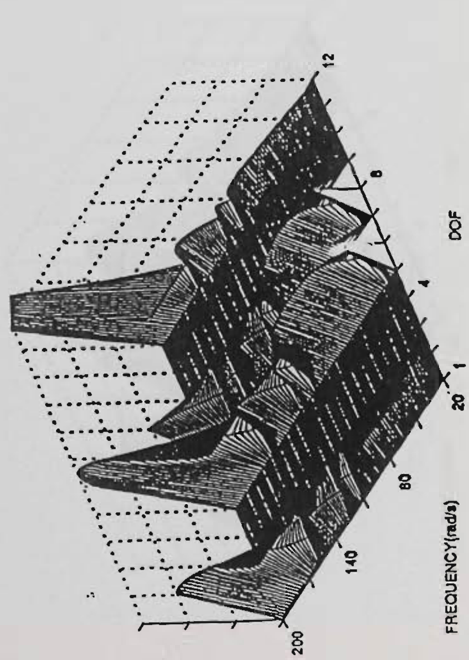

FIG.3.5A: 3-D DLP using D.E A (Case I/ Subcase 2 in section 3.4)

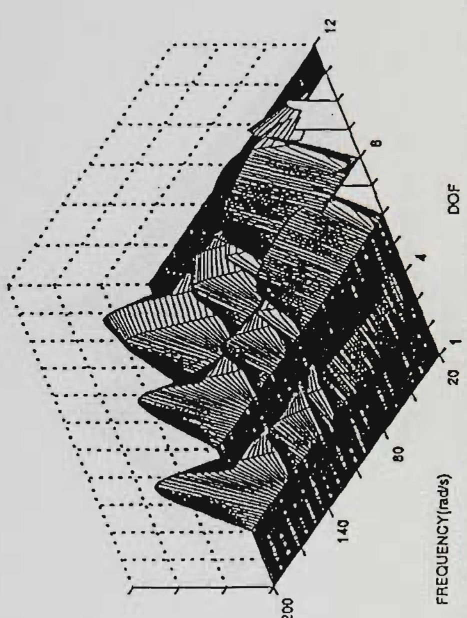

FIG.3.5B: 3-D DLP using D.E B (Case I/ Subcas 2 in section 3.4)

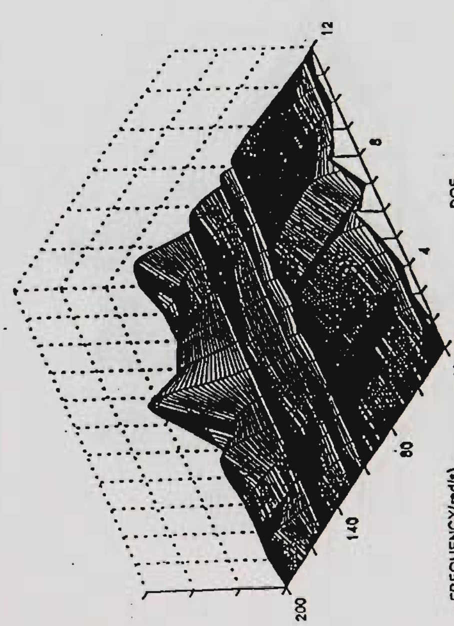

FIG.3.5C: 3-D DLP using D.E C (Case I/ Subcase 2 in section 3.4)

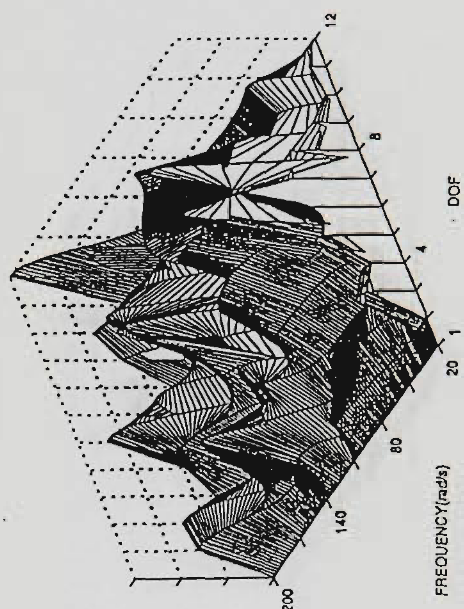

FIG.3.5D: 3-D DLP using RFRF mixing (Case I/ Subcase 2 in section 3.4)

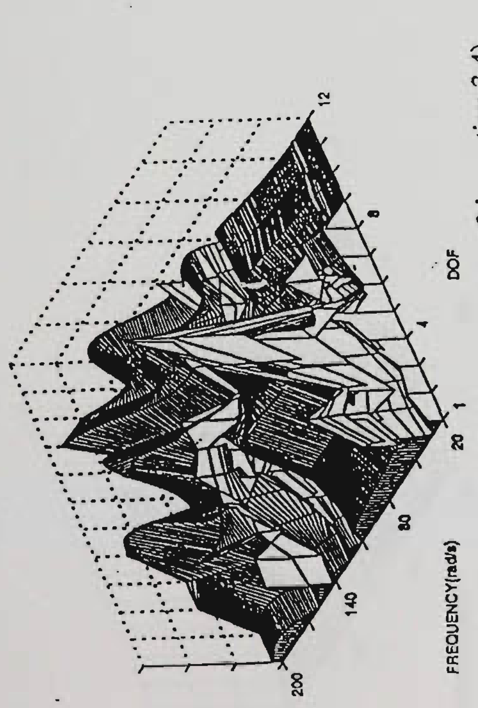

FIG.3.5E: 3-D DLP using SEREP 1 (Case I/ Subcase 2 in section 3.4)

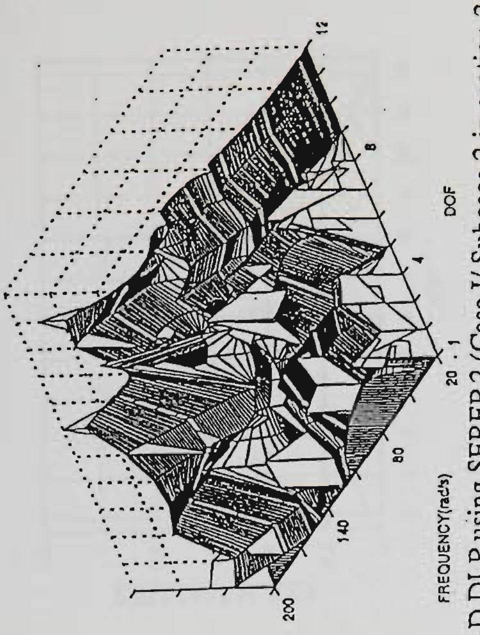

FIG.3.5F: 3-D DLP using SEREP 2 (Case I/ Subcase 2 in section 3.4)

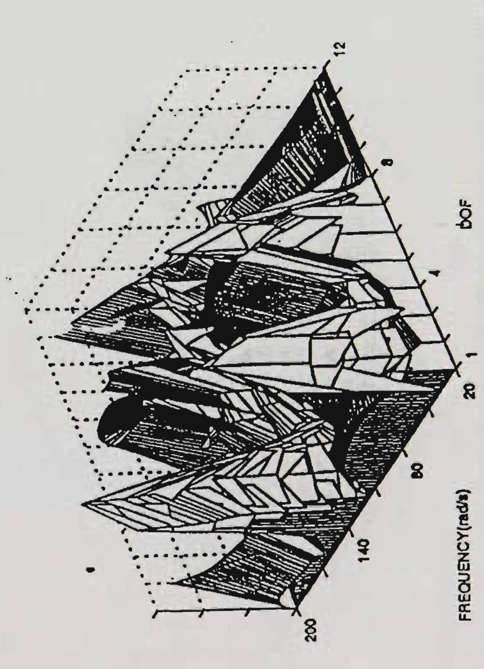

FIG.3.5G: 3-D DLP using SEREP 3 (Case I/ Subcase 2 in section 3.4)

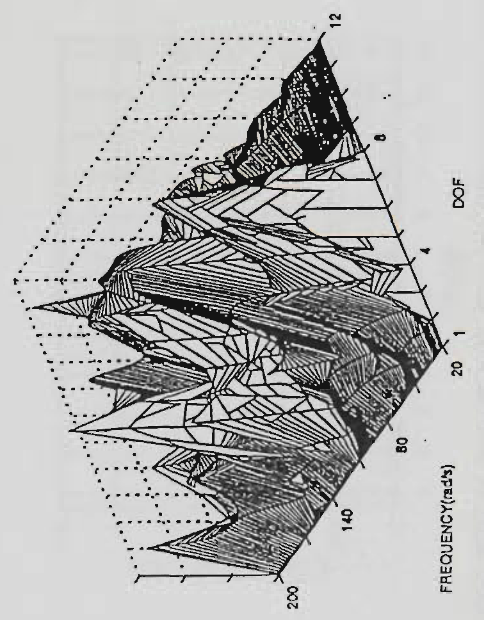

FIG.3.5H: 3-D DLP using SEREP 4 (Case I/ Subcase 2 in section 3.4)

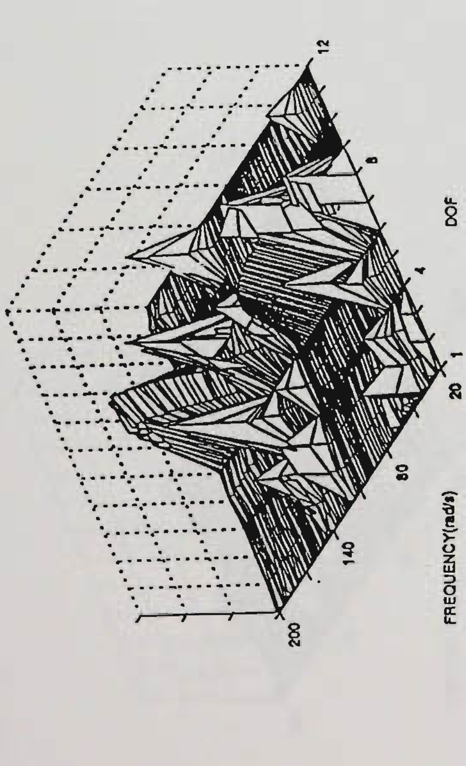

FIG.3.6A: 3-D DLP using D.E A (Case II/ Subcase1 in section 3.4)

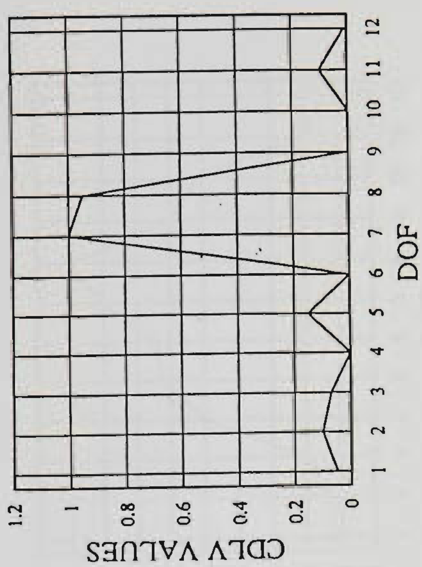

FIG.3.6A/1: CDLV using D.E A (Case II/ Subcase1 in section 3.4)

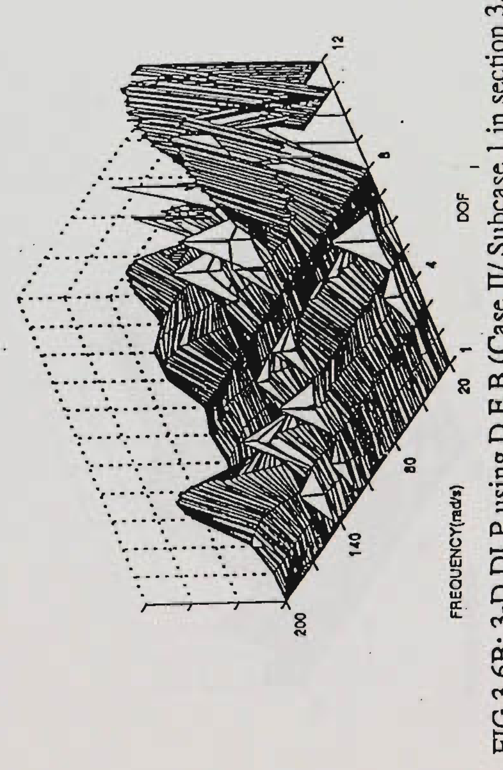

FIG.3.6B: 3-D DLP using D.E B (Case II/ Subcase 1 in section 3.4)

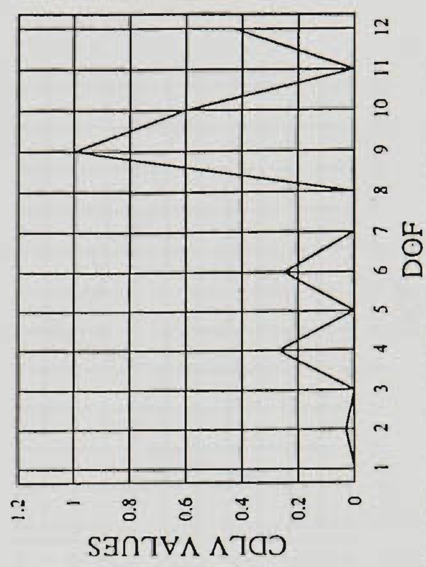

FIG.3.6B/1: CDLV using D.E B (Case II/ Subcase 1 in section 3.4)

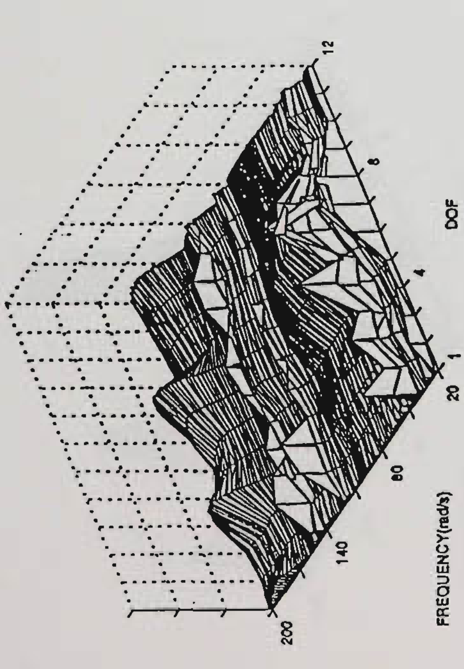

FIG.3.6C: 3-D DLP using D.E C (Case II/ Subcase 1 in section 3.4)

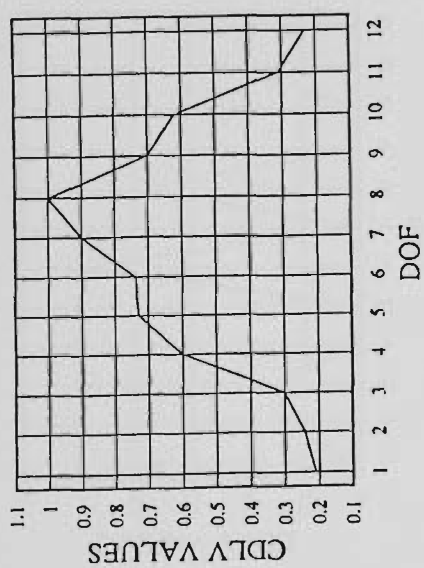

FIG.3.6C/1: CDLV using D.E C (Case II/ Subcase 1 in section 3.4)

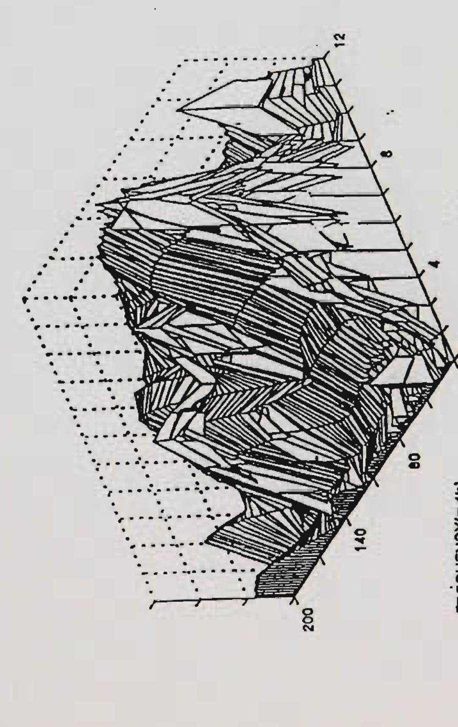

FIG.3.6D: 3-D DLP using RFRF mixing (Case II/ Subcase1 in section 3.4)

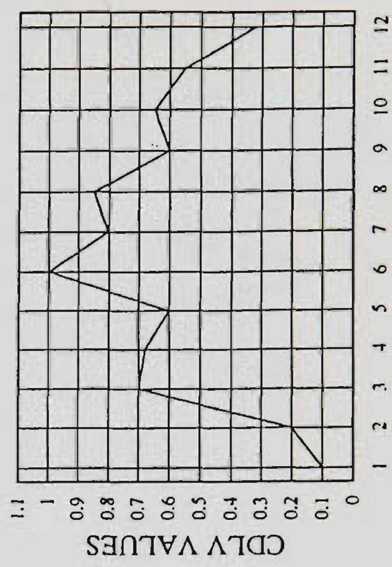

FIG.3.6D/1: CDLV using RFRF mixing (Case II/ Subcase1 in section 3.4)

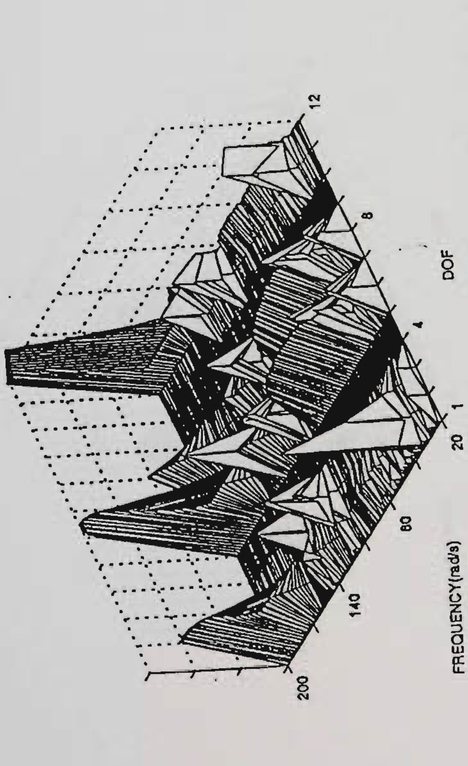

FIG.3.7A: 3-D DLP using D.E A (Case II/ Subcase 2 in section 3.4)

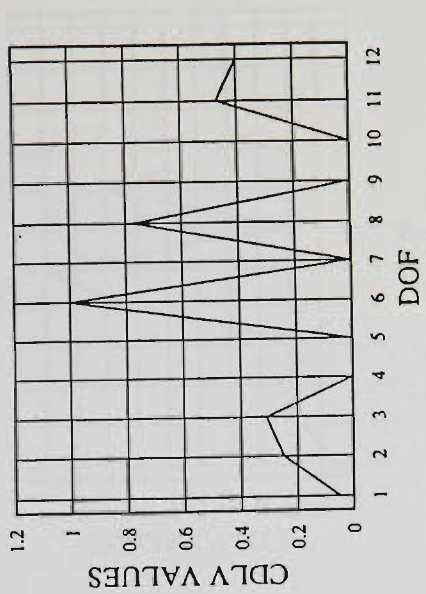

FIG.3.7A/1: CDLV using D.E A (Case II/ Subcase 2 in section 3.4)

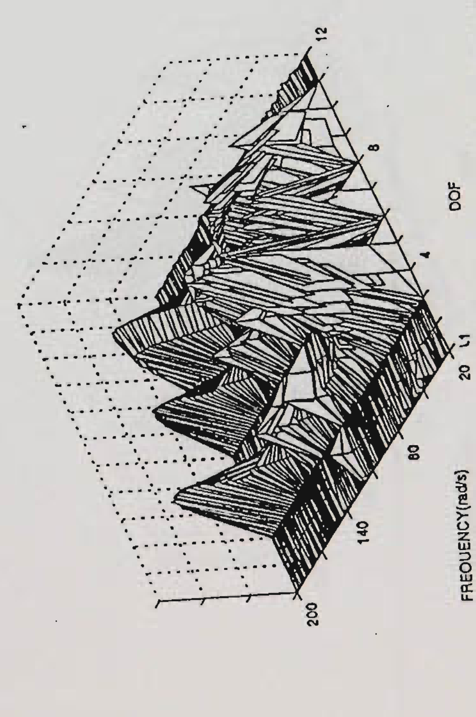

FIG.3.7B: 3-D DLP using D.E B (Case II/ Subcase 2 in section 3.4)

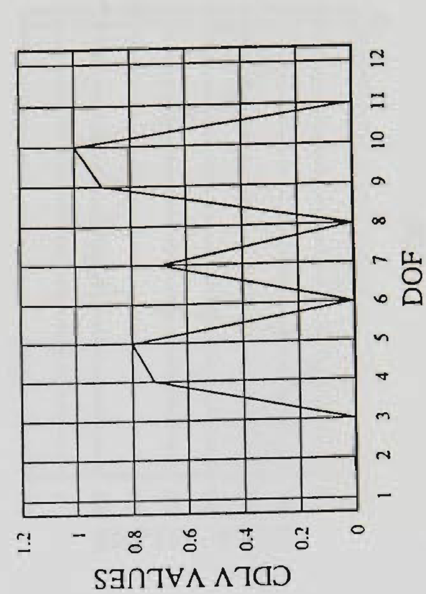

FIG.3.7B/1: CDLV using D.E B (Case II/ Subcase 2 in section 3.4)

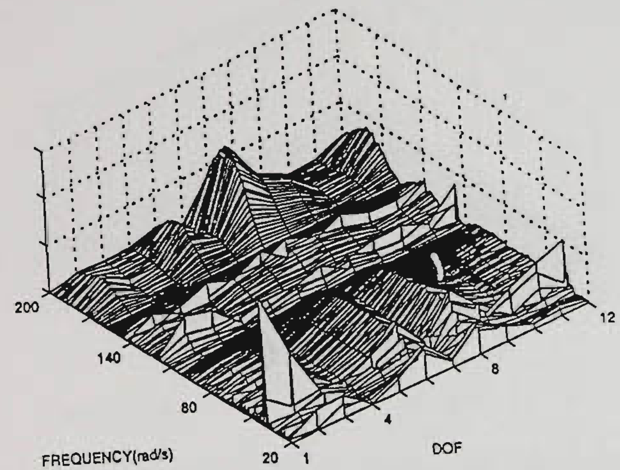

FIG.3.7C: 3-D DLP using D.E C (Case II/ Subcase 2 in section 3.4)

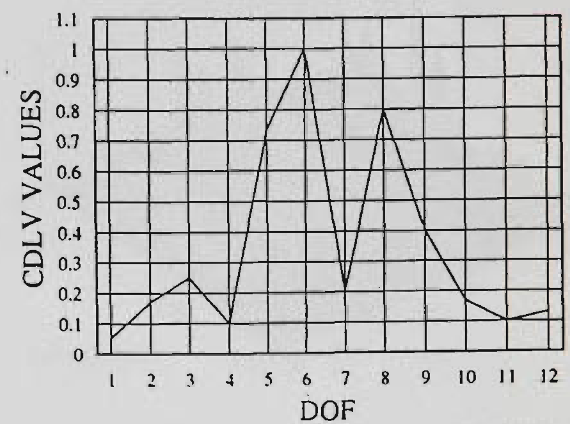

FIG.3.7C/1: CDLV using D.E C (Case II/ Subcase 2 in section 3.4)

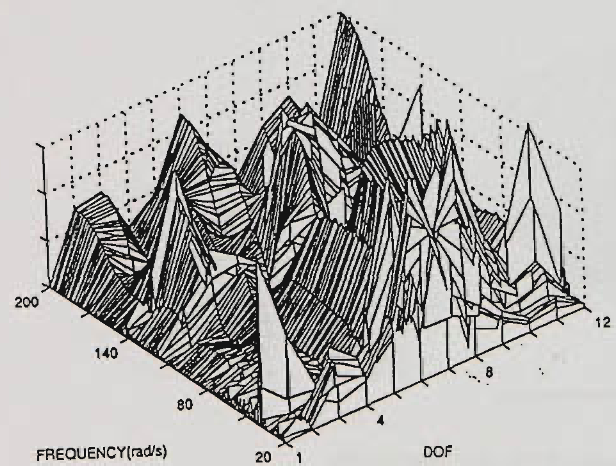

FIG.3.7D: 3-D DLP using RFRF mixing (Case II/ Subcase 2 in section 3.4)

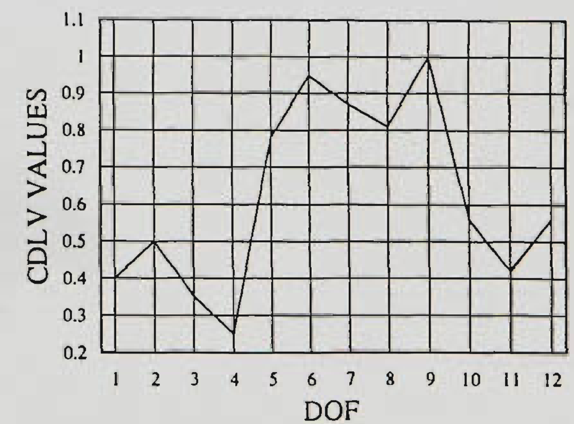

FIG.3.7D/1: CDLV using RFRF mixing (Case II/ Subcase 2 in section 3.4)

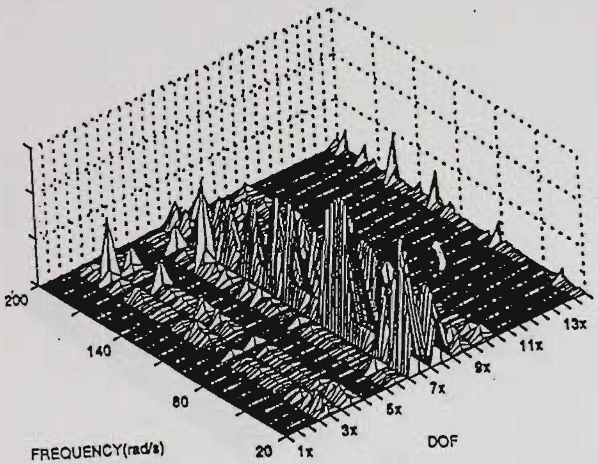

FIG.3.8A: 3-D DLP using D.E A for damage case 1 in Fig.3.3 structure
(measured DOFs 3-x, 4-x, 6-x, 7-x, 8-x, 9-x, 10-x, 14-y)

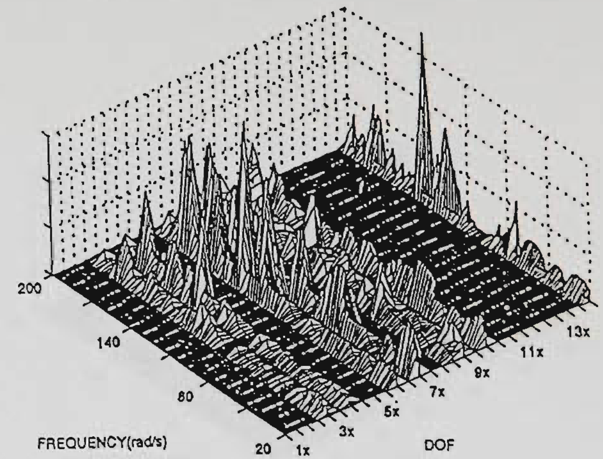

FIG.3.8B: 3-D DLP using D.E A for damage case 1 in Fig.3.3 structure
(measured DOFs 3-x, 4-x, 6-x, 7-x, 8-y, 9-x, 10-x, 14-y)

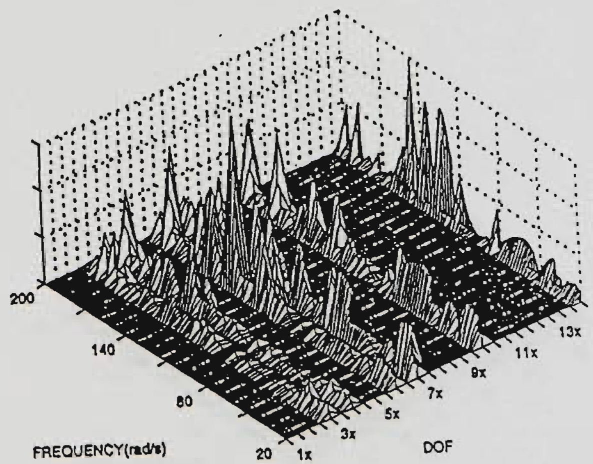

FIG.3.8C: 3-D DLP using D.E A for damage case 1 in Fig.3.3 structure
(measured DOFs 3-x, 4-x, 6-x, 7-x, 10-x, 14-y)

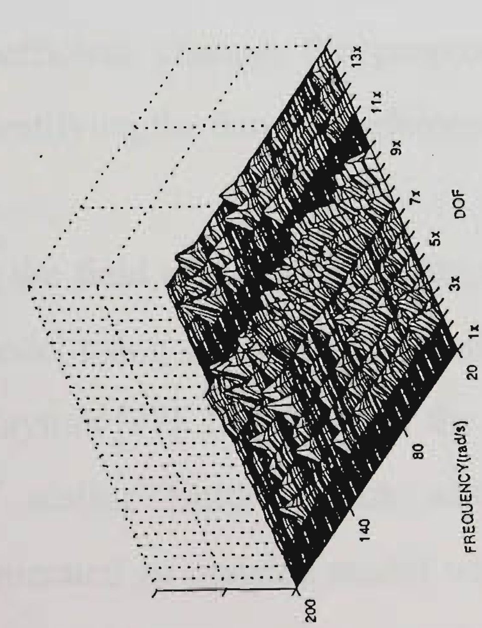

FIG.3.9A: 3-D DLP using D.E A for damage case 2 in Fig.3.3 structure (measured DOFs 3-x, 4-x, 5-x, 6-x, 7-x, 8-x, 8-y, 9-x, 9-y, 12-x, 13-x, 14-x)

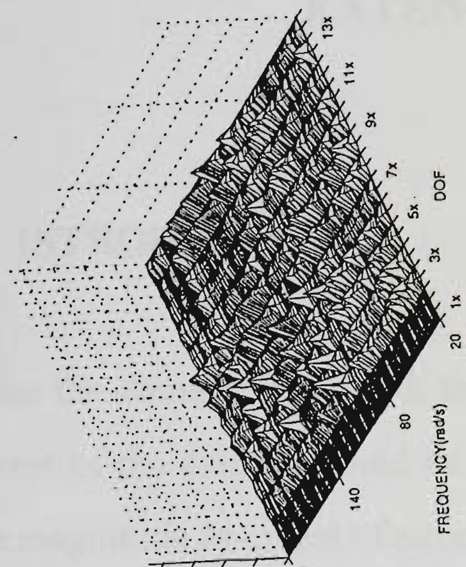

FIG.3.9B: 3-D DLP using D.E A for damage case 2 in Fig.3.3 structure (measured DOFs 3-x, 4-x, 5-x, 6-x, 7-x, 8-x, 9-x, 10-x, 11-x, 12-x, 13-x, 14-x)

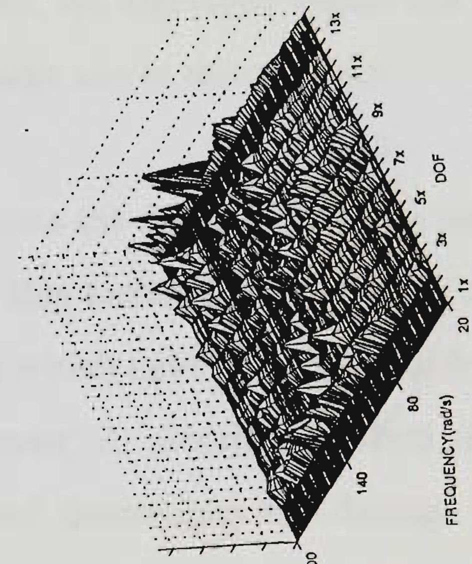

FIG.3.9C: 3-D DLP using D.E A for damage case 2 in Fig.3.3 structure (measured DOFs 3-x, 3-y, 4-y, 5-y, 6-y, 7-y, 8-y, 9-y, 10-y, 11-y, 12-y, 14-y)

CHAPTER 4

SUBMATRIX APPROACH FOR DETERMINING DAMAGE EXTENT IN A STRUCTURE

4.1 INTRODUCTION

After the damage is located, the severity of the damage can be assessed if the extent of the damage could be determined. An algorithm which can determine the magnitude or extent of structural damage serves this purpose.

The method proposed in this chapter utilizes the submatrix scaling technique to determine the extent of damage. Using this technique, it attempts to find the scaling factor for the particular elements which have been affected by damage. Unlike the method suggested in Chapter 2, which identified the matrix coefficient change, the proposed method determines the damage extent by identifying the damaged elements directly.

In the field of model updating, attempts to improve the accuracy of the global model using the submatrix approach had been already reported by White and Maytum [77]. In this work, the authors suggested a method of identifying a set of scaling factors which when multiplied by the prescribed submatrices, generated an updated model with the same connectivity of the FE model to be updated. However, the adjusted matrices computed by this method did not produce the expected modal data accurately unless the method went through an iterative process.

In addition to modal updating, efforts had been made by Stetson and Palma [78] to utilize the submatrix concept in the field of structural modification. In their work they made use of the inversion of first order perturbation theory and expressed the changes in matrix elements in terms of the changes in stiffness and mass of the individual structural elements. Sandstrom and Anderson [79] improved on Stetson and Palma's [78] method by making it computationally simpler. In their work , they expressed each element stiffness or mass change as a fractional change from the original stiffness or mass of that particular element.

In 1991, Lim [19] proposed a stiffness correction method based essentially on the submatrix method to improve the identification of White and Maytum's [77] method. In the same year, Lim [80] applied the method in the field of damage detection when he used modal data in a submatrix approach to detect structural damage. Lim presented a technique to calculate the stiffness reduction factor (SRF) for each submatrix which revealed the location and extent of structural damage. In addition to the above publications, limited application of the submatrix approach while using FRF data had been demonstrated by He [81,82]. In [81] the author presented the submatrix concept for stiffness correction in the field of model updating and suggested a method to estimate stiffness error using FRF data. In addition, He [82] used the submatrix concept along with FRF data to derive the damping matrix of a dynamic structure.

From the literature search carried out in the course of this research work, it appears that the existing submatrix based approaches have been mostly used along with modal parameters in the field of model updating and, to a much lesser extent, in damage detection. This chapter introduces a technique which extends the submatrix approach in the field of damage detection while using FRF data. The use of FRF data has enabled full exploitation of the advantages associated with FRF data.

Theoretically, the submatrix approach based method presented in this chapter can work with the mathematical model of a whole structure, thus allowing it to determine the damage extent directly without actually locating the damage. But as already found with the damage estimation algorithm proposed in Chapter 2, the capability of an algorithm to accommodate measurement noise and expansion errors is significantly reduced if damage is not located first. On the contrary, significant improvement in the performance of the algorithm for damage estimation can be achieved if the damage is located beforehand and the estimation algorithm works only with that part of the structure. This approach of damage location followed by determining its severity has been adopted in this chapter. Numerical examples have been presented to show the improvement in results obtained when the algorithm proposed in this chapter works with the knowledge of damage location.

4.2 THEORY OF DETERMINING DAMAGE EXTENT USING SUBMATRIX APPROACH

Using equation (3.2.2), it is possible to relate a single column of the receptance matrix for the damaged structure at a frequency Ω, to the dynamic stiffness matrix of the damaged structure by the following equation,

$$([K]_D - \Omega^2[M]_D)\{\alpha_D(\Omega)\}_K = \{\delta\}_k \qquad (4.2.1)$$

Using the concept of submatrix scaling factors, the mass and stiffness matrices of a damaged structure given in equation (4.2.1) can be expressed as a linear summation of submatrices of the undamaged structure, such that,

$$[K]_D = [K]_{UD} - \sum_{j=1}^{p} h_j [K]_{j,UD} \tag{4.2.2}$$

$$[M]_D = [M]_{UD} - \sum_{j=p+1}^{r} h_j [M]_{j,UD} \tag{4.2.3}$$

Here, h_j is the j^{th} scaling factor, $[K]_{j,UD}$ and $[M]_{j,UD}$ are the j^{th} submatrix of undamaged stiffness and mass matrix respectively transformed to global coordinates and p and r represents the number of submatrices. Each of the submatrices represent a single physical element of the structure. Equations (4.2.2) and (4.2.3) imply that before and after damage, the physical connectivity of the structure remains the same. Only the stiffness (and/or mass) values of certain physical elements which have been affected by damage are changed. Using equations (4.2.2) and (4.2.3), equation (4.2.1) may be modified as:

$$\left(\left([K]_{UD} - \sum_{j=1}^{p} h_j [K]_{j,UD}\right) - \Omega^2\left([M]_{UD} - \sum_{j=p+1}^{r} h_j [M]_{j,UD}\right)\right)\{\alpha_D(\Omega)\}_k = \{\delta\}_k \tag{4.2.4}$$

To illustrate the concept of submatrices, a 3 DOF mass-spring system as shown in figure 4.1 is considered here. A 3x3 matrix as shown below represents the stiffness matrix of the structure:

$$[K]=\begin{bmatrix} k_1 & -k_1 & 0 \\ -k_1 & (k_1+k_2) & -k_2 \\ 0 & -k_2 & k_2+k_3 \end{bmatrix}$$

The structure has three stiffness elements namely k_1, k_2 and k_3 and matrix [K] is made up of these elements together. In the submatrix approach, instead of using the combined matrix [K], each of these particular elements k_1, k_2 and k_3 is represented in the global coordinate system such that

$$[K]_1=\begin{bmatrix} k_1 & -k_1 & 0 \\ -k_1 & k_1 & 0 \\ 0 & 0 & 0 \end{bmatrix},\ [K]_2=\begin{bmatrix} 0 & 0 & 0 \\ 0 & k_2 & -k_2 \\ 0 & -k_2 & k_2 \end{bmatrix},\ [K]_3=\begin{bmatrix} 0 & 0 & 0 \\ 0 & 0 & 0 \\ 0 & 0 & k_3 \end{bmatrix}$$

These matrices are called stiffness submatrices and the total stiffness matrix [K] is the sum of these submatrices $[K]_1$, $[K]_2$ and $[K]_3$. Now if there is a damage in the structure it will affect only those elements which lie in the damage zone. As a consequence, the scaling factors corresponding to the damaged elements will assume non-zero values and undamaged element scaling factors remain zero. To elaborate the concept of scaling factors, equation (4.2.2) for the system in figure 4.1 becomes

$$[K]_D = [K]_{UD} - h_1[K]_{1,UD} - h_2[K]_{2,UD} - h_3[K]_{3,UD} \qquad (4.2.5)$$

Assuming that damage has affected only the stiffness element k_2, equation (4.2.5) becomes

$$[K]_D = [K]_{UD} - h_2[K]_{2,UD} \qquad (4.2.6)$$

the other two terms in the right hand side of equation (4.2.5) vanishes as the damage has not affected those elements. As a result, the scaling factors h_1 and h_3 corresponding to those elements become zero. In order to calculate the scaling factor h_2, equation (4.2.6) together with equation (4.2.4) gives:

$$([K]_{UD} - h_2[K]_{2,UD} - \Omega^2[M]_{UD})\{\alpha_D(\Omega)\}_k = \{\delta\}_k \tag{4.2.7}$$

From this equation, it is possible to obtain h_2. If all three stiffness elements had been affected, then equation (4.2.7) would have been modified to include the h_1 and h_3 terms in addition to the h_2 term. Then, the number of unknowns would have been three. In contrast, an approach which tries to correct individual matrix coefficients would have to adjust five upper triangular matrix coefficients for this system when all three springs in figure 4.1 has been affected. From this illustration it is not difficult to appreciate that a reduction in the number of unknowns can be achieved by using the submatrix approach for determining damage extent.

Equation (4.2.4) obtained using the concept of submatrices can be further modified and written as:

$$\left.\sum_{j=1}^{p} h_j[K]_{j,UD} - \Omega^2 \sum_{j=p+1}^{r} h_j[M]_{j,UD}\right)\{\alpha_D(\Omega\}_k = \{R\} \tag{4.2.8}$$

where $\{R\} = -\{\delta\}_k + \left([K]_{UD}\{\alpha_D(\Omega)\}_k - \Omega^2[M]_{UD}\{\alpha_D(\Omega)\}_k\right)$

It is apparent that the only unknowns in the above equation are the scaling factors and hence equation (4.2.8) can be written as:

$$\sum_{j=1}^{r} h_j \{L_j\} = \{R\} \tag{4.2.9}$$

where $\{L_j\} = [K]_{j,UD} \{\alpha_D(\Omega)\}$ for $j = 1$ to p

and $\{L_j\} = -\Omega^2 [M]_{j,UD} \{\alpha_D(\Omega)\}$ for $j = p+1$ to r.

Equation (4.2.9) is obtained by considering a single frequency point. However if 's' frequency points are chosen, then equation (4.2.9) may be modified to derive the following equation

$$[L]\{h\} = \{g\} \tag{4.2.10}$$

where

$$[L] = \begin{bmatrix} \{L_1\}_1 & \{L_2\}_1 & .. & .. & \{L_r\}_1 \\ \{L_1\}_2 & \{L_2\}_2 & .. & .. & \{L_r\}_2 \\ .. & .. & .. & .. & .. \\ .. & .. & .. & .. & .. \\ \{L_1\}_s & \{L_2\}_s & .. & .. & \{L_r\}_s \end{bmatrix}$$

$$\{g\} = \left\{ \{R\}_1^T \quad \{R\}_2^T \quad .. \quad .. \quad \{R\}_s^T \right\}^T$$

$$\{h\} = \{h_1 \quad h_2 \quad .. \quad .. \quad h_r\}^T$$

Approach 1

The vector $\{L_j\}_k$ corresponds to $\{L_j\}$ for the k^{th} frequency point and the vector $\{h\}$ is made up of all the scaling factors where each scaling factor corresponds to a particular element. Note that the size of the matrix [L] and the vector {g} are qxr and qx1 respectively, where q = Nxs. If the number of scaling factors to be identified "r" is less than the product of number of DOFs "N" and the number of frequency points "s", then

$$q \geq r \qquad \text{or,} \quad s \geq r/N \tag{4.2.11}$$

For such cases it is possible to solve equation (4.2.10) by using a least squares approach which gives

$$\{h\} = \left[[L]^T[L]\right]^{-1}[L]^T\{g\} \tag{4.2.12}$$

The values of individual scaling factors obtained by solving the above equation not only indicates the location of damage but also gives an estimate of the extent of the damage.

Approach 2

Instead of using a pseudo inverse mathematical technique as shown in Approach 1, it is also possible to calculate the scaling factors by using a classical inverse. Like Approach 1, Approach 2 is also based on equation (4.2.10). However instead of working with the whole equation, this approach works with each row of matrix [L] at a time along with the vector {h} and {g}. It is obvious that for different frequency points, matrix [L] and vector {g} will be different although the vector {h} will be the same. Therefore, while working with the first row of matrix [L] along with vectors {h} and {g}, if it is found that the number of unknowns are "x", then it is required to regenerate matrix [L] and vector {g} for "x" frequency points and use the first row of each of these matrices along with the corresponding vector {g} to compute the unknowns. This operation has to be repeated for other rows of matrix [L] until all the scaling factors have been identified. This concept is illustrated next by using an example.

A 3 DOF mass-spring system with 4 stiffness and 3 mass elements was considered. Assuming that due to damage all stiffness elements had been affected leaving the mass unchanged, equation (4.2.10) for a particular frequency point may be written as:

$$h_1\begin{Bmatrix} a \\ b \\ c \end{Bmatrix} + h_2\begin{Bmatrix} a_1 \\ b_1 \\ c_1 \end{Bmatrix} + h_3\begin{Bmatrix} a_2 \\ b_2 \\ c_2 \end{Bmatrix} + h_4\begin{Bmatrix} a_3 \\ b_3 \\ c_3 \end{Bmatrix} = \begin{Bmatrix} x \\ y \\ z \end{Bmatrix} \tag{4.2.13}$$

or,

$$\begin{bmatrix} a & a_1 & a_2 & a_3 \\ b & b_1 & b_2 & b_3 \\ c & c_1 & c_2 & c_3 \end{bmatrix} \begin{Bmatrix} h_1 \\ h_2 \\ h_3 \\ h_4 \end{Bmatrix} = \begin{Bmatrix} x \\ y \\ z \end{Bmatrix} \tag{4.2.14}$$

While using Approach 1 for this example, it is possible to form an overdetermined set of equations by using two frequency points. Approach 2 uses the classical inverse to solve the unknowns as given in equation (4.2.14). By using one frequency point, the first row of the matrix given in the left hand side of equation (4.2.14) may be used with the corresponding vector to generate the first equation. Using a second frequency point, the first row of the new matrix developed in equation (4.2.14) may be used again with the corresponding vectors to develop a second equation. Since the equations developed for this example using the first row of matrix has four unknowns, it is necessary to generate four such equations using four frequency points. Therefore, this results in a situation where there are four equations with four unknowns which can be solved easily. However, while using Approach 2 it is imperative to check that the set of equations built up by using different frequency points are independent of each other. If the equations are not, reselecting frequency points to obtain realistic results will be required.

4.3 DISCUSSION

The scaling factors used to identify the damaged elements in a system can be computed by using either Approach 1 or 2 in section 4.2. However, based on a comparative study of both approaches, it appears that Approach 2 is a better performer than Approach 1. Approach 2 uses classical inverse. This avoids possible numerical errors associated with pseudo inverse. By using more frequency points, each contributing to one equation, Approach 2 is based on a set of linearly independent equations. It has been found that with noisy FRF data, better estimates of damage extent can be made if the location of the damage is first ascertained. Following that, Approach 2 is used to determine the extent or severity of damage. Once the location of damage has been ascertained, it becomes relatively easy to identify only those scaling factors affected by damage. Other scaling factors can be safely assumed to be 'zero'. In this way, a significant reduction in the number of unknowns can be achieved. The number of equations to be solved is drastically reduced resulting in a significant reduction in computational burden and improvement in accuracy.

When FRF data are corrupted by noise, the results of damage estimation obtained using Approach 2 with damage location varied to some extent with the selection of frequency points. Although the variation is not significant, it is found that most accurate results are obtained if frequency points selected are in the neighbourhood of natural frequencies which are more affected by damage.

In the case of incomplete measurement coordinates, it is possible to expand the measured coordinates to the size of the analytical model of the undamaged structure. However, 'expansion errors' will affect the performance of the algorithm aimed at determining the severity of damage. As the ratio of the measured and unmeasured DOFs becomes smaller, the expansion error becomes more prominent which hampers the damage estimation.

Improvement can be achieved by first locating the damage and then working with the damaged portion of the structure to determine damage extent. After locating the area of damage, the proposed submatrix approach to determine damage extent can use FRF data only in the area of damage to determine its extent. This can be executed by:

1. actually measuring the additional DOFs in the area of damage; or
2. using an expansion method to interpolate the FRF data corresponding to unmeasured DOFs in the damaged structure.

A 10 DOF mass-spring system shown in figure 4.2 was used here to show how the submatrix approach successfully determined damage extent by using FRF data only measured for DOFs between which damage was located. Let the damage in system be located between DOFs 4 and 5 and let the FRFs measured be at DOFs 1, 3 and 7. Using the damage location algorithm suggested in Chapter 3, the location of damage can be identified to be lying between DOFs 3 and 7. Once the location of damage had been identified, the proposed submatrix approach required only FRF data at DOFs 4, 5 and 6 in addition to the FRFs already measured at DOFs 3 and 7 to determine the damage extent. This can be better appreciated by considering equation (4.3.1) given below. Since the damage had been located between DOFs 3 and 7, the scaling factors attached to stiffness elements k_1 to k_3 and k_8 to k_{11} could be safely assigned to zero. Hence equation (4.2.9) for this particular system becomes:

$$\begin{aligned}&\left(h_4[K]_4 + h_5[K]_5 + h_6[K]_6 + h_7[K]_7 - \Omega^2 h_{15}[M]_4 - \Omega^2 h_{16}[M]_5 - \right.\\&\left.\Omega^2 h_{17}[M]_6 - \Omega^2 h_{18}[M]_7\right)\{\alpha_D(\Omega)\}_k = \{R\}\end{aligned} \tag{4.3.1}$$

It is apparent that to solve for h_4 to h_7 and h_{15} to h_{18}, the FRF data for DOFs 3, 4, 5, 6 and 7 are needed. Since FRF data for 3 and 7 were known, additional FRF data required were for DOFs 4, 5 and 6. Measurements at 3 and 7 were required in equation (4.3.1) above, because these were the DOFs interfacing the area of damage. In general, it can be said that once the damage had been located, with incomplete DOFs the submatrix approach to determine damage extent requires FRF data in the area of damage and the data for DOFs which are connected immediately to the area of damage.

If the FRF data at the coordinates in the area of damage are unavailable, then the alternative is to use interpolated FRF data. In this case, it is found that the performance of submatrix method to determine the damage extent deteriorates progressively as the error introduced due to FRF data expansion increases.

4.4 RESULTS OF NUMERICAL ANALYSIS

To assess the effectiveness of the submatrix method, numerical analysis was carried out on the 12 DOF mass-spring system shown in figure 3.2 in Chapter 3 and the truss structure shown in figure 4.3.

The 12 DOF mass-spring system shown in figure 3.2 had 13 stiffness elements and the stiffness element between ground and DOF 1 had been named as Element 1, the element between DOFs 1 and 2 as Element 2 and so on. It was assumed that damage had only affected stiffness of element 8, leaving mass unchanged. Due to damage, the stiffness of element 8 had decreased from 20,000 N/m to 14,000 N/m. For such a change in stiffness, the actual scaling factor of element was given as:

scaling factor of element 8 = (20,000- 14,000)/20,000 = 0.3

and the scaling factor for remaining elements were zero. This has been shown in figure 4.4 where the scaling factor for stiffness element 8 has been given as 0.3 and that for remaining stiffness elements as zero.

For noise free FRF data both Approaches 1 and 2 were applied to identify the actual scaling factor. For Approach 1, using a single frequency point, equation (4.2.10) generated a set of 12 equations with 13 unknowns. Using just two frequency points, this equation can be made overdetermined. Initially just two frequency points within the first mode were used and the results obtained as plotted in figure 4.5 is not very encouraging. Not only the identified scaling factor corresponding to Element 8 was not accurate enough, but also non zero scaling factors have been identified for other stiffness elements. In the next instance, the number of frequency points were increased from two to four covering the first two modes and figure 4.6 shows the scaling factors identified for this case. Although the result obtained was better than that in figure 4.5, it was not perfect considering the fact that pure data was used.

The same example was repeated using Approach 2. For this 12 DOF system given in figure 3.2, by using a single frequency point in equation (4.2.10), [L] becomes a matrix of size 12x13, {h} is a 13x1 sized vector and {g} is a vector of size 12x1. To identify scaling factors corresponding to Elements 1 and 2, the equation derived from the first row of matrix [L] along with vector {h} and {g} was repeated at two frequency points. The resultant pair of equations were solved to obtain the scaling factors corresponding to Elements 1 and 2. The same operation was repeated using other rows of matrix [L] to compute the scaling factors for remaining elements. The frequency points were selected within the range of the first two modes. The equations derived were found to be independent of each other. The scaling factors thus computed are given in figure 4.7 and for noise free data was found to be independent of the frequency points selected. The identified scaling factors in figure 4.7 are almost identical to the correct answers.

Next, the same example was used with noisy FRF data. A random noise of 4% was introduced into the amplitude of the FRF data of the damaged structure. The scaling factors for stiffness elements were identified using both Approaches 1 and 2. While using Approach 1, two frequency points were theoretically sufficient to obtain the result. However, to reduce the effect of noise additional frequency points were used. FRF data at six frequency points covering the first three modes were used and the scaling factors were identified using Approach 1, as shown in figure 4.8. Approach 2 required FRF data at a minimum of two frequency points. However, to reduce the effect of noise, FRF data at the same six frequency points used in Approach 1 were used in Approach 2 and the resultant overdetermined equation set was solved using pseudo inverse. The scaling factors identified using Approach 2 have been plotted in figure 4.9.

Figure 4.8 obtained using Approach 1 provides a very inaccurate estimate of the scaling factors. In contrast, the identified scaling factors in figure 4.9 provides a much better estimate. However, in addition to deriving the scaling factor corresponding to Element 8, figure 4.9 has returned non zero values for scaling factors corresponding to undamaged elements.

To improve the accuracy of the derived scaling factors, the damage location was first identified using the 3-D DLP suggested in Chapter 3 and then Approach 2 was employed in the area of damage to estimate the scaling factor corresponding to damaged elements only. As already shown in the numerical examples in Chapter 3, the 3-D DLP successfully located damage for this system with FRF data contaminated by 4% noise. Once the location of damage is identified, Approach 2 was used to identify the scaling factor for stiffness element 8. Since the number of unknown for this case is just one, FRF data at a single frequency point was used to identify the scaling factor. The results plotted in figure 4.10 uses FRF data at 120 rad/s. FRF data at this frequency was selected as it was in the vicinity of the third natural frequency of this system which changed from 121.9 rad/s to 117.2 rad/s due to damage. In the course of carrying out the numerical studies, FRF data at different frequency points were also used. Although the scaling factors computed were found to vary with selection of frequency points, it always approached the correct answer whenever the FRF data close to one of the natural frequencies affected by damage were used.

For incomplete coordinates, the FRF data for unmeasured coordinates has to be interpolated before they can be used for damage location and/or estimation. As already demonstrated in Chapter 3, the best results of FRF expansion can be obtained when D.E A is used. For this 12 DOF system, it is assumed that the measured coordinates do not include the coordinates between which damage is located. The measured coordinates are 1, 4, 6 and 9 whereas damage is located between 7 and 8. With a measurement noise of 4% and using expanded values for unmeasured coordinates, Approach 2 was used. FRF data at six frequency points spanning the first three modes were used again to identify the scaling factors. The identified scaling factors for the stiffness elements have been plotted in figure 4.11 which does not exhibit the damage location. Hence, the 3-D damage location plot suggested in Chapter 3 was used to determine damage location. Once the damage has been located to be lying between DOFs 6 and 9, Approach 2 was applied to determine damage extent. This required FRF data in the region of damage which are coordinates 7 and 8. By taking additional 'measurements' corresponding to DOFs 7 and 8, the extent of damage was calculated for elements 7, 8 and 9 which are the elements lying between DOFs 6 and 9. The identified scaling factors as shown in figure 4.12 estimates the change in stiffness in element 8 accurately.

However in case of incomplete coordinates, it may be possible that coordinates in the region of damage are not accessible so that additional FRF measurements is not possible. As a result, the expanded FRF data have to be used to estimate damage. To simulate the situations, FRF data expanded by D.E A for coordinates 7 and 8 were used along with measured coordinates to calculate the extent of damage. The results for such a situation have been shown in figure

4.13. Although this figure provides a reasonable estimate of the damage, it showed a marked deterioration. In general, it has been found that the performance of the submatrix method to estimate damage deteriorates as more FRF data need to be interpolated in the region of damage.

The second example was a truss structure shown in figure 4.3. This structure has 20 nodes. The truss members were modelled using PAFEC-FE. Element number 34400 in PAFEC routine which has only 3 translational DOFs at each node was selected to model this truss structure. The PAFEC FE data file used to generate the mass and stiffness matrices of the undamaged structure is given in Table 4.1. The translational DOFs at y and z direction only at each node was retained for the element.The two nodes cantilevered to the wall were assumed rigidly fixed. The final FE model thus contained mass and stiffness matrices of dimension 36x36. Each horizontal member was assumed to have a length of 0.1 m, vertical member a length of 0.1m and diagonal members were assigned a length of 0.14 m. For generating the mass and stiffness of the structure, the material properties were assumed to be E = 208E4 N/m^2, Poisson's Ratio = 0.3 and Density = 7860 kg/m^3. For this structure, two damage cases were simulated separately:

<u>Case 1</u>

The vertical member between nodes 7 and 8 has been damaged.

<u>Case 2</u>

The vertical member between nodes 7 and 8 along with the diagonal member between nodes 12 and 13 have been damaged.

Damage was simulated by changing the Young's Modulus (E) of the damaged members by 50%. It was assumed that the FRF data were contaminated by 4% noise and this was done by introducing a random error of 4% on the FRF data.

The damage location method using 3-D DLP as suggested in Chapter 3 was used in conjunction with the Approach 2 of the submatrix method proposed in this chapter to locate and quantify damage. The damage in Case 1 had affected the stiffness of Element 15 and for the second case the damage had affected both Elements 15 and 28. Figures 4.14 and 4.15 show the actual magnitudes of scaling factors of the damaged elements for Cases 1 and 2 respectively. The damage location and the magnitude of the scaling factors for Case 1 were shown in figures 4.16 and 4.17 respectively. While plotting the 3-D damage location plot for the single damage as shown in Case 1, it was found that the damage location plot becomes prominent only after 20 Hz. This was quite expected for this structure since the natural frequencies of this structure upto 20 Hz were hardly affected due to the damage in member between node 8 and 9. The scaling factor plotted in figure 4.17 was obtained using a frequency of 24 Hz. This frequency was selected as the natural frequency corresponding to 24.3 Hz had been shifted to 23.3 Hz due to damage as described in Case 1. FRF data at a single frequency point was required to identify the scaling factor corresponding to the damaged member.

For Case 2, the 3-D damage location plot given in figure 4.18 clearly shows the existence of both damages. Unlike Case 1, the damage location plot showed appreciable and consistent peaks from 10 Hz onwards. The scaling factors for both the affected elements had been given in figure 4.19. Each of these scaling factors can be identified individually. The result plotted in figure 4.19 was obtained by using FRF data at frequency point of 25.4 Hz. which is adjacent to one of the affected natural frequencies.

Although, the scaling factors identified in Cases 1 and 2 were found to be somewhat frequency dependant, reliable and consistent results can be obtained. This can be achieved by using FRF data at frequency points which are in the proximity of the natural frequencies which have been more affected due to damage. From this truss structure example, an additional significance of the 3-D damage location plot can be appreciated. In case of multiple damages, the 3-D plot identifies the frequency region in which FRF have been more significantly affected due to damage in a particular member. Once the frequency region is thus identified, more accurate estimate of the damage in a particular member can be made by using FRF data at frequencies, which are more affected due to damage in that member.

4.5 SUMMARISING REMARKS

The damage location method using submatrix approach has been discussed in details in this chapter. The method introduced a different approach to determining damage extent by identifying the damaged physical elements directly instead of the DOFs. Two different approaches named in this chapter as Approaches 1 and 2 have been discussed. It has been found that Approach 2 is better when using FRF data with measurement noise. The capacity of Approach 2 to accomodate measurement noise is further enhanced when the damage is located prior to its estimation. With incomplete measured coordinates, it is suggested to locate the damage and then trying to determine its extent. Once the region of damage is located, two methods have been tried to obtain the FRF data corresponding to unmeasured coordinates in the area of damage : measuring the FRF data for unmeasured coordinates in the area of damage and interpolating them using D.E A.

With measured data the results obtained have been quite accurate but with interpolated coordinates, the quality of results starts deteriorating as the measured coordinates move further away from the damage location. In addition to that, while using FRF data contaminated by noise it was found that the results obtained often varied to some extent depending on the frequency points selected. However, it was found that the results obtained were very close to the actual value when the FRF data used were at frequency points in the vicinity of the most affected natural frequency within the frequency range measured.

A significant advantage of using this method is that it can identify the damaged elements directly. In addition, by determining the element scaling factors rather than the matrix coefficients, a significant reduction in the number of unknowns can be achieved. Finally, the use of measured FRF data instead of modal parameters eliminates the complexities and numerical errors associated with extracting modal parameters .

```
CONTROL
CONTROL.END
NODES
NODE    X     Y       NODE    X     Y       NODE    X     Y
1       0     0       2       0     .1      3       .1    0
4       .1    .1      5       .2    0       6       .2    .1
7       .3    0       8       .3    .1      9       .4    0
10      .4    .1      11      .5    0       12      .5    .1
13      .6    0       14      .6    .1      15      .7    0
16      .7    .1      17      .8    0       18      .8    .1
19      .9    0       20      .9    .1
ELEMENTS
ELEMENT.TYPE = 34400
NUMBER  PROP  TOPOLOGY  NUMBER  PROP  TOPOLOGY  NUMBER  PROP  TOPOLOGY
1       1     1 3       2       1     1 4       3       1     2 3
4       1     2 4       5       1     3 4       6       1     3 5
7       1     3 6       8       1     4 5       9       1     4 6
10      1     5 6       11      1     5 7       12      1     5 8
13      1     6 7       14      1     6 8       15      1     7 8
16      1     7 9       17      1     7 10      18      1     8 9
19      1     8 10      20      1     9 10      21      1     9 11
22      1     9 12      23      1     10 11     24      1     10 12
25      1     11 12     26      1     11 13     27      1     11 14
28      1     12 13     29      1     12 14     30      1     13 14
31      1     13 15     32      1     13 16     33      1     14 15
34      1     14 16     35      1     15 16     36      1     15 17
37      1     15 18     38      1     16 17     39      1     16 18
40      1     17 18     41      1     17 19     42      1     17 20
43      1     18 19     44      1     18 20     45      1     20 19
BEAMS
SECTION   MATERIAL   IYY        IZZ        TORSIONAL.CONST   AREA
1         11         1.666E-9   6.666E-9   4.6E-9            2.0E-4
MATERIAL
MATERIAL.NUMBER   E       NU   RO
11                208E4   .3   7860
LOADS
CASE   NODE   DIRECTIONS.OF.LOAD   VALUE.OF.LOAD
1      4      2                    10
ACTIVE.FREEDOMS
NODE      DIRECTION   PRINT.CONTROL
3         23          2
R17   1   00          0
RESTRAINTS
NODE      DIRECTION
1         0
2         0
3         1
R17   1   0
MODES.AND.FREQUENCIES
AUTOMATIC.MASTERS   MODES
0                   10
MASTERS
NODE.NUMBER   DIRECTION
3             23
R20   1       00
END.OF.DAT
```

Table 4.1: Data file in PAFEC FE for deriving mass and stiffness for truss in fig.4.3

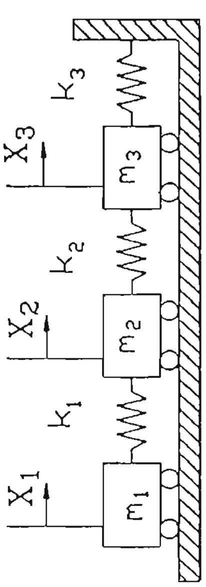

FIG.4.1: A 3 DOF mass-spring system

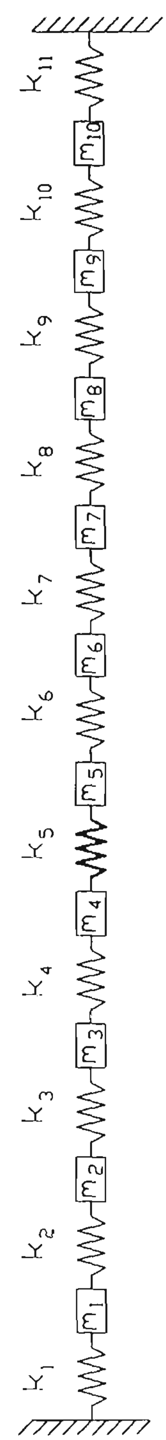

FIG.4.2: A 10 DOF mass-spring system

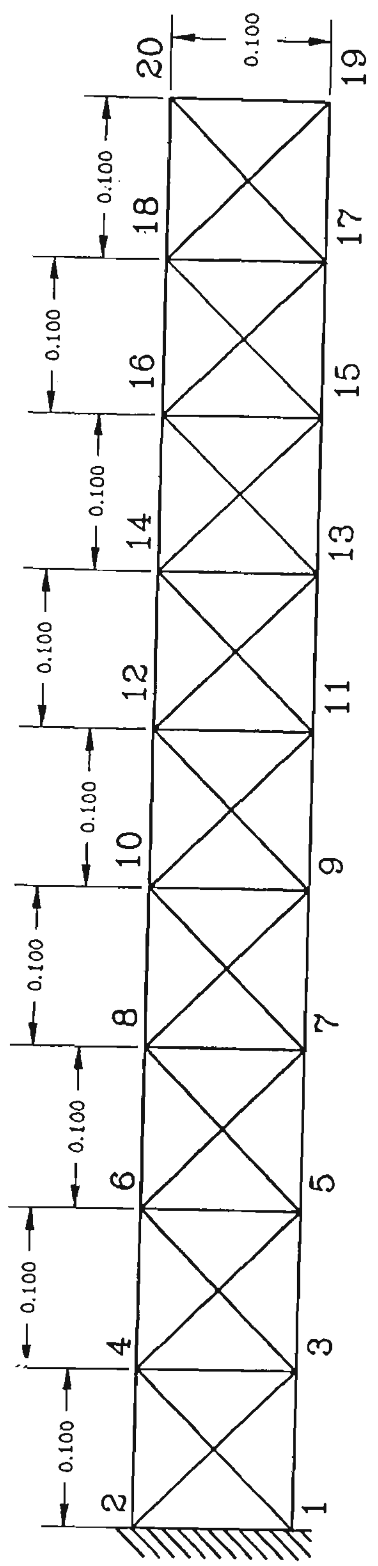

ALL DIMENSIONS IN METRES

FIG.4.3: A cantilever truss structure

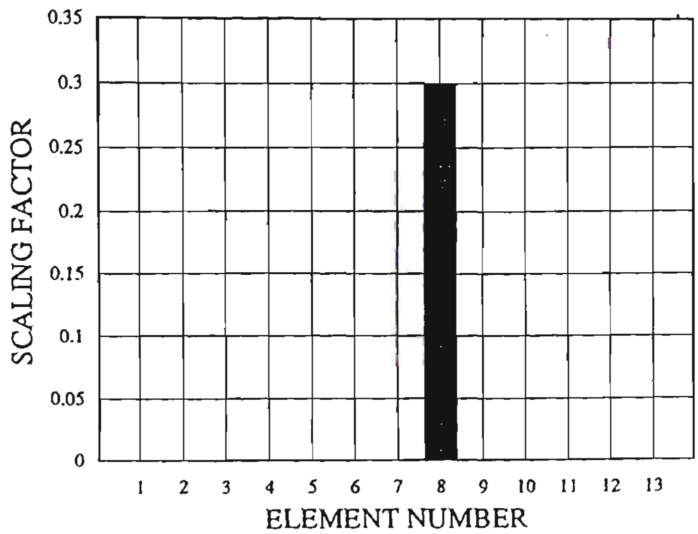

FIG.4.4: Scaling factor due to damage in model 3.2

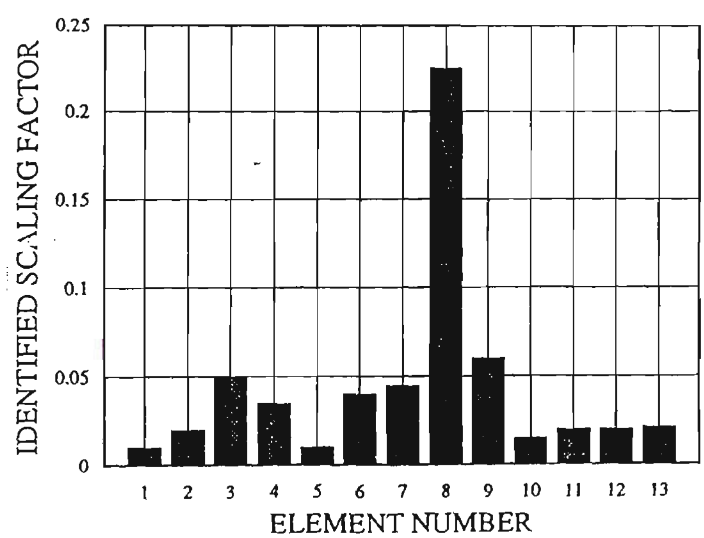

FIG.4.5: Identified scaling factor using approach 1 (with two frequency points and no noise)

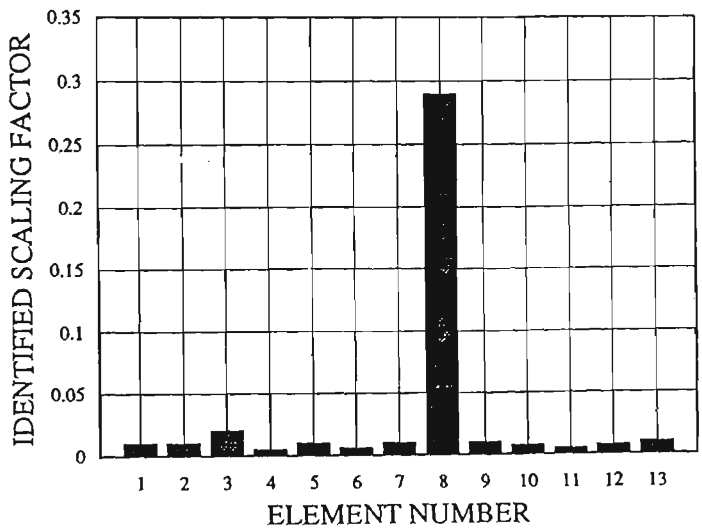

FIG.4.6: Identified scaling factor using approach 1 (with four frequency points and no noise)

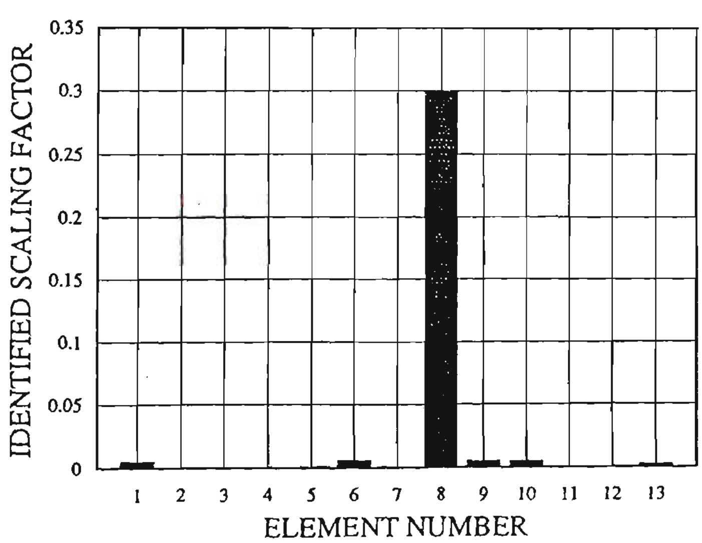

FIG.4.7: Identified scaling factor using approach 2 (with no noise)

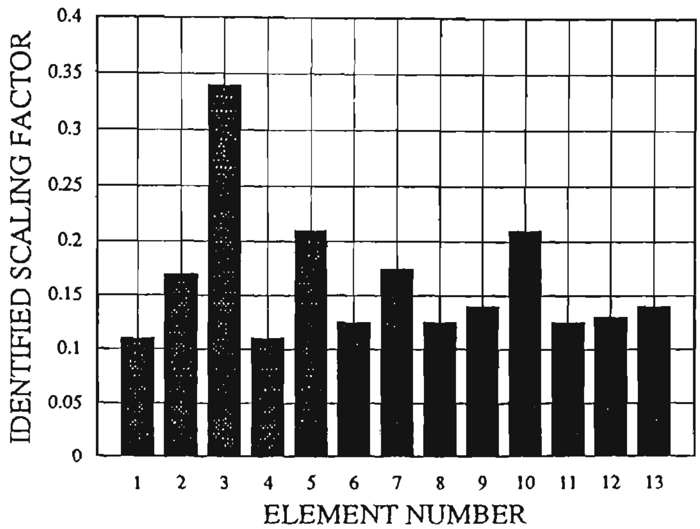

FIG.4.8: Identified scaling factor using approach 1 (with 4% noise)

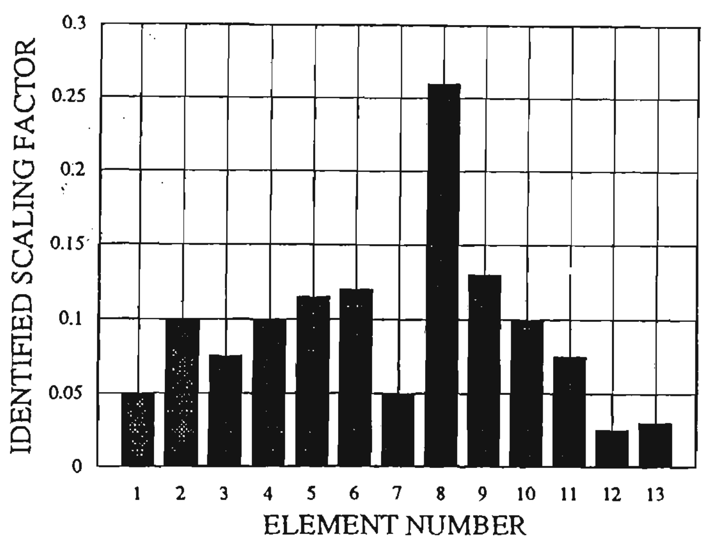

FIG.4.9: Identified scaling factor using approach 2 (with 4% noise)

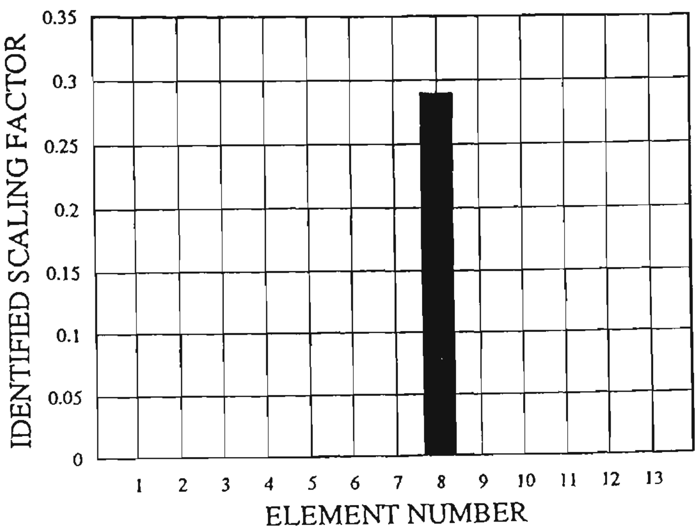

FIG.4.10: Identified scaling factor using approach 2 and DLP (with 4% noise and damage location known)

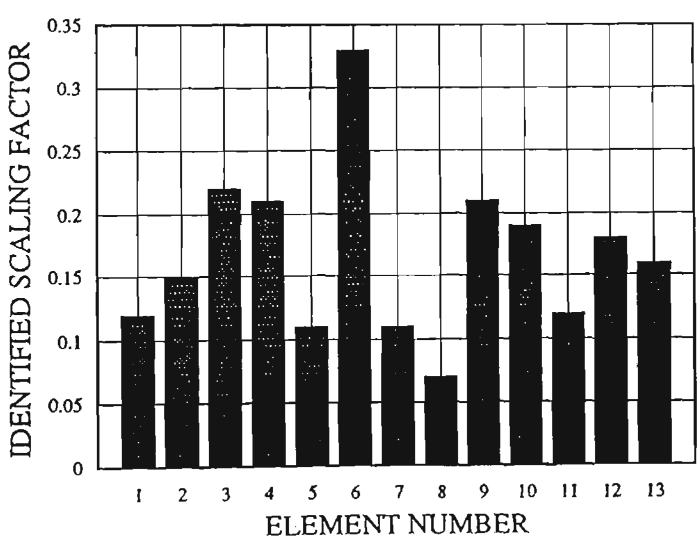

FIG.4.11: Identified scaling factor using approach 2 (with 4% noise and incomplete measurement)

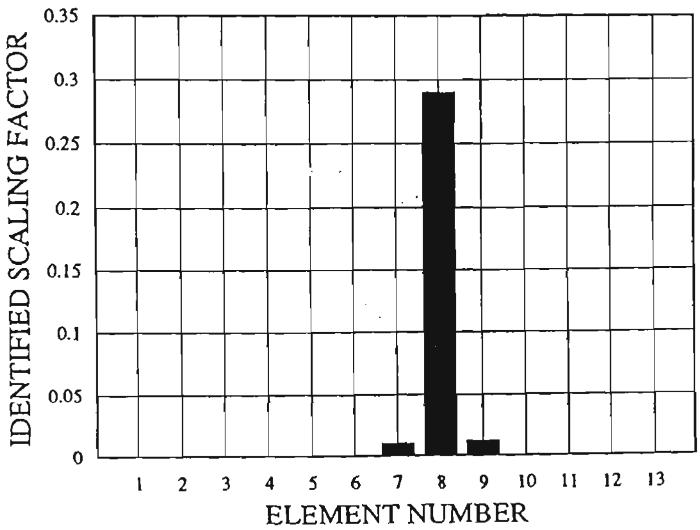

FIG.4.12: Identified scaling factor using approach 2 and DLP
(with 4% noise and measurement available)

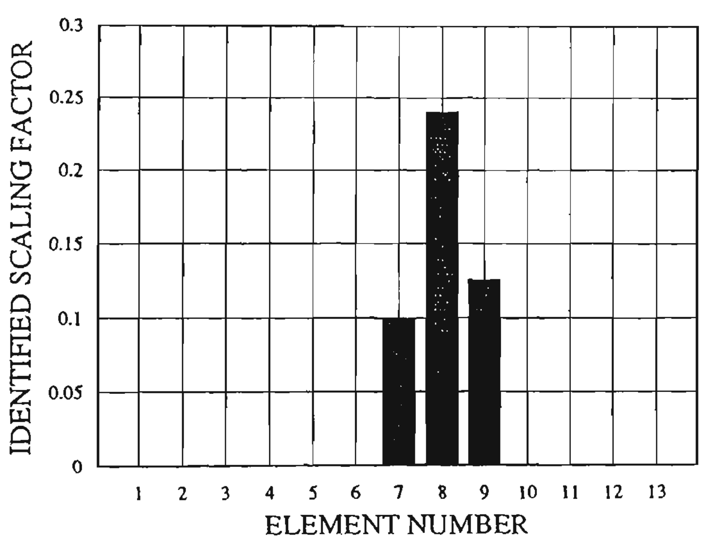

FIG.4.13: Identified scaling factor using approach 2 and DLP
(with 4% noise and interpolated data)

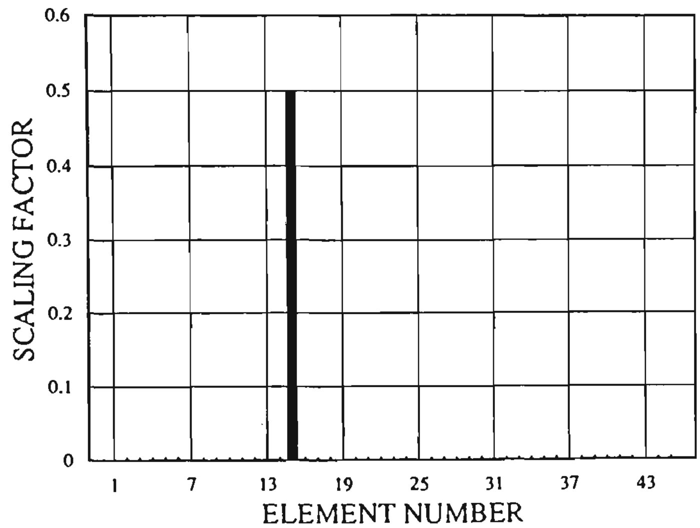

FIG.4.14: Scaling factor of the truss structure in fig 4.3 (Case 1)

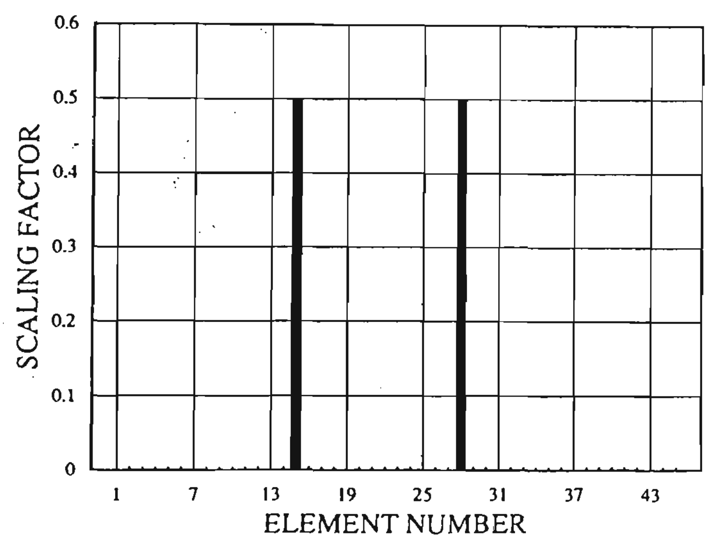

FIG.4.15: Scaling factor of the truss structure in fig 4.3 (Case 2)

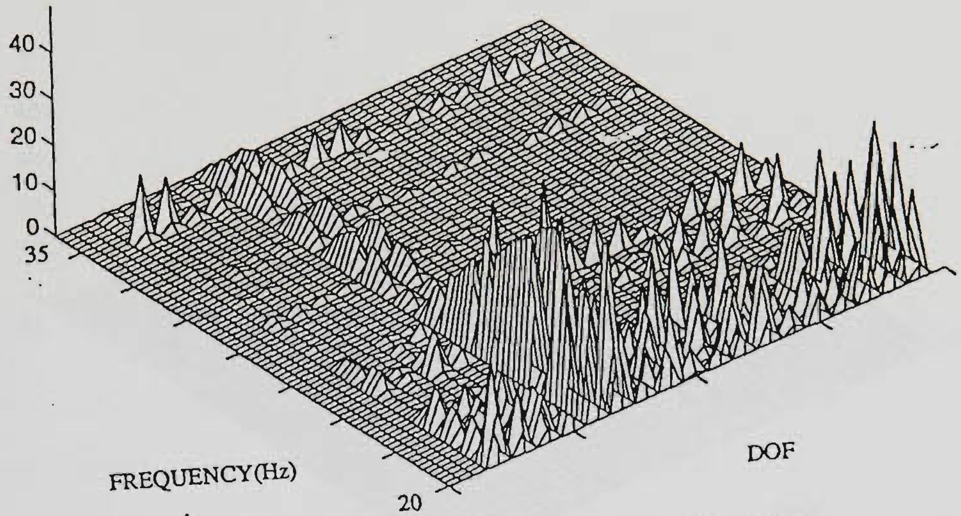

FIG.4.16: 3-D Damage Location Plot for case 1 damage in fig.4.3 model

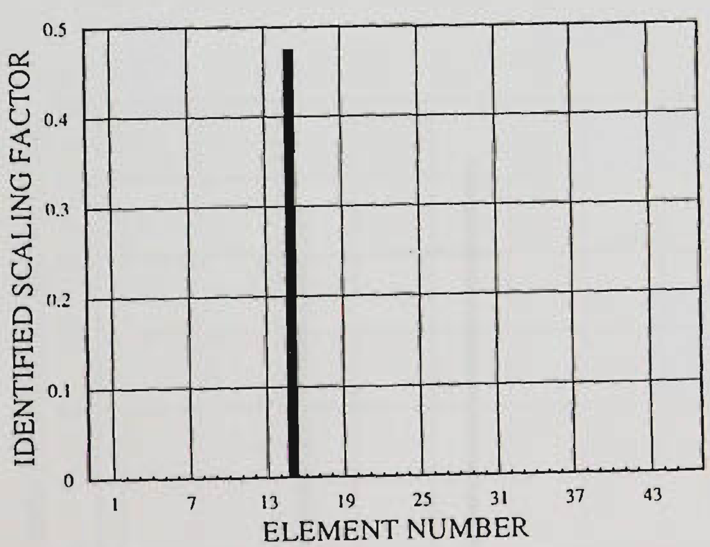

FIG.4.17: Identified scaling factor for case 1 damage in fig.4.3 truss structure.

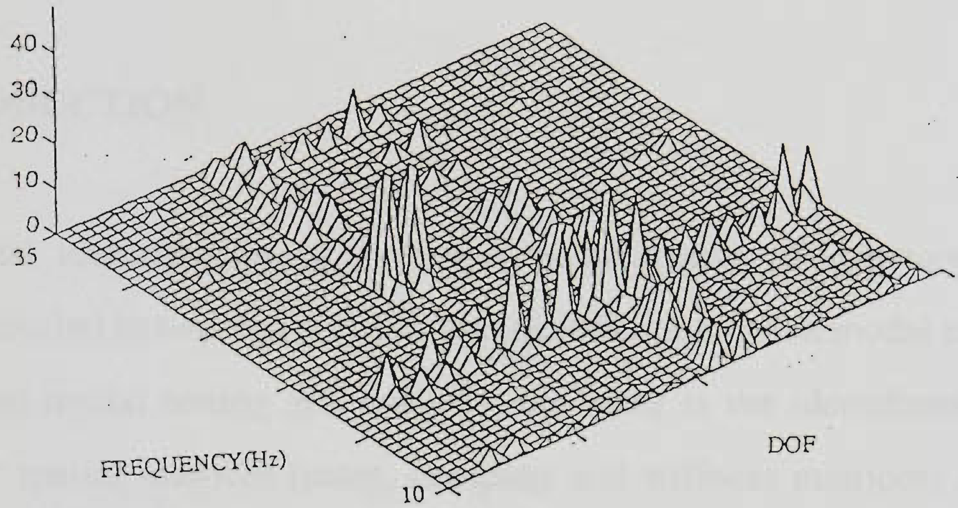

FIG.4.18: 3-D Damage Location Plot for case 2 damage in fig.4.3 model

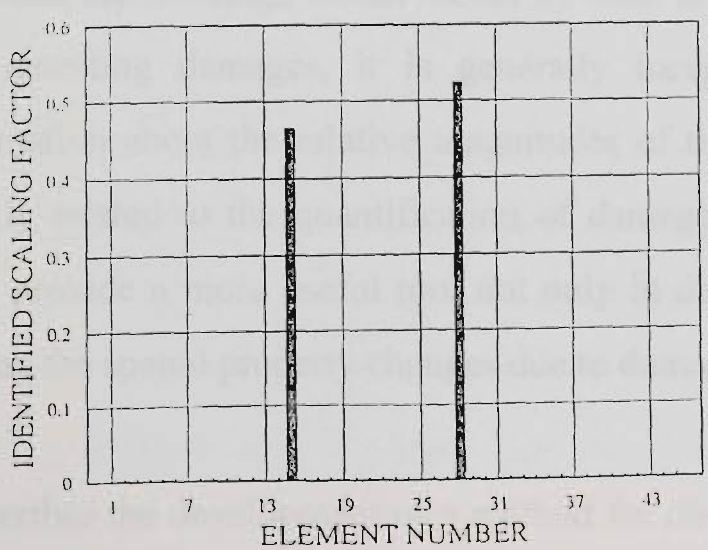

FIG.4.19: Identified scaling factor for case 2 damage in fig.4.3 truss structure.

CHAPTER 5

USING THE SPATIAL MODEL TO DETERMINE DAMAGE EXTENT

5.1 INTRODUCTION

Experimental identification of dynamic characteristics of structures can be broadly classified in two ways: one is the identification of the modal parameters and is called modal testing and analysis; the other is the identification of the physical or spatial matrices (mass, damping and stiffness matrices) which are often referred to as system identification.

The experimentally derived models can be used in a variety of applications, of which detection of damage in a structure is an important area. In damage detection, it is found that although modal model by itself is somewhat effective in locating or detecting damages, it is generally incapable of providing immediate information about the relative magnitudes of the spatial properties which are directly related to the quantification of damage. Generally, spatial properties could provide a more useful tool not only in detecting damage but also in quantifying the spatial property changes due to damage.

This chapter describes the development of a method for direct identification of the spatial properties from measured FRF data, and furthermore to extend the method in order to locate and quantify structural damage.

5.2 REVIEW OF PREVIOUS RESEARCH FOR SPATIAL MODEL DERIVATION

Derivation of a valid spatial model of a dynamic system from experimental data has been a focus of many researchers. Research in this field can be broadly classified under two categories: using frequency domain data and using time domain data to derive spatial parameters. Among the works using frequency domain data, one of the earlier publications can be traced back to the work by Raney [83] in which he showed ways of computing the mass, stiffness and damping co-efficients at selected locations in a structure using the results of near-resonance testing. Subsequent to that, Ross [84] had tried to synthesize [M] and [K] by using a normalisation procedure for the measured eigenvectors so that the known strain energy characteristics of the system could be preserved. Thoren [85] had proposed a technique similar to Ross [84] which used orthonormal modal vectors to derive mass, stiffness and damping matrices. In essence, his method made use of the orthogonality properties of the vibration modes.

Potter and Mark [86] introduced the concept of a transfer matrix (inverse of a system matrix) and had derived expressions to obtain [M], [C] and [K] in terms of the poles and the complex modal vectors of an elastic mechanical system. Tsang and Rider [87] proposed a method of deriving spatial parameters from measured frequency response function data. Lee and Dobson [88] also used experimentally measured FRF data to derive structural mass, stiffness and damping properties. They also tried with limited success to generate a reduced model from measurements which retains the dynamic characteristics.

Stanbridge, et al. [89] suggested that the values to be given to the mass, stiffness and damping constants of these modal elements can in principle be determined using the equations of motion of each mass in turn, from a small number of experimentally determined sinusoidal frequency responses. Although it was shown to be effective for a mass-spring-damper chain system, the effectiveness of the proposed method to more complicated structures is open to doubt. Muscia [90] introduced a methodology which was similarly based on the orthogonality conditions of the eigenvectors of the structure. Alvin, et al. [91] tried a method for determining minimum order mass and stifness matrices from modal test data. Chen, et al. [92] developed a transformation matrix between complex and the normal frequency response functions of a structure and used it to calculate the damping matrix of the system.

In addition to the methods discussed above, which were all frequency domain techniques, there have been efforts to estimate spatial parameters using time domain techniques. Among them, Rajaram and Junkins [94] derived a technique that used a Gauss-Newton least squares differential correction method to produce modal information that in turn would identify a unique lumped parameter model from forced response data. Juang and Pappa [95] employed the concept of Singular Value Decomposition to develop the Eigensystem Realization Algorithm for deriving spatial parameters. Fritzen [96] developed the Instrument Variable (IV) method and compared it with the Least Squares Method suggested by Lerudian, et al. [93] to reveal much improvement. However, in a more recent work by Roemer and Mook [99], the mass, stiffness and damping matrices were identified by using an integrated approach. In this method, the Eigensystem Realization Algorithm [95], the impulse response method [97], and the minimum modal error estimation method [98] had been combined to generate a more robust method for spatial parameter derivation from the sensitivity of measurement noise viewpoint.

The method presented in this chapter aims to develop a frequency domain technique using measured frequency response function data to derive spatial parameters. Besides enjoying the inherent advantage of using FRF data over modal data as described in Chapter 1, the proposed method identifies mass and stiffness completely independent of each other. This is in contrast to almost all the existing methods which derived mass, stiffness and damping parameters from measured FRF data simultaneously. This essentially means that for an N DOF system, existing methods work with matrices of size of 3Nx3N. This introduces an unnecessary computational burden which can be avoided if the mass and stiffness can be derived seperately. The method presented in this chapter addresses this problem. In addition to lessening the computational burden, this method will be more efficient in the case of damage detection, since the damage most often affects the stiffness of the structure more significantly than the mass and damping. Therefore, if this method is used to locate and estimate structural damage, the mass properties of the structure may be neglected. Finally and most importantly, even in absence of a FE model of the undamaged structure, this method can use the FRF data before and after damage to generate spatial models. Comparison of these two models will indicate the location and extent of damage.

The submatrix approach can also be used together with this method to identify the damaged elements of the structure directly instead of the matrix coefficients in the spatial matrices.

5.3 THEORY TO GENERATE SPATIAL MODEL

For an N DOF undamped system, the receptance matrix $[\alpha(\Omega)]$ is given by:

$$[\alpha(\Omega)] = ([K] - \Omega^2[M])^{-1}$$

or, $$([K] - \Omega^2[M])[\alpha(\Omega)] = [I] \tag{5.3.1}$$

where [K] and [M] are NxN real matrices of stiffness and mass respectively.

Rewriting equation (5.3.1) for a frequency Ω_1,

$$([K] - \Omega_1{}^2[M])[\alpha(\Omega_1)] = [I]$$

or, $$[K][\alpha(\Omega_1)] = [I] + \Omega_1{}^2[M][\alpha(\Omega_1)] \tag{5.3.2}$$

At another frequency Ω_2, equation (5.3.2) can be written as:

$$[K][\alpha(\Omega_2)] = [I] + \Omega_2{}^2[M][\alpha(\Omega_2)] \tag{5.3.3}$$

Transpose of equation (5.3.2) yields,

$$[\alpha(\Omega_1)][K] = [I] + \Omega_1{}^2[\alpha(\Omega_1)][M] \tag{5.3.4}$$

Post multiplying both sides of equation (5.3.4) by $[\alpha(\Omega_2)]$ will generate the following equation:

$$[\alpha(\Omega_1)][K][\alpha(\Omega_2)] = [\alpha(\Omega_2)] + \Omega_1^{\,2}[\alpha(\Omega_1)][M][\alpha(\Omega_2)] \tag{5.3.5}$$

Pre multiplying both sides of equation (5.3.3) by $[\alpha(\Omega_1)]$, the equation derived is:

$$[\alpha(\Omega_1)][K][\alpha(\Omega_2)] = [\alpha(\Omega_1)] + \Omega_2^{\,2}[\alpha(\Omega_1)][M][\alpha(\Omega_2)] \tag{5.3.6}$$

Subtracting equation (5.3.5) from equation (5.3.6) yields:

$$(\Omega_1^{\,2} - \Omega_2^{\,2})[\alpha(\Omega_1)][M][\alpha(\Omega_2)] = [\alpha(\Omega_1)] - [\alpha(\Omega_2)] \tag{5.3.7}$$

$$[M] = \frac{1}{(\Omega_1^2 - \Omega_2^2)}([\alpha(\Omega_2)]^{-1} - [\alpha(\Omega_1)]^{-1}) \tag{5.3.8}$$

Using equations (5.3.6) and (5.3.8) together the following equation is derived:

$$[K] = \frac{1}{(\Omega_1^2 - \Omega_2^2)}(\Omega_1^2[\alpha(\Omega_2)]^{-1} - \Omega_2^2[\alpha(\Omega_1)]^{-1}) \tag{5.3.9}$$

It is noted that the expression derived for mass [M] and stiffness [K] using equations (5.3.8) and (5.3.9) are similar to results derived by Klosterman [100]. However, Klosterman had used the results only for extracting modal parameters. From a practical viewpoint, an algorithm which relies on a full matrix $[\alpha(\Omega)]$ is not promising, since in reality it is not possible to measure the whole matrix of $[\alpha(\Omega)]$ and the re-constructed $[\alpha(\Omega)]$ will contain various errors. More realistically, a single column of RFRF matrix is all that is mostly measured. From this viewpoint, an algorithm to derive the mass and stiffness matrices has to rely only on one column of FRF data rather than the whole matrix $[\alpha(\Omega)]$.

Considering a single column of the receptance matrix, equation (5.3.1) at a frequency Ω_1 can be rewritten as:

$$([K] - \Omega_1^2[M])\{\alpha(\Omega_1)\}_k = \{\delta\}_k \tag{5.3.10}$$

$$\text{or,}\quad [K]\{\alpha(\Omega_1)\}_k = \{\delta\}_k + \Omega_1^2[M]\{\alpha(\Omega_1)\}_k \tag{5.3.11}$$

Again, at a different frequency Ω_2 :

$$[K]\{\alpha(\Omega_2)\}_k = \{\delta\}_k + \Omega_2^2[M]\{\alpha(\Omega_2)\}_k \tag{5.3.12}$$

The transpose of equation (5.3.11) yields:

$$\{\alpha(\Omega_1)\}_k^T[K] = \{\delta\}_k^T + \Omega_1^2\{\alpha(\Omega_1)\}_k^T[M] \tag{5.3.13}$$

Post multiplying both sides of equation (5.3.13) by $\{\alpha(\Omega_2)\}_k$ leads to:

$$\{\alpha(\Omega_1)\}_k^T[K]\{\alpha(\Omega_2)\}_k = \{\delta\}_k^T\{\alpha(\Omega_2)\}_k + \Omega_1^2\{\alpha(\Omega_1)\}_k^T[M]\{\alpha(\Omega_2)\}_k \tag{5.3.14}$$

Also, pre multiplying both sides of equation (5.3.12) by $\{\alpha(\Omega_1)\}_k^T$ yields:

$$\{\alpha(\Omega_1)\}_k^T[K]\{\alpha(\Omega_2)\}_k = \{\alpha(\Omega_1)\}_k^T\{\delta\}_k + \Omega_2^2\{\alpha(\Omega_1)\}_k^T[M]\{\alpha(\Omega_2)\}_k \tag{5.3.15}$$

Subtracting equations (5.3.14) from (5.3.15) yields:

$$\{\alpha(\Omega_1)\}_k^T[M]\{\alpha(\Omega_2)\}_k = (\alpha_{kk}(\Omega_1) - \alpha_{kk}(\Omega_2))/(\Omega_1^2 - \Omega_2^2) \qquad (5.3.16)$$

Replacing equation (5.3.16) into equation (5.3.14), it gives:

$$\{\alpha(\Omega_1)\}_k^T[K]\{\alpha(\Omega_2)\}_k = (\Omega_1^2\alpha_{kk}(\Omega_1) - \Omega_2^2\alpha_{kk}(\Omega_2))/(\Omega_1^2 - \Omega_2^2) \qquad (5.3.17)$$

In order to derive matrices [M] and [K] using equations (5.3.16) and (5.3.17), some mathematical manipulation is needed. In particular, the connectivity constraint of the structure needs to be imposed to ensure that non-existent load paths do not occur in the derived mathematical model. Two different approaches can be taken. Approach I tries to obtain the individual matrix coefficients of the spatial matrix and Approach II tries to identify the elements instead of the matrix coefficients.

Approach I

A 3 DOF undamped mass spring system shown in figure 5.1 is used to illustrate the procedure of deriving spatial parameters using this approach. Without loosing generality, the first column of receptance matrix $\{\alpha(\Omega)\}_1$ is used.

Let $\{\alpha(\Omega_1)\}_1 = \{a\ b\ c\}$ and $\{\alpha(\Omega_2)\}_1 = \{d\ e\ f\}$

Hence, equation (5.3.17) can be written as:

$$\begin{Bmatrix} a & b & c \end{Bmatrix} \begin{bmatrix} K_{11} & K_{12} & 0 \\ K_{21} & K_{22} & K_{23} \\ 0 & K_{32} & K_{33} \end{bmatrix} \begin{Bmatrix} d \\ e \\ f \end{Bmatrix} = x \qquad (5.3.18)$$

where x is the right hand side of the equation (5.3.17) and is known. Using simple matrix multiplication and knowing that the stiffness matrix is symmetric, the left hand side of equation (5.3.18) can be written as:

$$\begin{aligned}&K_{11}ad + K_{12}ae + K_{21}bd + K_{22}be + K_{23}cf + K_{32}ce + K_{33}cf\\&= K_{11}ad + K_{12}(ae + bd) + K_{23}(bf + ce) + K_{22}be + K_{33}cf\end{aligned}$$

$$= \{ad \quad be \quad cf \quad (ae+bd) \quad (bf+ce)\}\begin{Bmatrix} K_{11} \\ K_{22} \\ K_{33} \\ K_{12} \\ K_{23} \end{Bmatrix}$$

Therefore,

$$\{ad \quad be \quad cf \quad (ae+bd) \quad (bf+ce)\}\begin{Bmatrix} K_{11} \\ K_{22} \\ K_{33} \\ K_{12} \\ K_{23} \end{Bmatrix} = x \qquad (5.3.19)$$

Equation (5.3.19) has been generated using a pair of frequency points, Ω_1 and Ω_2. Since there are five unknowns in the equation, at least five independent equations requiring five different pairs of frequency points are needed in order to derive all the unknowns.

The above example for a 3 DOF system can be easily extended to an N DOF system. On closer inspection, it is found that the derivation for a 3 DOF system follows a pattern. The matrix coefficient corresponding to coefficient location

1-1 in the stiffness matrix is derived by using element 1 in $\{\alpha(\Omega_1)\}_1$ and element 1 in $\{\alpha(\Omega_2)\}_1$. The matrix coefficient for coefficient location 2-2 is obtained by using element 2 in $\{\alpha(\Omega_1)\}_1$ and element 2 in $\{\alpha(\Omega_2)\}_1$ and so on. For the off-diagonal matrix coefficients in [K], the matrix coefficient for coefficient location 1-2 or 2-1 is derived by using elements 1 and 2 in $\{\alpha(\Omega_1)\}_1$ and elements 1 and 2 in $\{\alpha(\Omega_2)\}_1$ respectively. The same process can be repeated for coefficient location of other off-diagonal matrix coefficients. Using this pattern, equation (5.3.19) can be implemented in a computer programme for an N DOF system.

Approach II

Instead of identifying the individual matrix coefficients in the stiffness or mass matrix, it is possible to identify individual mass or stiffness elements in the structure. In figure 5.1, k_1 is the stiffness element connecting DOF 1 to the ground, k_2 connect DOFs 1 and 2, and so on. In order to identify k_1, k_2, etc. directly, equation (5.3.18) can be written as:

$$\{a \quad b \quad c\}\begin{bmatrix} k_1+k_2 & -k_2 & 0 \\ -k_2 & k_2+k_3 & -k_3 \\ 0 & -k_3 & k_3+k_4 \end{bmatrix}\begin{Bmatrix} d \\ e \\ f \end{Bmatrix} = x \tag{5.3.20}$$

Matrix multiplication of left hand side of equation (5.3.20) yields the following:

$$\{ad \quad ((ad+be)-(ae+bd)) \quad ((be+cf)-(bf+ce)) \quad cf\}\begin{Bmatrix} k_1 \\ k_2 \\ k_3 \\ k_4 \end{Bmatrix} = x \tag{5.3.21}$$

Again, each coefficient of a particular stiffness element can be built up by considering only those DOFs which are connected to that particular stiffness element. For instance, the coefficient of k_2 in equation (5.3.21) is built up using elements 1 and 2 of $\{\alpha(\Omega_1)\}_1$ and $\{\alpha(\Omega_2)\}_1$ respectively because k_2 connects DOFs 1 and 2. By constructing an adequate number of equations using different pairs of frequency points, it is possible to identify individual stiffness elements k_1, k_2, k_3 and k_4. The same procedure can be repeated for identifying mass elements.

5.4 DISCUSSION

As shown above in the theory, it is possible to derive mass, stiffness and damping matrices by using receptance FRF data at different frequency points. Instead of the entire FRF matrix, the presented method is able to derive the spatial matrices by using a single column of receptance FRF matrix at different frequencies. However, in order to obtain accurate results using this method, a certain degree of judgement is warranted while selecting frequency points at which receptance FRF data are required. The frequency points selected should satisfy the following basic criteria :

(i) As already discussed above, equations (5.3.16) and (5.3.17) require a pair of frequency points. Depending on the number of unknowns, the same number of equations are required to generate mass or stiffness matrix. It is essential to realize that the pair of frequency points to be used in a particular equation should be always different to eliminate the possibility of division by zero in the right hand side of equations (5.3.16) and (5.3.17).

(ii) The number of unknowns in the mass, stiffness or damping matrix of a structure determine the minimum number of equations required. For instance if the stiffness matrix of a particular structure has three diagonal matrix coefficient and two off-diagonal matrix coefficient on each side of the diagonal, then to identify the five unknown matrix coefficients using Approach I at least five equations have to be generated. Instead of identifying the matrix coefficients, if elements are to be identified as shown in Approach II, then the number of equations required is guided by the number of unknown elements.

(iii) Although two particular frequency pairs should not have the same combination, the same frequency point can be used in different pairs. This may significantly reduce the number of frequency points needed for the execution of this algorithm. For "n" frequency points, it is possible to build up "d" different frequency pairs where

$$d = \Sigma\,(n-i) \quad \text{where } i = 1, 2, \ldots\ldots\ldots(n-1)$$

Equation (5.3.16) or (5.3.17) at different frequency points offers a set of simultaneous equations, which is in the form of:

$$[B]\{x\} = \{b\} \tag{5.4.1}$$

where $[B]$ = a square matrix constructed using receptance FRF data at different frequency points.

$\{x\}$ = an unknown vector comprising of elements of $[M]$ or $[K]$ to be determined.

{b} = a known vector constructed using point receptance FRF data at different frequency points.

To solve for this set of linear equations, it is essential that matrix [B] is non-singular. Therefore, it is always necessary to check the singularity of matrix [B]. However, from studies on simulated cases, it has been found that the most suitable frequency points for this method have certain properties which are identical to the findings by Lee and Dobson [88] regarding the selection of frequency points for their method of identifying spatial parameters. These properties are:

(i) frequency points should be scattered through out the frequency band over which it is required to establish the model;
(ii) it is better to avoid points where noise effect is significant;
(iii) frequency points selected should be close to resonances;
(iv) frequency points near anti-resonances should be avoided.

When FRF data are contaminated by noise, the effect of noise may be reduced by using additional frequency points. Consequently, equation (5.4.1) becomes overdetermined and can be solved mathematically for the optimum answers. However, when using noisy FRF data the [M] and [K] derived have been found to be frequency dependant. However, as long as the noise is not excessively large, the modal parameters generated by this spatial model do not show significant variations. Besides, the effect of noise can be reduced by using Approach II instead of Approach I. In the numerical examples to follow, different noise levels have been used to examine variation of results.

5.5 APPLICATION OF THE METHOD FOR DETERMINING DAMAGE EXTENT

The theory proposed in Section 5.3 for deriving spatial parameters can be also used effectively for determining damage extent. In the following section three different approaches have been suggested for identifying damage in a structure:

5.5.1 Method I: Direct Method using experimental data only

In some cases, the FE model of the undamaged structure might not be available. Instead the FRF data of the structure before and after damage is available. Method I proposes to use those FRF data to build the spatial models of the structure before and after damage. The connectivity of a structure is often derivable from the structure itself without any mathematical model. This can be imposed on the spatial models to be built by this method. As a result it is possible to ensure that both the derived models represent the connectivity of the structure. The location and extent of damage can be obtained by comparing the two models thus developed.

However, if the FE model of the undamaged structure is available, the need to derive the spatial model of the undamaged structure will not be there. For such a case, the FE model of the undamaged structure can be used with the FRF data of the damaged structure to locate damage. Following that Methods II and III can be used to determine the extent of damage as shown below.

5.5.2 Method II: Indirect Method

In this method once the area of damage is located, the spatial matrix coefficients for that area is computed only. This is illustrated by considering the example given in figure 5.1. It is assumed that the damage is located between DOFs 2 and 3 and equation (5.3.19) is again given here,

$$\{ad \quad be \quad cf \quad (ae+bd) \quad (bf+ce)\}\begin{Bmatrix} K_{11} \\ K_{22} \\ K_{33} \\ K_{12} \\ K_{23} \end{Bmatrix} = x \tag{5.3.19}$$

From the damage location it is known that K_{11} and K_{12} have not been affected by damage. Therefore they can be replaced by their original values and equation (5.3.19) is modified to give the following equation:

$$\{be \quad cf \quad (bf+ce)\}\begin{Bmatrix} K_{22} \\ K_{33} \\ K_{23} \end{Bmatrix} = x - K_{11}ad - K_{12}(ae+bd) = x_1 \tag{5.5.1}$$

Hence, by using at least three sets of frequency points it is possible to derive unknowns K_{22}, K_{23} and K_{33}. However, if the measurement is noisy, better results can be obtained by considering more than three sets of frequency points and solving the overdetermined equations.

5.5.3 Method III: Submatrix approach

Instead of determining the spatial matrix coefficients affected by damage, the proposed method can also be used together with the submatrix approach in Chapter 4 to determine damage extent. Using equation (4.2.8), the stiffness of the damaged structure for this model in figure 5.1 can be written as:

$$[K]_D = [K]_{UD} + h_1[K]_1 + h_2[K]_2 + h_3[K]_3 + h_4[K]_4 \tag{5.5.2}$$

$$[K]_{UD} = [K]_1 + [K]_2 + [K]_3 + [K]_4 \tag{5.5.3}$$

where h_1, h_2, h_3 and h_4 are the scaling factors.

Hence using equation (5.3.17), we get

$$\{\alpha_D(\Omega_1)\}_k^T\left[[K]_{UD} + h_1[K]_1 + h_2[K]_2 + h_3[K]_3 + h_4[K]_4\right]\{\alpha_D(\Omega_2)\}_k = x \tag{5.5.4}$$

$$\{a_1 \quad a_2 \quad a_3 \quad a_4\}\begin{Bmatrix} h_1 \\ h_2 \\ h_3 \\ h_4 \end{Bmatrix} = x_2 \tag{5.5.5}$$

The only unknowns in the above equation are the scaling factors. Once the damaged element is located, the scaling factors which have not been affected due to damage can be safely assigned to zero. For the model shown in figure 5.1, since h_3 is the only scaling factor affected by damage, equation (5.5.5) can be modified to become

$$a_3h_3 = x_2$$

or, $h_3 = x_2 / a_3$

Since x_2 and a_3 are already known from FRF data, h_3 can be easily computed which represents a measure of damage extent. Therefore, in contrast to Method II which requires at least three pairs of frequency points, Method III is able to quantify damage of the same system by using a single pair of frequency point.

While trying to detect damage extent using these methods proposed here, it is found that the results obtained are not unique when FRF data contaminated by noise. In general, it has been found that more accurate estimate of damage can be obtained by using FRF data more affected by damage. These FRF data are in the vicinity of natural frequencies which have been more severely shifted by damage.

5.6 RESULTS OF NUMERICAL CASE STUDIES

In this section, two numerical examples are given: the first shows its merits in regard to extracting spatial parameters from FRF data and the second one shows the effectiveness of the method in identifying and locating structural damage. In the second example, all three methods suggested in Section 5.5 for determining damage extent are used. In addition, FRF data contaminated by simulated measurement noise have been used.

The first example was based on the axial vibration of an undamped cantilever beam and is shown in figure 5.2. The beam was discretized into a lumped mass-spring system that has eight DOFs. The model consisted of eight masses with springs between them.

This eight DOF system was used to investigate the performance of the proposed method to develop spatial matrices from FRF data. The actual mass and stiffness matrices of this undamped system are given in Tables 5.1 and 5.2 respectively. In the simulation, it was assumed that the data from the first column of the FRF matrix were available. Calculations were carried out in two different ways. Firstly, each individual matrix coefficient of the mass and stiffness matrices were estimated using Approach I in Section 5.5. Since the diagonal mass matrix has 8 elements, it required 8 pairs of frequency points. For the stiffness matrix, there are 8 diagonal unknowns and 7 off- diagonal unknowns. Therefore, 15 pairs of frequency points were used. The 15 pairs of frequency points used to identify the matrix [M] and [K] are given in Table 5.3 and 5.4 respectively where the first eight pairs were used to derive [M].

These two different sets of frequency points were used to test the frequency independance of the results obtained by using the proposed method. While using Approach II, the individual mass and stiffness elements were obtained. There were eight mass and eight stiffness elements.

The frequency sets used to generate the mass and stiffness elements were the first sixteen frequency points given in Tables 5.3 and 5.4. It is worth mentioning that the frequency points considered in this exercise were within the first five modes of the system. In the next instance, the same example was repeated first with 0.5% noise and then with 1.5% noise. When using noisy

FRF data, additional frequency sets were used to make the spatial parameter derivation problem overdetermined so that the effect of noise may be reduced. Using Approach I, the stiffness and mass matrix co-efficients derived using noise free and noisy FRF data are given in Table 5.5.

Using different pairs of frequency points, it was found that the same [M] and [K] were derived if the FRF data were noise free. However, with noisy FRF data, the derived matrices varied with choice of frequency points and it was found that the accuracy of the derived matrices improved if the data selected were nearer natural frequencies and covered the frequency range of interest. For Approach II, the identified stiffness elements have been tabulated in Table 5.6. The natural frequencies generated by using the actual and derived spatial parameters using both the approaches have been given in Table 5.7. From the results obtained it might be concluded that for noise free FRF data the same results can be obtained by using different sets of frequency points as long as the matrix [B] in equation (5.4.1) is non singular. However, with noisy data better results can be obtained by using Approach II and using larger number of frequency points so that the problem becomes overdetermined which can be solved for the optimum answers.

The damage extent algorithm proposed in this chapter and referred to as Methods I, II and III were examined on the 12 DOF mass spring system given in figure 3.2. Figure 5.3 shows the true damage location and extent. Table 5.8 shows the shifts in natural frequencies due to the damage introduced. From the table it is clear that some natural frequencies have been affected more than others due to the damage.

Method I was first applied to derive the stiffness matrix of the undamaged and damaged structure and the [ΔK] obtained from their comparison is given in figure 5.4. From the result, the extent of damage can be ascertained quite accurately. With noisy FRF data (4% noise), the results obtained using Method I was found to deteriorate. However, for such cases, better results were obtained when using Method II and III as shown below.

While using Method II, the information regarding the location of the damage was utilised and the matrix elements only in the area of the damage was located. It was assumed that FRF data were available for a frequency range covering the first five modes. The frequency points utilised were in the vicinity of the natural frequencies which had been more severely affected than others within the 'measured' frequency range. The damage extent plotted in figure 5.5 gives a very good estimate of the magnitude of the damage. To obtain the result shown in figure 5.5, theoretically three frequency pairs are required to compute the three unknown matrix elements corresponding to area of damage in the stiffness matrix. However, to reduce the effect of noise, six frequency pairs were used involving four frequency points (frequency points used: 120 rad/s, 182 rad/s, 185 rad/s, and 204 rad/s) Using Method III for the damaged portion of the structure, the result obtained as shown in figure 5.6 is equally good, although it can be achieved by using a smaller number of frequency points compared to Method II. The result obtained in figure 5.6 was obtained by using a single pair of frequency points (183 rad/s and 185 rad/s).

Methods II and III were repeated by using a different set of frequency points and the frequency points were selected such that they were in the vicinity of the natural frequency (natural frequency corresponding to 31.6 rad/s) which had not been much affected by damage. Although, it still indicated the damage extent as given in figures 5.7 and 5.8, they are not as accurate as the results obtained in figures 5.5 and 5.6. Therfore, to obtain the best results, it is always better to select frequency points such that they are close to natural frequencies which have been most severely affected by damage.

The same example was repeated but with incomplete coordinates and noise of 4% in the FRF data. The 'measured' coordinates were assumed to be 1, 2, 3, 6, 8, 11 and 12. As already shown in figure 3.5A in Chapter 3, the damage location plot succeeded in locating the damage between coordinates 6 and 8.

Two different cases were studied:

a) the RFRF data for coordinate 7 were available.

b) the RFRF data for coordinate 7 was interpolated using D.E A.

For both the cases, the remaining ummeasured coordinates were interpolated using D.E A. For case (a), both methods II and III were used to quantify the damage extent and they have been shown in figures 5.9 and 5.10. It is clear that both Methods II and III produced accurate results. For case (b), the results obtained using methods II and III have been plotted in figures 5.11 and 5.12. The results obtained offer a reasonably accurate estimate of the extent of the damage although it is not as accurate as case (a). Based on simulation studies hitherto, it is suggested that once the damage is located, the best results for damage estimation can be obtained if it is possible to additionally measure the coordinates in the area of damage and then use the additional FRF data to determine the damage extent.

5.7 SUMMARISING REMARKS

A new method has been suggested to derive the spatial properties of dynamic system using FRF data. The method has the advantage of working only with the stiffness of the structure without dealing with the mass properties. This allows the user to calculate the changes in stiffness or mass due to structural damage seperately and results in substantial reduction in matrix size to be handled in damage location and estimation.

Because of its ability to derive spatial parameters directly from measured FRF data, theoretically Method I is able to determine damage extent without the FE model of the undamaged structure. With measured FRF data before and after damage, two spatial models with the correct connectivity can be derived and damage can be related to the difference between them.

For noisy FRF data, Methods II and III perform better than Method I. However, Method I has excellent potential in damage detection as it can work without an FE model. Further work is required to develop it to become a more robust method when dealing with measured FRF data with noise.

1	0	0	0	0	0	0	0
0	1	0	0	0	0	0	0
0	0	1	0	0	0	0	0
0	0	0	1	0	0	0	0
0	0	0	0	1	0	0	0
0	0	0	0	0	1	0	0
0	0	0	0	0	0	1	0
0	0	0	0	0	0	0	1.5

Table 5.1: Mass matrix of the cantilever beam model shown in Fig.5.2

4000	-2000	0	0	0	0	0	0
-2000	4000	-2000	0	0	0	0	0
0	-2000	4000	-2000	0	0	0	0
0	0	-2000	4000	-2000	0	0	0
0	0	0	-2000	4000	-2000	0	0
0	0	0	0	-2000	4000	-2000	0
0	0	0	0	0	-2000	4000	-2000
0	0	0	0	0	0	-2000	2000

Table 5.2: Stiffness matrix of the cantilever beam model shown in Fig.5.2

44.6 rad/s 19 rad/s	24.6 rad/s 48 rad/s	54.6 rad/s 18 rad/s	39 rad/s 46 rad/s
54.8 rad/s 23 rad/s	12.5 rad/s 36 rad/s	58 rad/s 29 rad/s	54.6 rad/s 21 rad/s
19.3 rad/s 25.8 rad/s	15 rad/s 60 rad/s	54.6 rad/s 40 rad/s	67 rad/s 22 rad/s
45.3 rad/s 40.5 rad/s	32 rad/s 25 rad/s	13 rad/s 45 rad/s	

Table 5.3: Frequency pairs used to generate [M] and [K] for the cantilever beam model shown in Fig.5.2

14.6 rad/s 17 rad/s	29.6 rad/s 49 rad/s	34.6 rad/s 28 rad/s	19 rad/s 26 rad/s
54.8 rad/s 27.5 rad/s	42.5 rad/s 46 rad/s	58 rad/s 29 rad/s	51.6 rad/s 21 rad/s
19.3 rad/s 20.8 rad/s	15 rad/s 40 rad/s	54.6 rad/s 10 rad/s	67 rad/s 22 rad/s
15.3 rad/s 65.0 rad/s	32 rad/s 25 rad/s	33 rad/s 45 rad/s	

Table 5.4: Second combination of frequency pairs used to generate [M] and [K] for the cantilever beam model shown in Fig.5.2

Spatial Matrix Coeff.	Frequency points as given in Table 5.3 *Noise Level*			Frequency points as given in Table 5.4 *Noise Level*		
	0%	**0.5%**	**1.5%**	**0%**	**0.5%**	**1.5%**
M_{11}	1.0	1.03	1.06	1.0	1.01	1.05
M_{22}	1.0	1.01	1.03	1.0	.98	1.04
M_{33}	1.0	1.0	.94	1.0	.99	.96
M_{44}	1.0	.99	.95	1.0	1.02	.95
M_{55}	1.0	.98	1.05	1.0	1.0	1.04
M_{66}	1.0	1.0	1.02	1.0	.98	1.05
M_{77}	1.0	1.02	.97	1.0	1.02	.98
M_{88}	1.5	1.52	1.46	1.5	1.47	1.53
K_{11}	4000	3990	3960	4000	3982	3953
K_{12}	-2000	-2005	-1978	-2000	-1990	-1969
K_{22}	4000	4041	3962	4000	4054	4100
K_{23}	-2000	-1992	-1963	-2000	-2031	-2057
K_{33}	4000	4007	4042	4000	4025	4093
K_{34}	-2000	-1960	-2031	-2000	-2007	-2033
K_{44}	4000	3960	4093	4000	3989	3980
K_{45}	-2000	-1985	-1959	-2000	-1958	-1950
K_{55}	4000	4027	4100	4000	4013	3945
K_{56}	-2000	-2009	-2123	-2000	-1993	-2064
K_{66}	4000	3996	4087	4000	3990	4032
K_{67}	-2000	-1992	-2058	-2000	-1983	-1967
K_{77}	4000	4005	3901	4000	4010	4021
K_{78}	-2000	-2017	-2100	-2000	-2013	-2067
K_{88}	2000	2017	2285	2000	2015	2023

Table 5.5: Mass and stiffness coefficients generated for the cantilever beammodel shown in Fig. 5.2 with different noise levels in FRF data (Approach I)

Stiffness elements	Frequency points as given in Table 5.3 *Noise Level*			Frequency points as given in Table 5.4 *Noise Level*		
	0%	**0.5%**	**1.5%**	**0%**	**0.5%**	**1.5%**
K1	2000	2005	2013	2000	2010	2017
K2	2000	2008	2015	2000	1997	1990
K3	2000	2003	2005	2000	2003	2007
K4	2000	1995	2016	2000	2006	1989
K5	2000	1995	1987	2000	2005	2020
K6	2000	1997	2016	2000	1996	2009
K7	2000	2001	1994	2000	1997	1983
K8	2000	1995	2010	2000	2007	2019

Table 5.6: Stiffness elements of the cantilever beam model shown in Fig. 5.2 with different noise levels in FRF data (Approach II)

	System natural freq.	Identified natural frequencies using Approach I *Noise Level*			Identified natural frequencies using Approach II *Noise Level*		
		0%	**0.5%**	**1.5%**	**0%**	**0.5%**	**1.5%**
1	7.80	7.86	8.24	6.60	7.84	7.78	7.86
2	23.30	23.24	23.70	24.70	23.32	23.24	23.57
3	38.37	38.45	38.40	38.60	38.37	38.28	38.10
4	52.46	52.46	52.30	52.90	52.46	52.24	52.62
5	64.97	64.97	64.80	65.30	64.91	64.71	65.00
6	75.31	75.4	74.90	75.20	75.28	75.00	75.30
7	83.05	83.14	82.80	83.30	83.05	82.80	82.92
8	87.82	87.82	87.90	88.80	87.82	87.90	88.50

Table 5.7: Natural frequency (rad/s) of the cantilever beam model shown in Fig. 5.2 with the regenerated mass and stiffness using Table 5.3 frequency points

	NATURAL FREQUENCY OF THE MODEL SHOWN IN FIG.3.2	
	BEFORE DAMAGE	**AFTER DAMAGE**
	rad/s	**rad/s**
I	31.6	31.5
II	110.8	109.2
III	121.9	117.2
IV	185.4	179.8
V	206.6	203.0
VI	229.1	226.4
VII	269.6	268.9
VIII	399.4	399.4
IX	734.7	732.1
X	751.2	739.4
XI	972.2	957.8
XII	1017.0	1013.4

Table 5.8 : Natural frequencies of the model shown in fig.3.2 before and after damage

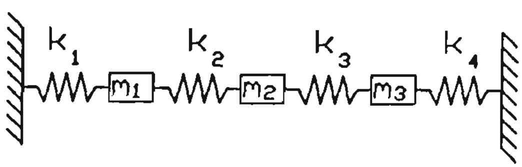

FIG.5.1: A 3 DOF mass-spring system.

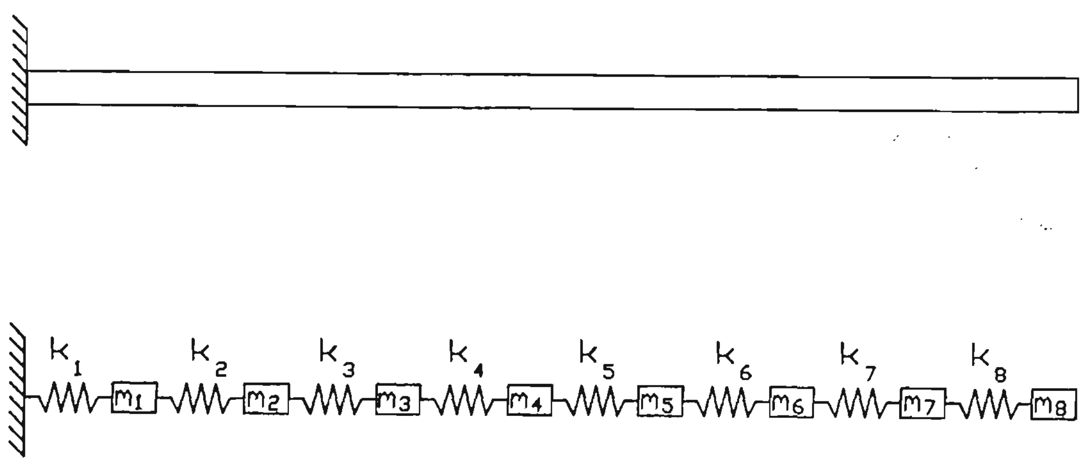

FIG.5.2: A continous beam and its lumped mass model.

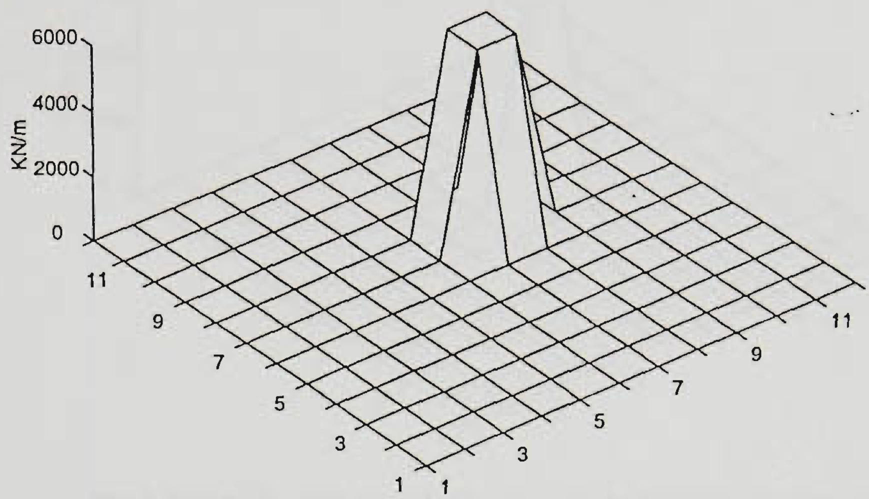

FIG.5.3: [ΔK] for the 12 DOF mass-spring system shown in fig.3.2

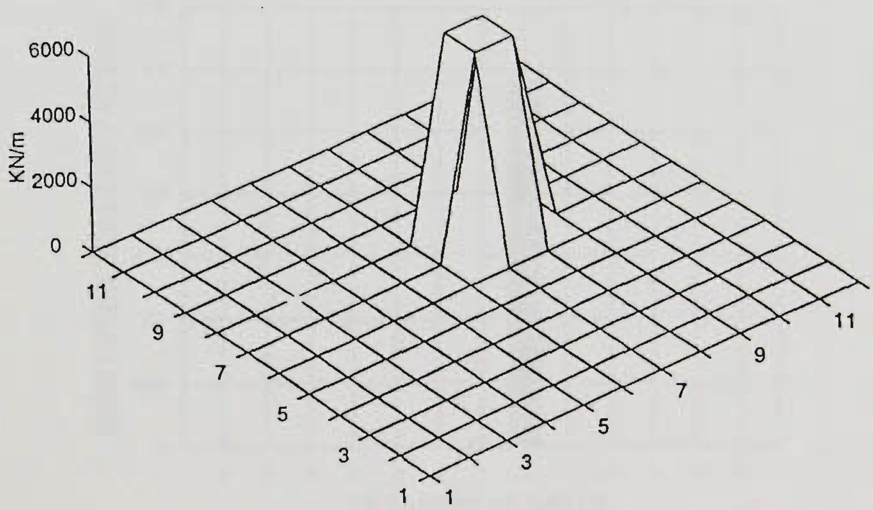

FIG.5.4: Calculated [ΔK] using Method I in section 5.5.1

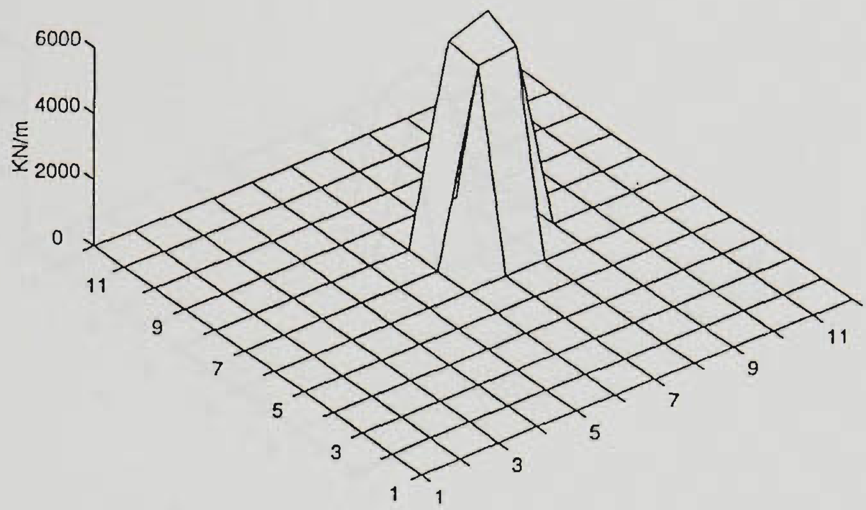

FIG.5.5: Calculated [ΔK] with 4% noise for the 12 DOF mass-spring system in fig.3.2 (using Method II in Section 5.5.2)

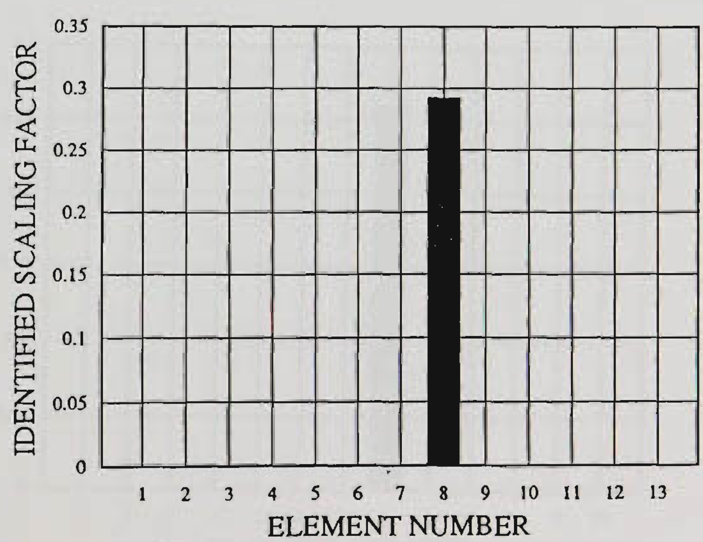

FIG.5.6: Identified scaling factor with 4% noise for the 12 DOF mass-spring system in fig.3.2 (using Method III in Section 5.5.3)

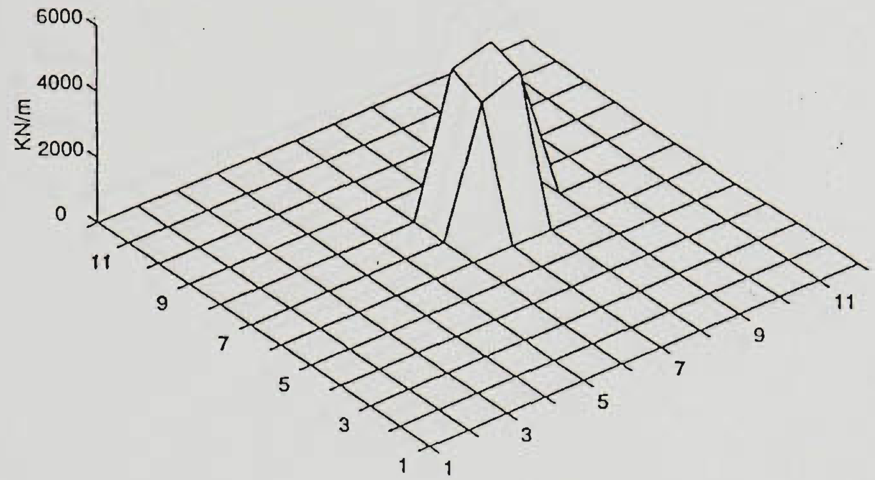

FIG.5.7: Calculated [ΔK] with 4% noise for the 12 DOF mass-spring system in fig.3.2 (using Method II with different frequency points)

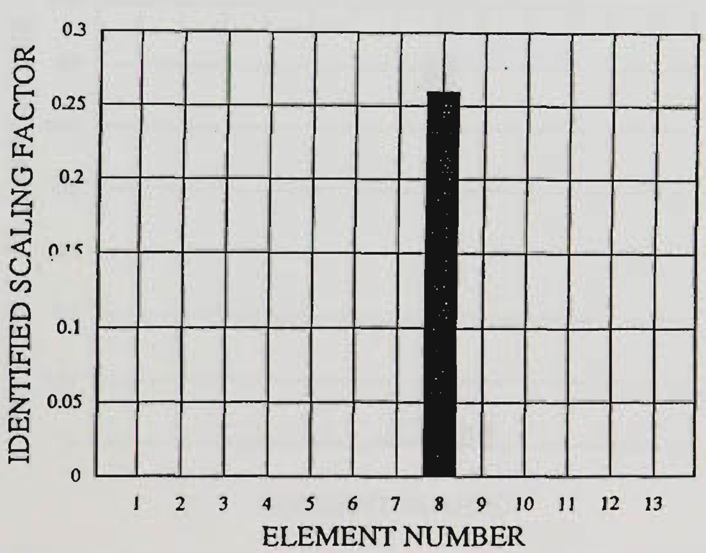

FIG.5.8: Identified scaling factor with 4% noise for the 12 DOF mass-spring system in fig.3.2 (using Method III with different freq. points)

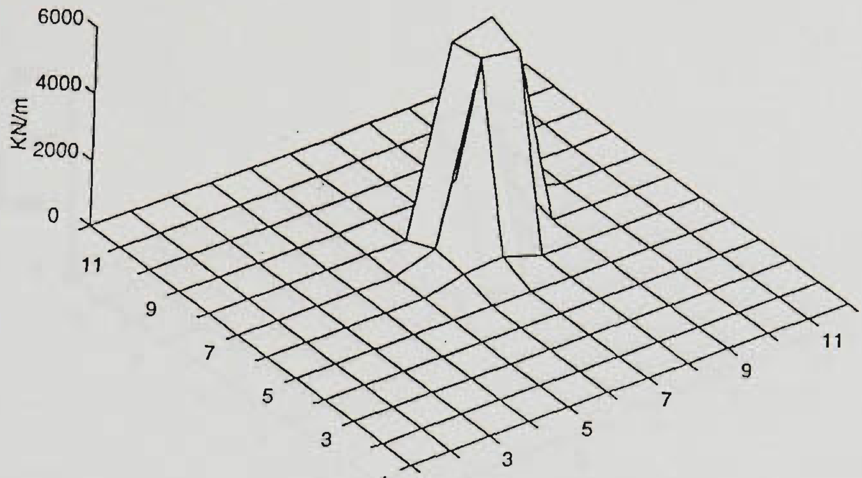

FIG.5.9: Calculated [ΔK] with 4% noise (incomplete coordinates in damage location measured) for the 12 DOF system in fig.3.2 (using Method II)

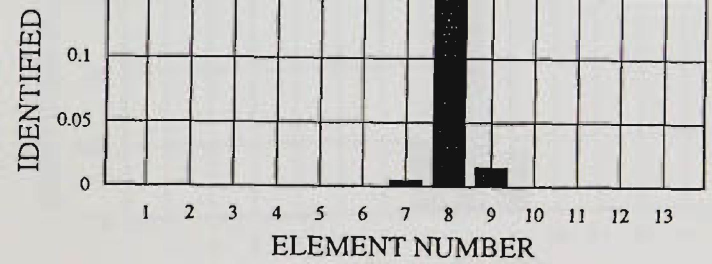

FIG.5.10: Identified scaling factor with 4% noise (incomplete coordinates in damage location measured) for the 12 DOF system in fig.3.2 (using Method III)

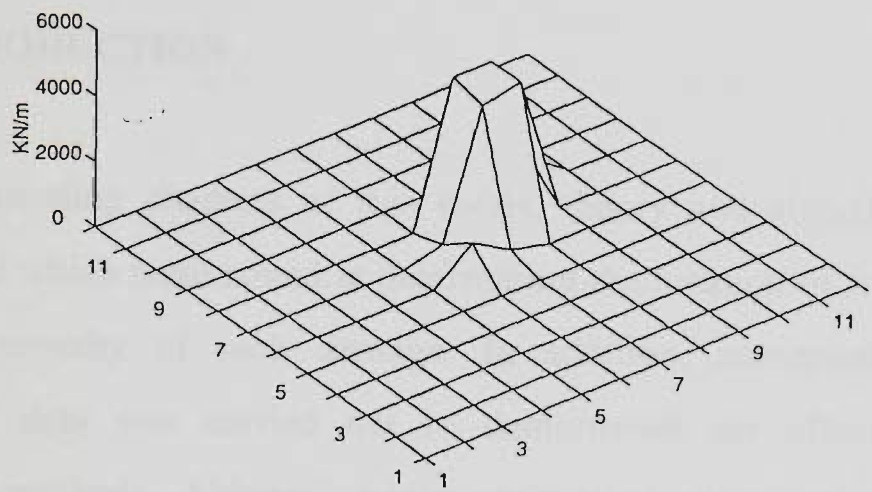

FIG.5.11: Calculated [ΔK] with 4% noise (incomplete coordinates in damage location interpolated) for the 12 DOF system in fig.3.2 (using Method II)

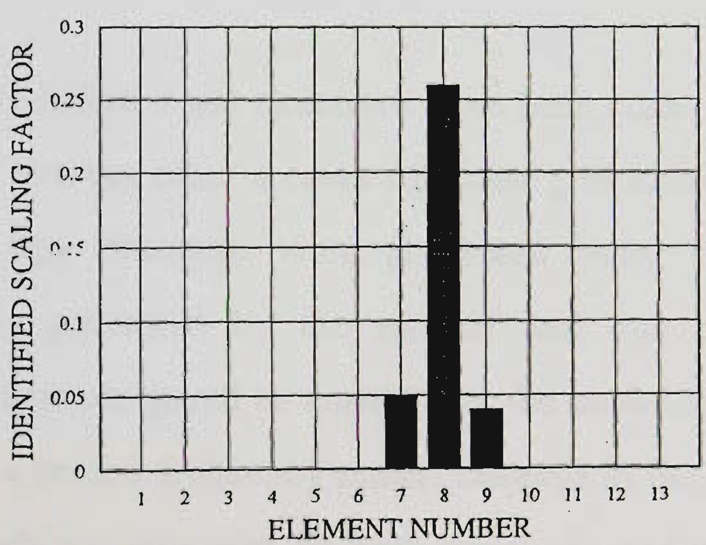

FIG.5.12: Identified scaling factor with 4% noise (incomplete coordinates in damage location interpolated) for the 12 DOF system in fig.3.2 (using Method III)

CHAPTER 6

EXPERIMENTAL STUDIES

6.1 INTRODUCTION

In the preceding chapters of this thesis, theory and algorithms have been developed which were aimed at determining the location of structural damage and the severity of such damage. In addition, numerical analysis with simulated data was carried out to demonstrate the effectiveness of the proposed methods. Although while conducting numerical analysis, efforts have been made to simulate complexities associated with practical structures and measurements, the ultimate confidence in the proposed algorithms cannot be achieved until they are applied to some practical structures.

In this work, two different test structures have been made and used, one was a cantilever beam and the other a cross stiffened grid structure. Finite element models of the test structures were generated using PAFEC-FE and the receptance FRFs generated by the models and that measured from the structures were first compared to ensure that the model truly represented the structure within a certain frequency range. Damage in the form of a hack saw cut of given depth was imposed on both structures and the damage location algorithms proposed in earlier chapters were applied. Subsequent to that, the algorithms proposed in Chapter 5 to determine the severity of the damage were applied on the beam and the cross grid structure. The effect of selection of frequency points on analysis of damage severity was also studied in detail.

Finally, a second damage was created in the grid structure to test the capacity of the location method to identify multiple damages.

6.2 THE TEST STRUCTURES

Two different test structures were used to carry out the experimental studies. The first was a simple cantilever beam structure made of mild steel of cross section 39 mm x 6 mm and 619 mm long. It was assumed that the material has a Young's Modulus of 209 GPa, Poisson's ratio of 0.3 and density of 7800 kg/m^3. Figure 6.3(a) shows the locations on the beam at which FRFs were measured. The points on the beam shown in this figure corresponds to nodal points in the data file for PAFEC FE given in Table 6.3. The beam was rigidly clamped at one end and was modelled as a cantilever.

The second was a cross stiffened grid structure shown in figure 6.2. Each member of the grid structure was an individual beam with a cross section of 20x10 mm with welded joints. Figure 6.3b shows the location on the grid structure at which FRF data were measured and they correspond to the nodal points in the data file in Table 6.6.

6.3 MEASUREMENT EQUIPMENT

An instrumented hammer (PCB 086B03) was used to excite the structure at one point and the response was measured at a different point using an accelerometer. The hammer was used with a plastic tip and a force transducer with a sensitivity of 2.10 mV/N. The hammer was connected to a power unit

(Model 480D06, Make: PCB) with gains of 1, 10 and 100. For this experiment, the gain was selected at 1. The output of the power unit was connected to channel A of the Dual Channel Analyzer (B&K 2032).

The translational responses of the structures were measured by using an accelerometer (PCB 10729). The accelerometer was small and light (2.4 gms) and was based on a simple configuration of piezo-electric slices clamped between a seismic mass and a centre post by a preloaded ring. This very light accelerometer ensured that its dynamic loading on the structure was negligible. The output of the accelerometer with voltage sensitivity of 0.804 mV/g was connected to a NVMS signal Conditioning Amplifier, which amplified the response signal to a suitable level before feeding it to channel B of the analyser. The gain of the Conditioning Amplifier was selectable in 10 dB steps covering the range -20 dB to 60 dB. The function switch could select low pass filter settings as well as velocity or displacement. Low pass filter settings included 25 kHz, 10 kHz and 1 kHz in the acceleration mode. Additionally, an all-pass wideband operation facility was available in the acceleration mode which covers 150 Hz to 100 kHz. For this particular experiment the setting selected was All pass with a sensitivity of 1.0 and a gain of 1.0 or 0 dB.

The B&K 2032 Dual Channel Analyser used for this test was a 2-channel real time analyser covering a wide range of standard functions. It had 801 lines of frequency resolution in dual channel operation and the user had the option of selecting frequency range. The window functions for the time domain signals of both channels could be selected. The function selected for channel A which was connected to the force transducer was of Transient type and the function for channel B connected to the accelerometer was of Exponential type. For both the windows, length was carefully selected so that noise effect was minimized and undue damping was limited due to the windows or functions. The FRF data from the analyser were downloaded using a GPIB connection to a PC for further analysis and storage.

Tables 6.1 and 6.2 describe the experimental setup and equipment settings used while conducting the experiments. In addition, a schematic diagram of the measurement equipment and set-up is given in figure 6.4. Figure 6.5 shows a photograph of the experimental rig.

6.4 CALIBRATION OF THE MEASUREMENT SETUP

Having prepared the experimental set-up as per the layout shown in figure 6.4, calibration of the set-up was performed using the technique proposed by Ewins [1]. A known cylindrical mass (weighing 2.6 kg) was freely suspended and the accelerometer to be used for measurement in this particular experiment was attached to the mass. This mass was then excited by the instrumented hammer in the same way as measurements would be otherwise made on the real structure. For this particular mass, it is possible to write:

$$m\ddot{X} = F$$

$$\text{or, } 20\log_{10}\left(\ddot{X}/F\right) = 20\log_{10}\left(1/m\right) = -8.29\text{dB}$$

Therefore, the measured inertance FRF from the mass was expected to have a constant value of -8.29 dB. The calibration units of the Dual Channel Analyzer were adjusted until the measured inertance FRF had an amplitude of -8.29 dB in the frequency range of interest.

This calibration technique has the advantage of being simple to perform and also ensured that the complete measurement set-up was calibrated rather than just the individual channels.

6.5 FE MODELLING OF UNDAMAGED STRUCTURES

The damage location algorithm discussed in Chapter 3 and employed here on the cantilever beam and the cross stiffened grid structure requires both the finite element model of the undamaged structure and the RFRFs of the damaged structure. For successful damage location, it was essential that the finite element model accurately represented the undamaged structure within the frequency range of interest. The finite element modelling of both the structures were carried out using PAFEC FE software.

6.5.1 Beam structure

The beam was modelled using PAFEC and beam elements (element number as per PAFEC reference: 34000) which have at each node six degrees-of-freedom: three translational and three rotational. However, when modelling the beam, for each node only the translational DOF in the z direction and rotational DOF in x-y plane as shown in figure 6.1 were considered. The beam was discretized into 13 elements and 14 nodal points as shown in the file in Table 6.3. The data file shown in Table 6.3 was created for PAFEC FE to generate the mass and stiffness matrices of the beam.

6.5.2 Cross stiffened grid structure

The grid structure used in this study is shown in figure 6.2. It has a cross sectional dimension of 20x10 mm. The structure was discretized into 20 elements and 21 nodal points, details of which are shown in PAFEC FE data file given in Table 6.6. The element type employed was again Element 34000 and the nodes were allowed translational movement in z direction, and rotational movement in x-y and y-z plane. The structure was modelled as freely supported and hence the mass and stiffness matrices generated by PAFEC had a size of 63x63.

6.6 TEST STRUCTURE PREPARATION FOR MEASUREMENT

The preparation of the test structure prior to starting experiments may be regarded as a most important phase of experimentation as an improper or faulty experimental set up affects the quality of data obtained.

6.6.1 Support conditions

The support condition of the structure is an important issue which needs to be addressed at the onset. The beam structure was grounded at one end so that it is regarded as a cantilever beam. This was done by rigidly clamping the beam to a work bench which was assumed to be sufficiently rigid to provide the necessary grounding. To confirm the above assumption, the mobility of the work bench which acted as the base structure was measured over the frequency range of interest. It was found that the base structure had a much lower mobility than the corresponding levels for the test structure at the point of attachment. This suggested that the base structure could be reasonably assumed to be rigid.

The cross stiffened grid structure was tested in a free-free condition. Although in practice it is not possible to provide a truly free support, this could be approximated by supporting the test piece on light elastic bands, so that the vibration modes of the support had very low natural frequencies compared to the first mode of the structure. To ensure minimum interference of the suspension on the structure's lowest bending mode, the suspension was attached as closely as possible to the nodal points of that mode, the location of which was predicted by the FE model of the grid structure.

6.6.2 Type of excitation

Different methods are available for exciting a structure and each one has its advantages and disadvantages. The selection of excitation is primarily dependent on the nature of application.

Impact excitation using an impact hammer was used in this study. This is a convenient means of excitation as it allows easy access to measurement locations on the structure and data can be acquired quite rapidly. In addition, there is minimal attachment between the structure and the excitation device, thus reducing unwanted interactions. The impulse response of the structure will contain information from all the modes of vibration of the structure, provided enough energy is put into the structure. However, using this type of excitation, the signal to noise ratio may not always be ideal. This problem can be partly alleviated by increasing the number of averages. While using this form of excitation, care needs to be taken to avoid multiple impacts as this can severely affect the quality of data obtained.

6.6.3 Attachment and location of transducer

It is important to ensure that the transducer has been located properly and attached correctly on the test structure. Various methods are available for accelerometer attachment, such as cemented stud, magnet, etc. The method used in this experimentation was to attach the accelerometer to the test structure by a thin layer of wax. This attachment ensures excellent contact and minimum effect on the stiffness of the test structure. From the frequency responses of different forms of attachment shown in figure 6.9 which is quoted from Ewins [1], it is clear that within a frequency range of 0 to approximately 7 kHz, the response signal from a structure remains reasonably accurate if wax is used for attachment. Since the frequency range of interest in this study was restricted to a maximum of 800 Hz, the selection of wax for attachment appears adequate.

From the FE models of the structures, an appreciation of their different modes of vibration and their corresponding nodal points was formed. The location of the transducer was then carefully selected to ensure that it was not positioned at, or very close to, a node of the structure's modes within the frequency range of interest.

6.7 INTRODUCTION OF DAMAGE IN THE STRUCTURE

In the beam structure a crack damage was introduced by making a cut at a distance of 255 mm from the free end between nodes 8 and 9. The cut which had a width of 1 mm and a depth of 6 mm extended for 15 mm on each side. Figure 6.1 shows the geometry of the cut.

For the grid structure, the damage was located at a distance of 235 mm from node 7 between nodes 8 and 9 and figure 6.2 shows the geometry of the cut.

6.8 EXECUTION OF THE MEASUREMENT

A description of the steps performed in execution of a typical test follows.

(i) *Verification of cable connections and joint tightness*

All the cable connections were checked to ensure that they were working properly and they have been properly connected.

(ii) *Calibration of the measurement set-up*

At the beginning of the test, the measurement set-up was calibrated with a known mass and the calibration technique as discussed earlier in Section 6.4 was used for calibration.

(iii) ***Examining the quality of data.***

For the beam structure the accelerometer was placed at node 11 as shown in figure 6.3(a) and for the grid structure it was located at node 7 as per figure 6.3(b). Once each FRF was measured, the data were examined to ensure that the quality of data was acceptable. This was done by checking the time functions of both channels, coherence function and cross spectrum to ensure that anomalies can be explained.

(iv) ***Storing Receptance FRFs***

Using a GPIB connection, the FRFs were downloaded from the B&K 2032 Analyzer to a PC for storage and post analysis. These data were then applied to the algorithms discussed earlier in this work to locate and estimate structural damage.

6.9 DAMAGE LOCATION

For the beam and grid structures, measurements were taken only for the translational DOFs in the z direction. However, the FE model of the beam structure generated mass and stiffness matrices using both the translational DOFs in z direction and the rotational DOFs in x-y plane. For the grid structure, the translational DOFs in z direction along with rotational DOFs in the x-y and y-z planes were used. Since the rotational DOFs could not be measured, the RFRFs of the damaged structure corresponding to the rotational DOFs were interpolated using D.E A. The interpolated RFRFs along with measured RFRFs for the damaged structure were used with the spatial matrices of the undamaged structure to locate damage. Both the 3-D DLP and the CDLV were generated. In the figures showing the 3-D DLP and the CDLV, only the values corresponding to measured DOFs have been plotted, as the damage location vector values corresponding to interpolated DOFs are zero. The reasons for this were explained in Chapter 3.

The natural frequencies obtained by using the FE mass and stiffness matrices of the beam were found to be in agreement with measurement as given in Table 6.4. The FE mass and stiffness matrices were then used in a programme written in Fortran to produce the RFRFs of the beam structure. The RFRFs thus computed were compared with RFRFs obtained from measurement. Figure 6.6 presents the point RFRF from measurement and that from FE model. It was found that the FE model of the beam is a reasonably accurate representation of the beam structure within a frequency range of 200 to 800 Hz. The validity of the measurements performed on the beam structure was confirmed by checking the coherence of measurement such as the one given in figure 6.7 for point measurement. For cross measurements, the coherence were also observed to be close to be one except in the region of anti-resonance. As the FE model represented the structure quite accurately in the frequency range of 200 to 800 Hz, it was decided to concentrate the study within this range.

The shift in natural frequencies caused by damage to the beam structure within the frequency range selected for study is given in Table 6.5. Figure 6.10 shows the plots of the point receptance FRF curves for the undamaged and damaged structures. From Table 6.5 it is possible to isolate the natural frequencies of the structure which have been most affected due to damage.

The 3-D Damage Location Plot in figure 6.11(a) over the frequency range of 200 to 800 Hz clearly shows a continuous peak at the DOFs 8-z and 9-z with the peaks becoming more distinct in the frequency region where the shift in the natural frequency is more prominent. From this, the location of damage can be correctly identified to be between nodes 8 and 9 since the DOFs 8-z and 9-z are associated with nodes 8 and 9. The CDLV was generated by using DLV between 200 and 800 Hz in steps of 1 Hz. The CDLV plotted for this case is shown in figure 6.11(b) which shows an appreciable peak occuring at DOFs 8-z and 9-z indicating that damage is located between nodes 8 and 9.

For the grid structure, the natural frequencies and RFRFs generated by the FE model and that from measurement were compared as given in Table 6.7 and figure 6.8. It was found that the FE model represented the grid structure accurately within a frequency range of 200 to 400 Hz. Therefore, the study on the grid structure was concentrated within this frequency range.

Due to damage in the cross grid structure between nodes 8 and 9, the resultant shift in natural frequencies and changes in the point receptance curve has been shown in Table 6.8 and figure 6.12 respectively. The 3-D Damage Location Plot drawn in figure 6.13(a) shows a continous peak running over the frequency range between DOFs 8-z and 9-z with the peaks becoming more prominent in the frequency region where the shift in natural frequencies is more notable. Therefore, it can be said that the damage in the cross grid structure is located between nodes 8 and 9. Figure 6.13(b) shows the CDLV obtained for the grid structure by using CDLV between 200 to 400 Hz in steps of 0.5 Hz. Again in this plot, a distinct peak is evident at DOFs 8-z and 9-z indicating correctly that the damage is located between nodes 8 and 9.

6.10 DISCUSSION OF LOCATION RESULTS

By using either the 3-D DLP or the CDLV, the location of damage can be identified. However, since CDLV is obtained by adding all the damage location vectors over a frequency range, the peaks due to damage becomes magnified. However, from the 3-D DLP it is possible to determine the variation in the effect of damage on the structure at different frequency points. This information proves very useful when trying to determine the damage severity by selecting FRF data at frequency points more affected by damage.

From the experimental studies in the beam and grid structures, it is clear that D.E A can be successfully used to interpolate the FRF data for rotational DOFs. These interpolated data can be used in conjunction with the damage location algorithm suggested in Chapter 3 to locate damage. This is mainly due to relatively smaller magnitudes of spatial matrix elements related to the rotational DOFs compared with those related to translational DOFs for these two structures. This is explained in more details by using a simple illustration given below. In the illustration, the frequency symbol of Ω has been eliminated from the dynamic stiffness and receptance terms for simplicity. For a certain structure, the first row of the Dynamic Stiffness Matrix is given as:

$$\{z_{11} \quad z_{12} \quad z_{13} \quad z_{14} \quad z_{15} \quad z_{16} \quad z_{17} \quad z_{18}\}$$

and the receptance FRF column at a particular frequency is:

$$\{x_1 \quad x_2 \quad x_3 \quad x_4 \quad x_5 \quad x_6 \quad x_7 \quad x_8\}$$

Hence the first element of the Damage Location Vector is given by:

$$\sum_{n=1}^{8} z_{1n} x_n$$

If x_2, x_4, x_6 and x_8 have to be interpolated instead of being measured, then the actual receptance column may become

$$\{x_1 \quad (x_2 + e_1) \quad x_3 \quad (x_4 + e_2) \quad x_5 \quad (x_6 + e_3) \quad x_7 \quad (x_8 + e_4)\}$$

where e_1, e_2, e_3 and e_4 are due to expansion error. Therefore, the first element of the damage location vector becomes:

$$\sum_{n=1}^{8} z_{1n} x_n + z_{12} e_1 + z_{14} e_2 + z_{16} e_3 + z_{18} e_4$$

However, if z_{11}, z_{13}, z_{15} and z_{17} are much greater than z_{12}, z_{14}, z_{16} and z_{18}, then the errors introduced in the element of the damage location vector due to expansion error becomes almost negligible. For this reason the damage location vector is not severely affected, even with the expansion error introduced while interpolating FRFs for rotational DOFs, as the dynamic stiffness elements related to rotational DOFs are significantly smaller than those related to translational DOFs.

6.11 DETERMINATION OF DAMAGE SEVERITY

As discussed in Section 6.5, the location of damage in the beam and the cross stiffened grid was determined by using the damage location algorithm suggested in Chapter 3. Subsequent to locating the damage, the next step was to estimate the severity of damage. While trying to do so, it was assumed that the hack saw cut in the beam and the cross grid has only affected the stiffness of the structure. Therefore, the algorithms to be used here for estimating damage severity were mainly aimed at computing the change in stiffness matrix of the undamaged structure due to damage.

In Sections 5.5.2 and 5.5.3, two different methods have been suggested for estimating the severity of damage. The method suggested in Section 5.5.2 and named Method II aimed at calculating the change in spatial matrix coefficients of the undamaged structure in the area of damage. Method III in Section 5.5.3 attempted to identify the damaged elements directly by using the submatrix approach. In the following sections, both Methods II and III as discussed in Sections 5.5.2 and 5.5.3 are employed on the beam and grid structure to determine the severity of their respective damage. Henceforth in this chapter, reference to Methods II and III will indicate the methods presented in Section 5.5.2 and 5.5.3 respectively for determining the damage severity.

6.11.1 Regenerated FRF

Methods II or III can be applied to the beam and cross grid structure to compute the resultant change in stiffness $[\Delta K]$ due to damage. To verify the reliability of the $[\Delta K]$ thus obtained, it can be added to $[K]_{UD}$ to generate $[K]_D$. The generated $[K]_D$ along with $[M]_{UD}$ can then be used to compute the FRF of the damaged structure. The FRF thus produced is called the 'regenerated' FRF of the damaged structure. If the measured and 'regenerated' FRF of the damaged structure are found to be in agreement, then it can be concluded that the computed $[\Delta K]$ gives a reliable estimate of the damage. Unlike the numerical case studies, the correct $[\Delta K]$ due to damage is not known for the beam and grid structures. The $[\Delta K]$ computed cannot be compared with some reference [ΔK] to check the correctness of the results. Therefore, this indirect method has been adopted here to check the accuracy of results.

However, while comparing the 'regenerated' and measured FRF of the damaged structure, it is important to bear in mind that unlike the measured FRF, the 'regenerated' FRF are truly undamped. In general, their magnitude will always be bigger than the measured FRF. To compare them, it is best to check whether the curves have the peaks due to resonance at the same frequency rather than magnitudes.

6.12.2 Beam structure

For the beam structure, the location of damage was already identified in Section 6.9 to be between nodes 8 and 9. Methods II and III were applied alternately on the beam structure to determine the [ΔK] .

Application of Method II to beam structure

When applying Method II to the beam structure, the main aim was to calculate the change in stiffness matrix coefficients of $[K]_{UD}$ in the area of damage. As shown in Section 6.5.1, this beam was discretized into 13 elements and 14 nodal points. Since one of the nodal points at one end was totally encastered, the mass and stiffness matrix of the beam generated by using the PAFEC-FE data file shown in Table 6.3 had a size of 26x26. Therefore, damage between nodes 8 and 9 will affect the following matrix coefficients in the stiffness matrix of the undamaged structure:

13-13, 13-14, 13-15, 13-16, 14-14, 14-15, 14-16, 15-15, 15-16, 16-16

Hence, the number of unknowns to be determined is 10. Theoretically, Method II require 10 pairs of frequency points to compute them. As already shown in the numerical examples in Chapter 5, additional pairs of frequency points prove helpful in reducing the effect of measurement noise. Therefore, in this case, 20 frequency points were used to generate 50 frequency pairs and FRF data at those points were used to identify the unknown stiffness matrix coefficients. To test the sensitivity of the $[\Delta K]$ computed by using Method II on frequency points selected, three different cases were tried. Since from the numerical examples in Chapter 5, it has been already established that better results are obtained by selecting frequency points near resonances, frequency points used here for different cases encompassed different resonances. The frequency points selected for the three different cases are given below:

CASE A

From Table 6.5 it is clear that for the beam structure, the natural frequency at 745 Hz has been most severely affected due to damage within the frequency range of interest. Twenty frequency points were selected such that they were in the vicinity of 745 Hz and they are given in Hz in the table below:

710	713	715	717	720	722	727	730	732	735
737	740	742.5	745	747	750	752	755	757	760

CASE B

The natural frequency at 446 Hz was the least affected due to damage among the natural frequencies within the range of 200 to 800 Hz. In case B, frequency points were considered in the neighbourhood of 446 Hz only and they are given in Hz in the following table:

415	417	419	422	424	428	431	432	434	436
438	440	443	445	446	448	450	452	454	456

CASE C

In case C, 20 frequency points encompassing 230 Hz were used. Due to damage 230 Hz changed to 226 Hz. For this particular natural frequency, the shift due to damage is not as large as the natural frequency at 745 Hz but slightly larger than the shift suffered at 446 Hz.

210	212	215	216	217	219	222	224	225	228
230	231	232	234	236	238	240	243	246	248

For all three cases, the magnitude of change in the affected matrix coefficients have been given in Tables 6.9A to 6.9C. Figures 6.14A to 6.14C plot the measured point RFRF for damaged and undamaged structure along with the regenerated point RFRF for the damaged structure.

Application of Method III to beam structure

In the next case, Method III was applied to calculate the scaling factors using the submatrix approach. This method works with elements directly and computes the scaling factors of the elements affected by damage. From the location of damage it is clear that only one element lying between nodes 8 and

9 had been affected. Therefore, the number of unknowns in this case was just one. This unknown can be computed by Method III using a single pair of frequency points. A wide spectrum of frequency points were used which mostly encompassed the natural frequencies most affected by damage.

The frequency ranges used separately were 220 Hz to 250 Hz, 430 to 470 Hz and 710 to 760 Hz which are the frequency ranges used for Method II. The calculated scaling factor for the element between nodes 8 and 9 varied in each frequency range. The variation in the identified scaling factor for different frequency ranges have been tabulated in Tables 6.10A to 6.10C and the highest value of scaling factor from each of these tables was used to obtain the regenerated RFRF. The regenerated point RFRFs obtained by using the highest value of scaling factor from Tables 6.10A to 6.10C have been plotted in figures 6.15A to 6.15C respectively along with the point RFRF of the damaged and undamaged beam.

6.11.3 Cross grid structure

For the cross grid structure, the location of damage was already identified to be between nodes 8 and 9 in Section 6.9. Methods II and III were also applied alternately on the grid structure to determine the $[\Delta K]$. The same study which was done on the beam structure was repeated.

Application of Method II to grid structure

The main objective in this case was to calculate the change in stiffness matrix coefficients of $[K]_{UD}$ in the area of damage. The grid was discretized into 20 elements and 21 nodal points. Since each nodal point was assumed to have 3 DOFs, the mass and stiffness matrix of the grid generated by using the data file shown in Table 6.6 had a size of 63x63. Therefore, damage between nodes 8 and 9 will affect the following matrix coefficients in the stiffness matrix of the undamaged structure.
22-22, 22-23, 22-24, 22-25, 22-26, 22-27, 23-23, 23-24, 23-25, 23-26, 23-27, 24-24, 24-25, 24-26, 24-27, 25-25, 25-26, 25-27, 26-26, 26-27, 27-27

Hence, the number of unknowns is 21, and theoretically, Method II requires 21 pairs of frequency points to compute them. Since additional pairs of frequency points prove helpful in reducing the effect of measurement noise, 30 frequency points were used to generate 100 frequency pairs and the FRF data at those points were used to identify the unknown stiffness matrix coefficients. To test the sensitivity of the $[\Delta K]$ computed by using Method II on frequency points selected, four different cases were tried by selecting frequency points near resonances which were affected to varied extents due to damage. The frequency points selected for four different cases are given below:

CASE A

The natural frequency corresponding to 370.5 Hz have been most severely affected due to damage within the frequency range of interest. Thirty frequency points were selected for this case such that they were at the vicinity of 370.5 Hz and they are given in Hz in the table below:

351	351.5	352	352.5	353	354	355	356.5	358	359
359.5	360	361.5	362.5	363.5	364	365	366	366.5	368
369	370	371	372	373	374	374.5	375	375.5	376.5

CASE B

In case B, 30 frequency points were used at the vicinity of 308.5 Hz, which changed to 307 Hz due to damage. For this particular natural frequency, the shift due to damage is the least among the natural frequencies within a frequency range of 200 to 400 Hz. The frequency points used are given in Hz in the following table.

301	302	303	304	305	306	307.5	308	309	310
311	312	313	314	315	316	317	318	319	320
320.5	321	321.5	322	322.5	323	324	325	326	326.5

CASE C

The natural frequency at 244 Hz is almost as severely affected by the damage as that at 370.5 Hz, but the shift for 244 Hz is slightly less than for 370.5 Hz. In case C, 30 frequency points were considered in the neighbourhood of 446 Hz and they are given in Hz in the following table:

232	233	233.5	234	234.5	235	235.5	236	236.5	237
237.5	238	239	240	240.5	241	241.5	242	243	243.5
244.5	245	245.5	246.5	247	248	248.5	249	249.5	250

CASE D

In case D, 30 frequency points were used encompassing 224.5 Hz, which changed to 222 Hz due to damage. For this particular natural frequency, the shift due to damage is much less compared to natural frequencies considered in cases A and C for the grid structure. The frequency points used are given in Hz in the following table.

201	202	203	204	205	206	207	208	209	210
211	212	213	214	215	216	217	218	219	220
221.5	222	222.5	223	223.5	224	225	225.5	227	227.5

For all four cases, the magnitudes of change in the affected matrix coefficients have been given in Tables 6.11A to 6.11D and figures 6.16A to 6.16D shows the plot of the measured point RFRF for damaged and undamaged structures along with the regenerated point RFRF for the damaged structure.

<u>Application of Method III to cross grid structure</u>

Method III was applied to the cross grid structure which aimed to directly compute the scaling factor of the element affected by damage. From the location of damage it is clear that only the element between nodes 8 and 9 had been affected. Since the number of unknowns in this case was just one, it can be computed by Method III by using a single pair of frequency points. A wide spectrum of frequency points was used which mostly encompassed the natural frequencies most affected by damage. The frequency ranges used separately were 350 to 375 Hz, 290 to 315 Hz, 230 to 250 Hz, 215 to 225 Hz and 350 to 375 Hz which are the same ranges used for Method II.

The calculated scaling factor for the element between nodes 8 and 9 varied in each frequency range. The variation in scaling factor for different frequency pairs in different range have been tabulated in Tables 6.12A to 6.12D and the highest value of scaling factor from each of these tables were used to obtain the regenerated RFRFs. The regenerated point RFRFs obtained by using the highest value of the scaling factor from Tables 6.12A to 6.12D have been plotted in figures 6.17A to 6.17D respectively along with the point RFRF of the damaged and undamaged grid structure.

6.12 DISCUSSION OF DAMAGE SEVERITY RESULTS

From the results obtained regarding the severity of damage for both structures, it is apparent that the selection of frequency points plays an important role in the computations. Two different methods of estimating the severity of damage have been undertaken: determining the matrix coefficients and evaluating the scaling factors.

When trying to compute the matrix coefficient, it is clear from Tables 6.9A to 6.9C and Tables 6.11A to 6.11D, that for both structures, there is an appreciable variation in the computed values. As a result there might be a degree of uncertainty regarding the final estimate. In order to identify the most accurate one of the results obtained, the regenerated RFRF of the damaged structure have been compared here with the measured RFRF of the damaged structure. Without loss of generality, the point RFRF have been compared for both the beam and grid structure.

While studying figures 6.14A to 6.14C for the beam structure, it is clear that for almost all selection of frequency points, the regenerated RFRF and measured RFRF of the damaged structure resemble each other reasonably well in the frequency range of 200 to 650 Hz. However, in the frequency range of 650 to 800 Hz, which encompasses the natural frequency most severely affected within the frequency range of interest, the only regenerated curve which most closely resembles the measured RFRF of the damaged structure is shown by figure 6.14A.

Therefore, among the different cases considered for the beam, the case represented by figure 6.14A where the FRF data used are at frequency points close to 745 Hz (which is the most severely affected natural frequency within 200 to 800 Hz) approximates the actual damage severity.

For the cross grid structure, two natural frequencies (i.e 244 & 370.5 Hz) within the frequency range of interest have been more severely affected than the rest. For this structure, the regenerated FRF resembles the measured FRF of the damaged structure more closely than the others in figures 6.16A and 6.16C. The results are similar to that obtained for the beam structure, since for both the structures the most accurate results are obtained when FRF data used are at frequency points which are in the vicinity of the most affected natural frequencies within the frequency range of interest. For the beam structure, only a single natural frequency was most severely affected. However, for the grid structure, two natural frequencies have been affected most severely and the shift in them is almost similar. Therefore, reliable damage estimate was obtained for both cases as given in figures 6.16A and 6.16C which represented the cases of using FRF data at frequency points in the vicinity of 370.5 and 244 Hz respectively. As against that, figure 6.16B represents the case when the frequency points selected are in the vicinity of natural frequency at 308.5 Hz. This particular natural frequency has been hardly affected by the damage. Therefore, the regenerated FRF for this case significantly deviates from the measured RFRF of the damaged structure. Even so, the shift in the regenerated RFRF appear to be in the right direction. From this it can be said that the severity computed in this case is an underestimate. Figure 6.16D shows the case when the frequency points selected are in the vicinity of 224 Hz. Although the shift in this natural frequency is almost as much as that in the natural frequency at 308.5 Hz, from figure 6.16D, it is apparent that the regenerated RFRF is much closer to the actual RFRF compared to that in figure 6.16B. This may be attributed to its proximity to the natural frequency corresponding to 244 Hz which have been quite significantly affected by damage.

Hence from the results obtained, it is clear that for both the structures the best estimate about the severity of damage can be attained when using FRF data at the vicinity of the natural frequencies more severely affected by damage.

Instead of trying to obtain the matrix coefficients, the second approach was to use Method III which attempted to calculate the scaling factor of the damaged element. For the beam structure, the calculated scaling factor varied from 0.12

to 0.265. For the cross grid structure the variation ranged from 0.20 to 0.38. A comparitive study of figures 6.15A to 6.15C for the beam structure and figures 6.17A to 6.17D for the grid structure reveals that the regenerated RFRF approximates the RFRF of the damaged structure most closely in figure 6.15C for the beam and figures 6.17A and 6.17C for the cross grid structure. Analysis of these cases show that figure 6.15C represents the case when the frequency points selected were close to 744 Hz and the regenerated RFRF in figures 6.17A and 6.17C used frequency points in the vicinity of 370.5 and 244 Hz. Besides, the variation in computed scaling factors remains reasonably small for the frequency ranges in the vicinity of the most affected natural frequencies. Therefore like Method II, the most accurate results are obtained with Method III when using FRF data at frequency points which are in the vicinity of natural frequencies affected by damage.

Therefore irrespective of the method used, the results obtained are frequency dependant. However, from the regenerated FRFs it appears that the results obtained are closer to the correct estimate when Method II is used instead of Method III. This might be attributed to the fact that Method II uses a larger number of frequency points compared to Method III and this results in the outcome reflecting the structure more accurately over a wider frequency band. But this improvement in accuracy obtained while using Method II can be offset by the significant reduction in computational burden that can be achieved while using Method III.

Therefore in brief it can be said that the severity of damage computed is on the lower side compared to the actual when the frequency points selected are away from the most severely affected natural frequencies within the frequency range of interest. In contrast to that, when the frequency points selected lie near the natural frequencies which have been more severely affected, the damage estimate approaches the correct estimate more closely. Therefore, it is suggested that in order to approach the correct result more closely and to eliminate the risks associated with underestimating the damage severity, frequency points selected for estimating damage severity should be in the vicinity of the most severely affected natural frequency.

6.13 LOCATION OF MULTIPLE DAMAGES

In addition to the existing damage, a second damage was introduced on the grid structure at a distance of 75 mm from node 13 and between nodes 13 and 18 in figure 6.3(b). The resultant shift in natural frequency and the point receptance curve has been given in Table 6.8 and figure 6.18. The 3-D DLP and the CDLV for these damages have been shown in figures 6.19(a) and 6.19(b). Damage between DOFs 8-z and 9-z could be identified quite accurately. Besides the continous peak running corresponding to DOFs 13-z and 18-z indicate the location of damage between nodes 13 and 18. This experimental results successfully demonstrates the capability of 3-D DLP and CDLV to identify more than one damage in a structure at the same time.

6.14 SUMMARISING REMARKS

This chapter presented the results obtained when the damage location and extent algorithms proposed in this thesis were used to locate damage and determine damage severity on two practical structures. The results obtained for both complement to the numerical studies carried out in the previous chapters.

Based on the results presented in this chapter, it can be concluded that the methods suggested in this thesis to detect damage using FRF data are feasible and can be applied to real structures. Even when FRF data are noisy, location of structural damage can be determined by using either the 3-D Damage Location Plot or the CDLV.

Both 3-D DLP and the CDLV have their respective advantages. By using CDLV, the location of structural damage becomes more distinct compared to using 3-D DLP. However, use of 3-D DLP makes it possible to ascertain frequency regions where the damage has affected the FRFs more. This information proves useful when trying to determine the damage severity.

When all coordinates have not been measured, it is possible that damage location may still be successfull using interpolated FRF data obtained by applying D.E A.

To determine the severity of damage, two distinct techniques referred to here as Methods II and III have been employed. Method II determines the matrix coefficients and Method III calculates the scaling factors of the damaged element. The computational effort required for Method III is significantly less than that for Method II. Irrespective of the method employed for computing damage severity, the results obtained are more accurate if the severity of damage is determined locally. This implies that the damage should be located before its severity is estimated.

The damage estimate using FRF data is frequency dependant. However, the most accurate estimate of damage can be obtained if damage severity is computed locally and if FRF data at frequency points close to natural frequencies more severely affected by damage are used.

Structures:	Cross Stiffened Grid and Beam
Dual Channel Analyser:	Bruel & Kjaer, Type 2032
Exciter:	PCB Hammer, Force Transducer Sensitivity: 2.10 mV/N
Power Unit:	PCB Make, Model 480D06
Signal Amplifier:	NVMS Conditioning Amplifier
Accelerometer:	PCB 10729 Voltage Sensitivity: 0.804 mV/g
Data Processor:	HP Workstation, Model
Plotter	HP, Model 7440A

Table 6.1: Experimental setup information for the Beam and Grid structures

DUAL CHANNEL ANALYSER		SIGNAL AMPLIFIER	
Frequency Range	0- 800Hz (Beam) 0- 400Hz (Grid)	Gain	1.0
Resolution	800 Lines	High Pass	5.0 Hz
Windows	Exc: Transient Res: Exponential	Freq. Filter	All Pass
Sensitivity (Calibrated)	Exc: 1.08 mV/N Res: 43.0 μV/G	Sensitivity Unit: (Calibrated)	Response: 1.00
Averages	10		

Table 6.2: Equipment setting for the Beam and Grid Structures

```
CONTROL
CONTROL.END
NODES
NODE        X     Y          NODE        X      Y
1           0     0           8         .333    0
2         .047    0           9         .380    0
3         .095    0          10         .428    0
4         .142    0          11         .476    0
5         .190    0          12         .523    0
6         .238    0          13         .571    0
7         .285    0          14         .619    0
ELEMENTS
ELEM= 34000
NUMBER        PROPERTIES    TOPOLOGY
1                  1          1 2
2                  1          2 3
3                  1          3 4
4                  1          4 5
5                  1          5 6
6                  1          6 7
7                  1          7 8
8                  1          8 9
9                  1          9 10
10                 1          10 11
11                 1          11 12
12                 1          12 13
13                 1          13 14
BEAMS
SECTION       MATERIAL              IYY          AREA
1                  11               .072E-8      2.34E-4
MATERIAL
MATERIAL.NUMBER    E        NU      RO
11                 209E9    .3      7800
LOADS
CASE          NODE          DIRECTIONS.OF.LOAD   VALUE.OF.LOAD
1              2                  3                   10
ACTIVE.FREEDOMS
NODE          DIRECTION             PRINT.CONTROL
2              35                      2
R12     1      00                      0
RESTRAINTS
NODE          DIRECTION
1              0
2              1246
R12     1      0000
MODES.AND.FREQUENCIES
AUTOMATIC.MASTERS   MODES
0                   10
MASTERS
NODE.NUMBER         DIRECTION
2                    35
R12         1        00
END.OF.DAT
```

Table 6.3: Data file in PAFEC FE for deriving mass and stiffness of the beam

NATURAL FREQUENCIES OF UNDAMAGED BEAM	
FROM MEASUREMENT	FROM FINITE ELEMENT MODEL
13.0	13.0
82.0	82.0
230	229.7
446	450
745	745

Table 6.4: Natural Frequencies of undamaged beam from measurement and FE model

NATURAL FREQUENCIES OF BEAM FROM MEASUREMENT	
BEFORE DAMAGE	AFTER DAMAGE
13.0	13.0
82.0	78.0
230	226.0
446	444
745	718

Table 6.5: Natural Frequencies of damaged and undamaged beam from measurement

```
CONTROL
CONTROL.END
NODES
NODE      X       Y        NODE     X       Y
1         0       0        2        .1      0
3         .1      .15      4        .1      .42
5         .15     0        6        .15     -.11
7         .4      0        8        .4      .15
9         .4      .42      10       .5      0
11        .6      0        12       .6      .15
13        .6      .42      14       .6      -.11
15        .8      0        16       .8      .42
17        .6      .53      18       .5      .42
19        .15     .42      20       .15     .53
21        0       .42
ELEMENTS
ELEMENT.TYPE = 34000
NUMBER  PROP  TOPOLOGY   NUMBER  PROP  TOPOLOGY
1       1     1 2        2       1     2 3
3       1     3 4        4       1     4 5
5       1     5 6        6       1     5 7
7       1     7 8        8       1     8 9
9       1     7 10       10      1     10 11
11      1     11 14      12      1     11 12
13      1     12 13      14      1     13 17
15      1     11 15      16      1     13 16
17      1     13 18      18      1     18 9
19      1     9 19       20      1     19 20
21      1     19 4       22      1     21 4
BEAMS
SECTION   MATERIAL   IYY        IZZ        TORS.CONST   AREA
1         11         1.666E-9   6.666E-9   4.6E-9       2.0E-4
MATERIAL
MATERIAL.NUMBER     E        NU     RO
11                  209E9    .3     7800
LOADS
CASE        NODE        DIRECTIONS.OF.LOAD        VALUE.OF.LOAD
1           2           3                         10
ACTIVE.FREEDOMS
NODE        DIRECTION           PRINT.CONTROL
1           345                 2
R20         000                 0
RESTRAINTS
NODE        DIRECTION
1           126
R20    1    000
MODES.AND.FREQUENCIES
AUTOMATIC.MASTERS          MODES
0                          10
MASTERS
NODE.NUMBER          DIRECTION
1                    345
R20          1       000
END.OF.DAT
```

Table 6.6: Data file in PAFEC FE for deriving mass and stiffness of the grid

NATURAL FREQUENCIES OF UNDAMAGED CROSS GRID (Hz)	
FROM MEASUREMENT	FROM FINITE ELEMENT MODEL
224.5	223.0
244.0	242
308.5	308.5
370.5	371

Table 6.7: Natural Frequencies of undamaged cross grid from measurement and FE model

NATURAL FREQUENCIES OF CROSS GRID FROM MEASUREMENT (Hz)		
BEFORE DAMAGE	AFTER DAMAGE	AFTER TWO DAMAGES
224.5	222	219
244	231.5	228
308.5	307	305.5
370.5	357	352

Table 6.8: Natural Frequencies of damaged and undamaged cross grid from measurement

6060000	-144300	-6069000	-144400
-144300	4580	144400	2290
-6069000	144400	6060000	144300
-144400	2290	144300	4580

Table 6.9A: Magnitude of change of affected stiffness matrix coefficients for beam (Case A)

3990000	-95010	-4000000	-9500
-95010	3020	95000	1507
-4000000	95000	3990000	95010
-9500	1507	95010	3020

Table 6.9B: Magnitude of change of affected stiffness matrix coefficients for beam (Case B)

2300000	-54820	-2310000	-54800
-54820	1740	54800	870
-2310000	54800	2300000	54820
-54800	870	54820	1740

Table 6.9C: Magnitude of change of affected stiffness matrix coefficients for beam (Case C)

Freq (Hz)	227,231	220,245	225,227	225,231	228,233	229,236	234,238	234,243	241,243
Scaling Factor	.14	.11	.15	.14	.14	.14	.13	.13	.11
Freq (Hz)	238,249	240,250	242,250	225,228	225,248	243,247	241,247	223,229	224,230
Scaling Factor	.11	.10	.10	.15	.12	.11	.10	.14	.14
Freq (Hz)	221,227	223,226	227,235	228,232	223,243	234,246	248,250	241,247	241,231
Scaling Factor	.145	.15	.143	.15	.12	.12	.10	.11	.11

Table 6.10A: Identified scaling factor vs frequency pair
for beam (220 to 250 Hz)

Freq (Hz)	437,431	430,445	455,437	445,442	448,463	439,436	434,438	434,443	441,463
Scaling Factor	.16	.15	.16	.17	.15	.16	.15	.16	.15
Freq (Hz)	438,449	440,470	452,470	465,468	435,448	443,447	441,447	453,459	463,470
Scaling Factor	.17	.15	.10	.1	.16	.17	.17	.16	.14
Freq (Hz)	451,461	453,463	437,443	431,468	439,447	434,441	448,450	441,451	431,441
Scaling Factor	.15	.15	.17	.15	.15	.15	.14	.16	.15

Table 6.10B: Identified scaling factor vs frequency pair
for beam (430 to 470 Hz)

Freq (Hz)	710,724	715,725	720,727	730,740	735,758	739,760	734,738	734,743	741,743
Scaling Factor	.24	.24	.24	.25	.24	.25	.26	.26	.25
Freq (Hz)	738,749	740,750	742,760	725,728	725,748	743,747	741,760	723,729	724,730
Scaling Factor	.24	.25	.25	.25	.26	.26	.25	.26	.25
Freq (Hz)	721,727	723,753	727,759	728,760	723,743	743,760	748,750	741,747	741,731
Scaling Factor	.24	.25	.25	.26	.25	.25	.26	.26	.26

Table 6.10C: Identified scaling factor vs frequency pair
for beam (710 to 760 Hz)

105000	14260	0	-105700	14260	0
14260	2560	0	-14260	1283	0
0	0	682	0	0	-682
-105700	-14260	0	106000	-14260	0
14260	1283	0	-14260	2572	0
0	0	-682	0	0	680

Table 6.11A: Magnitude of change of affected stiffness matrix coefficients for grid (Case A)

89000	12070	0	-89400	12070	0
12070	2170	0	-12070	1086	0
0	0	577	0	0	-577
-89400	-12070	0	89000	-12070	0
12070	1086	0	-12070	2177	0
0	0	-577	0	0	580

Table 6.11B: Magnitude of change of affected stiffness matrix coefficients for grid (Case B)

55000	7410	0	-54900	7410	0
7410	1330	0	-7410	666	0
0	0	354	0	0	-354
-54900	-7410	0	55000	-7410	0
7410	666	0	-7410	1338	0
0	0	-354	0	0	360

Table 6.11C: Magnitude of change of affected stiffness matrix coefficients for grid (Case C)

103000	13880	0	-93100	13870	0
13880	2470	0	-13870	1888	0
0	0	652	0	0	-650
-93100	-13870	0	73000	-13870	0
13870	1188	0	-13870	2482	0
0	0	-650	0	0	650

Table 6.11D: Magnitude of change of affected stiffness matrix coefficients for grid (Case D)

Freq (Hz)	351,355	351,357	351,361	353,363	355,360	357,367	359,369	361,373	362,374
Scaling Factor	.35	.35	.36	.36	.36	.37	.38	.37	.35
Freq (Hz)	363,369	372,375	355,358	356,362	356,367	367,350	372,360	372,362	372,364
Scaling Factor	.38	.35	.36	.37	.38	.37	.38	.38	.38
Freq (Hz)	372,366	372,368	375,370	374,354	352,356	352,359	352,361	352,363	361,371
Scaling Factor	.38	.38	.36	.36	.37	.37	.36	.37	.38

Table 6.12A: Identified scaling factor vs frequency pair for cross grid (350 to 375 Hz)

Freq (Hz)	291,293	291,295	291,297	291,299	291,301	293,303	295,305	297,305	299,306
Scaling Factor	.21	.21	.22	.22	.22	.22	.23	.22	.24
Freq (Hz)	299,308	300,305	300,308	300,310	312,307	312,315	315,303	315,307	308,306
Scaling Factor	.24	.24	.24	.23	.22	.21	.21	.22	.24
Freq (Hz)	300,312	300,315	305,307	305,309	306,314	295,313	297,314	301,304	296,306
Scaling Factor	.21	.21	.24	.24	.23	.22	.22	.24	.22

Table 6.12B: Identified scaling factor vs frequency pair for cross grid (290 to 315 Hz)

Freq (Hz)	230,232	232,236	236,238	238,242	243,245	246,248	248,250	231,233	241,243
Scaling Factor	.35	.37	.37	.37	.36	.35	.35	.37	.36
Freq (Hz)	238,249	240,250	242,250	231,233	231,235	231,237	235,239	235,241	239,241
Scaling Factor	.35	.35	.35	.37	.37	.37	.37	.36	.36
Freq (Hz)	239,242	239,244	239,246	239,248	239,250	234,246	249,250	230,250	235,250
Scaling Factor	.35	.36	.37	.36	.36	.36	.35	.35	.35

Table 6.12C: Identified scaling factor vs frequency pair for cross grid (230 to 250 Hz)

Freq (Hz)	225,215	220,225	225,217	225,219	221,220	225,216	224,218	224,222	221,223
Scaling Factor	.33	.34	.34	.32	.33	.34	.34	.33	.34
Freq (Hz)	215,220	217,220	224,220	225,218	225,223	218,219	218,215	223,215	219,220
Scaling Factor	.32	.32	.34	.33	.33	.34	.32	.33	.34

Table 6.12D: Identified scaling factor vs frequency pair for cross grid (215 to 225 Hz)

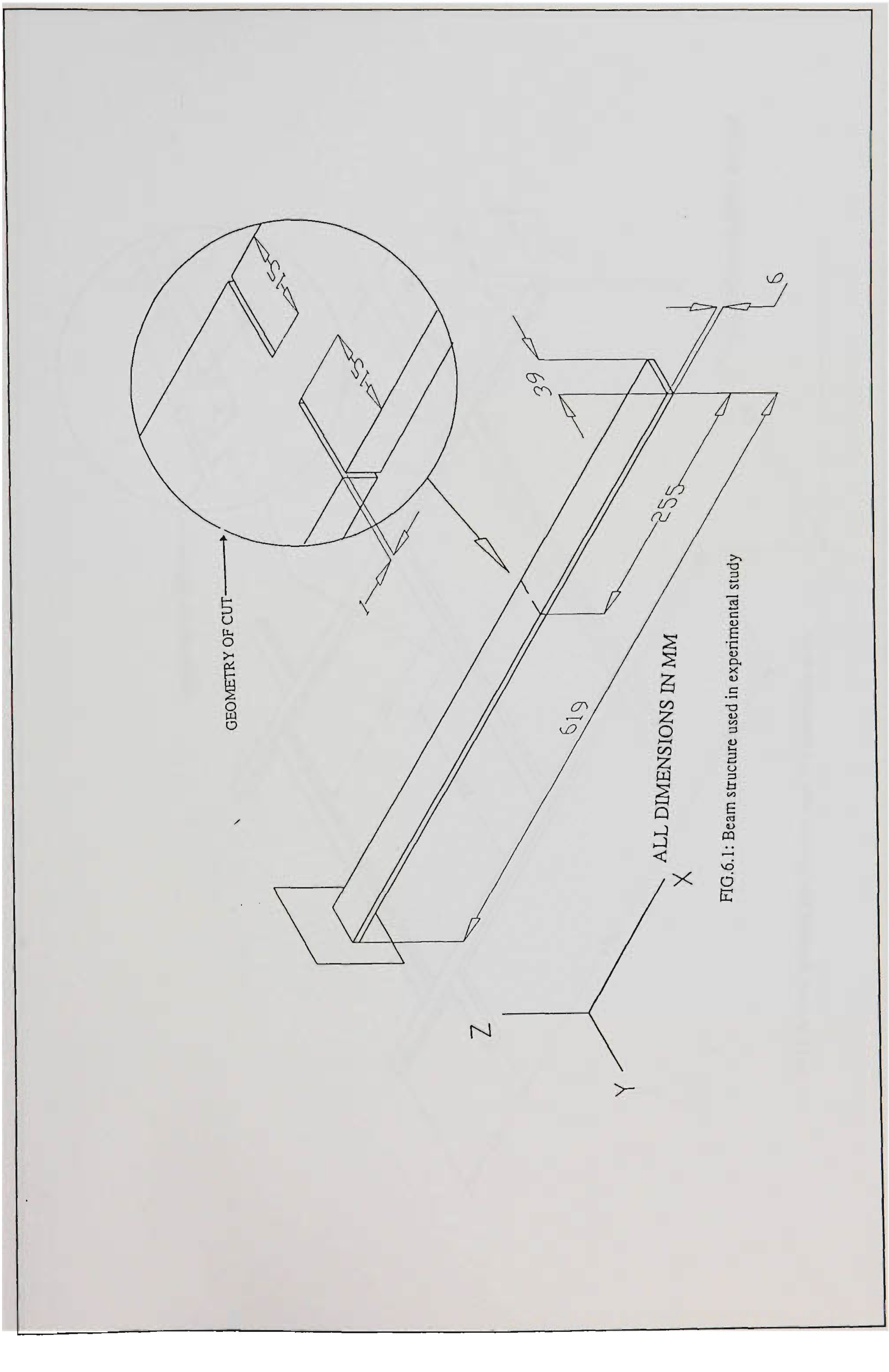

FIG.6.1: Beam structure used in experimental study

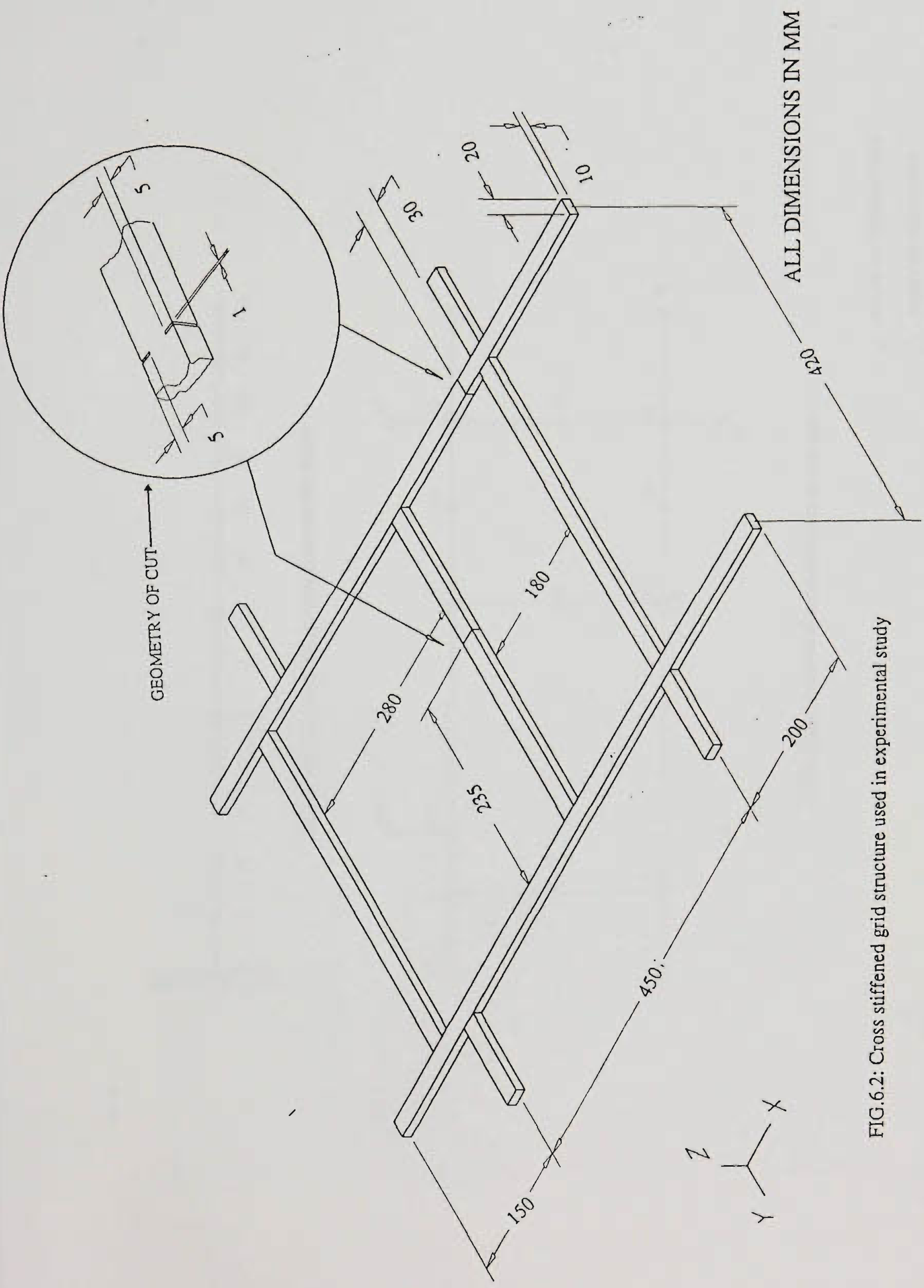

FIG.6.2: Cross stiffened grid structure used in experimental study

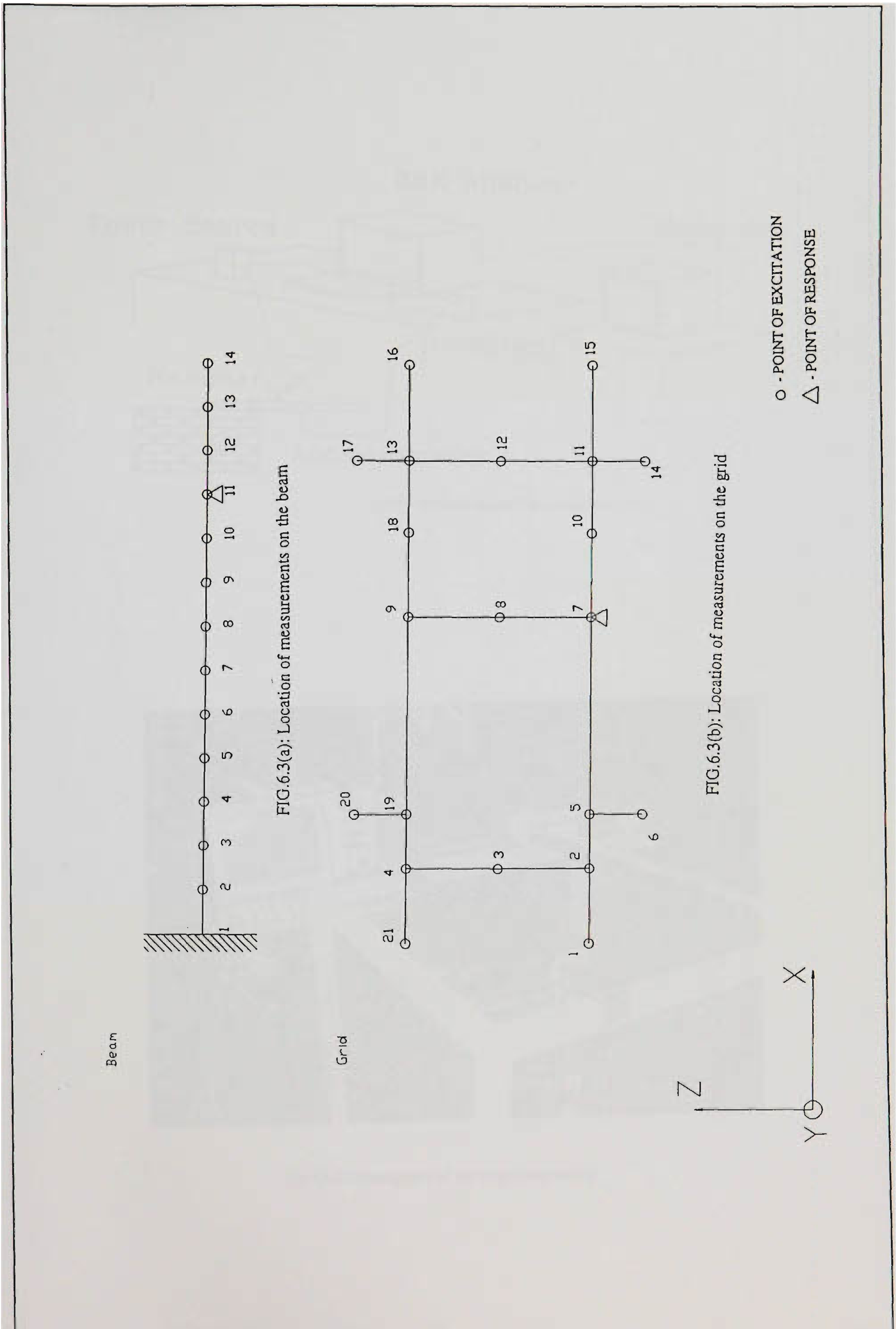

FIG.6.3(a): Location of measurements on the beam

FIG.6.3(b): Location of measurements on the grid

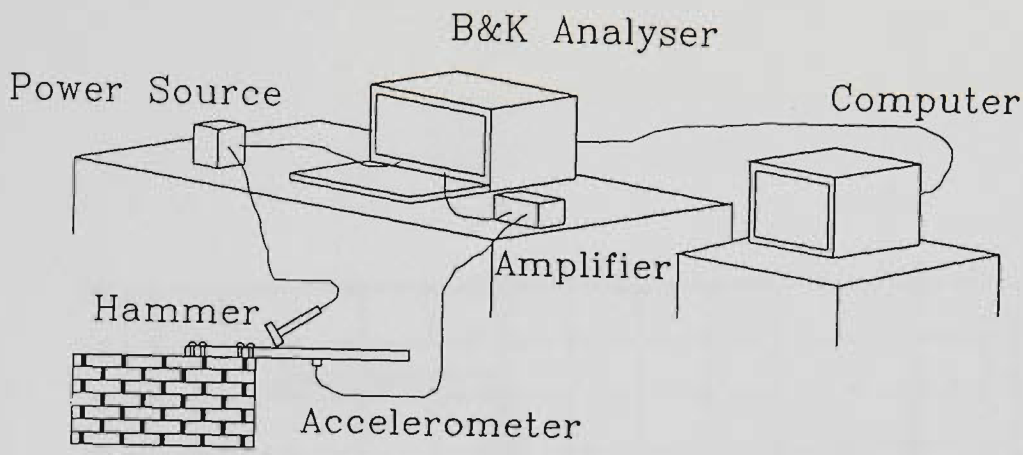

FIG.6.4: Schematic diagram of the measurement set up

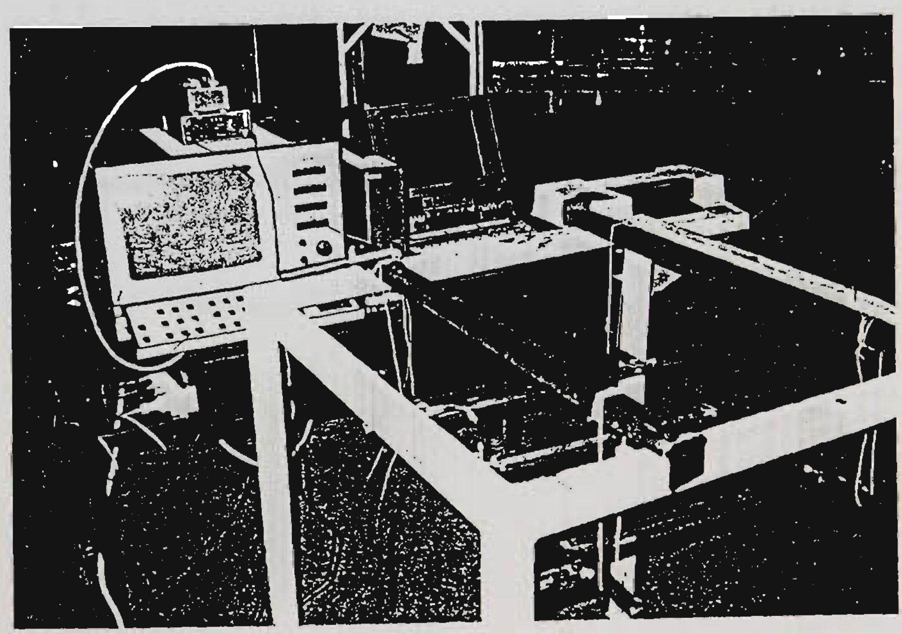

FIG.6.5: Photograph of the experimental rig

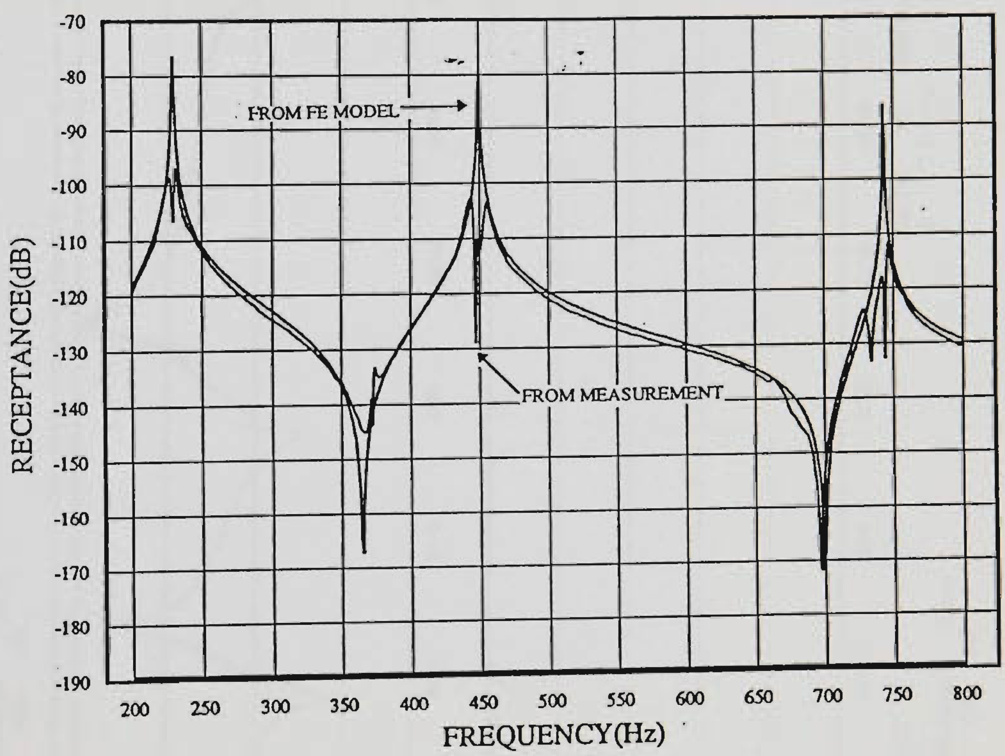

FIG.6.6: $\alpha_{11,11}(\Omega)$ for the beam from measurement and FE model

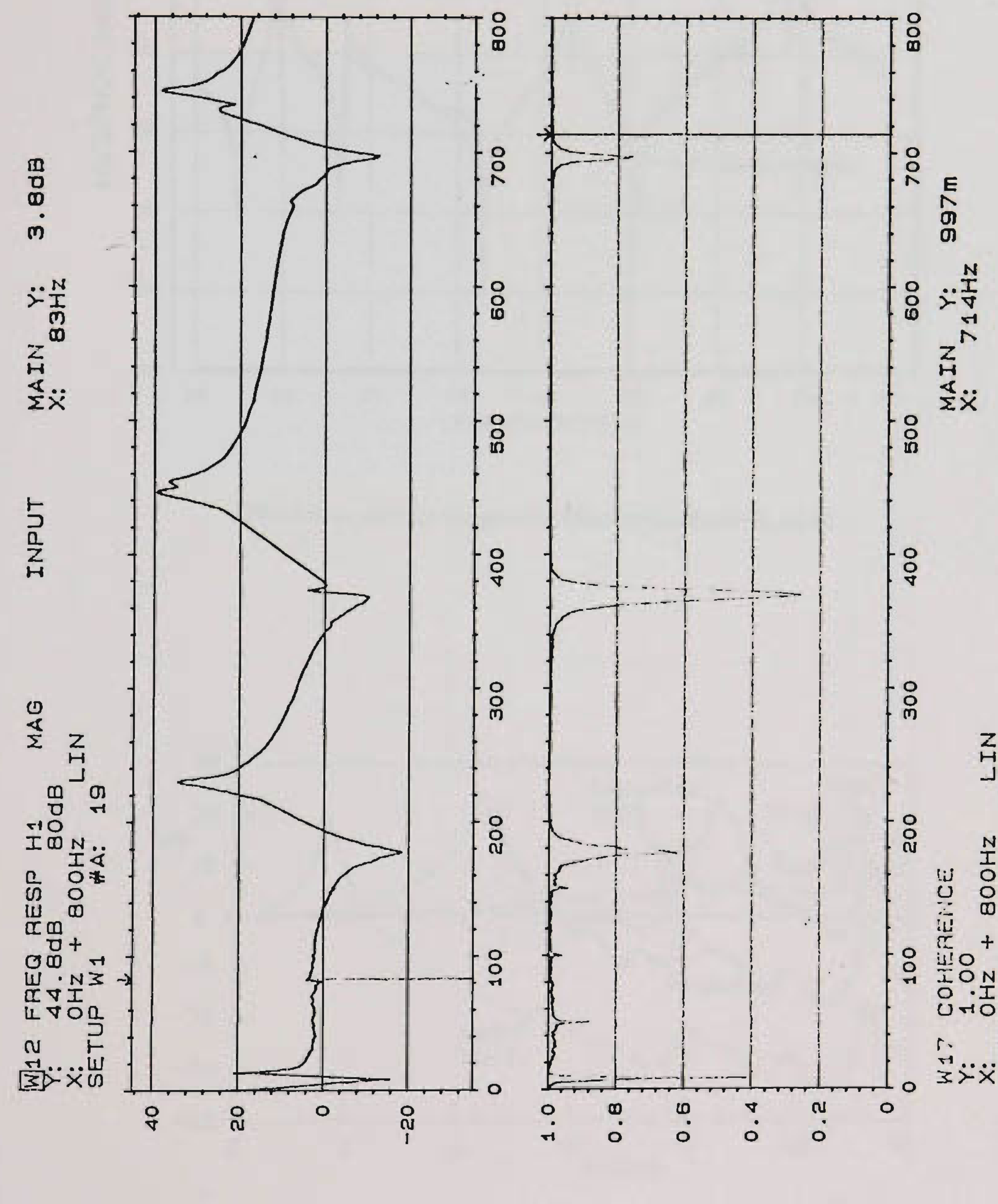

FIG.6.7: Coherence of $\bar{R}FRF$ ($\alpha_{11,11}(\Omega)$) for the undamaged beam

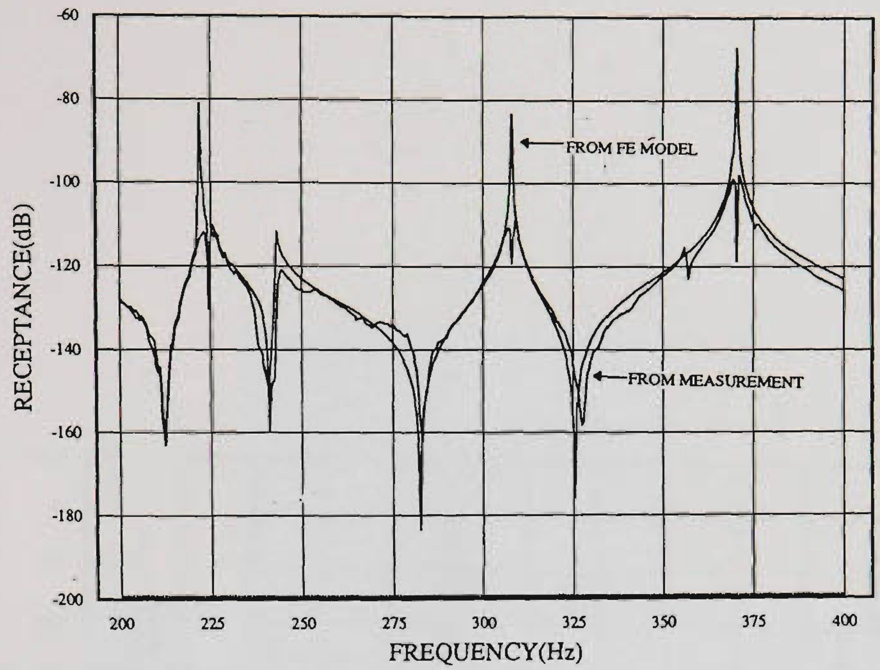

FIG.6.8: $\alpha_{7,7}(\Omega)$ for the grid from measurement and FE model

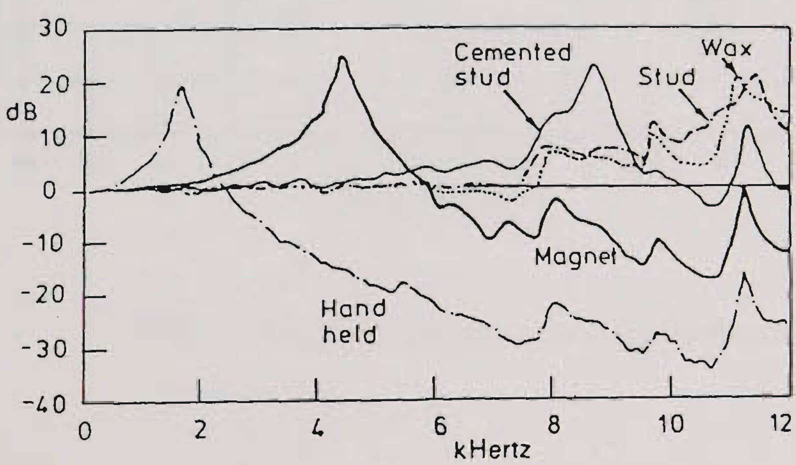

FIG.6.9: Frequency response of different forms of attachment
(Reference: Modal Analysis: Theory and Practice by D. J Ewins)

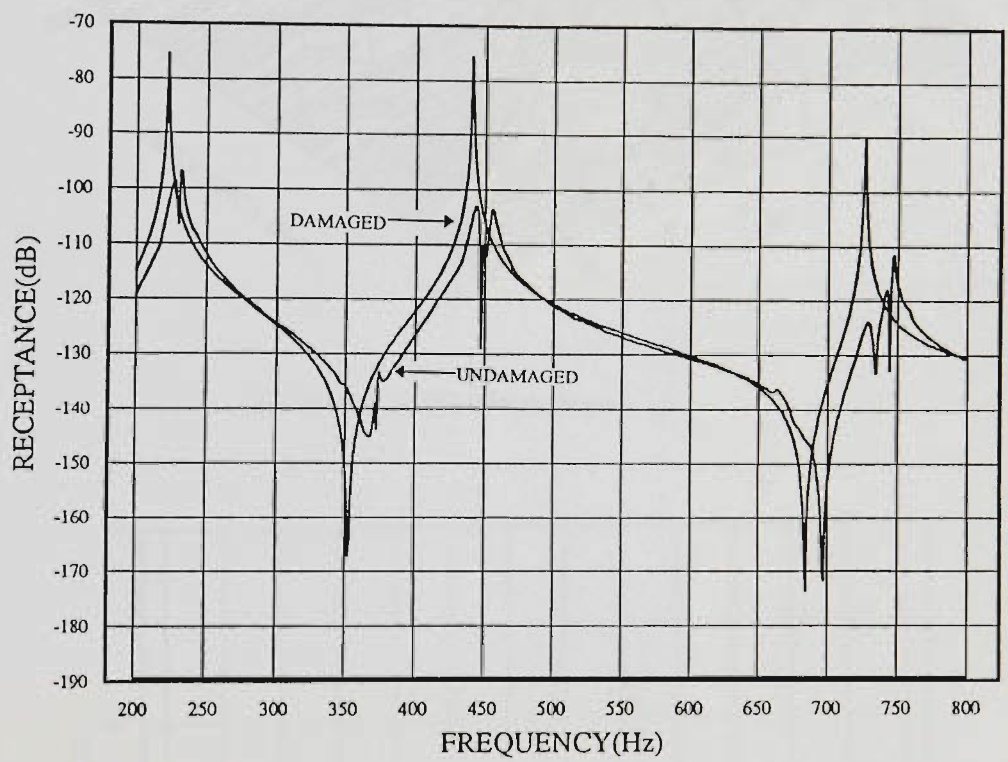

FIG.6.10: $\alpha_{11,11}(\Omega)$ for the beam before and after damage

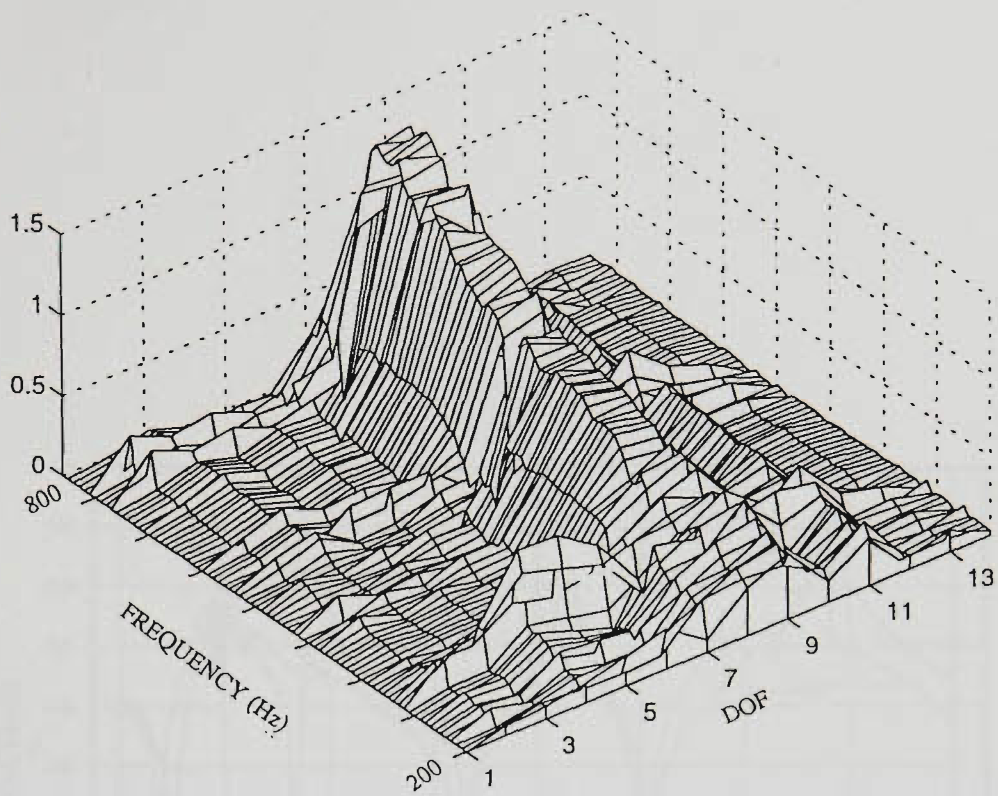

FIG.6.11(a): 3-D DLP for the beam

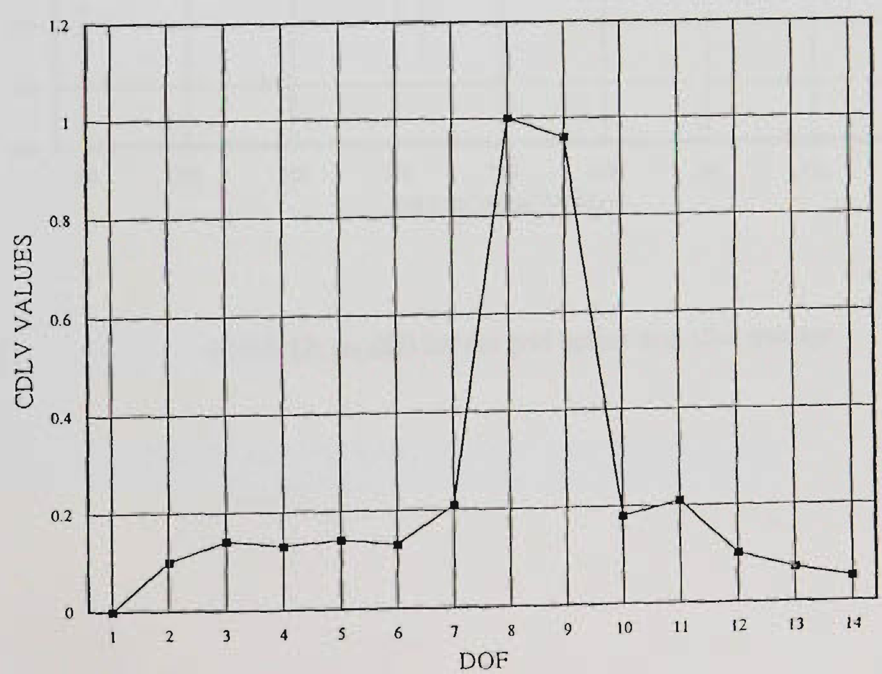

FIG.6.11(b): CDLV for the beam

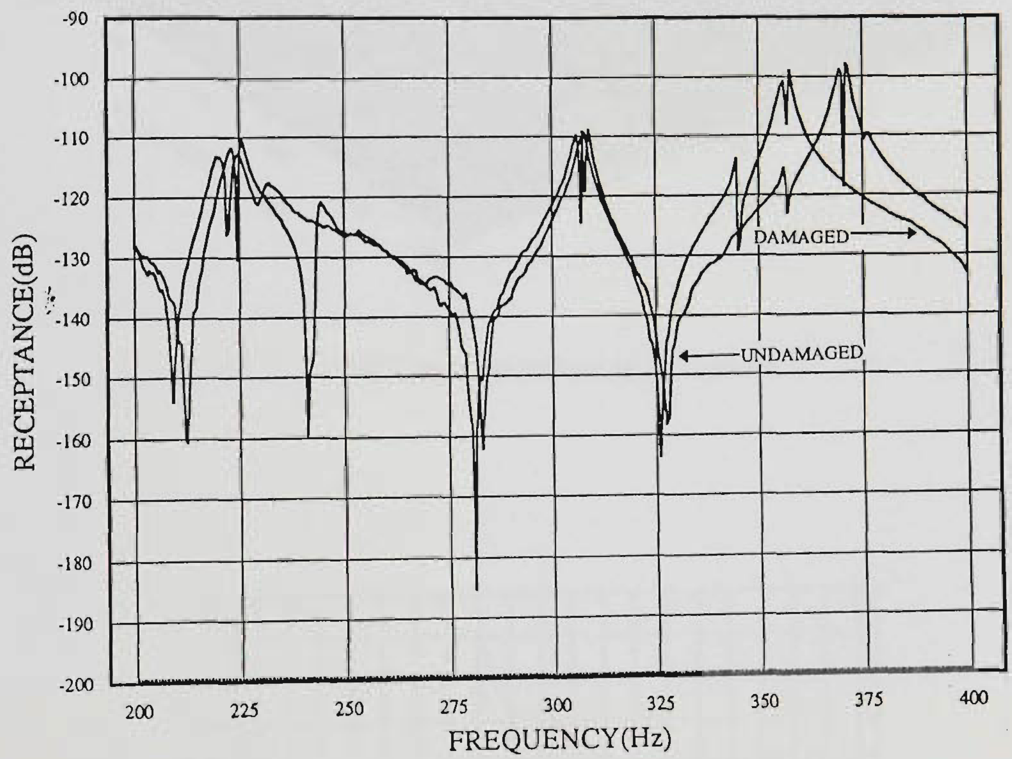

FIG.6.12: $\alpha_{7,7}(\Omega)$ for the grid before and after damage

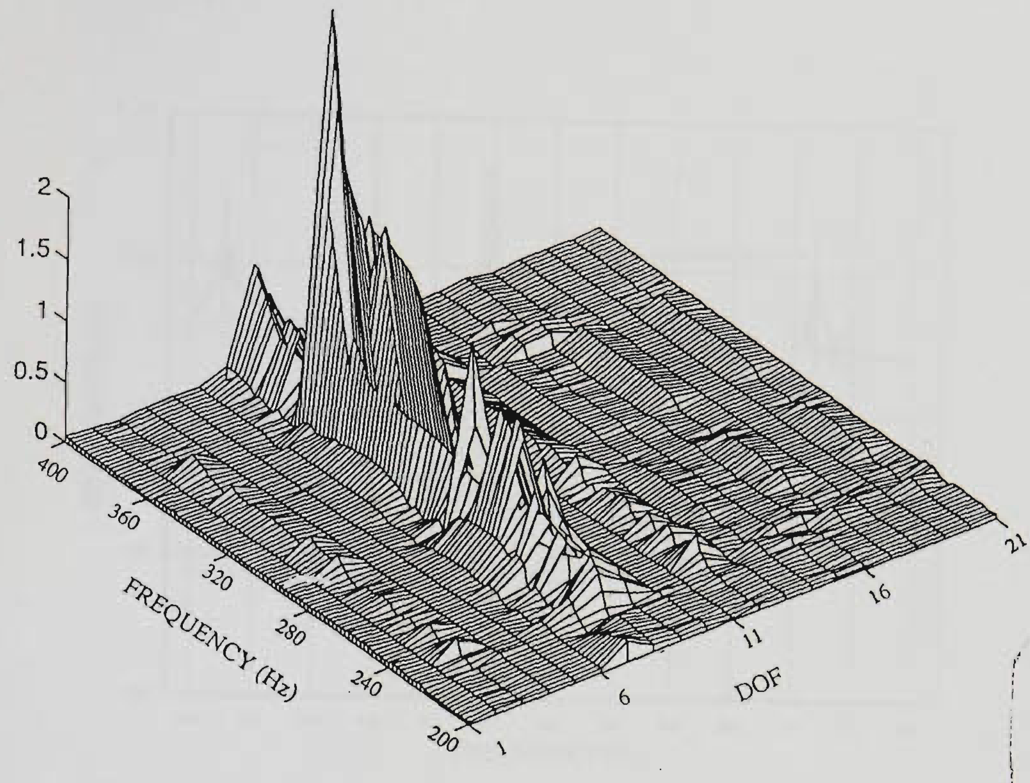

FIG.6.13(a): 3-D DLP for the grid structure

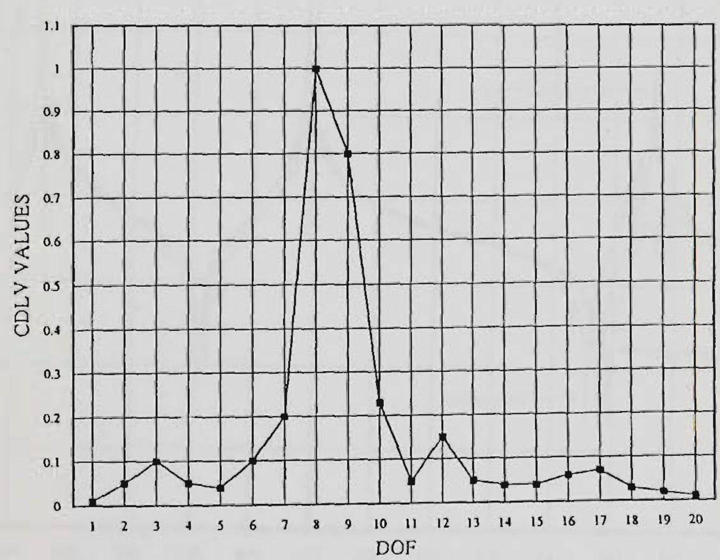

FIG. 6.13(b): CDLV for the grid structure

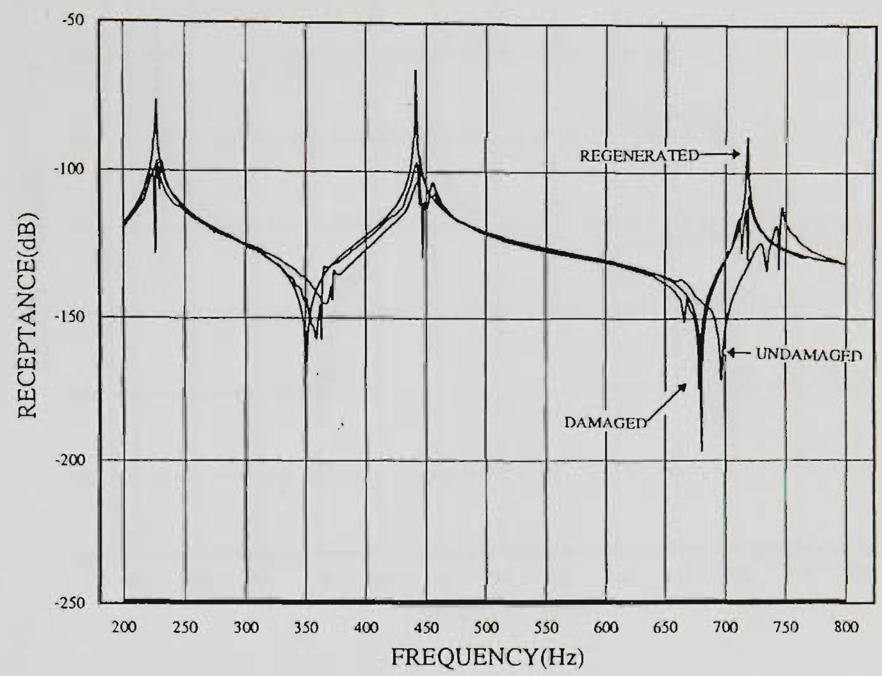

FIG.6.14A: $\alpha_{11,11}(\Omega)$ for the beam (regenerated, before and after damage) for case A

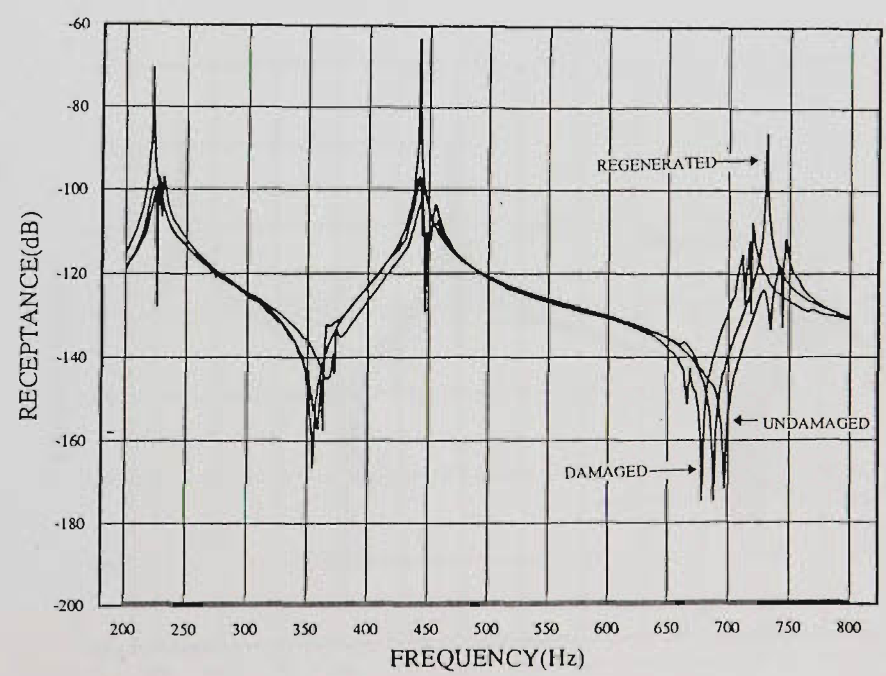

FIG.6.14B: $\alpha_{11,11}(\Omega)$ for the beam (regenerated, before and after damage) for case B

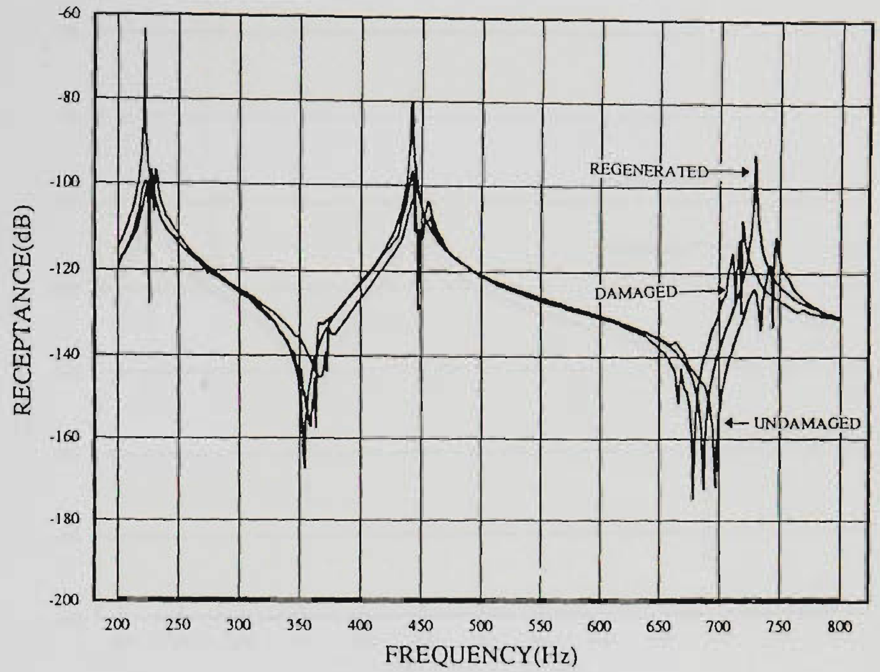

FIG.6.14C: $\alpha_{11,11}(\Omega)$ for the beam (regenerated, before and after damage) for case C

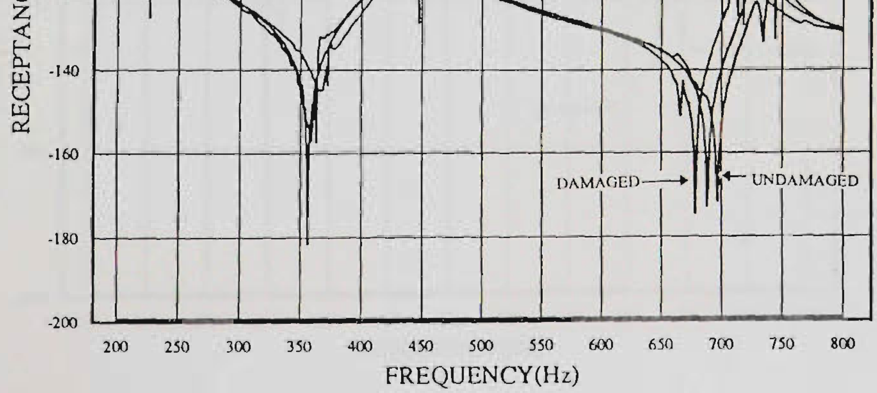

FIG.6.15A: $\alpha_{11,11}(\Omega)$ for the beam (regenerated, before and after damage) using scaling factor .15

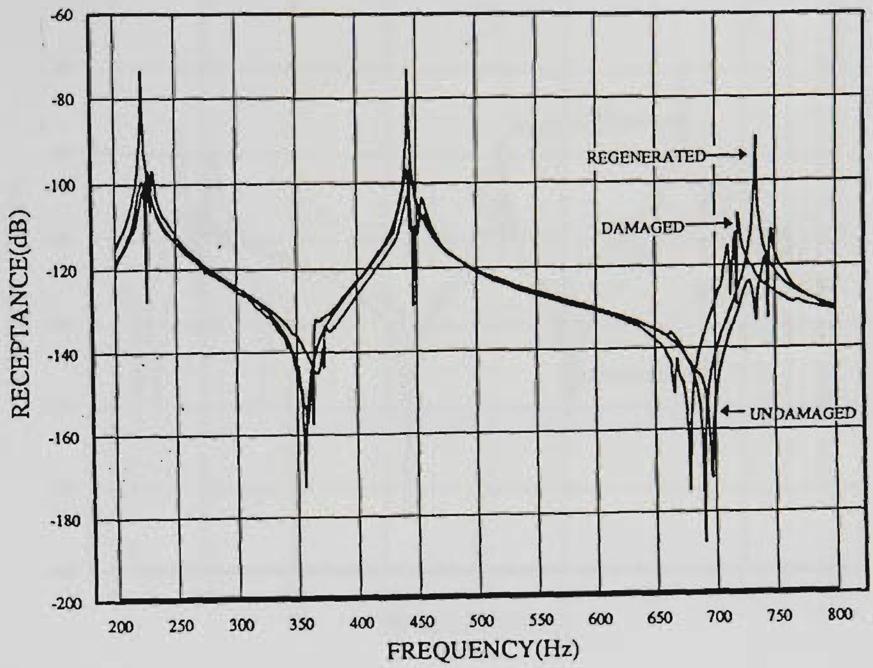

FIG.6.15B: $\alpha_{11,11}(\Omega)$ for the beam (regenerated, before and after damage) using scaling factor .17

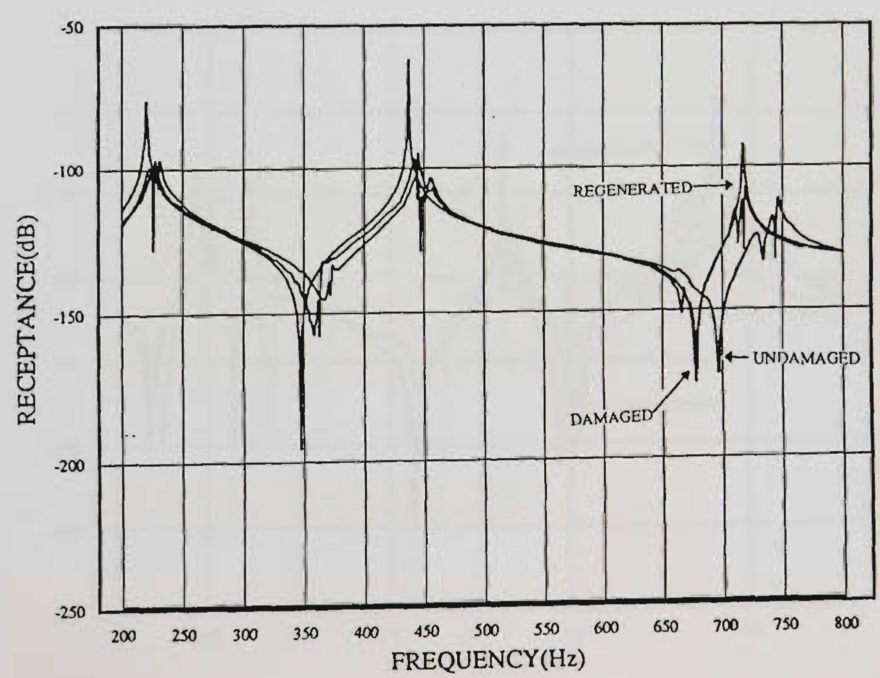

FIG.6.15C: $\alpha_{11,11}(\Omega)$ for the beam (regenerated, before and after damage) using scaling factor .26

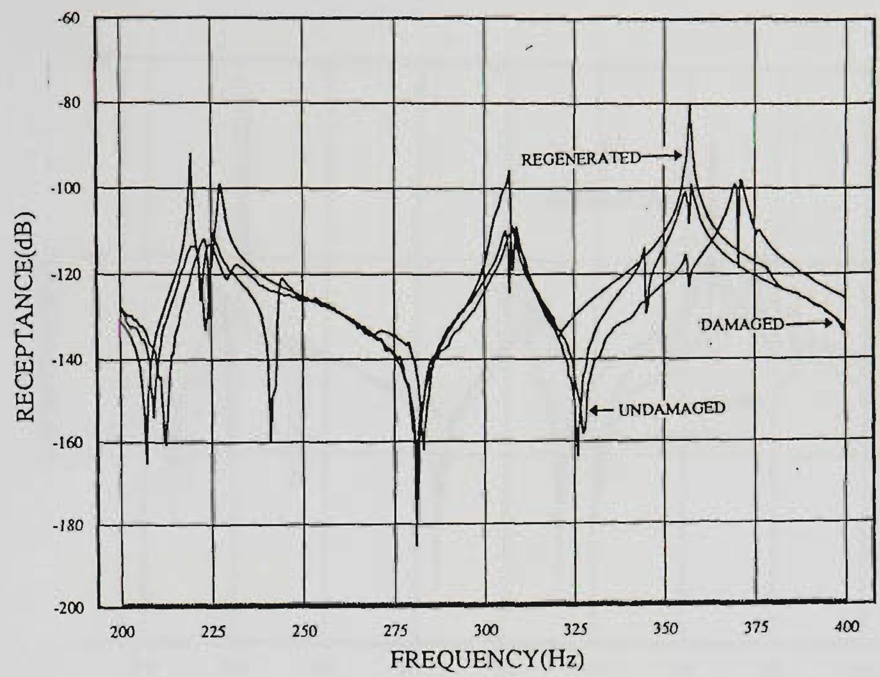

FIG.6.16A: $\alpha_{7,7}(\Omega)$ for the grid (regenerated, before and after damage) for case A

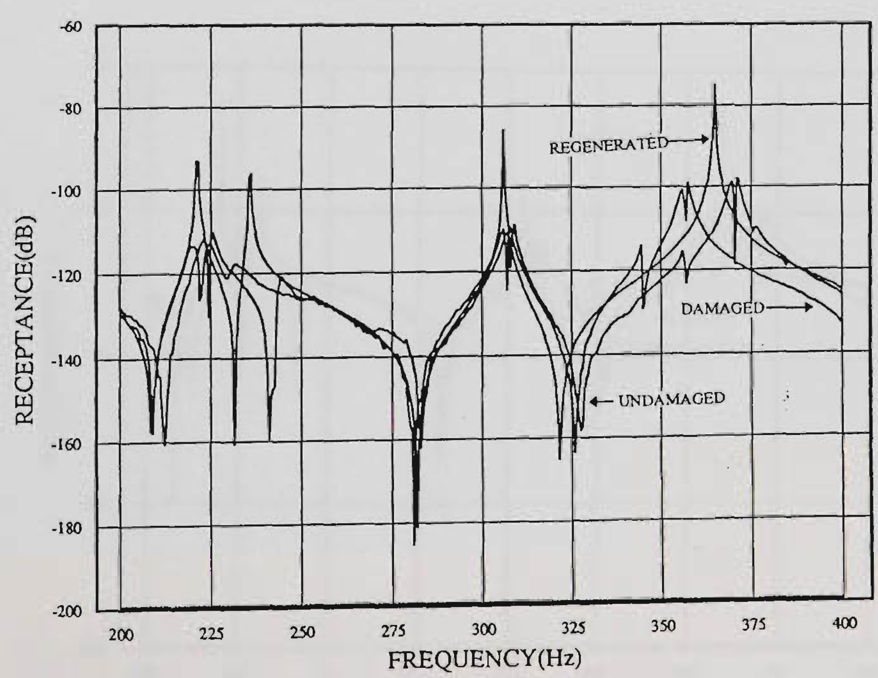

FIG.6.16B: $\alpha_{7,7}(\Omega)$ for the grid (regenerated, before and after damage) for case B

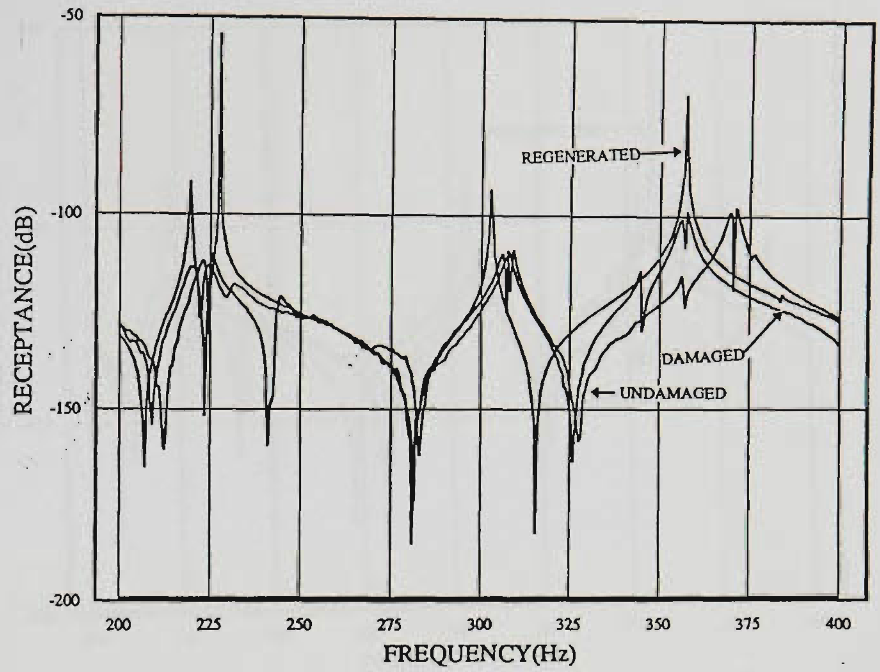

FIG.6.16C: $\alpha_{7,7}(\Omega)$ for the grid (regenerated, before and after damage) for case C

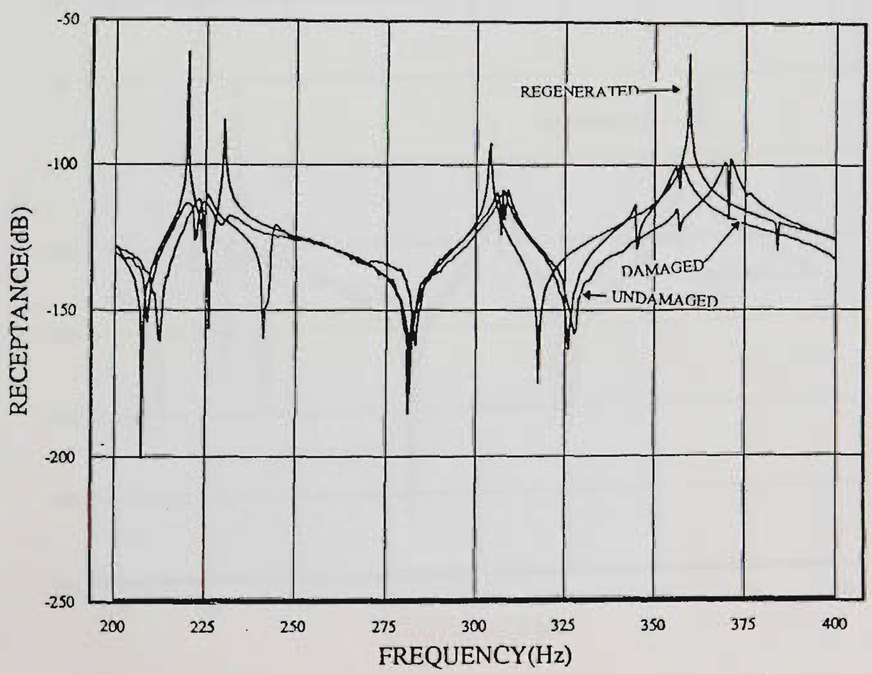

FIG.6.16D: $\alpha_{7,7}(\Omega)$ for the grid (regenerated, before and after damage) for case D

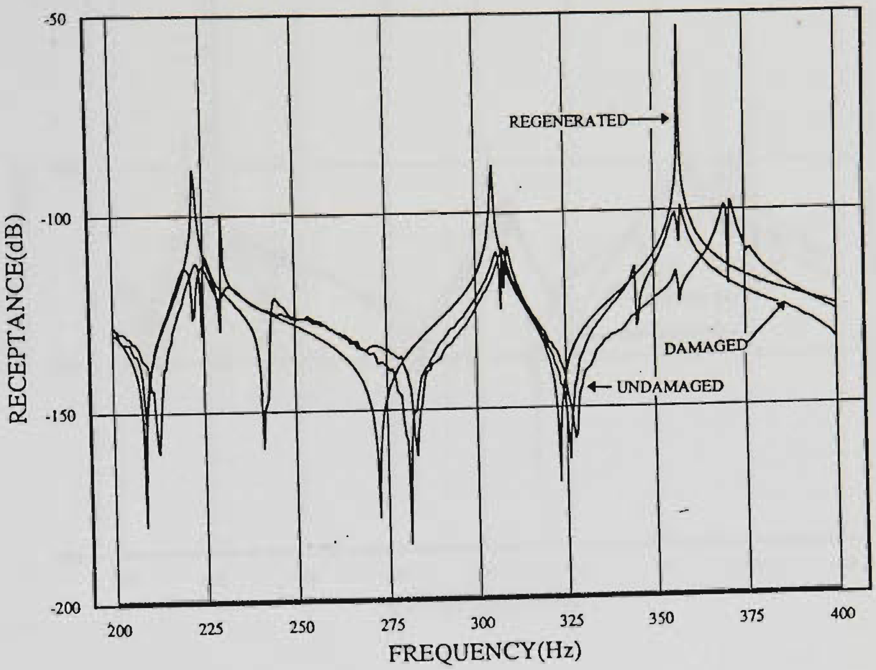

FIG.6.17A: $\alpha_{7,7}(\Omega)$ for the grid (regenerated, before and after damage) using scaling factor .38

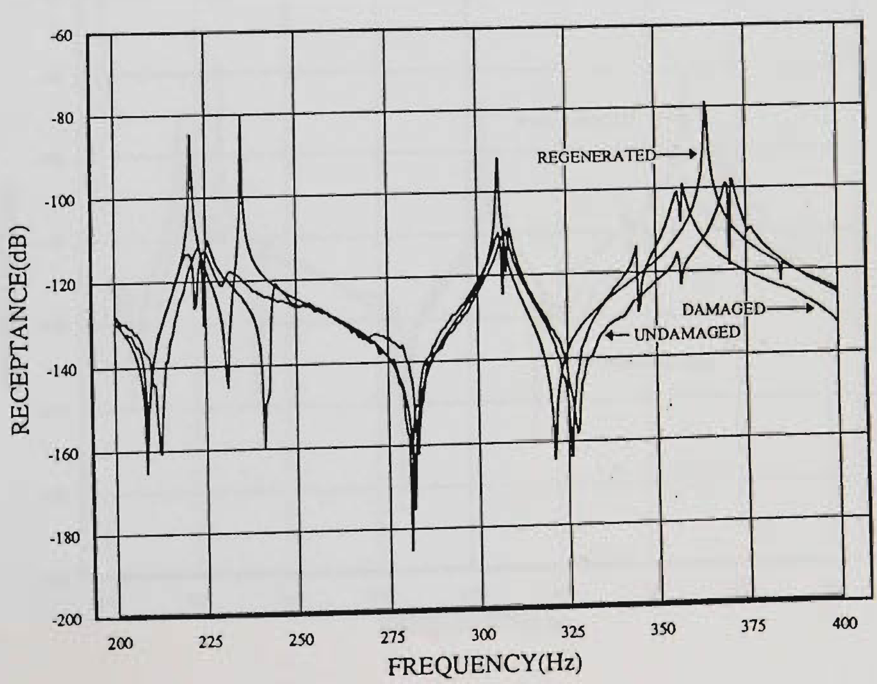

FIG.6.17B: $\alpha_{7,7}(\Omega)$ for the grid (regenerated, before and after damage) using scaling factor .24

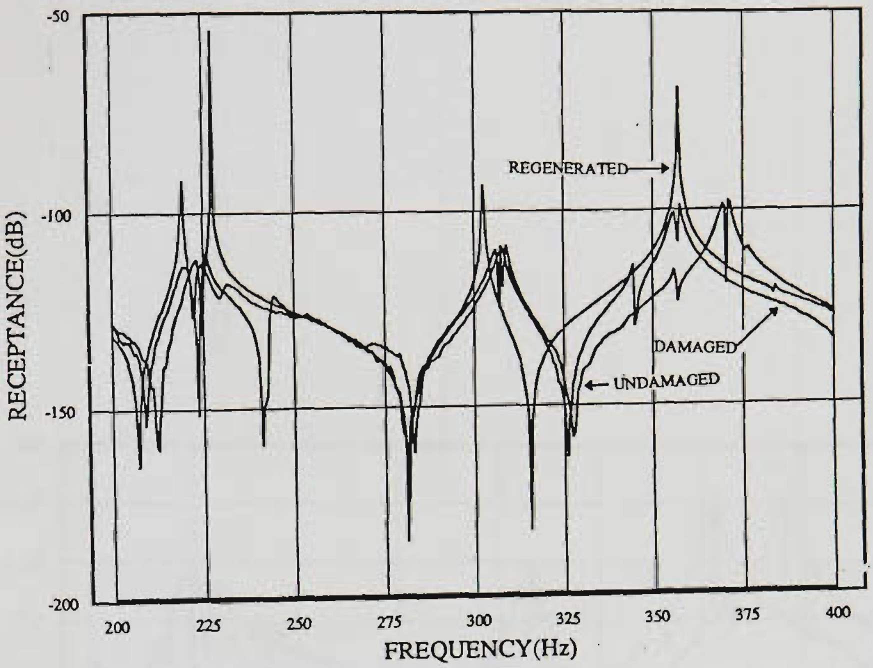

FIG.6.17C: $\alpha_{7,7}(\Omega)$ for the grid (regenerated, before and after damage) using scaling factor .37

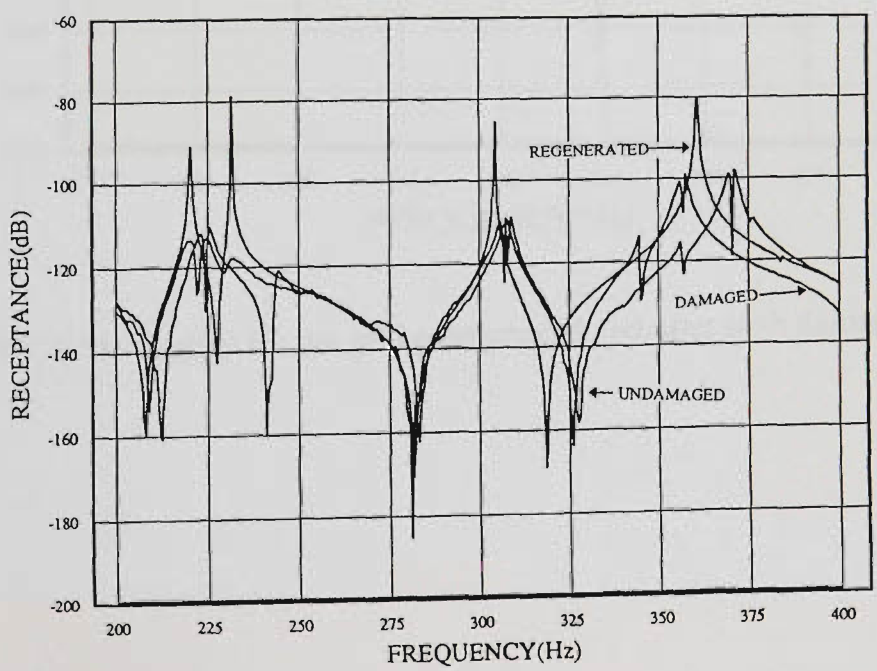

FIG.6.17D: $\alpha_{7,7}(\Omega)$ for the grid (regenerated, before and after damage) using scaling factor .34

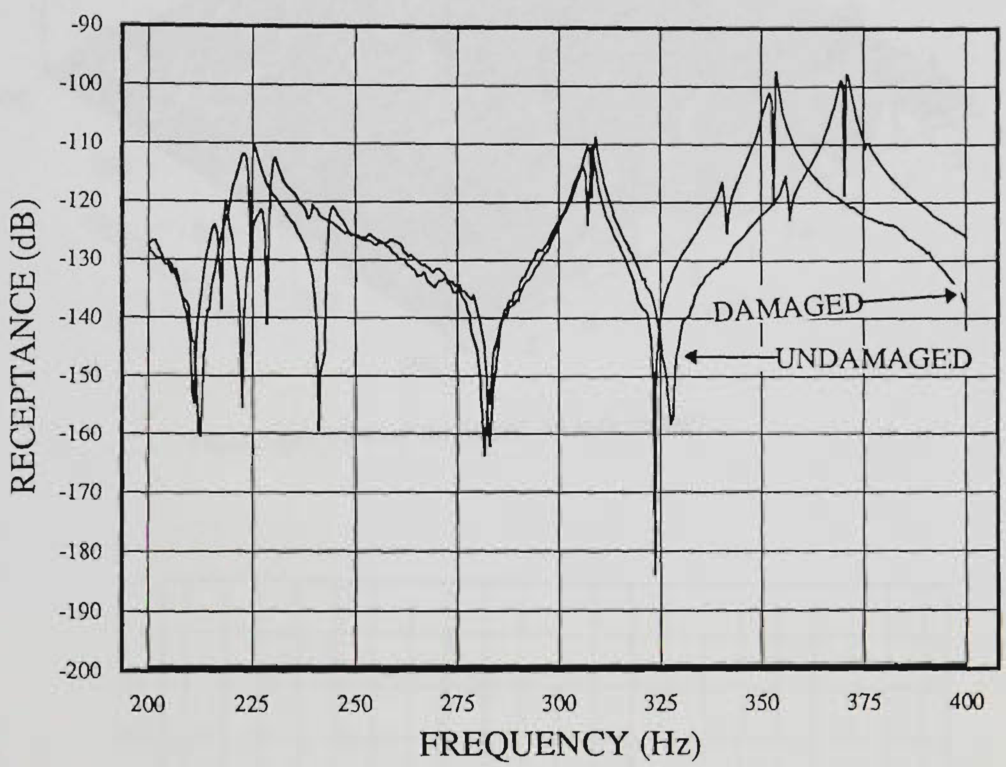

FIG. 6.18: $\alpha_{7,7}(\Omega)$ for the grid (undamaged and after both damages)

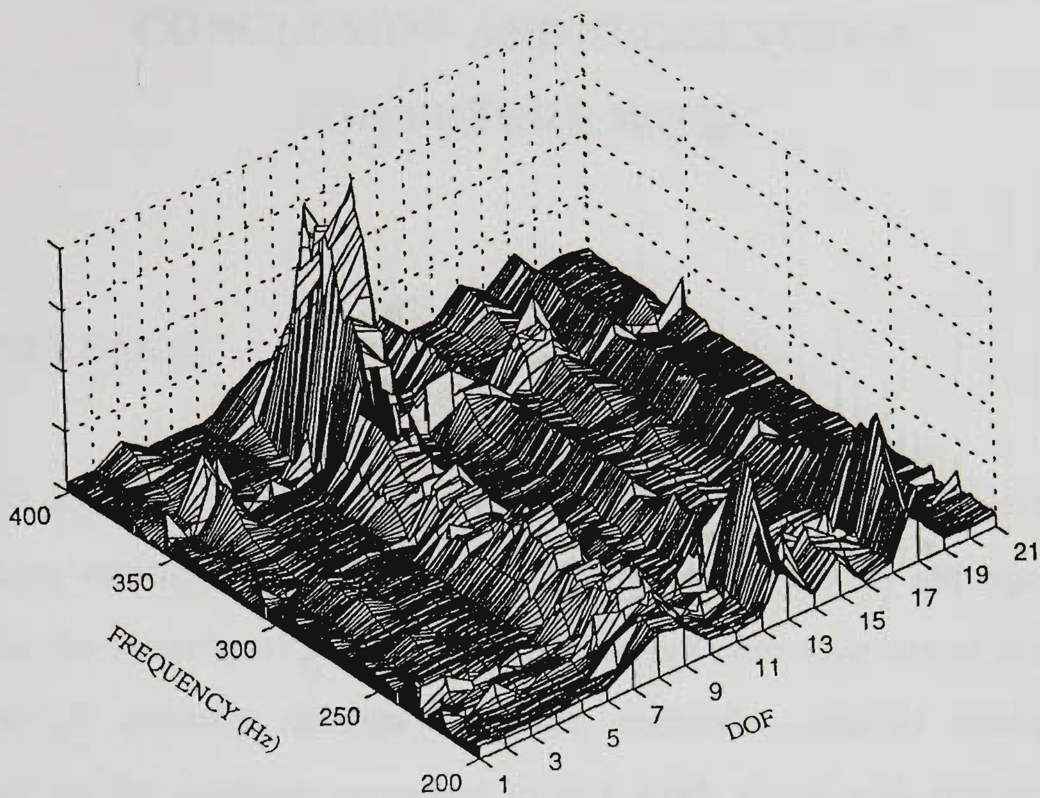

FIG.6.19(a): 3-D DLP for the grid for both damages

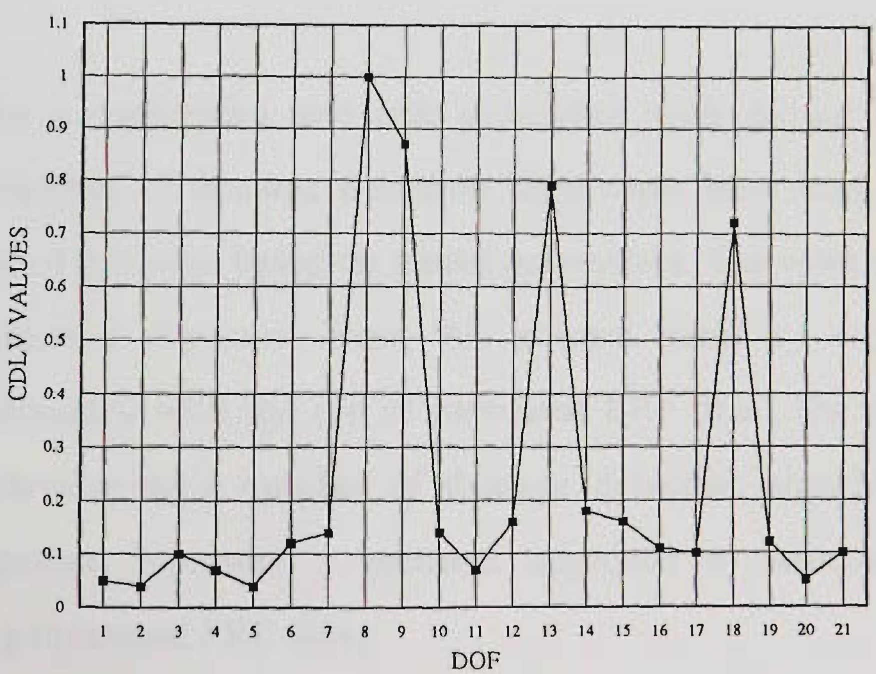

FIG.6.19(b): CDLV for the grid for both damages

CHAPTER 7

CONCLUSION AND SUGGESTIONS FOR FUTURE WORK

7.1 CONCLUSION

The main aim of this work was to develop a structural damage detection tool which uses measured FRF data to locate the existence of damage and to determine the severity of such damage. In the previous chapters of this thesis, a review of existing damage detection methods, detailed mathematical derivation of the methods proposed in this work along with numerical and experimental studies have been presented. This chapter provides a summary of conclusions and important findings of this research.

In view of the complexities and risk associated with failure of practical structures, a number of damage detection algorithms have been developed. However, most of them are based on modal parameters. The work presented in this thesis makes a departure from this current trend by exploiting the advantages associated with the use of measured FRF data. The research has focussed on developing a number of damage detection algorithms which, when put together, represent a coherent approach to structural damage detection using measured FRF data.

As found in this work, the use of FRF data in damage location can result in significant advantages compared to using modal data. In addition to avoiding the complexities of experimental modal analysis, use of FRF data provides the user with an abundance of data which i) locate damage with greater reliability while using noisy data; ii) allow use of FRF data at more frequency points for determining damage extent when the measurement is noisy.

The damage extent results using FRF data were found to be frequency dependant when the data used were noisy, but this can be readily overcome. More accurate estimates of damage can be made by using FRF data at frequency points near regions of resonance which have been more significantly affected than others within the measured frequency range.

The methods derived in this work have limitations regarding the extent of the expansion error it can withstand. Different expansion methods presently in use have been investigated and the best method was found to be D.E A but the quality of damage detection results were found to deteriorate as the expansion errors increased.

To ensure the damage detection algorithms developed in this work produce good results, the following steps should be taken :

- In order to enhance the sensitivity of damage and reduce systematic errors, it is imperative to have a baseline analytical model which can represent accurately the undamaged structure.
- To decrease the influence measurement noise and expansion errors, it is necessary to locate the damage before trying to quantify it.

- After locating the damage, the extent of damage can be obtained more accurately by appropriate selection of frequency points.

7.2 CONTRIBUTIONS OF THE PRESENT RESEARCH

A final review of the research work presented in this thesis have been detailed in this section. A chapter by chapter listing of the specific contributions of this research work have been given here.

In Chapter 2, the major contributions are as follows:

(i) the development of CMDQ method using measured FRF data and Constrained Minimization Theory to detect damage in a structure;

(ii)derivation of a noise filtering algorithm which, when used in conjunction with the damage detection theory proposed in this chapter, enhances its capacity to absorb more measurement noise;

(iii)providing guidelines regarding the minimum number of frequency points required for the success of this method.

The contributions made in Chapter 3 are the following:

(i) presentation of a method to locate damage in a structure by using measured FRF data;

(ii)introduction of the concept of 3-D Damage Location Plot to isolate the area of damage with greater confidence even when the measured FRF data are not of the highest quality;

(iii)a detailed analysis of the existing expansion algorithms for FRF data;

(iv)investigation of the performance of the Damage Location Algorithm when used with expanded measured FRF data and a study of conditions under which the algorithm succeeds.

In Chapter 4, the concept of the Submatrix Approach has been introduced into the area of damage location using measured FRF data in order to identify the damaged spatial elements directly. This has proven to be a promising method.

The new developments included in Chapter 5 for damage detection are as follows:

(i) formulation of a new algorithm aimed at identifying the matrix coefficients of a spatial matrix or the stiffness/mass elements directly by using measured FRF data;

(ii)the extension of the algorithm proposed for identifying spatial parameters into the area of damage detection;

(iii)providing guidelines about the most suitable frequency points for this application.

7.3 SUGGESTIONS FOR FUTURE WORK

As a consequence of this work, it is believed that an useful step has been taken towards making use of measured FRF data in the field of damage detection. However, further research is required to make the developments more suitable for ultimate and effective applications. It is felt that future direction of research in this area may be classified under two headings: short term and long term. The former implies extension of work presented in this thesis and the later includes strategic extension and further development of present research.

In the short term, it is envisaged that the areas to be explored should include:

- improvement of the methods suggested in this work so that their capacity to deal with FRF data contaminated by measurement noise can be further enhanced.
- For a damped structure, measured FRF data are damped while the analytical model is not. The effect of this discrepancy on the performance of damage detection methods should be investigated.

As for long term development, it is suggested:

- to develop an integrated system which automates the entire process of damage detection and make it an effective condition monitoring tool. This can perhaps be achieved by training a system so that it generates the 3-D Damage Location Plot, identifies the highest peaks as probable location of damage and then determines the change in spatial matrice due to damage by applying the extent algorithm. This change in matrices may be compared with a 'data bank' in which change in matrices corresponding to typical damages for different structures have been stored, and use the result of comparison to identify the type of damage and to estimate its extent.

REFERENCES

[1] **Ewins.D.J;** ***Modal Analysis: Theory and Practice***

[2] **Thomson.W.T;** ***Theory of Vibrations with applications***

[3] **Rodden.W.P;** ***A Method for Deriving Structural Influence Coefficients from Ground Vibration Tests,*** AIAA Journal, Vol.5/5, pp. 991-1000, 1967

[4] **Brock.J.E;** ***Optimal Matrices Describing Linear Systems,*** AIAA Journal, Vol.6, No.7, pp. 1292-1296, 1968

[5] **Berman.A and Flanelly.W.G;** ***Theory of Incomplete Models of Dynamic Structures,*** AIAA Journal, Vol.9, No.8, pp. 1481-1487, 1971

[6] **Baruch.M and Bar Itzhack.I.Y;** ***Optimum Weighted Orthogonalization of Measured Modes,*** AIAA Journal, Vol.16, No.4, pp. 346-351, 1978

[7] **Berman.A and Nagy.E.J;** ***Improvement of a Large Analytical Model Using Test Data,*** AIAA Journal, Vol.21, No.8, pp. 1168-1173, 1983

[8] **Kabe.A.M;** ***Stiffness Matrix Adjustment Using Mode Data,*** AIAA Journal, Vol.23, No.9, pp. 1431-1436, 1985

[9] **Smith.S.W and Hendricks.S.L;** ***Evaluation of Two Identification Methods for Damage Detection in Large Space Trusses,*** Proceedings of

the 6th VPI&SU/AIAA Symposium on Dynamics and Controls of Large Space Structure, Virginia Polytechnic Inst. and State Univ., Blacksburg, VA, pp. 127-142, 1987

[10] **Inman.D.J and Minas.C;** ***Matching Analytical Models with the Experimental Modal Data in Mechanical Systems,*** Control and Dynamics Systems, Vol.37, pp. 327-363, 1990

[11] **Zimmerman.D.C and Widengren.W;** ***Model Correction Using the Symmetric Eigenstructure Assignment Technique,*** AIAA Journal, Vol.28, No.9, pp. 1670-1676, 1990

[12] **Hajela.P and Soeiro.F;** ***Structural Damage Detection Based on Static and Modal Analysis,*** AIAA Journal, Vol.28, No.6, pp. 1110-1115, 1990

[13] **Soeiro.F;** ***Structural Damage Assessment by Using the Identification Techniques,*** Ph.D Dissertation, AeMES Dept., University of Florida, 1990

[14] **Jung.H and Ewins.D.J;** ***Error Sensitivity of the Inverse Eigensensitivity Method for Model Updating,*** Proceedings of 10th International Modal Analysis Conference, SanDiego, California, pp. 992- 998, 1992

[15] **Liu.S.C and Yao,J.T;** ***Structural Identification Concept,*** ASCE Journal of the Structural Division, Vol.104, No.ST12, pp. 1845-1858, 1978

[16] **Gudmundson.P;** ***The dynamic behaviour slender structures with cross sectional cracks,*** Journal of mechanics and physics of solids, Vol.31(4), pp. 329-345, 1983

[17] **Chondros.T.G and Dimarogonas.A.D;** ***Identification of Cracks in Welded Joints of Complex Structures,*** Journal of Sound & Vibration, Vol.69, No.4, pp. 531-538, 1980

[18] **Ju.F.D and Mimovich,M;** ***Modal Frequency Method in Diagnosis of Fracture Damage in Structures,*** Proceedings of the 4th International Modal Analysis Conference, LA, pp. 1168-1174, 1986

[19] **Lim.T.W;** ***Submatrix Approach to Stiffness Matrix Correction Using Modal Test Data,*** AIAA Journal, Vol.28, No.6, pp. 1123-1130, 1990

[20] **Hearn.G and Testa.R.B;** ***Modal Analysis for Damage Detection in the Structures,*** Journal of Structural Engineering, Vol.117, No.10, pp. 3042-3063, 1991

[21] **Adams.R.D, Walton.D, Flitcroft.J.E and Short.D;** ***Vibration Testing as a Non-destructive Test Tool for Composite Materials,*** Composite Reliability, ASTM STP 580, pp. 159-175, 1975

[22] **Cawley.P and Adams.R.D;** ***The Location of Defects in Structures from measurements of natural frequencies,*** Journal of Strain Analysis, Vol.14(2), pp. 49-57, 1979

[23] **Yuen.M.F;** ***A Numerical Study of the Eigenparameters of a damaged structure,*** Journal of Sound and Vibration, Vol.103/3, pp. 301-310, 1985

[24] **Cherng.A.P and Abdelhamid.M.K;** ***Signal Subspace Correlation (SSC) Index for Detection of Structural Changes,*** Proceedings of the 11th International Modal Analysis Conference, Florida, pp. 232-239, 1993

[25] **Chen.J.C and Garba.J.A;** ***On orbit Damage Assessment for the Large Space Structures,*** AIAA Journal, Vol.26, No.9, pp. 1119-1126, 1988

[26] **Ricles.J.M and Kosmatka.J.B;** ***Damage Detection in Elastic Structures Using Vibratory Residual Forces and Weighted Sensitivity,*** AIAA Journal, Vol.30, No.9, pp. 2310-2316, 1992

[27] **Penny.J, Wilson.D and Friswell.M.I;** ***Damage Location in Structures Using Vibration Data,*** Proceedings of 11th International Modal Analysis Conference, Kissimmee, Florida, pp. 861-867, 1993

[28] **Wang.J.H and Liou.C.S;** ***Structure damage detection via the behaviour of substructure,*** Modal Analysis, Modelling, Diagnostics and Control-Analytical and Experimental ASME, Vol.38, pp. 123- 130, 1991

[29] **Salawu.O.S and Williams.C;** ***Structural damage detection by using Experimental Modal Analysis - A comparison of some methods,*** Proceedings of 11th International Modal Analysis Conference, Kissimme, Florida, pp .254-260, 1993

[30] **He.J and Ewins.D.J;** ***Analytical Stiffness Matrix Correction Using Measured Vibration Modes,*** International Journal of Analytical and Experimental Modal Analysis, Vol.1, No.3, pp. 9-14, 1986

[31] **Adelman.H.M and Haftka.R.T;** ***Sensitivity Analysis of a Discrete Structural System,*** AIAA Journal, Vol.24/5, pp. 823-832, 1986

[32] **Wolff.T and Richardson.M;** ***Fault detection in structures from changes in their modal parameters,*** Proceedings of 7th International Modal Analysis Conference, SanDiego, California, 1989

[33] **Martinez, Red-Horse and Allen;** ***System Identification Methods for Dynamic Structural Models of Electronic Packages,*** Proceedings of 32nd Structures, Structural Dynamics and Materials Conference, Baltimore, pp. 2336-2346, 1991

[34] **Nobari.A.S, Robb.D.A and Ewins.D.J;** ***A new modal based method for structural dynamic model updating and joint identification,*** Proceedings of 10th International Modal Analysis Conference, SanDiego, California, pp. 741-750, 1992

[35] **Lallement.G, Berriet.R and Cogan.S;** ***Updating finite element model using static deformation,*** Proceedings of 10th International Modal Analysis Conference, SanDiego, California, pp. 494-499, 1992

[36] **Law.S and Li.X;** ***Structural Damage Detection based on Higher Order Analysis,*** Proceedings of Asia Pacific Vibration Conference, Kitakyushu, Japan, pp. 640-643, 1993

[37] **Dong.C, Zhang.P, Feng.W and Huang.T;** ***Sensitivity of the modal parameters of a cracked beam,*** Proceedings of 12th Int. Modal Analysis Conference, Hawaii, pp. 98 -104, 1994

[38] **Zimmerman.D and Kaouk.M;** ***Structural Damage Detection using a Minimum Rank Update Theory,*** Journal of Vibration and Acoustics, Vol.116, pp.222-231, 1994

[39] **Kaouk.M and Zimmerman.D;** ***Structural Health Assessment using a partition model update technique,*** Proc. of 13th International Modal Analysis Conference, Tennessee, pp. 1673- 1679, 1995

[40] **Lin.R.M and Ewins.D.J;** ***Model Updating using FRF data,*** Proceedings of 15th International Seminar on Modal Analysis, Leuven, 1990

[41] **Zimmerman.D, Simmermacher.T and Kaouk.M;** ***Structural Damage Detection Using Frequency Response Functions,*** Proceedings of 13th International Modal Analysis Conference, Tennessee, pp. 179-184, 1995

[42] **Tsai.T, Yang.J.C.S and Chen.R.Z;** ***Detection of Damages in Structures by the Cross Random Decrement Method,*** Proceedings of the 3rd International Modal Analysis Conference, Florida, pp. 691-700, 1985

[43] **Akgun.M and Ju.F.D;** ***Transmissibility as a means to diagnose damage in structures,*** Proceedings of 3rd International Modal Analysis Conference, Orlando, Florida, pp. 701-707, 1985

[44] **Rizos.P.F, et al;** ***Identification of crack location and magnitude in a cantilever beam from the vibration modes,*** Journal of Sound and Vibration, Vol.138(3), pp. 381-388, 1990

[45] **Lin.C.S;** ***Location of Modeling Errors Using Modal Test Data,*** AIAA Journal, Vol.28, No.9, pp. 1650-1654, 1990

[46] **Pandey.A, Biswas.M and Samman.M;** ***Damage detection from changes in curvature mode shapes,*** Journal of Sound& Vibration, Vol.145(2), pp. 321-332, 1991

[47] **Fox.C.H.J;** ***The Location of Defects in Structures: A comparison of the use of natural frequency and mode shape data,*** Proceedings of 10th International Modal Analysis Conference, SanDiego, Calfornia, pp. 522-528, 1992

[48] **Law.S.S, Waldron.P and Taylor.C;** ***Damage Detection of a Reinforced Concrete Bridge Deck using the Frequency Response Function,*** Proceedings of 10th International Modal Analysis Conference, SanDiego, California, pp. 772-778, 1992

[49] **Kim.J, Jeon.H and Lee.C;** ***Application of the modal assurance criteria for detecting and locating structural faults,*** Proceedings of 10^{th} International Modal Analysis Conference, SanDiego, California, pp. 536-540, 1992

[50] **Richardson.M and Mannan.M.A;** ***Correlating minute structural faults with changes in modal parameters,*** Proceedings of 11^{th} International Modal Analysis Conference, Kissimmee, Florida, pp. 893- 898, 1993

[51] **Doebling.S, Hamez.F, Barlow.M, Peterson.L and Farhat.C; D*amage Detection in a suspended scale model truss via model update*,** Proc. of 11^{th} International Modal Analysis Conference, Kissimmee, Florida, pp. 1083-1094, 1993

[52] **Lim.T.W and Kashangaki.T.A.L;** ***Structural Damage Detection of Space Truss Struct. using best achievable eigenvectors,*** AIAA Journal, Vol.32, No. 5, pp. 1049 -1057, 1994

[53] **Sheinman.I;** ***Damage Detection in Framed Structures,*** AIAA Journal, Vol.32, No.5, pp. 1103-1105, 1994

[54] **Guyan.R.L;** ***Reduction of Stiffness and Mass Matrices,*** AIAA Journal, Vol.3, No.2, pp. 380, 1965

[55] **Irons.B.M;** ***Structural Eigenvalue Problems: Elimination of Unwanted Variable,*** AIAA Journal, Vol.3, No.5, pp. 961-962, 1965

[56] **Kaufman.S and Hall.D.B;** ***Reduction of Mass and Loading Matrices,*** AIAA Journal, Vol.6, No.3, pp. 550-551, 1968

[57] **Hu.Y and Zheng.Z;** ***Improving the accuracy of Guyan Reduction by the Perturbation Technique,*** Proceedings of 7th International Modal Analysis Conference, Las Vegas, pp. 988-991, 1989

[58] **Conti.P;** ***A higher order generalization of the Guyan Reduction Method,*** Proceedings of 7th International Modal Analysis Conference, Las Vegas, pp. 529-532, 1989

[59] **Kidder.R.L;** ***Reduction of structural frequency equations,*** AIAA Journal, Vol.11, No.6, pp. 892, 1973

[60] **Leung.Y.T;** ***An accurate method of dynamic condensation in structural analysis,*** International Journal of Numerical Methods in Engineering, Vol.14, pp. 1241-1256, 1979

[61] **Downs.B;** ***Accurate reduction of stiffness and mass matrices for vibration analysis and a rationale for selecting master degrees-of-freedom,*** ASME, Journal of Mechanical Design, Vol.102, No.2, pp. 412-416, 1980

[62] **Paz.M;** ***Dynamic Condensation,*** AIAA Journal, Vol.22, No.5, pp. 724-727, 1984

[63] **Petersmann.N;** ***Calculation of eigenvalues using substructures and dynamic condensation,*** Proceedings of Second International Conference on Recent Advances in Structural Dynamics, Southampton, pp. 211-219, 1984

[64] **Suarez,L.E and Singh.M.P; A** ***Dynamic Condensation Method for the structural eigenvalue analysis,*** AIAA Journal, Vol.30, No.4, pp. 1046-1054, 1992

[65] **Moore.B.C;** ***Principal component analysis in the linear systems: controllability, observability and model reduction,*** IEEE Transaction of Auto. Control, AC-26(1), pp. 17-36, 1981

[66] **Yae.K.H and Inman.D.J;** ***Model reduction in a subset of the original states,*** Journal of Sound and Vibration, 155(1), pp. 165-176, 1992

[67] **O'Callahan.J;** ***A Procedure for an improved reduced system(IRS) model,*** Proceedings of 7th International Modal Analysis Conference, Las Vegas, Nevada, pp. 17-21, 1989

[68] **O'Callahan.J, Avitable.P and Riemer.R;** ***System equivalent reduction expansion process (SEREP),*** Proceedings of 7th International Modal Analysis Conference, Las Vegas, Nevada, pp. 29-37, 1989

[69] **O'Callahan.J, et al;** ***An efficient method of determining rotational degrees of freedom,*** Proceedings of 4th International Modal Analysis Conference, Los Angeles, 1986

[70] **Avitabile.P, et al;** ***Model correlations and the orthogonality criteria,*** Proceedings of 6th International Modal Analysis Conference, Orlando, 1988

[71] **Avitabile.P, et al;** ***Effects of various model reduction techniques on computed response,*** Proceedings of 7th International Modal Analysis Conference, Las Vegas, 1989

[72] **O'Callahan.J, et al;** ***Optimization of mass and stiffness matrices using generalized inverse technique on the measured modes,*** Proceedings of 3rd International Modal Analysis Conference, Orlando, 1985

[73] **Williams.E.J and Green.J.S;** ***A Spatial Curve fitting technique for estimating rotational degrees of freedom,*** Proceedings of 8th International Modal Analysis Conference, pp. 376-381, 1990

[74] **Waters.T.P and Lieven.N.A.J;** ***A modified surface spline for modal expansion,*** Proceedings of the 12th International Modal Analysis Conference, Hawaii, pp. 66-73, 1994

[75] **Harder.R.L and Desmaris.R.N;** ***Interpolation Using Surface Splines,*** Journal of Aircraft, Vol.9, No.2, pp. 189-191, 1972

[76] **Roy.N.A, Girard.A and Bugeat.L-P;** ***Expansion of experimental mode shapes -an improvement of the projection technique,*** Proceedings of the 11th International Modal Analysis Conference, Florida, pp. 152-158, 1993

[77] **White.C.W and Maytum.B.D;** ***Eigensolution Sensitivity to Parametric Model Perturbations,*** Shock and Vibration Bulletin, Bull.46(5), pp. 123-133, 1976

[78] **Stetson.K.A and Palma.G.E;** ***Inversion of the first-order perturbation theory and its application to structural design,*** AIAA Journal, Vol.14, No.4, pp. 454-460, 1976

[79] **Sandstrom.R.E and Anderson.W.J;** ***Modal perturbation methods for marine structure,*** SNAME Transactions, Vol.90, pp. 41-54, 1982

[80] **Lim.T.W;** ***Structural damage detection using modal test data,*** AIAA Journal, Vol.29, No.12, pp. 2271-2274, 1991

[81] **He.J;** ***On model correlation using the measured frequency response function data,*** Proceedings of the International Conference on Structural Dynamics Modelling- Test, Analysis and Correlation, UK, 1993

[82] **He.J;** ***Derivation of an accurate damping matrix of dynamic structure using its FE model and measured FRF data,*** Journal of Computers and Structures, Vol.53, No.2, pp .367-374, 1994

[83] **Raney.J.P**; ***Identification of Complex Structures using near resonance testing,*** Shock and Vibration Bulletin, No.38, August 1968, pp. 23-32

[84] **Ross.R.G**; ***Synthesis of Stiffness and Mass Matrices,*** SAE Paper No. 710787, Annual SAE Meeting, LA, 1971

[85] **Thoren.A.R**; ***Derivation of Mass and Stiffness Matrices from Dynamic Test Data,*** AIAA Paper 72-346, 1972

[86] **Potter.R and Richardson.M**; ***Mass, stiffness and damping matrices from measured modal parameters,*** ISA International Instrumentation Symposium- Automat. Conference, NY, 1974

[87] **Tsang.W.F and Rider.E**; ***The technique of the extraction of structural parameters from experimental forced forced vibration data,*** Proceedings of 7th International Modal Analysis Conf., Las Vegas, pp. 1627-1631, 1989

[88] **Lee.H.G and Dobson.B.J**; ***The direct measurement of structural mass, stiffness and damping properties,*** Journal of Sound and Vibration, 145(1), pp. 61-81, 1991

[89] **Stanbridge.A.B, Imregun.M and Ewins.D.J**; ***A simple approach to experimental identification of vibration systems,*** 17th International Seminar on Modal Analysis, KU Leuven, pp. 489-502, 1992

[90] **Muscia.R;** ***Identification of Mass and Stiffness Matrices based on incomplete modal analysis of the structures,*** 17th International Seminar on Modal Analysis- KU Leuven, pp. 471-483, 1992

[91] **Alvin.K.F, Peterson.L.D and Park.K.C;** ***A method of determining the minimum order mass and stiffness matrices from modal test data,*** Proceedings of 12th International Modal Analysis Conference, 1994

[92] **Chen.S.Y, Ju.M.S and Tsuei.Y.G;** ***Estimation of mass, stiffness and damping matrices from frequency response functions,*** Proceedings of International Conference on Vibration Engg., Beijing, pp. 279-285, 1994

[93] **Leuridan.J.M, Brown.D and Allemang.R.J**; ***Direct System Parameter Identification of Mechanical Structures with application to Modal Analysis,*** Proceedings of the 8th International Seminar on Modal Analysis, Leuven, 1983

[94] **Rajaram.S and Junkins.J.L;** ***Identification of the vibrating flexible structures,*** AIAA Journal of Guidance, Control and Dynamics, Vol.8(4), pp.463-470, 1985

[95] **Juang.J and Pappa.R.S;** ***An Eigensystem Realization Algorithm (ERA) for Modal Parameter Identification and Model Reduction,*** AIAA Journal of Guidance, Control and Dynamics, Vol.8(5), pp. 620-627, 1985

[96] **Fritzen.C.P;** ***Identification of Mass, Damping and Stiffness Matrices of Mechanical Systems,*** ASME, Journal of Vibration, Acoustics, Stress and Reliability in design, Vol.108/9, 1986

[97] **Yeh.F.B and Yang.C.D;** ***New time domain identification technique,*** AIAA Journal of Guidance, Control and Dynamics, Vol.10/3, 1987

[98] **Mook.D.J and Junkins.J.L;** ***Minimum modal error estimation for poorly modelled dynamic system,*** AIAA Journal of Guidance, Control and Dynamics, Vol.11/4, pp. 367-375, 1988

[99] **Roemer.M.J and Mook.D.J;** ***Mass, stiffness and the damping matrix identification: an integrated approach,*** Journal of Vibration and Acoustics, pp. 358-363, 1992

[100]**Klosterman.A;** ***On the Experimental Determination and use of modal representation of Dynamic characteristics,*** Ph.D Thesis, University of Cincinnati, 1971

APPENDIX A

A1. EXTENSION OF CMDQ METHOD FOR DAMPED SYSTEM

The CMDQ method proposed in Chapter 2 can be readily modified for damped systems. For damped systems, the mathematical procedure remains the same except that, the constraint equation given by equation (2.2.25) in Chapter 2, includes the damping term so that it gets modified. In the following equation viscous damping has been considered although the data is valid for other forms of damping as well:

$$([K]_{UD} \otimes [Q_K])[A_D] - [M]_{UD}[A_D][\Omega_n^2] + i[C][A_D][\Omega_n] - [\{\delta\}_k, \ldots, \{\delta\}_k] = [0]$$

where $[\Omega_n^2]$ is the diagonal matrix. Ω_i $(i = 1, 2, \ldots, n)$ is the frequency at which RFRF data have been measured , and

$$[A_D] = [\{\alpha_D(\Omega_1)\}_k, \ldots \{\alpha_D(\Omega_n)\}_k]$$

The second physical constraint is still the symmetry of matrix $[Q_K]$. However while doing derivation, the damping terms do not make any contribution. However, the [D] matrix in equation (2.2.31) and the receptance matrix will be complex. Therefore while trying to use equation (2.2.32), to obtain the Lagrange multiplier, the real and imaginary parts may be isolated and then $\{\underline{\lambda}\}$ can be derived.

A2. EXTENSION OF METHOD FOR DERIVING SPATIAL MODELS FOR DAMPED SYSTEM.

For damped system, the derivation follows the same method as for undamped systems, with the exception that the stiffness matrix term was considered complex. For the mass matrix, the equation remains as:

$$\{\alpha(\Omega_1)\}_k^T[M]\{\alpha(\Omega_2)\}_k = (\alpha_{kk}(\Omega_1) - \alpha_{kk}(\Omega_2))/(\Omega_1^2 - \Omega_2^2)$$

However, the stiffness term become complex and the equation derived is:

$$\{\alpha(\Omega_1)\}_k^T[K + iH]\{\alpha(\Omega_2)\}_k = (\Omega_1^2\alpha_{kk}(\Omega_1) - \Omega_2^2\alpha_{kk}(\Omega_2))/(\Omega_1^2 - \Omega_2^2)$$

Since the receptance terms are also complex, the real and imaginary parts on both sides of the equation may be isolated and then equated against each other to derive mass, stiffness and damping properties.

APPENDIX B

A NEW METHOD OF DERIVING MODAL PARAMETERS

For an N DOF system as already explained in Chapter 5, it is possible to derive equation (5.3.16) and (5.3.17) by using a single set of frequency points where each set comprises of a pair of points. Therefore, by considering N sets of frequency points, equations derived in Section A2 of appendix A may be modified to yield the following equations:

$$[A][M][B] = [X_M] \tag{B1}$$

$$[A][K+iH][B] = [X_{KH}] \tag{B2}$$

where

$$[A] = \begin{bmatrix} \begin{Bmatrix} \alpha_{1k}(\Omega_1) \\ .. \\ .. \\ \alpha_{Nk}(\Omega_1) \end{Bmatrix} & \begin{Bmatrix} \alpha_{1k}(\Omega_2) \\ .. \\ .. \\ \alpha_{Nk}(\Omega_2) \end{Bmatrix} & \begin{matrix} .. \\ .. \\ .. \\ .. \end{matrix} & \begin{Bmatrix} \alpha_{1k}(\Omega_N) \\ .. \\ .. \\ \alpha_{Nk}(\Omega_N) \end{Bmatrix} \end{bmatrix}$$

$$[B] = \begin{bmatrix} \begin{Bmatrix} \alpha_{1k}(\Omega_{N+1}) \\ .. \\ .. \\ \alpha_{Nk}(\Omega_{N+1}) \end{Bmatrix} & \begin{Bmatrix} \alpha_{1k}(\Omega_{N+2}) \\ .. \\ .. \\ \alpha_{Nk}(\Omega_{N+2}) \end{Bmatrix} & \begin{matrix} .. \\ .. \\ .. \\ .. \end{matrix} & \begin{Bmatrix} \alpha_{1k}(\Omega_{2N}) \\ .. \\ .. \\ \omega_{Nk}(\Omega_{2N}) \end{Bmatrix} \end{bmatrix}$$

$$X_{M,mn} = (\alpha_{kk}(\Omega_m) - \alpha_{kk}(\Omega_n))/(\Omega_m^2 - \Omega_n^2)$$

$$X_{KH,mn} = (\Omega_m^2\alpha_{kk}(\Omega_m) - \Omega_n^2\alpha_{kk}(\Omega_n))/(\Omega_m^2 - \Omega_n^2)$$

Therefore, $[X_{KH}]$ and $[X_M]$ in equations (B1) and (B2) can be built up by using a single point FRF at different frequency points. Assume there exists a eigenvectors of such a system can be obtained by solving the following generalised complex eigenproblem:

$$[[X_{KH}] - \underline{\lambda}_r[X_M]]\{\underline{\psi}_r\} = \{0\} \qquad \text{(B3)}$$

or, $$[[X_M]^{-1}[X_{KH}] - \underline{\lambda}_r[I]]\{\underline{\psi}_r\} = \{0\} \qquad \text{(B4)}$$

Now using equations (B1) and (B2) to replace $[X_{KH}]$ and $[X_M]$ in equation (B4), the following equation may be obtained:

$$[[B]^{-1}[M]^{-1}[A]^{-1}[A][K + iH][B]- \underline{\lambda}_r[I]]\{\underline{\psi}_r\} = \{0\} \qquad \text{(B5)}$$

or, $$[[B]^{-1}[M]^{-1}[K + iH][B] - \underline{\lambda}_r[I]]\{\underline{\psi}_r\} = \{0\} \qquad \text{(B6)}$$

or, $$[[B]^{-1}[R][B]- \underline{\lambda}_r[I]]\{\underline{\psi}_r\} = \{0\} \qquad \text{(B7)}$$

where $[R] = [M]^{-1}[K+ iH]$

or, $$[[P] - \underline{\lambda}_r[I]]\{\underline{\psi}_r\} = \{0\} \qquad \text{(B8)}$$

where $[P] = [B]^{-1}[R][B]$

However, for the actual system, whose mass, stiffness and damping are represented by [M], [K] and [H] respectively, the eigenparameters may be obtained by solving the following equation:

$$[[M]^{-1}[K + iH] - \lambda_r[I]]\{\psi_r\} = \{0\} \qquad \text{(B9)}$$

or, $$[[R] - \lambda_r[I]]\{\psi_r\} = \{0\} \qquad \text{(B10)}$$

Comparing equations (B8) and (B10), it is clear that the square matrices [P] and [R] are similar if the matrix [B] is non- singular. Thus

- Matrices [P] and [R] have the same eigenvalues, i.e $\lambda_r = \underline{\lambda}_r$

- If $\{\underline{\psi}_r\}$ is the eigenvector of [P] corresponding to the eigenvalue $\underline{\lambda}_r$, then $\{\psi_r\} = [B]\{\underline{\psi}_r\}$ is the eigenvector of [R] corresponding to the same characteristic root λ_r of [R].

Therefore once the eigenvalues and eigenvectors of the 'Pseudo system' are derived, the eigenparameters of the actual system given by λ_r and $\{\psi_r\}$ can be easily derived by using the following relationships

- $\lambda_r = \underline{\lambda}_r$
- $\{\psi_r\} = [B]\{\underline{\psi}_r\}$

Since λ_r is the r^{th} eigenvalue of the system which for a damped system is a complex quantity, it can be written as:

$$\lambda_r^2 = \omega_r^2 (1 + i\eta_r)$$

where ω_r is the natural frequency and η_r is the damping loss factor for the r^{th} mode. Hence all the parameters needed to construct the modal model of the system can be obtained from FRF measurements.

However, it might be mentioned that the mode shapes derived here are not mass-normalized. To derive mass-normalised mode shapes, it is suggested to obtain [M] by using equation (B1) and then derive the modal mass by using the orthogonality equation:

$$[\psi]^T [M] [\psi] = [m_r]$$

Once the modal mass is obtained, the mass normalised mode shapes can be derived by using the following equation:

$$\{\varphi\}_r = (m_r)^{-1/2}\{\psi_r\}$$

An alternative approach to derive modal parameters is as given next. From equations (B1) and (B2), it is possible to calculate [M] and [K] as given below:

$$[M] = [A]^{-1}[X_M][B]^{-1}$$
$$[K+ iH] = [A]^{-1}[X_{KH}][B]^{-1}$$

[M] and [K+ iH] thus obtained do not retain the connectivity of the original structure unlike the method suggested in Chapter 5 to derive spatial parameters. However, since the main intention here is to derive the eigen parameters, it does not really make any difference if the connectivity of the original structure is not preserved as long as the eigenparameters obtained are accurate. Knowing [K+ iH] and [M], it is possible to solve equation (B9) to obtain the eigenparameters, which yields the natural frequencies, damping ratios and mass normalised mode shapes of the structure.

APPENDIX C

OPTIMIZATION PROBLEMS WITH CONSTRAINTS

The problem of finding the maximum or minimum values of z = f(x, y) subject to constraint can be approached by solving the constraint equations for one of the independent variables and substituting the result into the expression for f(x, y). This reduces f to a function of a single variable and the relative extrema for the function can be obtained by equating the derivative of f to zero.

However, this method is not always ideal, since the constraint equations may be difficult to solve, or the resulting function of a single variable may be difficult to work with.

Mathematician Joseph L. Lagrange (1736-1813) discovered a more superior method for solving such problems. The Lagrange method of finding the extreme values of a function subject to constraints is based on the following theorem:

> Let f and g be differentiable at (x_0, y_0). Let C be the level curve $g(x, y) = c$ that contains (x_0, y_0). Assume that C is smooth, and (x_0, y_0) is not an endpoint of the curve. If grad $g(x_0, y_0) \neq 0$ and if f has an extreme value on C at (x_0, y_0), then there is a number λ such that
>
> $$\text{grad } f(x_0, y_0) = \lambda \text{ grad } g(x_0, y_0) \qquad \text{(C1)}$$

The number λ in equation (C1) is called a Lagrange multiplier for f and g. The proof of the above theorem proceeds as follows:

If grad $f(x_0, y_0) = 0$, then equation (C1) is satisfied with $\lambda = 0$. Thus for the rest of the proof it is assumed that grad $f(x_0, y_0) \neq 0$. Let I be an interval and

$$r(t) = x(t)i + y(t)j \text{ for t in I}$$

a smooth parametrization of C. Let t_0 be such that $r(t_0)$ corresponds to the point (x_0, y_0). Then t_0 is not an endpoint of I since (x_0, y_0) is not an endpoint of C. Finally let F be defined by

$$F(t) = f(x(t), y(t)) \text{ for t in I}$$

$$F'(t) = \frac{dF}{dt} = \frac{\partial f}{\partial x}\frac{dx}{dt} + \frac{\partial f}{\partial y}\frac{dy}{dt} = grad\ f(x_0, y_0).r'(t)$$

Since f has an extreme value on C at $(x_0, y_0) = (x(t_0), y(t_0))$, it follows that F has an extreme value on I at t_0. Since F is differentiable on I and t_0 is not an endpoint of I it follows that $F'(t_0) = 0$. Therefore

$$0 = F'(t_0) = grad\ f(x_0, y_0).r'(t_0)$$

But $r'(t_0) \neq 0$ since r is a smooth parametrization of I, and grad $f(x_0, y_0) \neq 0$ by assumption. Thus grad $f(x_0, y_0)$ is perpendicular to $r'(t_0)$, which itself is tangent to C. Therefore grad $f(x_0, y_0)$ is normal to C. But grad $g(x_0, y_0)$ is normal to C, since C is smooth and grad $g(x_0, y_0) \neq 0$. Consequently grad $f(x_0, y_0)$ and grad $g(x_0, y_0)$ are parallel. This yields equation (C1).

The method of applying Lagrange multiplier follows:

(i) Form the function $L = f + \lambda g$ with values

$L(x, y, \lambda) = f(x, y) + \lambda g(x,y)$

(ii) Set all partial derivatives of L equal to zero, obtaining the equations

$$\frac{\partial L}{\partial x} = 0, \quad \text{or,} \quad \frac{\partial f}{\partial x} + \lambda \frac{\partial g}{\partial x} = 0 \qquad \text{(a)}$$

$$\frac{\partial L}{\partial y} = 0, \quad \text{or,} \quad \frac{\partial f}{\partial y} + \lambda \frac{\partial g}{\partial y} = 0 \qquad \text{(b)}$$

$$\frac{\partial L}{\partial \lambda} = 0 \quad \text{or,} \quad g(x,y) = 0 \qquad \text{(c)}$$

(iii) The desired value can be obtained by solving equations set up in step (ii).

The method of applying Lagrange multiplier as described above was exactly applied in Chapter 2. Unlike x and y in the example described above, the variables in Chapter 2 were $Q_{Z,ij}$ and $Q_{K,ij}$ for different values of i and j. As described in step (ii) above, equation (2.2.16) was obtained by differentiating with respect to $Q_{Z,ij}$. Differentiating L in equation (2.2.14) with respect to λ and μ generated equations (2.2.11) and (2.2.12) respectively. Equations (2.2.16), (2.2.11) and (2.2.12) were solved together to obtain the desired value.

APPENDIX D

MATRICES: SELECTED DEFINITIONS AND MANIPULATIONS

Matrix theories that were frequently used in course of this thesis have been highlighted here. Symbols used here are arbitrary and imply no particular physical meaning.

D1. SUM OF MATRICES

If $A = [A_{ij}]$ and $B = [B_{ij}]$ are two m x n matrices, their sum (difference), $A \pm B$, is defined as the m x n matrix $C = [C_{ij}]$, where each element of C is the sum (difference) of the corresponding elements of A and B. Thus, $A \pm B = [A_{ij} \pm B_{ij}]$

Two matrices of the same order are said to be conformable for addition or subtraction.

D2. Matrix multiplication

If $A = [A_{ij}]$ is a m x n matrix and $B = [B_{ij}]$ is a n x q matrix, then their product C is defined as $C = AB$ where $C_{ij} = \Sigma A_{ik}B_{kj}$ where k ranges from 1 to n, i ranges from 1 to m and j ranges from 1 to q. The product AB is defined or A is conformable to B for multiplication when the number of columns of A is equal to the number of rows of B. The transpose of a product is the product of the transpose in reverse order, that is $([A][B])^T = [B]^T[A]^T$

D3. Linear Dependance of Vectors

The m n-vectors $\{x_1\}$, ..., $\{x_m\}$ are said to be linearly dependent provided there exists m scalar elements k_1, k_2,.........,k_m, not all zero, such that: $k_1\{x_1\}$ + $k_2\{x_2\}$ + -------------$k_m\{x_m\}$ = 0.

Otherwise, the m vectors are said to be linearly independent.

D4. Rank, Singularity

A non-zero matrix [A] is said to have rank r if at least one of its r-square minors is different from zero while every (r + 1) square minor, if any, is zero. A null or zero matrix is said to have zero rank. An equivalent definition of rank is the maximum number of linearly independent rows (or columns) in [A].

A matrix whose rank is less than its order is said to be rank deficient. An n-square matrix A is called non-singular if its rank is equal to its order. Otherwise, the matrix is called singular.

D5. Elementary transformations

The following operations, called elementary transformations, may be performed on a matrix without changing its order or its rank.

(1) The interchange of the i^{th} and j^{th} rows, denoted by H_{ij};

The interchange of the i^{th} and j^{th} columns, denoted by K_{ij}

(2) The multiplication of every element of the i^{th} row by a non-zero scalar k, denoted by $H_i(k)$;

The multiplication of every element of the i^{th} row by a non-zero scalar k, denoted by $K_i(k)$.

(3) The addition to the elements of the i^{th} row of k, a scalar, times the corresponding elements of the j^{th} row, denoted by $H_{ij}(k)$;

The addition to the elements of the i^{th} row of k, a scalar, times the corresponding elements of the j^{th} column, denoted by $K_{ij}(k)$.

The transformations H are called elementary row transformations; the transformations K are called elementary column transformations.

D6. Similarity transformations

A similarity transformation possesses the following properties:

1. $[C]^{-1}[A_1][C] + \text{-----} + [C]^{-1}[A_n][C] = [C]^{-1}([A_1] + \text{------} + [A_n])[C]$
2. $([C]^{-1}[A_1][C])^n = [C]^{-1}[A_1]^n[C]$

where [C] is a non-singular matrix. The matrix [D] is said to be similar to matrix [A] when $[D] = [C]^{-1}[A][C]$. The most important property common to similar matrices is the fact that they have the same eigenvalues, for

$$[A] - \lambda\, [I] = 0$$

implies $\quad [C]^{-1}([A] - \lambda\, [I])[C] = 0$

and $\quad [C]^{-1}[A][C] - \lambda\, [I]) = 0$

so that $\quad [D] - \lambda[I] = 0$

Therefore the eigenvalues of [A] and [D] coincide. However, matrices having the same eigenvalues are not necessarily similar.

D7. Basis

A basis of a vector space is any ordered set of vectors of the space that

(i) is linearly independent

(ii) spans the vector space

D8. Orthonormal

A basis $\{x_1\}, \ldots\ldots\ldots\ldots, \{x_N\}$ is called orthonormal if

$$\{x_i\}^H\{x_j\} = \begin{cases} 0 \; whenever \; i \neq j \;\; giving \; the \; orthogonality \\ 1 \; whenever \; i = j \;\; giving \; the \; normalization \end{cases}$$

D9. Element by element matrix multiplication

In Chapter 2, operator ⊗ has been used to perform element by element matrix multiplication. Relevant properties of the operator are given below:

1) $[c] = [a] \otimes [b]$

   defines $c_{ij} = a_{ij}b_{ij}$

2) $[c] = [d]([a] \otimes [b])$

   implies $c_{ij} = \sum d_{ik}(a_{kj}b_{kj})$

   where k ranges from 1 to n

3) $[a] \otimes [b] = [b] \otimes [a]$

4) $\{[d]([a] \otimes [b])\}^T = ([a]^T \otimes [b]^T)[d]^T$

D10. Matrix differentiation

Differentiation of a matrix is accomplished by differentiating each of its terms. Let $\{x\} = \{x_1 \ \ x_2 \ , \ldots\ldots, x_n\}^T$ and let [A] be an arbitrary n by n square matrix that does not depend on the x_i. Suppose that the quadratic form

$$\phi = 0.5 \ \{x\}^T[A]\{x\}$$

is to be differentiated with respect to each of the x_i. The result is conveniently stated as a vector,

$$\left\{\frac{\partial\phi}{\partial x}\right\} = \left[\frac{\partial\phi}{\partial x_1} \quad \frac{\partial\phi}{\partial x_2} \quad \cdots \quad \frac{\partial\phi}{\partial x_n}\right]^T = [A]\{x\}$$

APPENDIX E

METHOD OF LEAST SQUARES

When the number of equations (m) > n, the number of unknowns in the equations $y = Ax$, then rank $(A) \leq n < m$, and rank $(A/y) \leq n + 1 \leq m$; in such cases, the equations may be inconsistent, that is, there may not be an exact solution. In cases like that, we look for an approximate solution minimizing the error

$$e = y - Ax$$

The solution minimizing the usual norm of e, assuming real vector space for simplicity,

$$\|e\|^2 = e^T e = (y - Ax)^T (y - Ax)$$

is called the least squares estimate of x. The vectors y, Ax, and e belong to an m - dimensional vector space, say V_m, but Ax belongs to M(a), the column space of A. Then

$$V_m = M(a) + M(a)^{\perp}$$

$$y - Ax = e = e_1 + e_2$$

$$\|e\|^2 = \|e_1\|^2 + \|e_2\|^2$$

Since y is given and $Ax \in M(a)$, the choice of x cannot affect e_2. The least squares solution vector $\underline{x}$ is therefore the one for which $\|e_1\|^2 = 0$ or $e_1 = 0$, so that

$$y - A\underline{x} = e = e_2 \in M(a)^{\perp}$$

that is,

$$a_i^T e = 0, \quad i = 1, 2, \ldots\ldots, n$$

$$A^T e = A^T(y - Ax) = 0 = A^T y - A^T A\underline{x}$$

or,

$$A^T A\underline{x} = A^T y$$

which are known as normal equations for the least squares problem. If the square matrix is nonsingular, then

$$\underline{x} = (A^T A)^{-1} A^T y$$

which is the usual least squares formula. For weighted least squares, the norm is taken as $e^T Qe$ and yields

$$\underline{x} = (A^T QA)^{-1} A^T Qy$$

If $A^T A$ is singular, its usual inverse does not exist. Then the least squares estimates can be obtained by using pseudo (or genaralized) inverse with the help of singular value decomposition (SVD).